A GOUGING MODEL FOR A FIRST-YEAR ICE RIDGE PENETRATING THE SEABED

S.A. Vershinin[1], P.A. Truskov[2], and K.V. Kouzmitchev[3]

ABSTRACT

A physical model of a first-year pressure ice ridge (hummock) interacting with the seabed in drift is derived with the purpose to tackle the problem of pipeline burial depth profile offshore Sakhalin Island.

This paper improves the existent computational models by a more substantial description of the ice ridge keel behavior as it penetrates into bottom soil. The hummock is modeled by a loose-cohesive body with three degrees of freedom, which is forced by inertia and ice floe bearing to penetrate into bottom soil − also modeled as a loose medium.

The process of hummock penetration into the seabed and disintegration of both media is described by equations of motion of solids and a theory of limit equilibrium of solid-plastic bodies. Both sets of equations are adjusted for the friction of ice over soil to justifiably estimate the quantitative parameters of seabed gouging by ice pressure ridges as a function of sea depth, bottom slope and relevant geometrical and physical parameters of interacting media.

INTRODUCTION

Reported interaction models of first year hummocks with bottom soil have been derived under strong influence of existent methods used to estimate the interaction of icebergs with the seabed (Alekseev et al., 2001). Unlike first-year hummocks, icebergs are high-strength ice formations with high inertia of motion; therefore, their interaction with the seabed may be modeled rather accurately for practical applications by equations describing penetration of a solid with one degree of freedom into a loose medium whereby the kinetic energy of this solid converts into a work against braking forces of reacting medium.

The pressure ice ridge modeled as a solid is an element of ice cover. It interacts with this cover and has strength characteristics comparable with those of bottom soil. Its interaction with bottom soil requires adequate representation in the model.

---

[1] Morneftegasproect, Moscow, Russia
[2] Sakhalin Energy, Moscow, Russia
[3] Rosneft, Moscow, Russia

A major objective of this paper is to adjust the model for the physical processes describing the interaction of finite-strength first-year hummock keel with bottom soil, and also to include in it mathematical models of motion and destruction of solid and deformable bodies. This deterministic approach will further evolve into a probabilistic model.

The importance of theoretical estimates of gouge depths should not be underestimated, because observations of gouges dug by ice ridge keels in the seabed provide only indirect evidence of gouge size (as a rule undervalued). Observations of bottom-bound hummocks do not yield accurate measures of the actual gouge depth because of the screening effect of surrounding bands of soil expelled from the bottom by penetrating hummocks and the effects of soil erosion by sea currents around their keels.

Model parameters of hummock geometry

Choosing the angle of attack for a bottom penetrating hummock keel
The pitch angle of hummock keel is normally between 30 deg. and 60 deg. and this angle defines the geometry and strength of the entire hummock. The reaction of seabed soil is in general a function of hummock's angle of attack (gouging) along the hummock's contact with seabed soil. The depth of a gouge in soil is comparable with the size of ice rubble constituting the keel, therefore the gouging angle is defined by the angle at which ice rubble are set in the hummock.

Front face rubble's attack angles are almost random in view of the random orientation of rubble in the hummock; therefore, the model's local gouge angle should be selected on the condition of the least resistance to hummock keel when it cuts a gouge of a given depth. From the standpoint of gouging hazard, the maximum penetration potential is found in a hummock with a vertical gouging face (90 deg.). This fact has been proved experimentally (Green et al., 1983). Indeed, attack angles below 90 deg. produce an upward (lifting) force, and in order to proceed gouging the hummock needs an additional downward pressing force which would increase friction and its horizontal bulldozing work – a trend found in experiments.

Orientation of pressure ice ridges with respect to bottom slope

Actual ice ridges are almost prismatic in shape and differ in width and length only. They may drift in different directions and the result of their interaction with the bottom depends on the hummock width to ice ridge length ratio. For large pressure ice formations, these aspect parameters are comparable in size; therefore, we approximate the ice formation by an axially symmetric flattened cone with the top and bottom diameters selected on the conditions of balance of hummock weight and keel buoyancy, and the general slope of actual hummock keels. The bottom diameter will define the gouge width. Under these assumptions, the hummock orientation is invariant to the bottom fall direction.

The hummock strength model has been adopted as a ball-shaped discrete rubble formation adjusted for rubble size and hummock age (Vershinin et al., 2003b). This model treats the pressure ice ridge as a layered medium with $2h$-thick layers (h is the ice rubble thickness). In this medium, the strength increases with depth, depending on ice ridge geometry, conditions in which the ridge was formed and its age.

Physical model of hummock-seabed interaction

Loads acting on the pressure ice ridge are depicted in Fig. 1.

When a pressure ice ridge of mass M drifting along with an ice floe at a velocity V meets the seabed, its gouging effort gives rise to a passive reaction of soil $F_p(x)$, which is a major force causing hummock deceleration to a complete halt. Decelerating hummock to a velocity $V(x)$ results in an additional bearing of the drifting ice floe on the hummock $F_D(V - V(x))$ due to a reduced drag. Physically the hummock drive force is exerted by wind sail push and sea currents F_W and opposed by the hydrodynamic drag F_H, inertia and compacting ice floes $Fi(V - V(x))$, viz.,

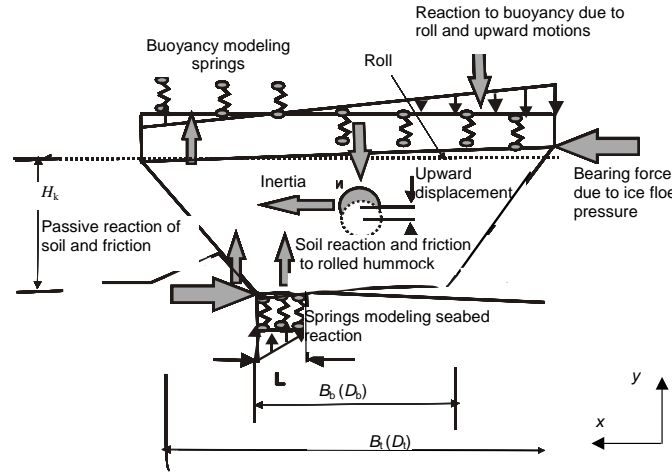$$F_D\big(V - V(x)\big) = F_W - F_H\big(V - V(x)\big) + Fi(V - V(x)). \tag{1}$$

Fig. 1. Computation model of a pressure ice ridge interacting with the seabed:
B_t = top width (D_t = diameter for axially symmetric hummock);
B_b = bottom width (D_b = diameter for axially symmetric hummock);
H_k = depth of the keel; L = line of keel-gouge bottom contact

The strongest reaction force $F_p(x)$ is governed by whatever passive reaction, exerted by the subsurface part of hummock or soil, is lower and this depends on their physical and mechanical characteristics. The height of passive pressure zone depends on the volume of soil bulldozed out of the gouge. The balance of vertical forces yields the unbalanced hummock weight, which occurs when the hummock is forced to ascend, thus producing the downward tracking force. The downward force owes its existence also to hummock's off-center loading.

The maximum bearing force (1) produced by ice drift at complete halt of the hummock is also known as the ultimate drive force. When the ice bearing force reaches its ultimate level (conditioned by the ice strength or floe stability) and the hummock is ground to halt, broken ice rubble start piling up on the bottom, i.e., a grounded hummock is being formed. Thus, the maximum gouging depth is also limited by the strength or stability of the floe. In an alternative scenario, a drifting floe drives the halted hummock deeper into bottom soil.

The moment causing hummock turnover through an angle ψ is balanced by the reaction of soil at the hummock bottom and unbalanced buoyancy.

Thus, the hummock is involved in three movements in accord with the number of degrees of freedom in plane motion, namely, horizontal, vertical, and rotary motions. Motion parameters depend on ice ridge's aspect ratio (width to height), in other words, on the offset of forces about to the ridge base.

Modeling assumptions are as follows:

- The hummock roll ψ is small (<< 1) and varies slowly. The inertia of rotation and transverse forces that arise in bending the floe are neglected, thus setting the moment about the hummock's center of mass to zero.
- The acceleration and velocity of hummock's vertical motion (y) are small, that is, its vertical motions occur under static equilibrium.

- The hummock of mass M moving horizontally (x) with an initial velocity V comes under the effect of external forces dependent on the velocity of motion.

- The kinetic energy of hummock and the work of the floe bearing drive is expended mainly on the work against the resistance of ground to motion producing a pressure wedge sliding along the front face of the hummock and on the work against the friction of bottom soil brought about by the downward pressing force.

The equation of horizontal (x) motion of the hummock center of mass at the initial condition $V(0) = V_0$ has the form

$$M \frac{dV}{dt} = F_D - F_r - F_c \cdot f \ . \tag{2}$$

Here, F_D is the force due to floe bearing on the hummock (bounded by the force of hummocking $F_{\lim}$), F_r is the resistance of soil to hummock's dozing push, F_c is the normal component of the reaction of hummock bottom soil to hummock rotation, and f is the ice against soil friction factor.

The equation includes the force F_c which may be defined by analysis of hummock's rotation and uplift; thus, the equations of hummock motion in three degrees of freedom should be combined in a system of equations.

Mechanical model of grounded hummock interaction with the bottom

The mechanical model of hummock's horizontal motion reflects the process of self-oscillations of soil-hummock system.
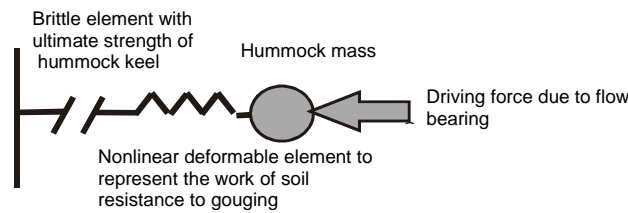

Fig. 2. Mechanical model of hummock horizontal motion

Assumptions of the mechanical model

- The driving force due to ice floe bearing on the hummock does not exceed the force of its hummocking, i.e., $\sum F_i \le F_{\lim}$.

- The bearing force is assumed to be $F_{\lim}[1 - V(x)/V]^2$ to reflect the changing resistance to ice floe decelerating to velocity $V(x)$.

The variable motion of the hummock may be represented by an energy integral (in addition to equation (2)). For bottom gouging started with velocity V, the energy integral is

$$\int_0^S F_{nf}(x)\,\mathrm{d}x = \frac{M \cdot V^2}{2} - \frac{M \cdot V(S)^2}{2} + \int_0^S F_{\lim}\left(1 - \frac{V(x)}{V}\right)^2 \mathrm{d}x. \tag{3}$$

Here, $F_{nn} = F_r + F_c \cdot f$ is the resistance of soil to horizontal bulldozing push and hummock bottom friction against the soil of a gouge dug to a length S.

Assuming that the hummock velocity decreases uniformly over S, its current velocity is

$$V(x) = V - \cdot\frac{x}{S}[V - V(S)]. \tag{4}$$

Here, $S = h/\tan(i)$, and h is the gouge depth.

Rotation of hummock (we assume that both velocities and accelerations are small)
Figure 1 shows applied forces and reactions that occur in turnover of the hummock (ψ is the hummock's angle of roll).

Hummock's roll in turnover

We determine the moment about the center of mass (the moment arm is the distance of the center of mass from the top of the hummock keel, Z_c).
The moment of rotation due to the action of active forces and passive pressure of the soil pressure wedge is

$$M(x) = F_{\lim} \cdot \left(1 - \frac{V(x)}{V}\right)^2 \cdot Z_c + F_{nn}(x) \cdot (H_k - Z_c) - F_r(x) \cdot f \cdot \frac{D_b}{2}. \tag{5}$$

We determine the width of keel contact with soil (letting for simplicity that this is a rectangle of length L) assuming that the sum of the vertical projections of forces causing hummock roll is zero, viz.,

$$\left(\frac{D_t + D_b}{2} - L\right)^2 \cdot \gamma_w - \left(\frac{D_t - D_b}{2} + L\right)^2 \cdot \gamma_w - \cdot L^2 \cdot C_x = 0, \tag{6}$$

where γ_w is the unit weight of water modeled by the spring force due to buoyancy, $C_x = C_i \cdot C_g /(C_i + C_g)$ is the spring force representing the stiffness of ground C_g and ice ridges C_i.
We determine the angle of hummock roll ψ using the fact that the resultant moment about the center of mass is zero

$$\frac{1}{3} \cdot L^2 \cdot C_x \cdot \psi + \frac{1}{3} \cdot \left(\frac{D_t + D_b}{2} - L\right)^3 \cdot \gamma_w \cdot \psi + \frac{1}{3} \cdot \left(\frac{D_t - D_b}{2} + L\right)^3 \cdot \gamma_w \cdot \psi - \frac{M(x)}{D_b} = 0. \tag{7}$$

In order to determine the reactions that occur in rotation of the hummock, including the reaction of soil, the two last equations for the vertical projections and moment about the center of mass should be treated as a system in conjunction with the equation of horizontal motion.

Moving the hummock's center of mass upwards

The friction along the contact with the ground knockout wedge and resultant tilt of the hummock cause its center of mass to go up and when the hummock is ground to halt in the seabed and becomes a grounded hummock, the magnitude of this uplift is the largest.

The upward slide the hummock caused by the friction in forming a soil knockout prism is

$$Y_p = \frac{F_r(x) \cdot f}{\gamma_w \cdot \pi D_t^2 / 4} \,.$$

(8)

The upward displacement of the center of mass for the rolled hummock is

$$Y_\psi = \left(\frac{D_b}{2} - L \right) \cdot \psi \,.$$

(9)

The full displacement of the center of mass is given by the sum of these quantities.

Estimating the ultimate strength of bottom gouging keels

Level shear case

The shear reaction of gouged bottom soil can shift the bottom part of the keel with respect to its upper part. Keel ice disintegration may proceed by sequential cutting layers of the keel penetrating the soil until hummocks complete halt (Fig. 3).
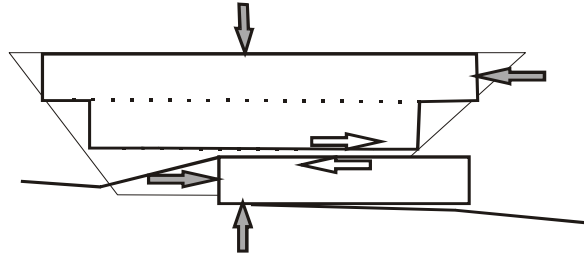

Fig. 3. Horizontal shear of keel's bottom layers by a seabed reaction to gouging

Keel depth shear by horizontal forces

Structural destruction of the hummock over slide surfaces progresses over the front face, as shown in Fig. 4.
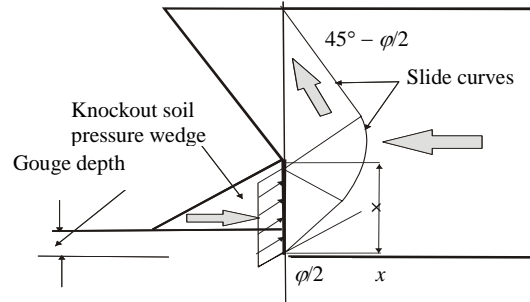

Fig. 4. Resistance to gouging and structural shear over the front of the hummock

In order to estimate the ultimate resistance of hummock to shear we resort to the Sokolovsky solution derived for a non-horizontal load on the keel disregarding the weight of ice rubbles in water. We assume that the normal component of the sliding force is $P_n = N_c C$, where N_c is a function of internal friction and the sliding force of bottom soil resistance, which depends on the ice friction over ground (Tsytovich, 1968); for zero friction, N_c is the Prandtl number. For non-vertical front face of the keel, the resistance to bottom shear increases (similar to Prandtl solution for a wedge).

Seabed soil dislocation models

When the keel penetrates the seabed, the soil undergoes a few types of structural dislocation. Two most probable types include the horizontal shear and bulldozing a soil pressure wedge above the keels bottom.

Formation of a knockout soil wedge by horizontal pressure

In view of a finite width of hummock B_t (D_t) and the knockout wedge of undisturbed soil (height H), and an additional weight of the knockout wedge in from the hummock, the estimation model of soil resistance should be three-dimensional, as shown in Fig. 5.
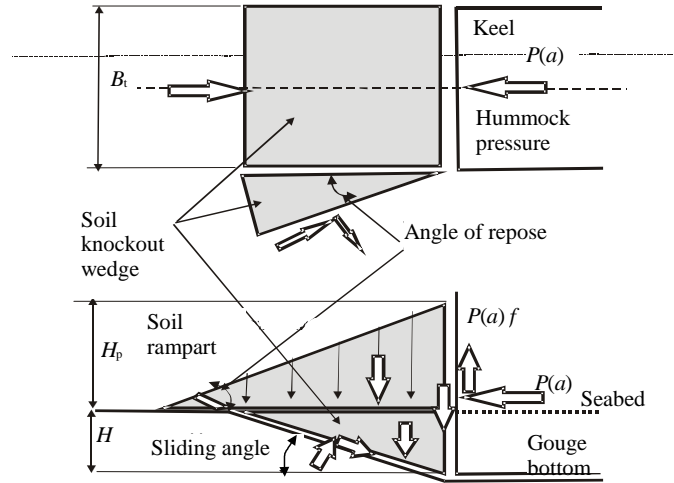

Fig. 5. Soil rampart and pressure-wedge forming forces

We will seek a solution to this problem by the energy methods of plasticity theory. The bottom soil slide wedge will be viewed as a rigid-plastic body in a given kinematically feasible velocity field. The wedge configuration is selected from physical considerations and the properties of loose-cohesive medium: angle of internal friction (φ) and cohesion (C) − an initial shear parameter for sand, which is treated as a Mohr-Coulomb medium. The rampart of soil ahead of the hummock loses cohesion and is treated as a loose medium.

We assume that the energy is dissipated over the knockout wedge surface only (we neglect the discontinuity of velocity inside the wedge and assume that this prism is moving as a solid). In this estimation, the knockout front surface will be treated as a plane. The effect of bottom slope within the wedge length is neglected. The sliding velocity of the wedge along the slide plane is V_p (the horizontal component is the hummock velocity $V(x)$) inclined to the horizon at an angle a which need be determined from the condition of the minimum force P). The balance between the power of external forces and energy dissipation rate has the form:

$$P \cdot \cos(a) \cdot V_p = T_1 \cdot V_p + G_s \cdot V_p \sin(a) + 2(N_{02} + T_{03}) \cdot V_p$$
$$+ P \cdot \sin(a) \cdot f \cdot V_p + P \cdot f \cdot \cos(a) \cdot \tan(\varphi) \cdot V_p, \tag{10}$$

where f is the friction factor of ice rubble over the bottom soil.
The pressing force normal to the slide surface is:

$$P_n(a) = P(a) \cdot \sin(a). \tag{11}$$

The normal component due to the weight of knockout wedge of height H and soil rampart G_{up} is :

$$G_{sn}(a) = G_s(a) \cdot \cos(a),$$
(12)

where the weight of the slide wedge and soil rampart prism is

$$G_s(a) = \frac{1}{2}H^2\gamma\frac{Bt}{\tan(a)} + \frac{1}{3}\pi\left(\frac{H}{\tan(a)}\right)^2\gamma \cdot H\frac{x}{2\pi} + G_{up}.$$
(13)

Here, γ is the specific weight of soil in water defined as: $\gamma = (\rho - \rho_w) \cdot g \cdot (1-n)$ ρ_w is the density of sea water; ρ is the density of sand; $g = 9.81$ m/s^2 is the acceleration of free fall; and n is the porosity of sand.

Assuming that there is no cohesion in the rampart soil and adjusting the model for rampart soil spread aside in gouging, we have

$$G_{up} = \frac{1}{2}\gamma\left[\frac{H^2}{\tan i} - \frac{1}{2}\left(\frac{H_p}{\tan\varphi} - \frac{H}{\tan a}\right)^2\sin 2a\right]B_t - \frac{1}{6}\gamma \cdot \frac{H_p^2 H}{\tan\varphi \cdot \tan i},$$
(14)

where φ is the angle of repose for rampart sand, i is the bottom slope, and the negative term reflects the soil lost in spreading aside from the bulldozed rampart.

The force of wedge sliding along the slide surface is

$$T_1(a) = [P_n(a) + G_n(a)]\tan\phi + c \cdot \frac{H.B_t}{\sin a} + c \cdot b(a)\frac{H}{\sin a},$$
(15)

where $b(a) = \frac{H}{\tan a}\varphi$.

The force component normal to the side surface of discontinuity multiplied by $\sin(x)$ is:

$$N_{02}(a) = c \cdot \tan(\frac{\pi}{4} - \frac{\phi}{2})^2\sin(x)\frac{H^2}{\tan a}.$$
(16)

The component of force tangential to the side surface of discontinuity multiplied by $\cos(x)$ is:

$$T_{03}(a) = \tau(\phi)\frac{H^2}{2\tan a}\cos x,$$
(17)

where $\tau(\varphi) = c - 2c \cdot \tan(45° - \phi/2) \cdot \tan\phi$.

The horizontal resistance to motion of the subsurface part of hummock F_p when it meets the seabed can be determined by minimizing the following equation with respect to a:

$$P(a) = \frac{G_{sn}(a)\tan(\phi) + c\frac{H \cdot B_t}{\sin(a)} + cb(a)\frac{H}{\sin(a)} + G_s(a)\sin(a) + 2T_{03}(a) + 2N_{02}(a)}{F(a) - \sin(a) \cdot \tan(\phi)},$$
(18)

where $F(a) = \cos(a) - \sin(a) \cdot f - f \cdot \cos(a) \cdot \tan(\phi)$.

The depth shear of soil by the pressing force due to hummock roll

Rolling the ice pressure ridge (contacting the seabed over a surface *L*) aside gives rise to contact stress causing a shear of soil beneath the ridge bottom, as shown in Fig. 6. This shear of soil may affect the trenching depth of offshore pipelines laid in the area.
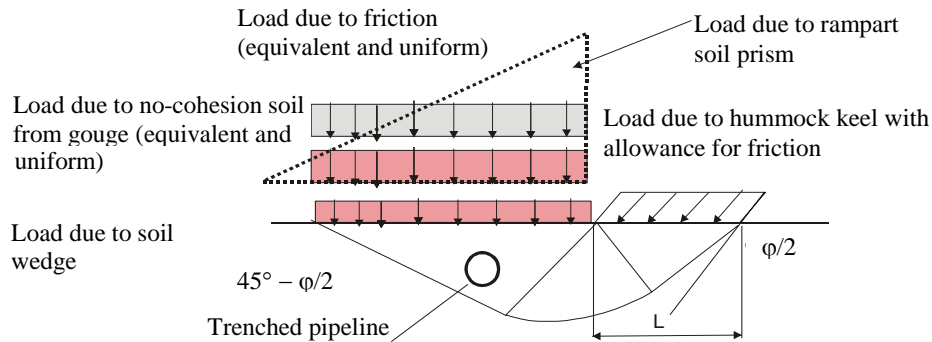

Fig. 6. Loads produced by hummock's keel gouging the seabed

We resort to the Sokolovsky solution to estimate the maximum force due to inclined keel loading.

The normal component of this load is $P_n = N_\gamma \cdot \gamma \cdot X + N_q \cdot q + N_c \cdot c$.

The horizontal component is $P_t = P_n \tan \delta$, where $\delta = \arctan(f)$, N_i are coefficient of soil bearing capacity taken as functions soil internal friction and bottom soil load slope angle, i.e., they depend on the friction of ice over ground (Tsitovich, 1968).

The average value of critical pressure is $P_{cr} = [P(L = 0) + P(L)]/2$.

Conclusion

The model of a hummock interacting with the seabed is based on the mechanics of movement and disintegration of solids. It yields quantitative parameters of gouging from the geometrical and physical parameters of the hummock and bottom soil.
The process of soil gouging is treated as a three-dimensional motion of an ice pressure ridge accompanied by upward static motions, roll, and self-oscillatory motions along the horizontal axis.

Hummock penetration into the bottom proceeds in cycles as the keel crushes under bottom soil resistance. A penetration model should not overlook the friction of the keel against the bottom soil.

The ice ridge is driven by inertia forces and floe bearing, the driving force being limited by hummocking. The bearing force increases as the hummock velocity decreases, for the floe drag is proportionate to the square of relative velocity.

REFERENCES

Alekseev, Yu.N. et. al. (2001) Ice engineering problems in offshore oil and gas field development. *Gidgometeoizdat*, St. Petersburg. (In Russian).

Green, H., Reddy, A.S. and Chari, T.R. (1983) Iceberg scouring and pipeline burial depth. *Proc. of POAC -83,* Espoo, Helsinki, vol. 1, pp. 280–288.

Tsytovich, N.A. (1968) Mekhanika gruntov (Soil mechanics), *Vysshaya Shkola*, Moscow.

AN APPROACH FOR RIDGE LOAD DETERMINATION IN PROBABILISTIC DESIGN

Tuomo Kärnä[1] and Esa Nykänen[1]

ABSTRACT

This paper addresses the methods of determining ice loads caused by first-year ice ridges in connection with a probabilistic analysis of the ice loads. A typical probabilistic analysis is done using the Monte Carlo simulation technique. While using this method, the ice loading formulas should not require extensive computations. Two solutions are proposed to evaluate the keel force component of the ridge load with a very small computational effort. First, an advanced ridge model is used to teach a neural network to provide the same results as the basic model. Second, the same advanced model is used to derive small modifications to the Dolgopolov's keel force model. After these modifications this model can be considered as a reliable method to provide an upper bound value for the keel load.

INTRODUCTION AND OBJECTIVES

The determination of forces caused by keels of first-year ice ridges is one of the current problems in ice engineering. Timco et al. (1999) evaluated twelve different models that have been proposed for the determination of forces caused by ridge keels. The methods are different variants of the passive-earth-pressure theory (Tsytovich, 1986 and Bowles, 1988 and). Timco et al. (1999) found that the ice forces predicted by different methods vary greatly, and recommend more efforts in new numerical techniques that should provide realistic ice force predictions. Using classical concepts of soil mechanics, Kärnä et al. (1996, 2001) and Croasdale (1999) have proposed such numerical models for the determination of the keel load. Based on extensive field measurements, Heinonen (2004) has developed a more advanced material model for first-year ridges, to be used in numerical FE models.

Recent field observations on first-year ice conditions have shown (Timco et al, 2000; Kärnä and Jochmann, 2003) that the structure does not penetrate a first-year ice ridge in its strongest area. Instead, a dodging behaviour will occur in one of several possible variants. These include spine failure, shear fracture, failure behind or stopping and a subsequent failure by creep buckling. These failure modes were illustrated and further discussed by Wright and Timco (2001). The ice floe may also rotate so that the penetration can continue along a weak zone of the ridge field. The area of the ridge sail is a potential

---

weak zone. Field observations (Kärnä and Jochmann, 2003) show several conditions where the penetration of a ridged ice area occurs for a along distance along the ridge sail or along the boundary between an area of rafted ice and level ice. An obvious explanation of the observed dodging behaviour is based on the large-scale behaviour of the drifting ice fields. The first-year ice cover always has several weak zones. Therefore, ridge failure behaviour is very complicated. Large-scale deformations and rotation of the ice field can occur owing to the interaction forces caused by the bottom-founded structure.

The dodging behaviour of the ice ridges is a force limiting mechanism. Unfortunately, it is difficult to construct models that would consider all the failure mechanisms that have been observed. Therefore, there is still a need to make use of models where the structure is assumed to directly penetrate the ice ridge. These models will yield upper bounds for the realistic ice forces.

The objective of this paper is to derive an approach of ridge load determination for the probabilistic design. The paper will address only forces caused by the ridge keel. While using the Monte Carlo simulation technique, there is a need to obtain values of the keel force with a minimum computational effort. Numerical tools that are available for the deterministic estimation of the ridge forces appear to consume too much computing time. As a first solution to this problem we will apply a neural network. An advanced passive failure model is used to teach a neural network to provide the same results as the basic model. As a second option, we will compare the advanced failure model with the Dolgopolov's formula and show how this formula can be used to yield realistic values for the keel force component.

AN ADVANCED RIDGE MODEL

Kärnä et al. (1996, 2001) derived a passive failure model for the ridge keel. This model considers ice ridges having a cross section depicted in Fig. 1. The figure shows the geometrical characteristics of the ice feature in an initial condition of ridge penetration. The model simulates the ridge penetration as a sequence of discrete failure events. Figure 2 illustrates the assumed failure mechanism with an inclined and two vertical failure planes. Depending on the amount of penetration and the internal strength properties of the ridge, an individual failure event can be characterised either as a local failure or as a plug failure (Brown et al. 1996, Croasdale, 1999). The model considers the evolution of the ice ridge by redistributing the failed ice rubble below and behind the original keel profile. Accordingly, the model considers the surcharge effect that arises while the keel height increases during the interaction.
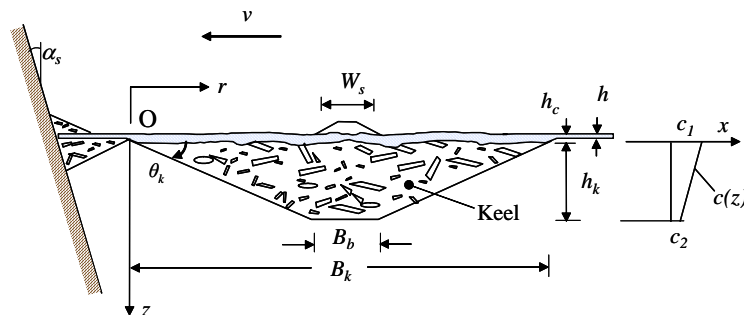

Fig. 1. Cross section and parameters of a first-year ice ridge.
The parameter $c(z)$ shows the distribution of the cohesion strength

The shape of the ice ridges has been a subject of active research (e.g. Timco and Burden, 1997). Parametric studies carried out with the present model indicate that the maximum keel force depends on the initial volume of the ridge keel. The keel profile is of less importance.
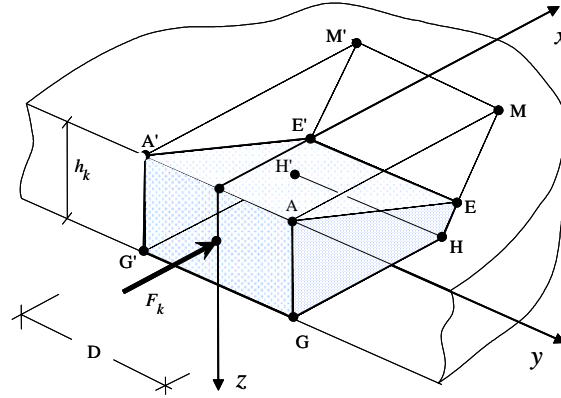

Fig. 2. Assumed failure mechanism with an inclined and two vertical slip planes

Figures 2 and 3 illustrate a typical step in the numerical simulation. The forces acting on the inclined slip plane AEE'A' and vertical slip planes AEHG, A'E'H'G' are evaluated based on the stress conditions at the Mohr-Coulomb failure envelope. The reactive force S is then solved from an equation of equilibrium where also the volume force Q and friction at the ice-structure contact are considered. This calculation is repeated for several tentative slip planes that are kinetically possible. The horizontal component of S is defined as the keel force F_k. The minimum value of F_k found at each step is defined as the actual keel force.

The original passive failure model described by Kärnä et al. (1996, 2001) was upgraded for this paper. First, the stress state within the keel was assumed to consist of three components $(\sigma_x, \sigma_y, \sigma_z)$ where σ_z is the main stress component arising directly from the buoyancy forces. The lateral stresses σ_x and σ_y arise due to the lateral confinement provided by the keel material (Tsytovicy, 1986, Sect. 2.1). Second, the cohesion strength $c(z)$ of the ridge keel was assumed to vary linearly within the keel as shown in Fig. 1. This assumption takes account of the fact that the keel strength is higher in the upper keel layers than in the keel bottom (Blanchet 1998). It was assumed in all subsequent calculations that the cohesion vanishes at the keel bottom ($c_2 = 0$).
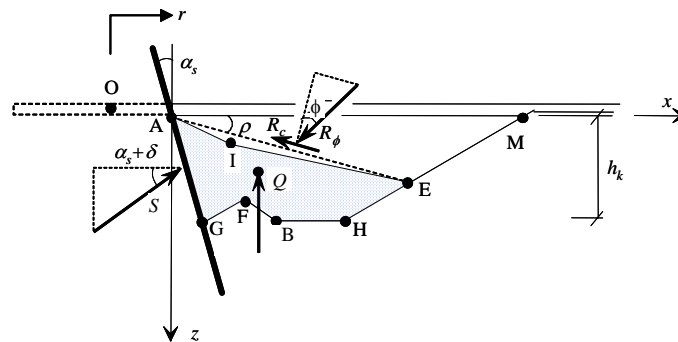

Fig. 3. Forces acting on the failing rubble volume. The parameters δ and ϕ are the angle of friction at the contact surface and the internal friction, respectively

The frictional and cohesion forces of the Mohr-Coulomb theory can not be mobilized simultaneously in full extent. Corresponding to the concepts of soil mechanics (Tsytovich, 1986, p. 52), the cohesion is considered to consist of two components. One of them is a structural rigid cohesion due to refrozen bonds between the ice blocks. The second component is a plastic cohesion, which arises during large slippage at the failure plains, as large ice fragments rotate and experience damage. The rigid cohesion is mobilized in an initial phase while the failure planes are forming. We assume that this component is not acting simultaneously with the internal friction, which attains its maximum level only after a relatively large deformation (Ramiah and Chickanagappa, 1990 and Bowles, 1988, Fig. 11-3). Quantitative data on the rigid and plastic cohesion is not available at present. Therefore, we assume that an estimate of the total cohesion is used as input to the advanced ridge model. Then, this total cohesion is reduced slightly (by 25%) to consider the non-simultaneous mobilization of the cohesion and friction.

Bowles (1988) recognises that a passive-pressure theory, which assumes linear failure planes consistently overestimate the actual passive pressure. In a more advanced application to the theory of plasticity, non-planar failure surfaces can be assumed. Therefore, the inclined failure plane AEE'A' depicted in Fig. 2 is likely to be slightly curved when the actual failure occurs. The advanced model of the present paper considers this by using a bi-linear failure plane. This is shown in the cross-sectional presentation of Fig. 3 by the line AIE.

In the advanced passive failure model, frictional and cohesion forces are active both in the inclined and in the two vertical failure planes. Figure 3 shows the resultant forces R_ϕ and R_c on the inclined failure surface. Corresponding force resultants act on the vertical failure planes AEHG and A'E'H'G' shown in Fig. 2. Both the internal stresses and the cohesion strength vary in accordance with the parameter z. Therefore, the internal force resultants are evaluated by integration over the failure surfaces concerned.

A NEURAL NETWORK APPROXIMATION

As a next step of this study, a trained Neural Network was developed to allow a much faster force evaluation than while using the advanced ridge model. In order to train the Neural Network, the advanced ridge model was first used to create a wide set of data on keel forces. The input variables of this calculation were selected as

- D is the width of the structure (m),
- h_k keel depth (m),
- α_s angle of inclination of the structure (deg),
- δ friction angle at the ice-structure contact (deg),
- ϕ internal friction angel of the keel material (deg),
- c_1 cohesion at the upper part of the ridge keel (kPa).

A total of 4143 combinations of these parameters were selected and the horizontal keel force component F_k was evaluated for each combination of the input. The results were then transformed to a line load $Q_k = F_k/D$, which was used to train the neural network. The NeuroShell 2 $^®$ software was used to develop the neural network. The network was designed so that 80 % (3315) randomly selected data lines were used as the training set and 20 % of the data was used for testing.

The method used for training was GRNN (General Regression Neural Network) with the type *Ward* net that has 3 three hidden layers with totally 67 neurons. The trained net

provides a value of the line load Q_k for any combination of the six input parameters within the trained range.

As shown in Fig. 4, the Neural network has learned quite well the data. At present, there are still some high individual absolute errors when comparing the "net" value to the "actual" value. This problem can be solved by using further data and improving the training process.
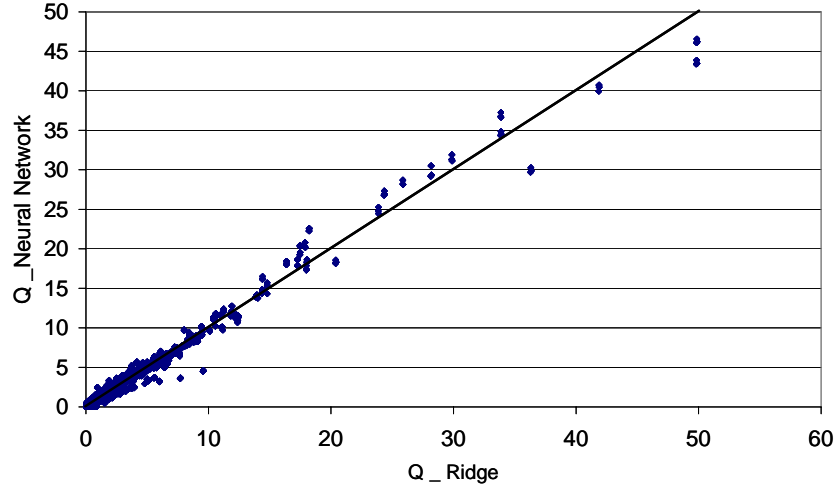

Fig. 4. The keel resistance values Q_k obtained by the advanced ridge model vs the corresponding values provided by the trained neural network

NeuroShell 2 provides a possibility to create different runtime versions based on the trained net. In this case, the most potential possibility is to create DLL (dynamic linked library) files to be called directly from a main program.

COMPARISONS WITH DOLGOPOLOV'S MODEL

Timco et al. (1999) recognise that the model proposed by Dolgopolov et al. (1975) considers most of those essential parameters that influence the keel forces. Using the notation of the present paper, Dolgopolov's formula for the keel load is given by

$$F_k = \mu \, h_e \, D \left(\frac{h_e \, \mu \, \gamma_e}{2} + 2c \right) \left(1 + \frac{2 \, W_s}{3 \, D} \right), \tag{1}$$

where $\mu = \tan\left(45^0 + \dfrac{\phi}{2} \right)$, ϕ is the angle of internal friction, c is the apparent cohesion, D is the width of the structure, h_e is an effective keel depth, W_s is the width of the ridge sail and γ_e is the effective buoyancy given by

$$\gamma_e = (1-n)(\rho_w - \rho_{ice}) \, g \,. \tag{2}$$

Here, n is the keel porosity, g is the acceleration due to gravity and ρ_w, ρ_{ice} are water and ice densities, respectively. The factor $q = \left(1 + \dfrac{2}{3} \dfrac{W_s}{D} \right)$ of Eq. (1) contains a parameter W_s, which in Dolgopolov's original paper was defined as a the width of the ridge sail (Fig. 1) and was related to the keel depth h_k by an assumption that h_k is equal to four to five times W_s. It is of interest to notice that Dolgopolov et al. (1975, Fig.1) used the

character H for the width of the ridge sail. Apparently due to this special notation, most subsequent discussions on Dolgopolov's model show Eq. (1) in a form where the sail width W_s is replaced by the keel depth h_k. This leads to an approach where Eq. (1) yields significantly higher keel force estimates than the original formula.

The effective keel depth h_e considers the surcharge effect that arises during the ridge penetration. Dolgopolov et al. (1975) assume that $h_e \leq h_k + D/2$ but provide no exact definition for this parameter.

A parametric study was conducted to compare the keel forces predicted by the advanced ridge model and the Dolgopolov's model. The aim of this effort was to clarify the influence of the parameters q and h_e. For these comparisons, it was tentatively assumed that the advanced ridge model yields "correct" keel forces and can be used to tune Eq. (1). It should be appreciated that Eq. (1) does not consider the effects of the inclination angle α_s and friction angle δ at the contact surface Therefore, the initial comparisons were made for vertical structures ($\alpha_s = 0$) assuming that the friction between the keel rubble is defined by $\delta = 0°$. The keel geometry was defined by assuming $\theta_k = 30°$ and $B_b = \frac{1}{2} h_k \cot \theta_k$ (see Fig. 1). The keel porosity was set as $n = 0.30$.

First parametric studies were made by assuming that the surcharge effect in Eq. (1) varies with the structure width as $h_e = h_k + D/10$. The results showed that the keel force predicted by Eq. (1) becomes excessive for wide structures. Therefore, further studies were made with $h_e = h_k$. The influence of the shape factor q was then studied assuming that in the equation of q, the parameter W_s is either replaced by the keel depth h_k or is given in its original form by $W_s = h_k/5$ or $W_s = h_k/4$. Parameters that influence the keel resistance were varied as $\phi = 10°$ to $50°$ and $c = 1$ kPa to 20 kPa. The geometrical parameters were varied as $D = 2$ m to 60 m and $h_k = 2$ m to 40 m. This study showed that the best fit with the Dolgopolov's formula and the advanced ridge model arises when Eq. (1) is used in its original form with $W_s = h_k/4$.

One of the differences between the advanced ridge model and Eq. (1) is that the advanced model considers the keel resistance arising in the inclined and two vertical failure planes. Eq. (1) considers explicitly only the resultant forces R_ϕ and R_c on the inclined failure surface AEE'A' (Figs. 2 and 3). The numerical comparisons between the two models clearly show that the shape factor q successfully compensates the deficiency that arises while Eq. (1) ignores the effects of the vertical failure planes AEHG and A'E'H'G' (Fig. 2).

As a final step of the comparisons, the influences of the contact friction and the cohesion were studied. First, the input value of the cohesion was reduced in computations by 25% on both models. Second, while using the advanced ridge model, the friction angle δ was varied from $0°$ to $20°$ (kinetic friction coefficient $\mu_k = \tan(\delta)$). It was found that the outputs from the advanced ridge model are close to each other while Eq. (1) is used with $h_e = h_k$ and $W_s = h_k/4$ and when the friction angle is assumed as $\delta = 10^0$.

As a result of these comparisons, it is proposed that the Eq. (1) is modified to

$$F_k = \mu \, h_k \, D \left(\frac{h_k \, \mu \, \gamma_e}{2} + 2c \right) \left(1 + \frac{h_k}{6 \, D} \right). \tag{3}$$

PARAMETRIC STUDIES

A parametric study was conducted to examine how the three models developed above compare with each other. Table 1 shows values of the input parameters in six cases that were studied. The results are shown in Figs. 5 to 7. The keel force was plotted in terms of the global keel pressure defined by $p_k = F_k/(D\, h_k)$

Table 1. Input parameters for the sample calculations

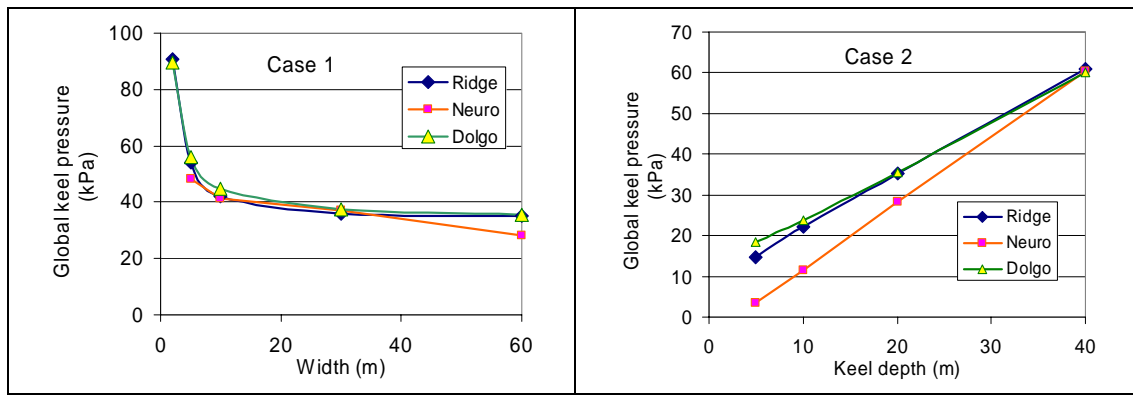|	Case1	Case2	Case3	Case4	Case5	Case6
D (m)	varied	60	30	30	30	30
h_k (m)	20	varied	20	20	20	20
α_s (deg)	0	0	varied	0	0	varied
δ (deg)	10	10	10	10	varied	10
ϕ (deg)	30	30	30	30	30	30
c_1 (kPa)	5	5	5	varied	5	5

Fig. 5. Influence of the structure width and the keel depth on the pressure p_k

The results in Figs. 5 and 6 concern a vertical structure where the kinetic friction coefficient is about 0.18 ($\delta = 10º$). In these conditions, the slightly modified Dolgopolov's formula (3) ("Dolgo") gives a keel force that is mostly very close to the value predicted by the advanced model denoted in the figures as "Ridge". While varying the contact parameters α_s and δ (Fig. 7), the Dolgopolov's model provides a constant value that can be significantly different from the prediction of the advanced ridge model. This problem can be solved by replacing in Eq. (3) the term μ by a passive pressure coefficient that considers the two contact parameters α_s and δ. Bowles (1988, Sect. 11-4) show the necessary derivations in the case of the Coulomb earth pressure theory. This modification is not done in this paper.
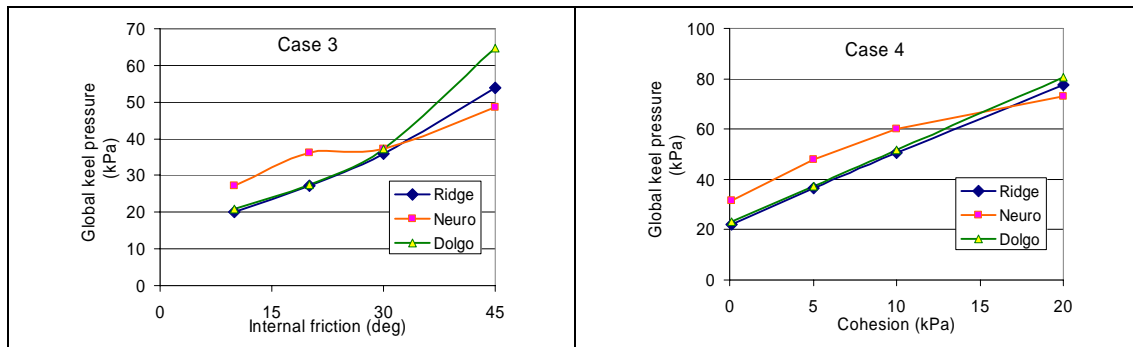

Fig. 6. Influence of the internal friction and the cohesion on the pressure p_k

48

Figures 5 to 7 show that the neural network solution derived in this paper shows in all conditions the same trends as the advanced ridge model. Occasionally, excessive errors are found in the neural network solutions. This problem could be solved by improving the training process.
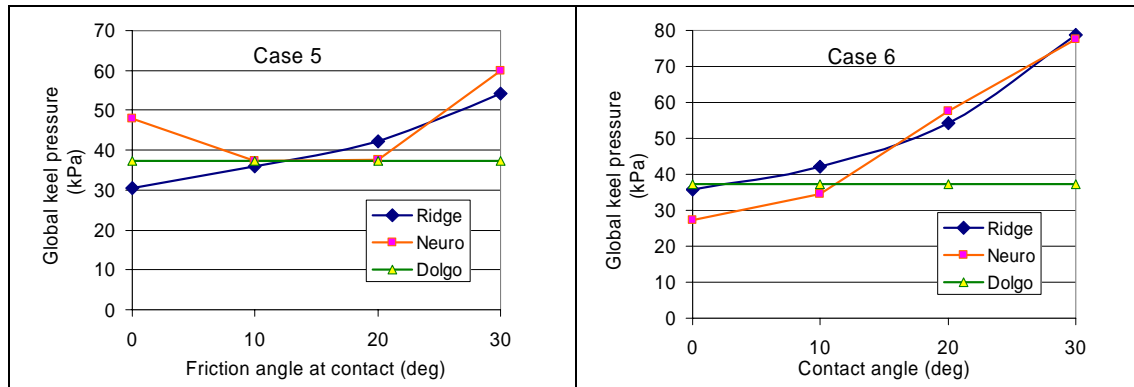

Fig. 7. Influence of the contact angle and the friction angle at the contact surface

SUMMARY

An advanced model on ridge keel forces was upgraded. This model was then used to develop a neural network application for the same problem. As a further effort, Dolgopolov's model for keel forces was studied. It was found that while using this model in a special way, the advanced model and the Dolgopolov's model provide practically the same results for vertical structures where the frictional forces at the ice-structure contact surface are within a specified range. The paper also refers to a possibility to extend the validity of Dolgopolov's model.

ACKNOWLEDGMENTS

REFERENCES

Blanchet, D. Ice load from first-year ice ridges and rubble fields. *Can. J. Civ. Eng*. 25: 206-219 (1998).

Bowles, J. E. Foundation Analysis and Design. *McGraw-Hill Civil Engineering Series. 4th Ed.* New York (1988) 1004p.

Brown, T., Croasdale, K. and Wright B. Ice loads on the Northumberland straight Bridge Piers - An approach. *Proc. 6th Int. Offshore and Polar Eng. Conf.,* Los Angeles. Vol. II, 367 - 372 (1996).

Croasdale, K. A study of ice loads due to ridge keels. *Proc. 4th Int. Conf. Development of Russian Arctic.* St. Petersburg, 268-274 (1999).

Dolgopolov, Y., Afanasiev, V., Korenkof, V and Panfilov, D. Effect of hummocked ice on the piers of marine hydraulic structures. *Proc. 3rd IAHR Ice Symp.,* Hanover, NH. 463-477 (1975)

Heinonen, J. 2004. Constitutive modelling of ice rubble in first-year ridge keel. *VTT Publications. Dissertation for the degree of Doctor of Technology.* (in review).

Kärnä, T & Rim, C.W., Model for global first-year ice loads. *VTT Building Technology, Internal Report* RTE39-IR-9/1996. 43 p.

Kärnä, T., Chae W. R. and Shkhinek, K. Global loads due to first-year ice ridges. *Proc. 16th Int. Conf. Port and Ocean Eng. under Arctic Cond.*, Ottawa, Canada, August 12-17. Vol 2, 627-638 (2001).

Kärnä, T and Jochmann, P. Field observations on ice failure modes. *Proc. 17th Int. Conf. Port and Ocean Eng. under Arctic Cond.*, Trondheim, Norway, June 16-19, Vol 2, 839-848 (2003).

Ramiah, B and Chickanagappa, L. Soil Mechanics and Foundation Engineering. 2nd ed. *Balkema*, Rotterdam (1990), pp. 168-179.

Tsytovich, N. Soil Mechanics (Concise Cource). Translation from English, *Mir Publishers* 1986, Moscow. 176p.

Timco, G., Frederking, B., Kamesaki, K. and Tada, H. Comparison of ice load calculation algorithms for first-year ridges. *Proc. Int. Workshop on Rational Evaluation of Ice Forces on Structures, REIFS99.* Mombetsu, Japan, February 2-4, 1999. 88-102 (1999).

Timco, G., Croasdale, K. and Wright, B. 2000. An overview of first-year ice ridges. Canadian Hydraulics Centre*, Technical report HYD-TR-047. PERD/CHC* Report 5-112. (2000) 159p.

Timco, G. and Burden, R. An analysis of the shapes of sea ice ridges. *Cold Regions Science Technology* 25(1997) 65-77.

Wright, B and Timco, G. First-year ridge interaction with the Molikpaq in the Beaufort Sea. *Cold Regions Science Technology* 32(2001) 27-44.

FIRST-YEAR ICE RIDGE LOADS ON CYLINDRICAL SUPPORTS

Surkov G.A.[1]

ABSTRACT

Loads due to first-year ice ridges on cylindrical support structures have been estimated with models based on the ratio of structure diameter to ice ridge keel thickness. A method has been suggested to estimate load due to first-year ice ridges from laboratory and field experiments. Various estimation techniques of loads due to first-year ice ridges have been compared to demonstrate that the suggested approach to hummock load estimation yields the best-justified (and smallest) load values.

INTRODUCTION

Available theoretical models of ice loads on offshore structures are known to produce a wide spectrum of highly overestimated results. Indeed, ice loads derived by different authors may differ as far as 15 times (Schwarz, 1999). Recent field experiments (Fitzpatric, 1994) demonstrated that calculated loads considerably exceed (almost 10 times) those measured on actual offshore structures.

Estimation of loads on offshore structures due to first-year ice ridges is a more complicated problem than estimation of loads due to level ice. For ice ridges, the model uncertainty is still higher. Ice-ridge loads calculated by different authors differ several times in magnitude (Croasdale and Brown, 2000). Until recent time, theoretical and field-measured values of the load have not been compared because of small number of field tests and absence of a method of comparison for data obtained under different conditions. In respond to this demand, this paper presents such a comparison as well as a method for estimating ice ridge loads from laboratory and field experiments.

AN OVERVIEW OF ICE-RIDGE LOAD CALCULATIONS

Fairly detailed analyses of published models of ice-ridge loads on cylindrical supports may be found in the papers of Krankkala and Maattanen (1984) and Frederking et al. (1999). Some of these models overlook the effect of the support diameter as a fraction of keel depth (draft) or thickness of level ice surrounding the ridge. However, experimental studies (including field tests) of ice ridge impact on cylindrical supports have demonstrated that such an effect does exist.

---

[1] JSC "Sakhalin Projects", Okha, Sakhalin, Russia

Afanasyev (1972) introduced the ice ridge (hummock) load coefficient k_h as a load on a cylindrical support exerted by an ice ridge in proportion to that exerted by level ice surrounding this ice ridge.

Figure 1 shows k_h calculated from experimental data as a function of D/h_i, where D is the support diameter, and h_i is the thickness of level ice surrounding the ice ridge. Field experiments studying the impact of ice ridges were conducted in Cook Inlet in 1963-1964 (Blenkarn, 1977), in the Baltic Sea at the Kemi-1 lighthouse (Maattanen, 1977), and in the Beaufort Sea at the Molikpaq platform (Timco, 1999).

Figure 1 demonstrates that k_h correlates well with D/h_i. The curve fitted on these data has the form (Surkov, 2001):

$$k_{\mathrm{h}} = \exp\left[1.35 - 0.34\ln(D/h_{\mathrm{i}})\right]. \tag{1}$$
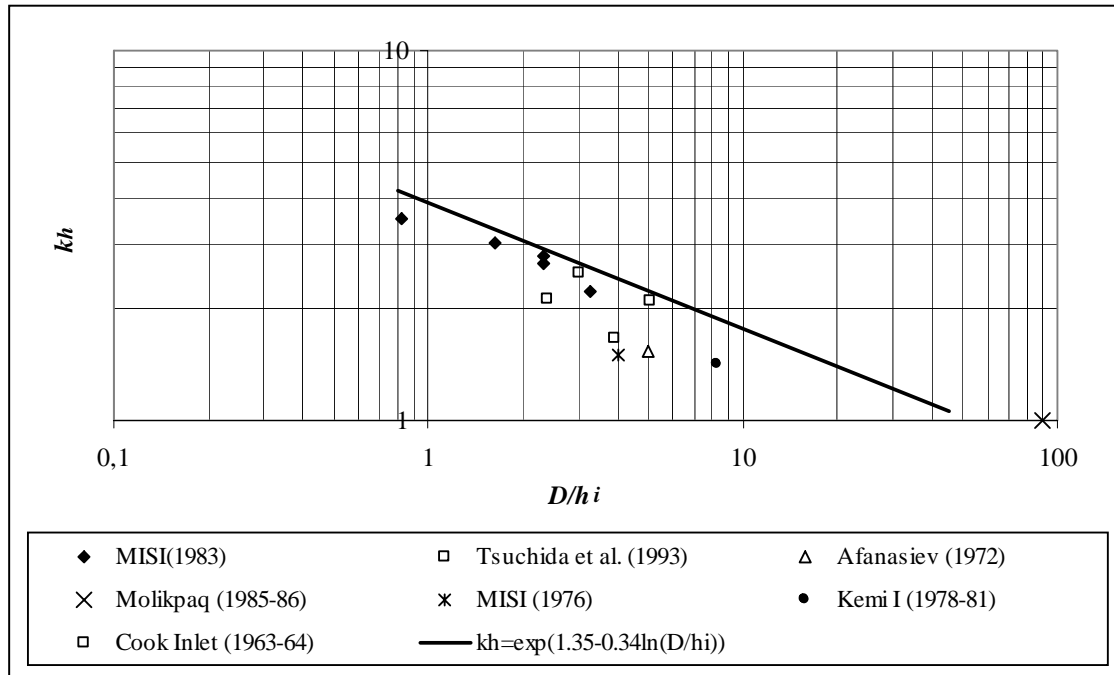

Fig. 1. Ice ridge load coefficient versus D/h_i

A common approach to this problem today is to represent the load F_H on a cylindrical support due to first-year hummock as a sum of the load F_c due to the consolidated layer of ice and the load F_{Hk} due to the hummock keel:

$$F_H = F_C + F_{Hk}. \tag{2}$$

This model does not include, by complexity reasons, the mutual effect of the consolidated layer and keel when the keel crushes. Some authors include also the load due to the hummock sail in this sum, but this addition is insignificant.

The load due to hummock's consolidated layer (and level ice) is mostly determined by the classic expression due to K.N. Korzhavin, which may be given in the form:

$$F_{Hk} = I k_1 k_2 \, \sigma_C \, D h_i, \tag{3}$$

where I is the indentation coefficient, k_1 is the shape factor, and k_2 is the ideal contact coefficient.

A number of reference documents recommend the Korzhavin equation as a model to determine the horizontal load due to ice fields (API 1982, 1988, 1994; SNiP 2.06.04 – 82*).

Application of this equation is hampered by the choice of specific values of I, k_1, and k_2. The ideal contact coefficient may vary in a rather wide range – normally, from 0.3 to 1. For the initial loading cycle, $k_2 = 1.0$ implies an ideal contact between the ice and support. Usually, this coefficient is smaller for cold brittle ice and equals unity for warm ice. The shape factor is 0.9 for cylinders and 1.6 for flat-face supports.

The indentation coefficient depends on the ratio of support width to ice thickness (D/h_i) and on ice structure. Many rule of thumb formulas have been devised for this parameter. An earlier model derived from laboratory experiments (Afanasiev, 1972) has the form

$$I = \begin{cases} \sqrt{5\frac{h}{D}+1}, & \text{for } 1 < \frac{D}{h} < 6; \\ 4 - 1.55\frac{D}{h}, & \text{for } \frac{D}{h} < 1. \end{cases} \tag{4}$$

An exhaustive review of these formulas may be found in a paper of Loset et al. (1999).

Fitting these dependencies by least squares yields the formula

$$I = 2.77 \, (D/h)^{-0.22}. \tag{5}$$

Similar to equation (3) one may write an expression to determine the load due to hummock's keel as

$$F_H = Jim\sigma_H DH_k^*, \tag{6}$$

where J is the indentation coefficient which is a function of D/H_k^*, i is the shape factor, m is the ideal contact coefficient for a keel–support interaction, σ_H. is the keel uniaxial compressive strength, and H_k^* is the keel thickness (keel thickness is equal to its draft H_k minus the thickness of the hummock's consolidated layer h_c).

The keel crushing strength σ_H is more frequently expressed in terms of Coulomb–Mohr loose-connected medium parameters: cohesion c, and the angle of internal friction φ. However, despite enormous amount of effort expended to determine these parameters, they are still in the realm of uncertainty. Therefore, it would be justified to express σ_H in terms of the crushing strength of consolidated layer σ_c which has been well reported by the present time (Surkov, 2000):

$$\frac{\sigma_H}{\sigma_c} = 1 - 0.255n(n \cdot 100), \tag{7}$$

where n is the porosity of hummock's keel ice.

Modern calculation schemes take both i and m equal to unity.

Of a host of such schemes reported only three include the indentation factor J different from unity, i.e., allow for the effect of D/H_k^*, namely,

- (Dolgopolov et al., 1975) $$J = 1 + \frac{2}{3}\frac{H_k^*}{D}, \tag{8}$$

- (Prodanovic, 1979)
$$J = 1 + a\frac{H_k^*}{D}\left(1 + b\frac{H_k^*}{D}\right),$$
(9)

where, for φ varying between 30° and 60°, and the coefficients a and b may be approximated as:

$$a = 0.61 \times 1.03\,\varphi, \quad b = 0.29 \times 1.02\,\varphi; \quad \text{and}$$

- (Coon et al., 1984)
$$J = 1 + C_1\frac{H_k^*}{D},$$
(10)

where C_1 is a coefficient dependent on the angle of internal friction φ; for $\varphi = 40°$, $C_1 = 2.42$.

COMPARISON OF LOAD ESTIMATION MODELS

For the sake of comparison, we make a few assumptions. The uniaxial compressive strength of level ice is assumed equal to 2.0 MPa. The thickness of ice around hummocks h_i and the thickness of ice blocks that form these hummocks are also assumed equal to 1.0 m. For these assumptions, the empirical relations due to Surkov (2001) and Surkov et al. (2001, 2002), yield:

the thickness of consolidated layer $h_c = 2h_i = 2$ m,
the sail height $H_s = 4.05\,h_i^{0.5} = 4.05 \times 1.0^{0.5} = 4.05$ m,
the keel draft $H_k = 4.21\,H_s = 4.21 \times 4.05 = 17.01$ m,
the keel thickness $H_k^* = H_k - h_c = 17.01 - 2.0 = 15.01$ m.

The behavior of coefficient J as a function of D/H_k^* determined by equations (8)-(10) is plotted in Fig. 2.
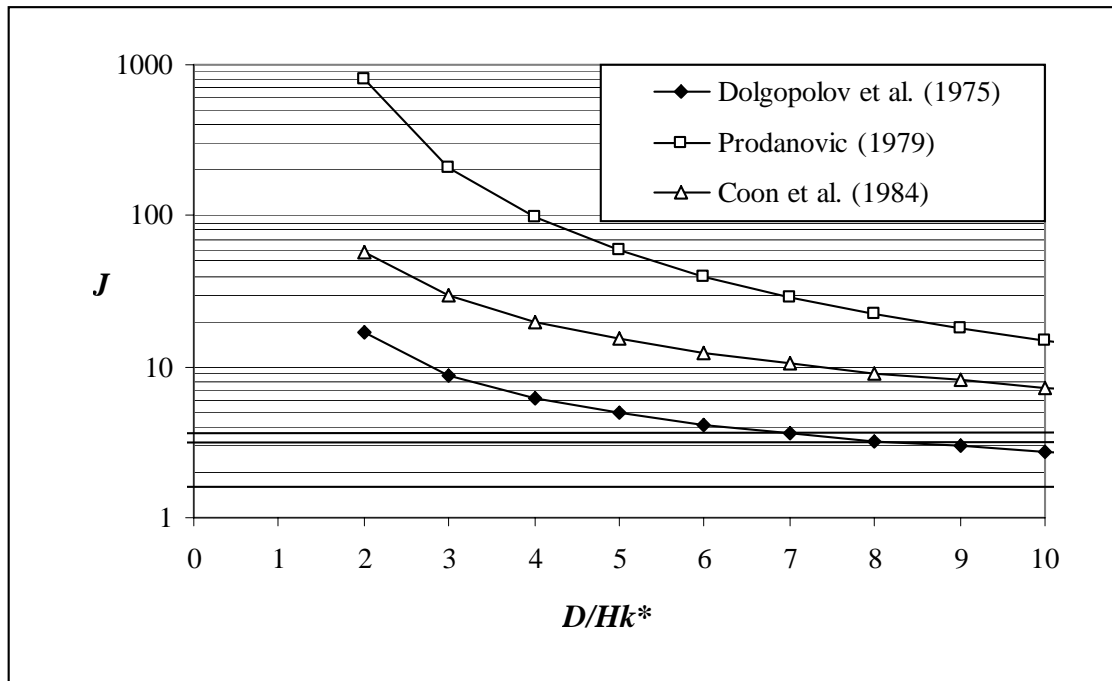

Fig. 2. Indentation coefficient J as a function of D/H_k^*

Analysis of Fig. 2 indicates that the model of Prodanovic (1979) yields unrealistically overestimated values. The model of Coon et al. (1984) also yields overestimated values: for $D/H_k^*=1$, it yields $J = 37.3$. This means that the load due to the hummock keel is 3 to 4 times that due to the consolidated layer, and the ice-ridge load coefficient k_h exceeds 10.

Thus, the more realistic values of J can be obtained with the model of Dolgopolov et al. (1975). An additional point in favor of this model is that it has been built on experimental data.

Now we refer to formula (2) to determine the load exerted by a hummock in the context of different models. We determine the load due to consolidated layer by equation (3), the indentation factor I by formula (5), and that due to the hummock keel by equation (6) with coefficients (8)-(10).

For the sake of comparison, we use the assumption of Maattanen (1983) who demonstrated that

$$F_H = 2.5F_i, \tag{11}$$

where F_i is the load due to level ice surrounding the hummock.

Also, an assumption following from equation (1) may be used, namely,

$$F_H = k_h F_i . \tag{12}$$

Figure 3 shows ice loads on supports of different diameters as calculated by models of different authors.
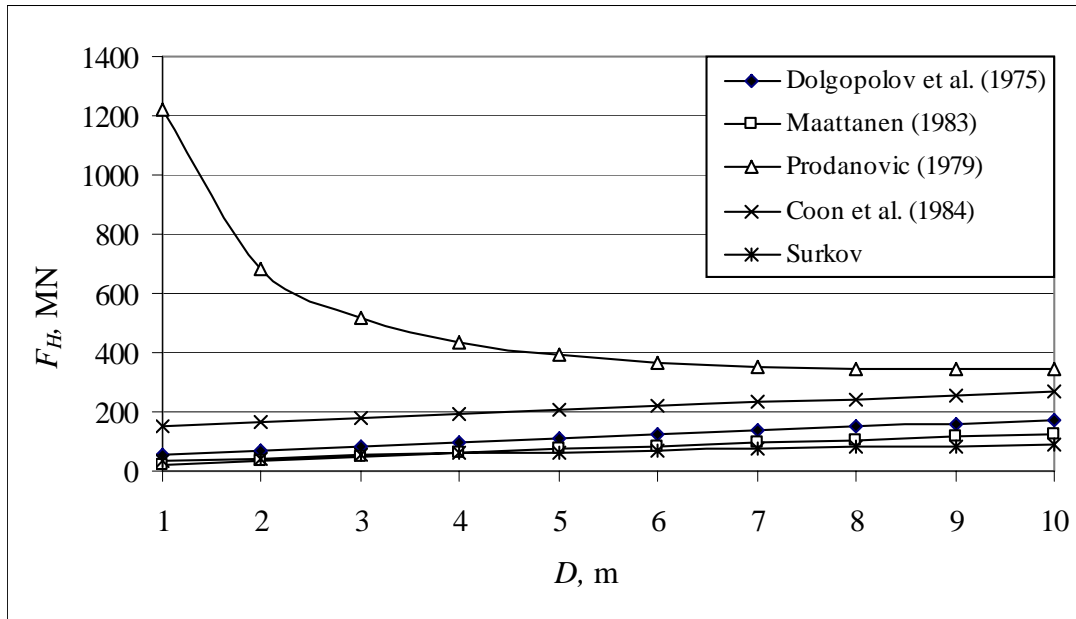

Fig. 3. Load due to ice ridge versus support diameter (for $D \leq 10$ m)

The method of Prodanovic (1979) is seen to produce unrealistic values. The method of Coon et al. (1984) also yields overestimated load values.

The models of Dolgopolov et al. (1975), Maattanen (1984) and equation (12) produce close results with the lowest loads predicted by equation (12).

If we observe that the ice-ridge load coefficient (1) has been derived not only from laboratory experiments but also from field test data, the developed approach to ice-ridge load estimation should be recognized as the one yielding the most realistic (and lowest of all) load estimates.

This approach may be recommended for $D/h_i \leq 10$, because this interval has been tested experimentally. Loads calculated for $D/h_i \leq 100$ are presented in Fig. 4.

In this interval, all theoretical methods give results several times higher than those on the experimental curve. This discrepancy can be attributed to the fact that the theoretical methods are incapable of allowing for the effect of spatial inhomogeneity that comes into play when the size of ice field with embedded ice ridges increases. For wider contacts, the inhomogeneity of hummock keel thickness and its consolidated layer increases. Hummocks begin to act on wider contacts as chains embedded in ice fields rather than as single bodies. Meeting a wide contact structure, such a chain finds the coupling between its links starting to broke and the field of ice ridges splitting into a broken array of hummocks. Nonetheless, recognizing that the interval $D/h_i > 10$ enjoys only one experimental value obtained at the Molikpaq platform, the proposed method should be used with caution in a severe ice environment. However, it suits well for use under moderate ice conditions such as those in the Baltic Sea, Cook Inlet, and Bohai Bay.
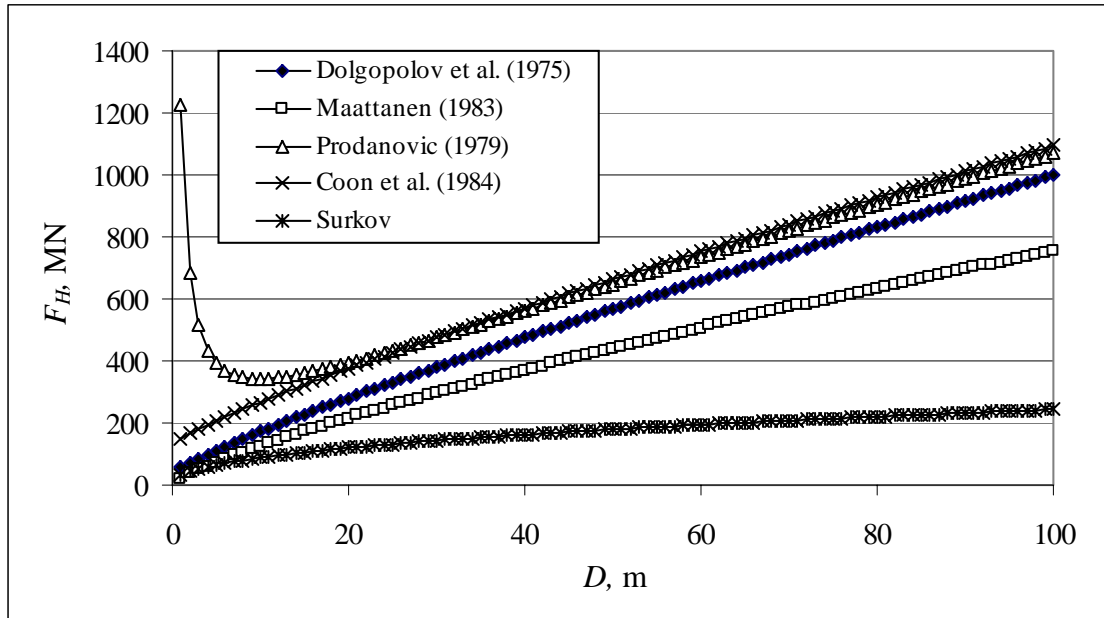

Fig. 4. Load due to ice ridge versus support diameter (for $D \leq 100$ m)

CONCLUSIONS

As has been expected, an ice-ridge-load estimation method, based on the load of level ice and an ice-ridge load coefficient obtained from experimental data, has predicted the least loads of all the known models. For narrow cylindrical supports, it gives loads half as large as those calculated by a classical method of Dolgopolov et al. (1975). Moreover, this deviation considerably increases with support diameter

For wider support structures, this method should be applied with caution, since these supports do not enjoy an adequate experimental database. Nonetheless, the model may be recommended for areas with moderate ice conditions.

REFRENCES

Afanasyev, V.P. Ice loads on offshore vertical support structures. *Cand. Sci. Thesis*, (1972).

Blenkarn, K.A. Measurement and Analysis of Ice forces on Cook Inlet structure. In *Proc. OTC-1261*, Dallas, Texas (1977) 11, 363-378.

Coon, M.D., Evans, R.J., and Gibson, D.H., Failure criteria for sea ice and loads resulting from crushing. In *Proc. of IAHR Ice Symposium*, Hamburg, (1984) V.III, pp. 1-16.

Croasdale, K.R. and Brown, T. Ice load uncertainties – progress in their resolution. In *Proc. of the 10th Int. Offshore and Polar Eng. Conference*, Seattle (2000) V.I., pp. 583-588.

Dolgopolov, Y.V., Afanasev, V.A., Korenkov, V.A., and Panfilov, D.F. Effect of Hummocked Ice on Piers of Marine Hydraulic Structures. In *Proc. IAHR Symposium on Ice*, Hanover, NH, U.S.A. (1975) 469-478.

Fitzpatrick, J., State-of-the Art of Bottom-Founded Arctic Steel Structures. *Canadian Marine Drilling*, Calgary (1994).

Krankkala, T. and Maattanen, M. Methods for Determining Ice Forces Due to First- and Multi-Year Ridge. In *Proc. of IAHR Ice Symposium*, Hamburg, Germany (1984) V.IV, 263-287.

Loset, S., Shkhinek, K., and Uvarova, E. An overview of the influence of structure width and ice thickness on the global ice load. In *Proc. of the POAC Conf.*, Helsinki (1999) V.I., 425-434.

Maattanen, M. Design recommendations for ice effects on aids-navigation, third draft. *IALA Technical Committee to study the effect of ice on lighthouses*, Oulu (1983).

Maattanen, M. Ice force measurements at the Gulf of Bothnia by the instrumented Kemi-I lighthouse. In *Proc. of POAC-77*, Newfoundland (1977) 2, 730-740.

Schwarz, J. The LOLEIF Project. In *Proc. of the International Workshop on Rational Evaluation of Ice Forces on Structures* (REIFS'99), Mombetsu (1999) 51-63.

Surkov, G.A. Loads on Cylindrical Support Structures due to First-Year Hummocks. In *Proc. of the 16th International Conference on Port and Ocean Engineering under Arctic Conditions* (POAC'01), Ottawa (2001) VI, 441-449.

Surkov, G.A. Strength parameters of one-year hummocks. In *Proc. of "On Okhotsk Sea and sea ice and Ice scour and Arctic marine pipeline"*, Mombetsu (2000) 179-187.

Surkov, G.A. Thickness of the consolidated layer in first-year hummocks. In *Proc. of the 16th International Conference on Port and Ocean Engineering under Arctic Conditions* (POAC'01), Ottawa (2001) VI, 245-252.

Surkov, G.A., Truskov, P.A., Zemliuk, S.V., Astafiev, V.N., and Polomoshnov, A.M. Geometry of ice hummock pieces on the north Sakhalin offshore. In *Proc. of the 16th Int. Symp. on "Okhotsk Sea and Sea Ice"*, Mombetsu (2001) 149-152.

Surkov, G.A., Zemlyuk, S.V., Khlebnikov, P.A., and Polomoshnov, A.M. Ratio of First-Year Hummock Sails and Keels. In *Proc. of the 17th Int. Symp. on "Okhotsk Sea and Sea Ice"*, Mombetsu (2002) 350-353.

Timco, G.W., Frederking, R., Kamesaki, K. and Tada, H. Comparison of ice load calculation algorithms for first-year ridges. In *Proc. of the International Workshop on Rational Evaluation of Ice Forces on Structures* (REIFS'99), Mombetsu (1999) 88-102.

Timco, G.W., Wright, B., Johnston, M., and Frederking, R. First-year ice ridge loads on the Molikpaq. In *Proc. of RAO'99 Conference*, St. Petersburg (1999) 172-179.

CASPIAN SEA SPRAYED ICE PROTECTION STRUCTURES

J. Bastian[1], A. G. Strandberg[1], W. P. Graham[1] and D. Mayne[2]

ABSTRACT

Design procedures and construction methods are documented for spray ice operations in the Kashagan Field of the North Caspian Sea. This spray operation was in support of off-shore oil exploration carried out by Agip Kazakhstan North Caspian Operating Company (Agip KCO). The Sunkar drilling barge, Aktote and Kairan Islands were structures in the North Caspian Sea where spray ice was employed. The spray ice was generated on or as an ice protection structure. The spray equipment consisted of pumps that output water in the pressure range of 1 to 2 MPa through a distribution and nozzle system. The aim of the procedure was to throw a water stream through the air such that small water droplets formed and became frozen or almost frozen before the droplet came to rest. The varied winter temperatures for the North Caspian required that the spray system selected be able to operate in an air temperature from -2°C to -25°C. The freezing degree day index for the Kashagan Field area was an important indicator for spray ice operation.

KEY WORDS

Agip KCO, spray ice, Kashagan Field, North Caspian, Sunkar, Aktote, Kairan, ice protection, horizontal ice sheet load, factor of safety, water pressure, water droplets, spray ice mass, air temperature, freezing-degree-day index (FDD).

SPRAY ICE INTRODUCTION

In the late 1970s and early 1980s the use of spray ice became a popular means of constructing grounded ice drilling pads in Alaska and the Canadian north. Oil exploration in the Beaufort Sea and adjacent Prudhoe Bay required large scale gravity structures that could resist the forces of moving ice sheets. The sprayed ice structures proved their merit in terms of ease and economics of construction. After the winter drilling period the ice structures would melt in the warming spring conditions which was a cost effective means of dismantling the island structure with minimal environmental impact.

Panarctic Oils Ltd at Cape Allison, Amoco Production Co. at Mars Island, Chevron USA Inc. at Karluk, Sohio Petroleum Company at Prudhoe Bay, were some of the early pro-

---

[1] Sandwell Engineering Inc., Suite 805, 900-6 Avenue SW, Calgary, Alberta T2P 3K2 Canada
[2] Agip Kazakhstan North Caspian Operating Company N.V. (Agip KCO), Kazakhstan

jects where spray ice was employed on a large scale in the 1980's. These projects form the basis for a number of documents listed in the reference section of this paper (Allyn et al 1989, Bugno et al 1990, Geotech/Golder 1985, Geotech 1988, Ice Construction and Engineering 1989, Masterson et al 1987 and Weaver 1991). The island building projects of this period typically employed in the order of 700,000 m^3 to 1,000,000 m^3 of spray ice.

Into the 1990s and to-date the use of spray ice on projects has continued at a slower but consistent rate, relative to the rapid pace of the 1980s. The Thetis Island, Pioneer Natural Resources project over the 2002/2003 winter period (Masterson et al, IAHR 2004 Symposium) was a recent project where spray ice was employed in a large scale island building effort in the Prudhoe Bay area. The Government of the Northwest Territories of Canada, Department of Transportation, has employed spray ice on the Mackenzie River crossing at Fort Providence since 1989. The Mackenzie River crossing is typically opened a month earlier then usual because of the use of spray ice (Government of the Northwest Territories 1991 and Masterson et al 1997).

In the summer of 2001 Agip KCO retained Sandwell Engineering Inc to design a spray system that could be employed on the drilling structures that were operating in the North Caspian Sea (Sandwell Report, 2001). The Sunkar drilling barge was to be the focus of spray operations over the 2001/2002 and 2002/2003 winter season. The spray equipment was not operational over the 2001/2002 winter season which gave a base case with no spray ice. The 2002/2003 winter season in the North Caspian was unusually cold and resulted in a good test of the spray method in protecting the Sunkar installation. The barge and island facilities at Aktote and Kairan were protected from incoming ice with sprayed berms during the unusually warm 2003/2004 winter season in the Caspian area.

NORTH CASPIAN SPRAY OPERATION SUMMARY

Figure 1 illustrates the Kashagan Field North Caspian Sea area where Agip KCO is conducting offshore oil exploration.

Agip KCO have adopted the use of ice protection system (IPS) barges that are placed around key offshore installations. These IPS barges as illustrated in Figure 2, keep the main ice forces away from an offshore installation and serve to create an inner area of operation where the supply vessels can be sheltered in a safe harbour. The spray plan over the 2001/2002 and 2002/2003 winter season was to have the vertical sided IPS barges loaded with spray ice in order to increase stability.
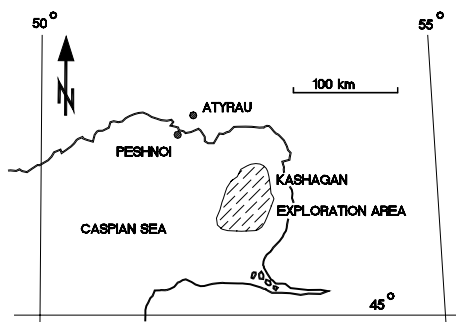

Fig. 1. North Caspian Sea Offshore Oil Exploration

Fig. 2. IPS Barges and Sunkar, Dec. 8, 2002 North Caspian Sea

Over the 2001/2002 winter season spraying was not carried out on the IPS barges.

During the colder winter season of 2002/2003 (FDD index at Sunkar just over 700 degree-days-Figure 15) two of the vertical sided IPS barges that were placed around the Sunkar platform were sprayed with the 1200 m^3/hour VN Pump to increase stability, as illustrated in Figure 3. The VN pump is a fire fighting (FiFi) class pump manufactured by VN-Pumpen Volker Nienstädt GmbH & Co KG. The IPS barges for Sunkar were 98.2 meters long and 12.78 meters wide, with an on-bottom weight in the order of 4,000 to 8,000 tonnes. If 2,000 tonnes of ice was sprayed onto a barge the factor of safety against sliding would be increased by approximately 25%.

The spray ice on the barge of Figure 3 will be present for the entire winter season and in the spring will melt away to allow the barge to be floated away to a new location. The ice on the Sheat IPS barge of Figure 3 was removed in a 2 day period during the first week of April 2003 through the use of a water cannon, as illustrated in Figure 4. This allowed the ship crews to move the IPS barge from the Sunkar location to another location at an early date. The same VN pump that was employed to produce the spray load was employed to cut the spray ice away.

Fig. 3. The Sheat IPS Barge with Sprayed Ice in place, December 2002

Fig. 4. Water Cannon Removing the Spray Ice from the IPS Barge, April 3, 2003

During the warmer 2003/2004 winter season (FDD Index less than 300 degree-days) an Areco fan was employed to produce an ice mass in front of the fuel tanks at Aktote Island to ensure that the ice sheet did not top the island west wall. The Areco fan and created spray ice are illustrated in Figures 5 and 6.

Fig. 5. Areco Fan Spray Material from West Side Aktote Island, December 24, 2003

Fig. 6. Fuel Tank Spray Ice Protection Mound West Side Aktote Island, Jan. 8, 2004

60

CASPIAN SEA WEATHER PATTERNS

Sunkar weather data from the North Caspian Sea winter seasons prior to the 2001 summer season was available for spray planning purposes. The air temperature data is important to a spray program as the type of spray equipment selected will vary with the expected temperature range. Wind direction is also important as spraying is generally carried out in a downwind direction. Figures 7 and 8 depict weather data from the winter seasons prior to 2001 in the Kashagan Field, North Caspian Sea.
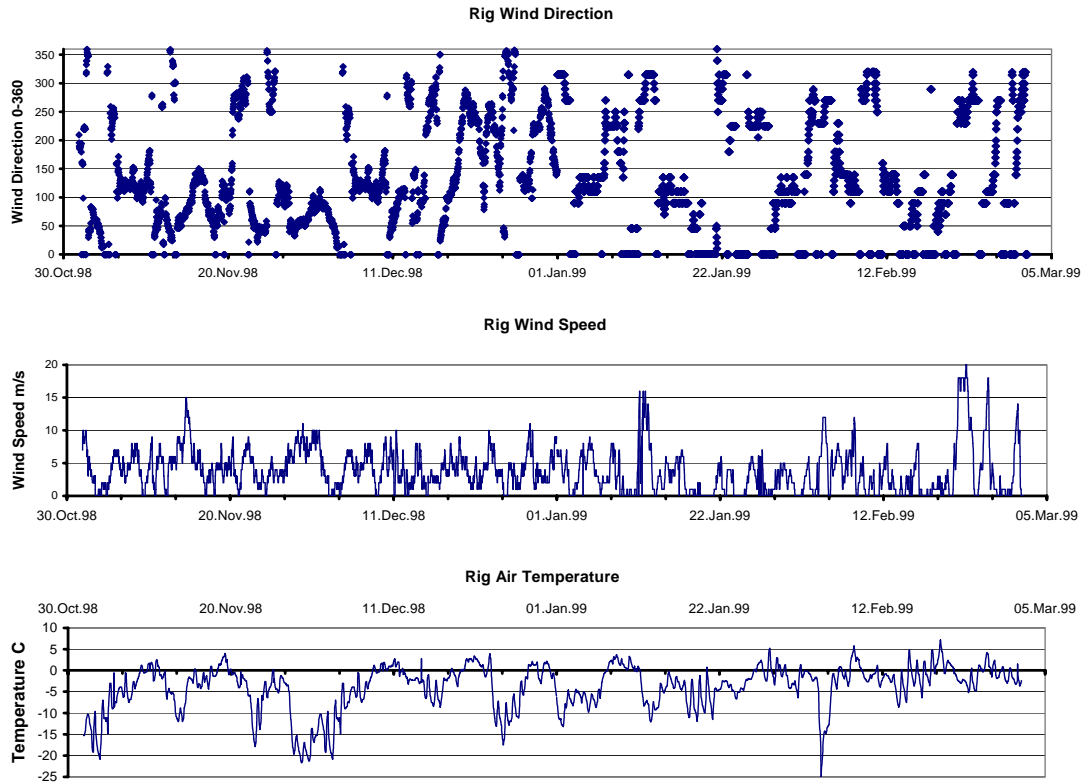

Fig. 7. Weather Data Sunkar location, North Caspian Sea, Winter 1998/1999

The FDD index is defined as $FDD = \text{ABS}(\text{sum } fdd)$ (freezing-degree-days is the sum (absolute) of 0°C minus the daily mean temperature). The FDD index is a measure of the freezing index which relates to spray operation since the spray freezing mechanism is heat/cold transfer as a water droplet is projected through the air. Table 1 summarizes the FDD index for the two winter season data set of Figures 7 and 8.

Table 1. FDD Index for the Weather Data
Sunkar location, North Caspian Sea

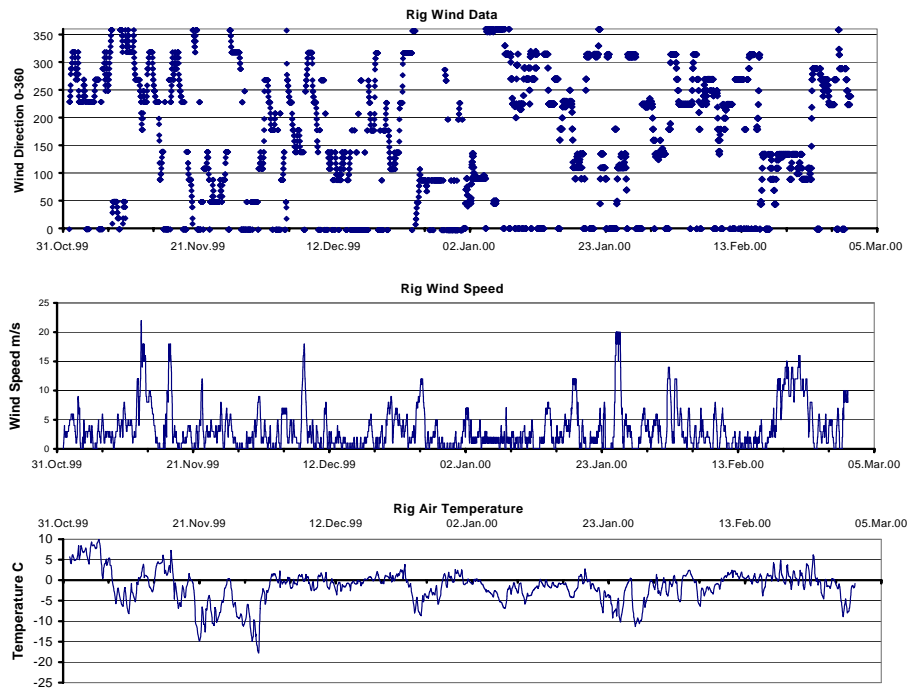| Year	1998/1999	1999/2000
FDD Index °C day	413	222
Peshnoi (Figure 9)	487	259

61

Fig. 8. Weather Data Sunkar location North Caspian Sea, Winter 1999/2000

Figure 9 illustrates the historic FDD index from 1900 recorded at Peshnoi and Atyrau.(Evers et al, 2001) Peshnoi and Atyrau are located where the Ural River reaches the Caspian Sea as illustrated in Figure 1. Figure 9 illustrates that the FDD index for Peshnoi and Atyrau is in close agreement. Historic Caspian Sea offshore weather data is not available, since offshore weather stations did not exist prior to the oil exploration of the late 1990s. The Peshnoi/Atyrau weather stations typically have a FDD index approximately 100 °C days colder than the weather data from the North Caspian Sea Kashagan Field area. The Kashagan Field 1998/1999 winter season at 413 °C days (FDD index) represents an average winter season with respect to 1990's weather data while the 222 °C days (FDD index) recorded for 1999/200 represented a warmer than usual winter.
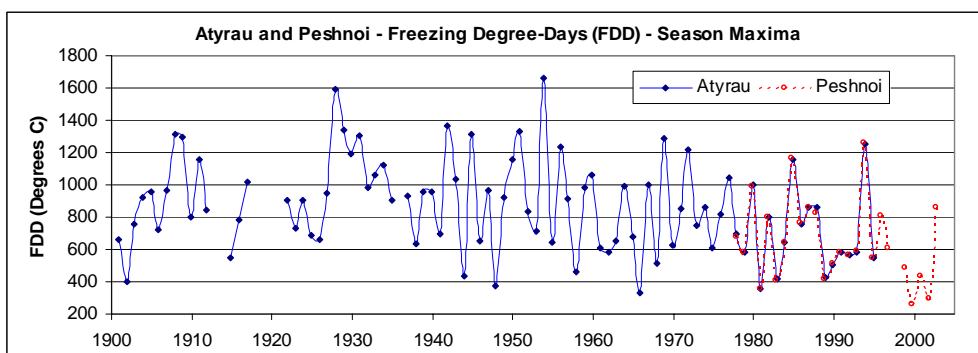

Fig. 9. Freezing Degree-Days Peshnoi North Caspian Sea, 1900-2003

SPRAY EQUIPMENT

With the weather patterns observed from the historic Peshnoi data and 1998/1999 and 1999/2000 winter seasons at Sunkar on location in the Kashagan Field, Sandwell recommended spray equipment as follows.

When the air temperatures were colder than -10°C, a 1200 m^3 per hour VN water cannon/pump was recommended to create the required ice mass needed to stabilize the IPS barges. Since the tonnage required was in the order of a few thousand tonnes such a pump could complete the job in less than a day or two, when the weather became sufficiently cold. The VN pump unit employed at the Sunkar site is illustrated in Figure 10.

For air temperatures between 0 and -10°C, an Areco fan system with a capacity of 40 t /hr. was recommended. The fan equipment, while having low production rates, can achieve the tonnage production goals of a few thousand tonnes since the majority of the expected air temperatures were in the 0 and -10°C range. This system was employed at Aktote to spray the material illustrated in Figures 5 and 6 during the 2003/2004 winter season. The 2003/2004 season was unusually warm with air temperatures rarely, if at all, falling below -10°C in the Kashagan Field area.

As a third option, a smaller scale Waterous, Figure 11, cannon/pump with output of 60 tonnes water per hour was recommended for the Kairan site over the 2003/2004 winter season to protect the fuel tanks. The lower pumping rate of this unit allowed the water cannon spraying to be conducted at temperatures as high as -6°C where reasonable material freezing occurred.

Fig. 10. VN 1200 m^3/hour Pump employed in the Agip KCO Spray Program, Caspian Sea

Fig. 11. Waterous 60 m^3/hour Pump

SPRAY OPERATION AT SUNKAR, WINTER 2002/2003

Table 2 summarizes ice material production on the IPS barges Sheat and the Rystar at Sunkar during December 2002. Due to the unusually cold weather during the month of December 2002 only the 1200 m^3 per hour VN pump was needed to complete the required spray ice production on the IPS barges Sheat and Rystar. Table 2 also summarizes the spraying that was completed on the rubble field behind the IPS barges. This was done to give an added degree of stability to the rubble field and IPS barge mass combination.

The material production onto the Sheat and Rystar barges in terms of tonnage is summarized in Table 3. The material production of Table 3 indicates the fraction of the water pumped that came to rest as ice and remained on the Sheat and Rystar barge top side. The remaining material either came to rest on the adjacent rubble field or ran off as water or sloughed back into the Caspian Sea. Note that the top side dimension of the Sheat and Rystar is 98.2m long by 12.78m wide. Table 4 summarizes the spray operation of the 1200 m^3 pump at the Sunkar location in December 2002.

Table 2. Sunkar Spray Operation Summary, December 2002

DATE	TEMP. Deg. C	L. SHEAT (NE IRG) DAILY PUMP Hrs	TOTAL PUMP Hrs	TOTAL BUILD-UP % / M	RUBBLE NE of SHEAT DAILY PUMP Hrs	TOTAL PUMP Hrs	DAILY BUILD-UP	L. RYTSAR (SE IRG) DAILY PUMP Hrs	TOTAL PUMP Hrs	TOTAL BUILD-UP % / M	RUBBLE SE of RYTSAR DAILY PUMP Hrs	TOTAL PUMP Hrs	DAILY BUILD-UP
13-Dec-02	-12	0	0	0	0	0	0	1	1	65% .3m	0	0	0
14-Dec-02	-4	0.5	0.5	0		0			1			0	
15-Dec-02			0.5			0			1			0	
16-Dec-02	-13.3	4	4.5	60%1.3m		0			1			0	
17-Dec-02	-17.5	14.5	19	75% 2.3m		0		7	8	35%1m		0	
18-Dec-02	-16.7	9	28	100% 2m		0			8			0	
19-Dec-02	-15.7	2	30	100%4m		0			8	35%1m		0	
20-Dec-02	-14.5	9	39	100%5.5m		0			8			0	
21-Dec-02			39			0			8			0	
22-Dec-02			39			0			8			0	
23-Dec-02	-10.2		39	100%4.4m		0		4.5	12.5	100%1m		0	
24-Dec-02			39	COMPLETE		0			12.5			0	
25-Dec-02			39			0			12.5			0	
26-Dec-02			39			0		14.4	26.9	100%4.8M		0	
27-Dec-02			39			0			26.9	COMPLETE		0	
28-Dec-02	-17.5		39		2	2			26.9		6	6	.5M
29-Dec-02			39			2			26.9			6	
30-Dec-02			39			2			26.9			6	
31-Dec-02			39			2			26.9			6	
1-Jan-03			39			2			26.9			6	
2-Jan-03	-9		39	100%4.2M	8.2	10.2	.5 TO 1.5M		26.9			6	
3-Jan-03			39			10.2			26.9			6	
4-Jan-03			39			10.2			26.9			6	
5-Jan-03			39			10.2			26.9			6	
6-Jan-03			39			10.2			26.9			6	
7-Jan-03			39			10.2			26.9			6	
8-Jan-03			39			10.2			26.9			6	
9-Jan-03			39			10.2			26.9			6	
10-Jan-03			39			10.2			26.9			6	
11-Jan-03			39			10.2			26.9			6	
12-Jan-03			39			10.2			26.9			6	
13-Jan-03			39			10.2			26.9			6	
14-Jan-03			39			10.2			26.9			6	
15-Jan-03			39			10.2			26.9			6	
TOTALS			39	100%4.2M		10.2			26.9	100%4.8M		6	

Average ice thickness measurements verified via total station by Ice Advisor Rig 257

All thicknesses are visual estmates except those in red.

Please note: while spraying IRGs, rubble was also being sprayed.

Table 3. Material Production on the Rystar and Sheat Barges, December 2002

Barge	Hours pumped	Height of material (m)	Produced on the IPS m^3	Produced on the IPS (tonnes)	Water pumped (tonnes)	Percent on the IPS
Sheat	39	4.2	5271	2899	46,800	6.2
Rystar	26.9	4.8	6024	3313	32,280	10.3

Table 4. Spray Summary for the 1200 m^3 VN Pumping Unit

Temperature	Observations
-4.0°C to -10°C	Little to minimum ice content in spray, large amount of "run-off". Pooling of water in and around target area. -10°C recommended minimum temperature for ice production.
-10°C to -15°C	Reasonable ice content, slow build-up, some "run-off observed, "sloughing off" occurring, monitor adjustment approximately every 4 hrs.
-15°C to -22°C	Stiff to firm ice production, little "run-off" observed, rapid build-up, "ice fog" thicker as temperature drops. Little monitor adjustment required.

WEATHER AT SUNKAR 2002/2003 WINTER SEASON

The hourly recorded temperatures for the 2002/2003 winter season at Sunkar are illustrated in Figure 12. The entire winter season is considered in order to allow the severity of the 2002/2003 winter season to be assessed. Figure 13 illustrates the FDD index for the Peshnoi weather station, the Sunkar location KEF over the 2002/2003 winter season and for the KE 4 island located to the east of the Sunkar site. The FDD index of Figure 13 is calculated from a daily average temperature taken as the average of the daily maximum and daily minimum. Figure 13 gives a cumulative seasonal FDD index of 741 °C days for the KEF Sunkar site.
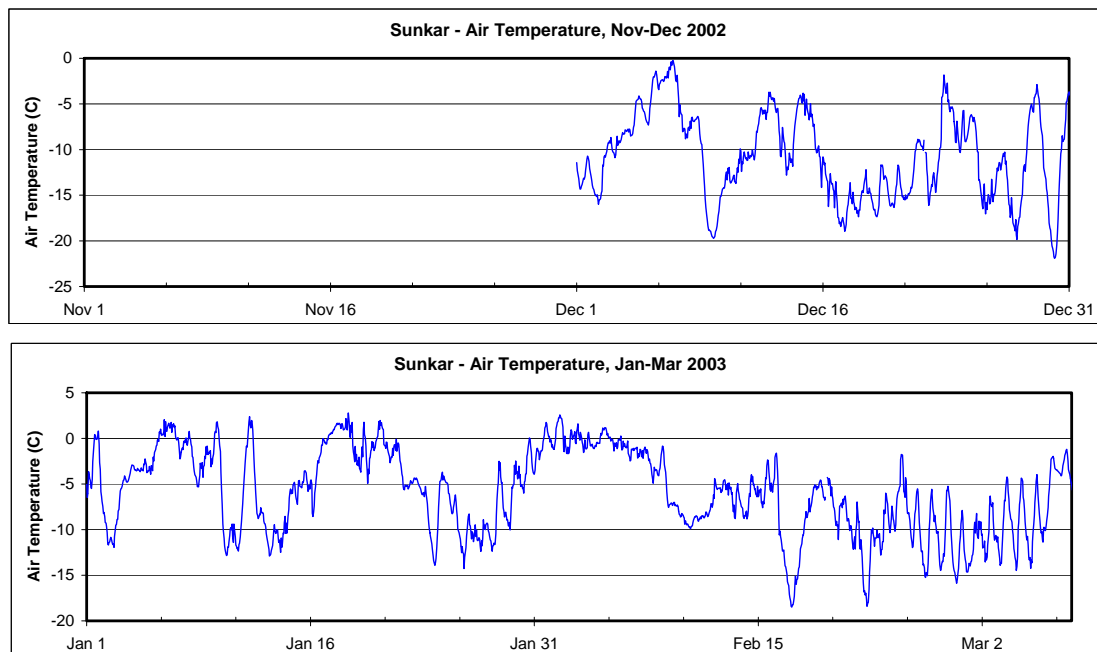

Fig. 12. Hourly Recorded Temperatures, Sunkar, Winter 2002/2003

Figure 13 illustrates the difference in FDD nearshore to offshore in the North Caspian. The nearshore temperatures represented by the Peshnoi data gave a FDD index that was 116 °C days greater than the offshore Sunkar location. This is an important observation for pipeline installation spraying operation through the near shore area.
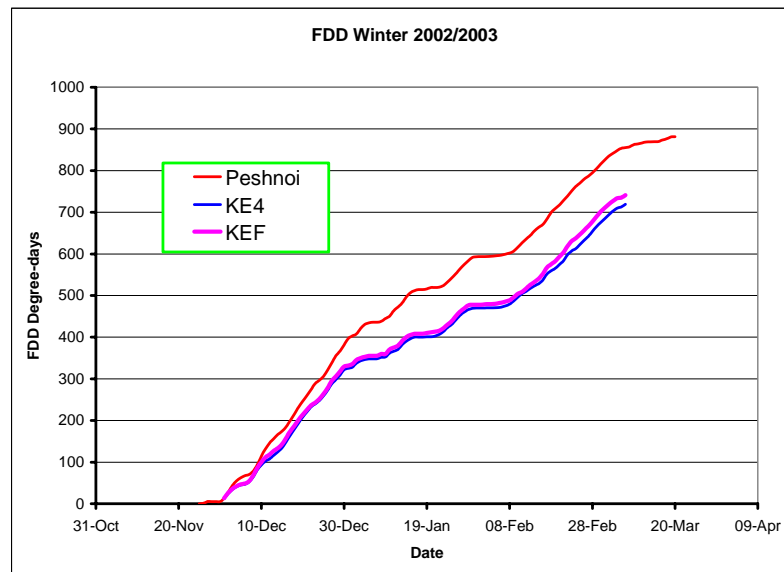

Fig. 13. FDD Index Winter 2002/2003 North Caspian Sea

NORTH CASPIAN SEA SPRAY ICE CONCLUSIONS

Conclusions that can be made with respect to spraying in the North Caspian are as follows.

• During a cold winter season in the North Caspian with an FDD index in the order of 400 to 1000 °C days spraying is practical with large capacity pump units that would output water in the order of 1200 tonnes per hour. It is during these colder winter seasons that the most spray ice would be required since greater lateral ice forces would be generated by the thicker ice sheet that would result from the colder weather. IPS barges can be loaded with several thousand tonnes of ice in 1-2 days with such a pump when a period of -10 °C to -20 °C air temperature is encountered. Smaller scale water cannon sprayers such as the Waterous pump operating at 60 tonnes per hour can create spray material in the temperature range -6 °C to -20 °C.

• When a warm winter is encountered with a FDD index less than approximately 300 °C days an Areco fan sprayer can be employed to produce in the order of 40 tonnes of spray ice material per hour. The Areco fan sprayers work well in air temperatures from -2 °C to -10 °C and colder if need be.

REFERENCES

Allyn, N., and Masterson, D.M., Spray Ice Island Construction and Simulation. *Proceedings, Offshore Mechanics and Arctic Engineering (OMAE 89)*, The Hague, 1989.

Bugno, W., Masterson, D., Kenny, J., Gamble, R., Karluk Ice Island. *Proceedings of The Ninth International Conference of Offshore Mechanics and Arctic Engineering,* Book No. 10296F, 1990.

Collins, J. and Masterson, D., The State of the Art in Snowmaking and its Application to Arctic Construction. *Proceedings Offshore Mechanics and Arctic Engineering (OMAE 89),* The Hague 1989.

Croasdale, K. and Metge, M. Sunkar Protection-Ice Load and Barge/Spray Ice Requirements. *Preliminary Report to Offshore Kazakhstan International Operating   Company*, July 2001.

Evers, K., Spring, W., Foulkes, J., Kuehnlein, W. and Jochmann, P. Ice Model Testing of an Exploration Platform for Shallow Waters in the North Caspian Sea. *Proceedings of the 16th International Conference on Port and Ocean Engineering under Arctic Conditions* (POAC 2001), August 12-17, 2001.

Geotech/Golder Associates (1985), *Report on Construction, Testing & Monitoring of Sohio et al Spray Ice Island*, Prudhoe Bay, Alaska, September, 1985.

Geotech (1988), Chevron Karluk Ice Island – Design Basis, November 1988.

Goff, R.D. and Masterson, D.M., Construction of a Sprayed Ice Island for Exploration, *Offshore Mechanics and Arctic Engineering (OMAE 86)*, Tokyo, Japan,April 13-17, 1986.

Government of the Northwest Territories, Department of Transportation, Highways Operations Division, Fort Providence Ice Crossing 1990/91 Construction Report, 1991.

Ice Construction and Engineering (Catco and Sandwell Swan Wooster Inc. Partnership) Chevron Karluk Ice Island, *Project report to Chevron USA Inc.* 1989.

Masterson, D.M., A Critical Barrier in the Construction of Spray Ice Islands, *Proceedings of CSME Mechanical Engineering Forum 1990*, University of Toronto Campus, Vol. II, June 3-9, 1990.

Masterson, D.M. (1992), Ambient Temperature Effects on Spray Ice Island Construction Using Saline (Sea) and Fresh Water, *Offshore Mechanics and Arctic Engineering (OMAE 92)*, Calgary, Alberta, Canada, 1992.

Masterson, D.M., Baudais, D.J., Pare, A. and Bourns, M. Drilling of a Well From a Sprayed Floating Ice Platform – Cape Allison C-47. *Offshore Mechanics and Arctic Engineering (OMAE 87)*, Houston, Texas, Paper No. 162 1987.

Masterson, D.M., W.P. Graham, S.J. Jones, G.R. Childs, A comparison of uniaxial and borehole jack tests at Fort Providence ice crossing, 1995, *Canadian Geotechnical Journal* 34: 471-475 (1997).

Masterson, D.M., R. Cooper, P.A. Spencer, W.P. Graham, Thetis Spray/Chip Ice Islands for Harrison Bay, Alaska *IAHR 04 Symposium*, St. Petersburg, Russia, 2004.

Sandwell Engineering Inc. Caspian Sea Sunkar Protection-Barge Spray Ice Requirements, *Report to K. R. Croasdale* & Associates Ltd., 18 September 2001.

Spencer, P.A., Smith, T.R. and Masterson, D.M., On the Creep Properties of Field-Retrieved Sprayed Ice, *Proceedings, POAC`87*, August, Fairbanks, Alaska 1987.

Weaver, J.S. Investigation of Spray Ice Spraying Techniques. *Report to Esso Resources Canada Ltd., Research Centre, ERCL.* RS.88.12, October 1991.

PROBABILISTIC ANALYSIS OF SEASONAL ICE LOADS ON THE MOLIKPAQ

G.W. Timco[1] and R. Frederking[1]

ABSTRACT

A probabilistic analysis is made to predict the seasonal evolution of first-year ice loads on the Molikpaq offshore structure throughout a winter in the Canadian Beaufort Sea. The analysis is based solely on the failure modes of the ice, the ice thickness, and the number of weekly ice loading events. The paper illustrates the use of the probabilistic approach using these basic input values. The results of the analysis show good agreement with the measured ice loads on the Molikpaq in the Beaufort Sea.

INTRODUCTION

An offshore structure placed in ice-covered waters experiences loading due to the ice. Observations from structures in the Beaufort Sea and Sea of Okhotsk have clearly shown that the ice can fail in a variety of modes during its interaction with the offshore structure. Recently, Timco and Johnston (2004) have shown that the global loads on offshore caisson structures reflect the failure mode of the ice. The analysis showed quantitatively that for level first-year ice, the ice loads dramatically increased as the failure mode changed from flexure, to mixed-mode, to crushing. The question is: "Is it possible to use this information to predict the global loads on an offshore structure throughout a winter season?". This paper explores this question.

A previous study by Wright and Timco (1994) has characterized the failure mode behaviour at the Molikpaq caisson (Figure 1) during its deployment at the Amauligak I-65 site. With this information and information on the ice thickness throughout the winter, a simple probabilistic model will be developed to predict weekly ice loads. Probabilistic analysis has traditionally been focused on defining the maximum annual load at some level, say at the 10^{-4} exceedance level, for design. While the maximum annual load is needed for design, information on the likely maximum weekly load has operational applications. The present paper introduces a new factor, failure mode, to probabilistic analysis of ice loads and as well presents the seasonal evolution of ice loads.

---

[1] Canadian Hydraulics Centre, National Research Council Canada, Ottawa, Ont. K1A 0R6 Canada

Fig.1. Photograph showing the Molikpaq in the Canadian Beaufort Sea

BACKGROUND INFORMATION

Defining Equations

Timco and Johnston (2004) provided information on over 170 ice load events on three caisson structures (Molikpaq, SSDC, Tarsiut caissons) that were used for exploratory drilling in the Canadian Beaufort Sea. The paper provides complete details of the ice loading events. Timco and Johnston showed that the ice loads could be directly related to the failure mode of the ice. They proposed the following equation for predicting global ice loads:

$$L_{gl} = T_{fm}\, w\, h,\qquad(1)$$

where the L_{gl} is the global load (in MN) on the structure, w is the width (in m) of the structure and h is the ice thickness (in m). T_{fm} is a failure-mode parameter with the following values:

T_{fm} = 1.09 MN/m^2 for ice crushing

$\quad$ = 0.83 MN/m^2 for long-term creep (i.e. thermally-induced creep)

$\quad$ = 0.63 MN/m^2 for mixed-mode failure

$\quad$ = 0.18 MN/m^2 for flexure failures.

This equation and these values for T_{fm} represent data on a <u>wide</u> caisson structure subjected to ice loading. This equation can be used in this analysis if information is known of the failure mode pattern at an offshore site. This information is known for one site in the Beaufort Sea. Also, the ice thickness at the site throughout the winter is required.

Failure Modes on the Molikpaq

The Molikpaq structure (Figure 1) was developed by Gulf Canada Resources Ltd. and operated by Beaudril, a subsidiary of Gulf. It is a Mobile Arctic Caisson (MAC) which was deployed in the Canadian Beaufort Sea in 1984 and used for exploration drilling for four winter seasons in the Canadian Arctic. It consists of a continuous steel annulus on which sits a self-contained deck structure. The core of the annulus was filled with sand, which provided over 80 percent of the horizontal resistance. The outer face of the

69

Molikpaq was designed for extreme ice features. The structure was extensively instrumented to monitor both ice loads and structural response.

Wright and Timco (1994) provided information on the observed failure mode of first-year sea ice as it interacted with the Molikpaq at the Amauligak I-65 site in the winter of 1985/86. The ice at this site was very dynamic since it was in the shear zone region in the Canadian Beaufort Sea. Figure 2 shows a pie chart of the ice behaviour and associated failure modes (modified from Wright and Timco, 1994). This figure is based on a review of over 6000 hours of video recordings.

The observed ice behaviour has been categorized according to the failure modes presented in Equation (1):

- 55% of the time the structure experienced no load (open water or no ice movement)
- 31% of the time the ice failed in a mixed mode (mixed mode, miscellaneous, sliding/glancing, isolated floes)
- 9% of the time the ice failed in creep
- 4% of the time the ice failed in flexure (ice/rubble interaction)
- 1% of the time the ice failed in crushing.

These values will be used in the present analysis. It is very important to understand that this failure mode pattern is not representative for all offshore structure sites. Figure 2 is, in fact, unique to the Molikpaq at the Amauligak I-65 site for the winter of 1985/86. This must be considered if the proposed probabilistic approach is used at other offshore regions and sites.
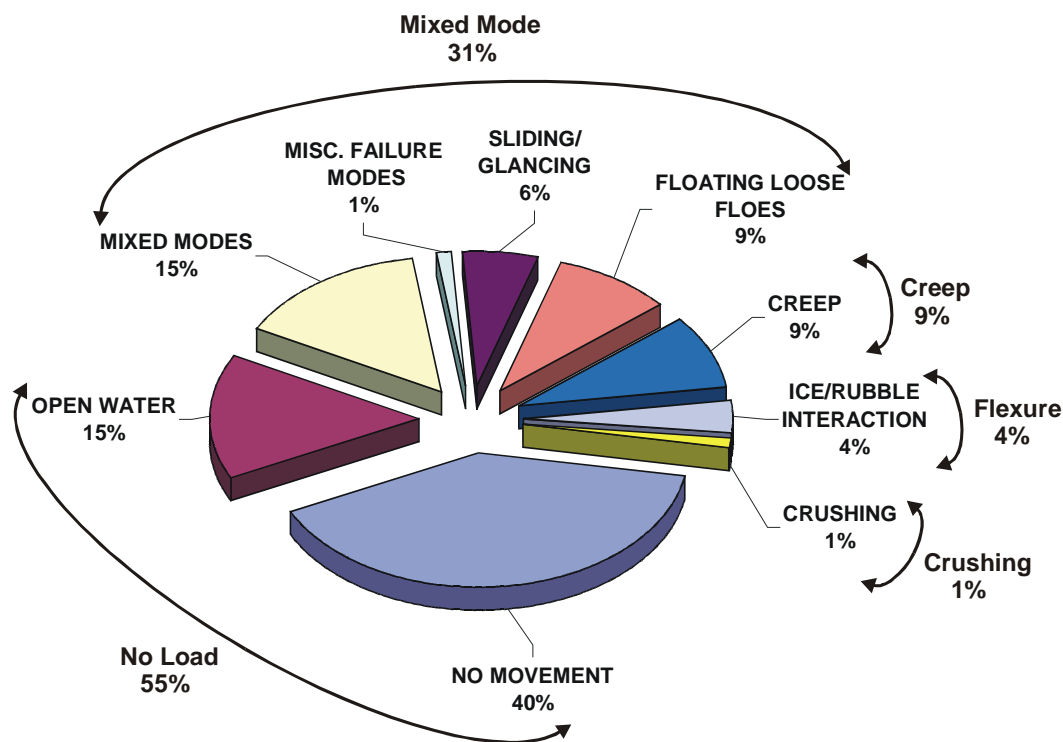
Fig. 2. Pie chart illustration of the ice failure modes observed on the Molikpaq at the Amauligak I-65 site (modified from Wright and Timco, 1994). The failure patterns have been mapped to those identified in Equation (1)

Ice Thickness

Knowledge of the ice thickness is required for Equation (1). The thickness of the ice interacting with the structure can vary considerably throughout the year with typically

thinner ice in the autumn and thicker ice later in the winter season. Recorded observations and ice maps from the Molikpaq showed a wide variability in the ice thickness. For the present analysis, a simplified approach is adopted. Information on landfast sea ice thickness for the Beaufort Sea is shown in Figure 3 for a cold winter, an average winter and a mild winter. The plot shows the ice growing throughout the winter and a gradual decrease in thickness in the late spring and early summer season. Given the dynamic nature of ice in the Beaufort, a random pick of thickness within a range is reasonable since it is possible for older (thicker) or newer (thinner) ice to move past the structure. In actual fact, ice thickness in the drifting pack ice is likely to be even more variable, ranging from only a few cm for newly formed ice to more than 5 m for multi-year ice floes. Note that in this analysis, only first-year level ice is considered in determining the loads on the structure.

Exposure

The amount of ice interacting with the structure will determine the number of ice loading events that will take place. This is a key part of any probabilistic model. Since this type of information is not available in the open literature, a simplified approach is used in this analysis. Wright et al. (1986) have provided information on the global ice loads on the Molikpaq at the Tarsiut P-45 site during the winter of 1984/85 (see Figure 4). This site is in less severe ice conditions than the Amauligak I-65 site. To gain an initial estimate of the number of weekly events, the figure by Wright et al. was digitized to extract the ice loading events from first-year ice. Using this simple approach indicated that on average, there were 18 loading events per week, with a standard deviation of 12 events. Thus, for this analysis, a random number of events between 0 and 30 were chosen for each week. In reality, the actual number of weekly events is quite variable and is related to ice concentration and the amount of ice drift past the structure. The amount and direction of drift in turn is dependent on major weather patterns that provide the driving force for ice movements. In future development of the model, a link between weather patterns, drift and number of events will be incorporated.
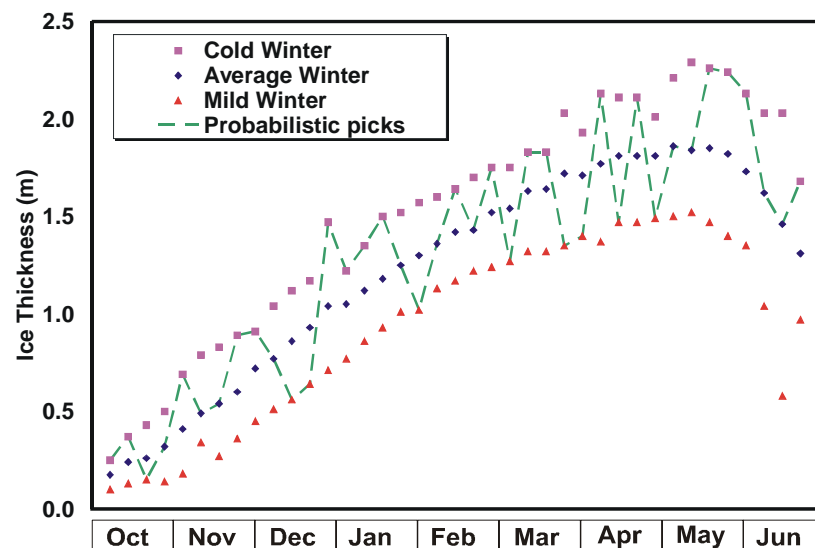

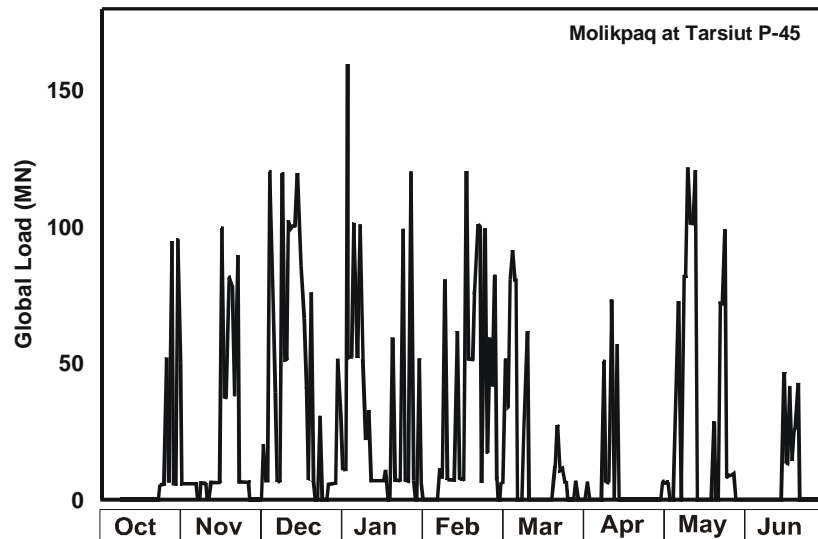Fig. 3. Ice thickness throughout a winter in the Beaufort Sea showing a cold, average and mild winter

Fig. 4. Global first-year ice loads on the Molikpaq at the Tarsiut P-45 site during the winter of 1984/85 (after Wright et al. 1986)

PROBABILISTIC APPROACH

A very simple probabilistic approach was developed to predict the ice loads on the Molikpaq throughout the winter. It was assumed that the **failure mode pattern** for the ice behaved throughout the year as shown in Figure 2. This implies that the failure mode pattern is independent of the ice thickness and ice speed. Since there is little quantitative information in the literature on thickness and speed effects on failure modes, this simple assumption was made here. However, the dependence of failure mode on thickness and speed will be the subject of future investigations. In this analysis, only first-year level ice is considered. A more comprehensive analysis would also include ridges, rubble fields and different ice types.

The steps for performing the probabilistic analysis for each week are shown schematically in Figure 5 and are discussed below. Note that the steps shown in this figure represent just one winter. In a full probabilistic model, many "winters" have to be simulated in order to predict load at the 10^{-4} or whatever exceedance level is desired.

1. The **ice thickness** was chosen by a random number generator to give three possible values for the week - a cold winter (upper curve in Figure 3), and average winter (middle curve in Figure 3) or a mild winter (lower curve in Figure 3). The distribution of the three values was uniform. The values that were selected using the random number generator for the one winter simulated are shown in Figure 3. In further development of the model it is envisioned that other distributions of weekly ice thickness will be developed. In actual practice, past records of ice conditions at the specific (drill) site could be used as an input into the model.

2. The **number of events** in a week was selected such that they could vary between zero and thirty. The choice was again based on a random number generation and selected from a uniform (linear) distribution.

3. For each event in the total selected for that week, the **failure mode** was chosen based on the probability of occurrence shown in Figure 2. The **ice load** was calcu-

72

lated for each failure mode using Equation (1) with the appropriate failure mode co-efficient (T_{fm}).

4. The **highest value** of the calculated ice loads for the week was selected and used in the analysis.

The highest calculated ice load for each week is plotted in Figure 6 for one winter of simulation. It can be seen that there is a general increase in the weekly loads. This is a reflection of the ice thickness increase over the winter. Also, due to the random pick of the number of events there were four weeks for which there were no events, and hence a zero weekly load. Similar behaviour was observed in the original Tarsiut P-45 data, where there were also weeks in which there was no ice movement or open water around the structure, and hence, no ice loads during that week.

A comparison between the loads measured on the Molikpaq and those simulated for one winter is shown in Figure 7. The deterministic value of the global load based on the Korzhavin (1971) equation is also included on the figure. This was calculated using a compressive strength of 3 MPa, which corresponds to an indentation rate of 0.1 m/s, a contact factor of 0.6, structure width of 90 m, and the average ice thickness. It can be seen that the Korzhavin equation predicts significantly higher loads than the probabilistic simulation and the measured loads, except in the early winter when measured loads exceeded the Korzhavin prediction.
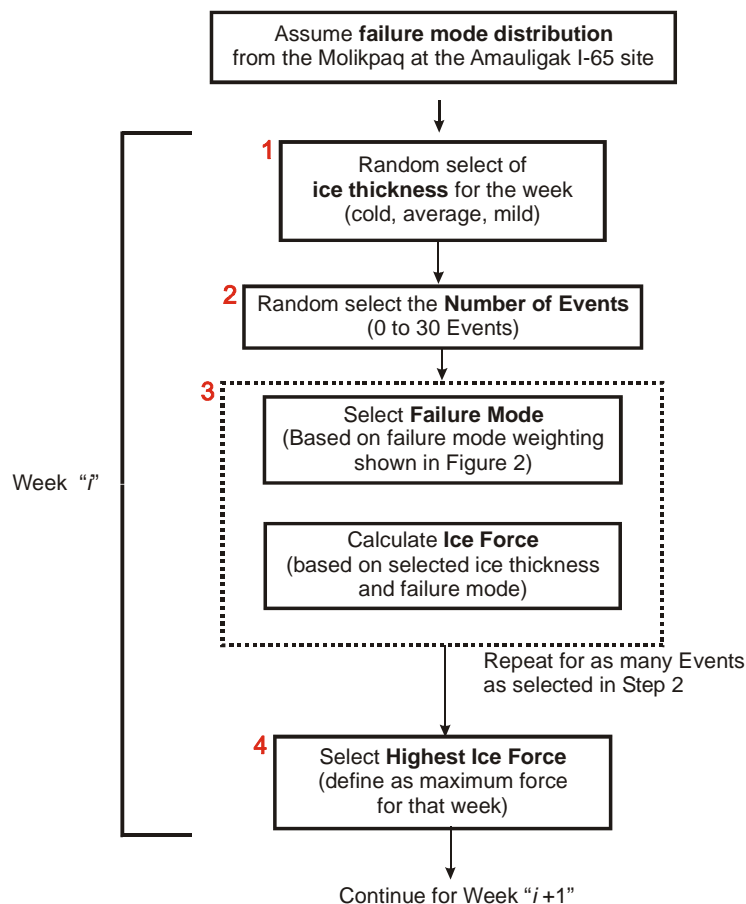
Fig. 5. Schematic illustration of the method used for the probabilistic analysis

Figure 7 shows that the load values determined from the probabilistic simulation are generally comparable with those measured on the Molikpaq at the Tarsiut P-45 site. They show weekly fluctuations in a manner similar to that observed on the structure. The present approach provides a much more realistic estimate of the loads on the structure than the Korzhavin deterministic approach.
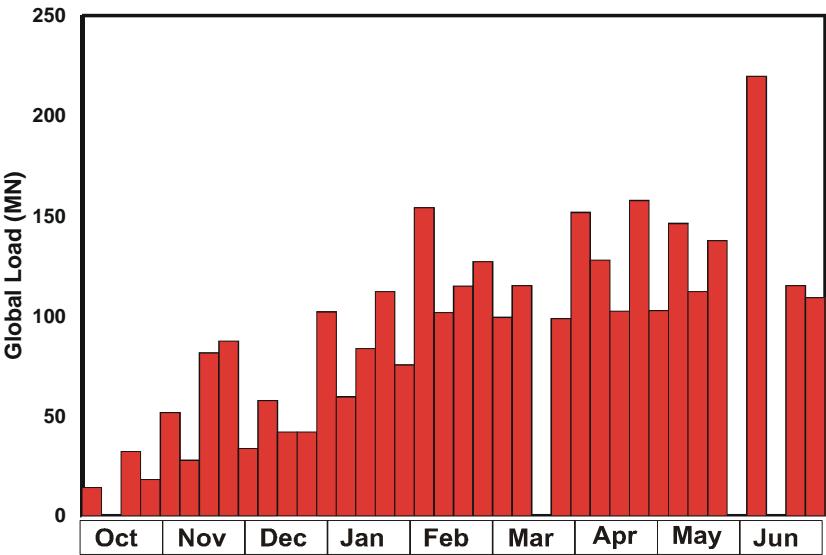

Fig. 6. Global Loads throughout the winter based on the probabilistic analysis. These represent the maximum load for each week based on the approach outlined in Figure 5
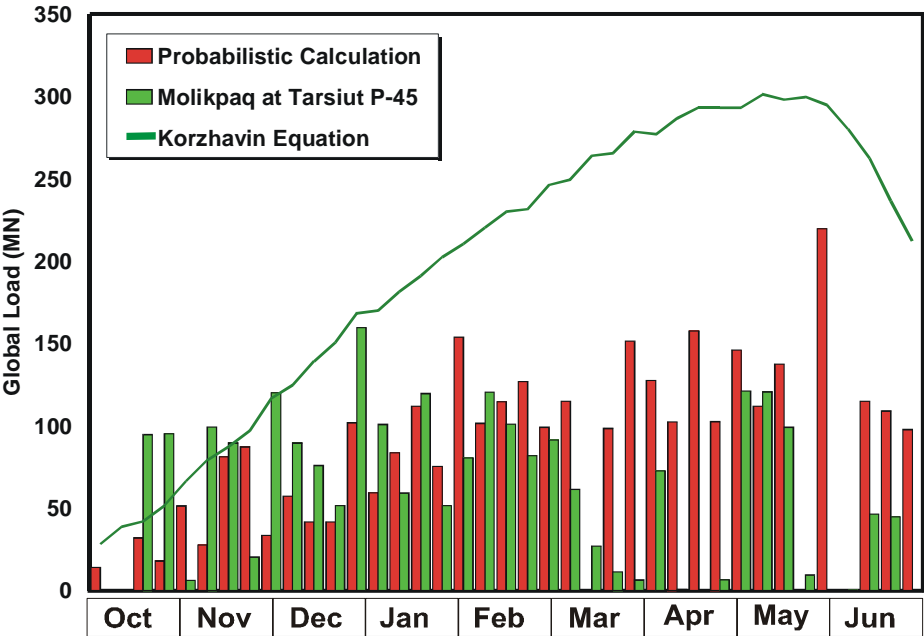
Fig. 7. Comparison on the global first-year ice loads measured on the Molikpaq at Tarsiut P-45 site with those calculated using the probabilistic approach. The deterministic Korzhavin equation is also included for comparison

Figure 7 represents a single winter simulation. To explore variability more systematically, multiple simulations were carried out for two one-week periods, one for the first week of December and the other for the first week in February. A hundred simulations were run for each week period with ice thickness, number of events and failure mode being the variables. The results are plotted in Figure 8 as cumulative distributions. Since there are only three ice thickness values each week and four failure mode parameters, there are just twelve possible weekly maximum loads, ignoring a zero load. Thus the plot is "steppy". This type of an analysis could be used to estimate expected loads at various times during the winter. It provides a basis for comparing weekly measured loads with those predicted for design load validation purposes, and for guiding operational procedures.
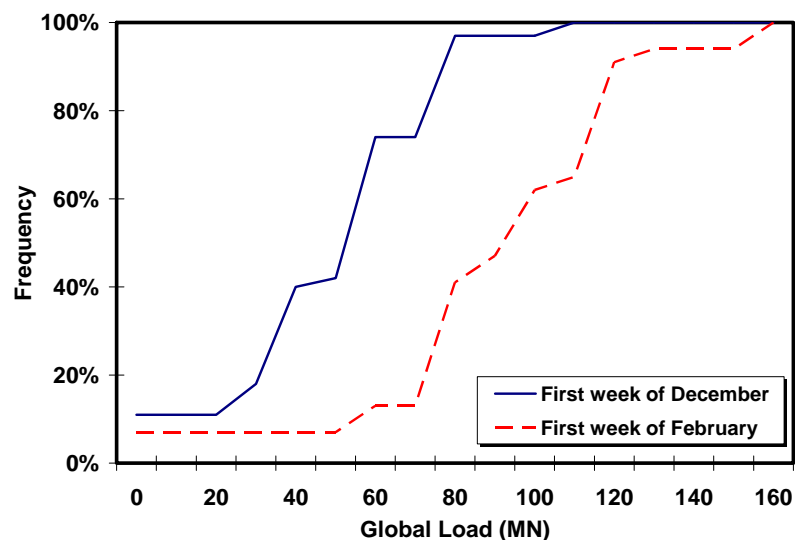
Fig. 8. Cumulative distribution of predicted weekly maximum global loads on the Molikpaq for two different weeks in the winter

SUMMARY

A simple probabilistic model has been developed that incorporates a number of ice failure modes. It has been shown that loads calculated using this model quantitatively agree with observed ice loads on a wide offshore structure. The output from the probabilistic model shows that maximum weekly loads can vary greatly throughout the winter. It provided a more realistic prediction of the ice loads than the deterministic Korzhavin equation. Various improvements to the model have been discussed in this paper. In applying this model for a structure to be located at a specific site, there are a number of environmental parameters that must be known. These include details on the annual variation of the ice thickness, ice types, ice macrostructures, and ice movement. Details regarding the structure, including the waterline width, angle of outer face, and water depth are also key inputs into the model. An estimate of the potential for ice grounding around the structure is also important since this can alter the failure mode distribution on the structure. It is planned to implement these features in the analysis in the near future. Overall, this approach should provide realistic load levels and information on the evolution of loads throughout the winter season.

REFERENCES

Korzhavin, K.N. 1971. Action of Ice on Engineering Structures. *US Army CRREL Translation TL260*, Hanover, N.H., USA.

Timco, G.W. and Johnston, M. 2004. Ice Loads on the Caisson Structures in the Canadian Beaufort Sea. *Cold Regions Science and Technology* 38, pp 185-209.

Wright, B., Pilkington, G.R., Woolner, K.S. and Wright, W.H. 1986. Winter ice Interactions with a Arctic Offshore Structure, *IAHR Symposium on Ice*, Vol. III, pp 49-73, Iowa City, Iowa, USA.

Wright, B.D. and Timco, G.W. 1994. A Review of Ice Forces and Failure Modes on the Molikpaq. *Proceedings of the 12th IAHR Ice Symposium*, IAHR'94, Vol. 2, pp 816-825, Trondheim, Norway.

TIDE AND WIND INDUCED SEA-ICE DRIFT AND ICE COVER DEFORMATIONS IN THE VICINITY OF THE MOLIKPAQ DRILLING PLATFORM, NORTHEASTERN SAKHALIN

Victor Tambovsky[1], Pavel Truskov[2] and Georgy Shevchenko[3]

ABSTRACT

This paper presents the results of investigations of ice drift and ice cover deformations on the northeastern shelf of Sakhalin Island. Ice drift data was obtained during operations near ice resistant platform Molikpaq (Sakhalin Energy Investment Company, LTD) in the spring of 2003. Using radar deployed on the Molikpaq, the time series of the ice drift were obtained in several points around the platform. Tidal and wind-induced components of ice drift were analyzed separately in each point. The differences of ice drift velocities in shallow water and deep areas were used to estimate parameters of ice cover deformations. Forecast of ice drift velocity and ice cover deformations can be useful for ships operation support in the area adjacent to Molikpaq platform.

INTRODUCTION

Oil production on the northeastern shelf of Sakhalin Island is carried out in severe ice conditions. For protection of the Molikpaq drilling platform and also for safe approach of vessels thereto, ice drift measurements are made every year using a Furuno radar. Investigation of ice drift peculiarities on the northeastern shelf of Sakhalin Island is based on the observations conducted in 1985-1995 years. The coastal radars were used for ice drift measurements. The radar's antennas were deployed on the top of the special tower in 40-50 meters high to provide the best measurements. These radars were deployed on the shore in Odoptu settlement, Komrvo settlement and on Levenshtern Cape (Shevchenko, Putov, 1999; Tikhonchuk et al, 2001).

New method of ice drift measurement using coastal radar was developed by Eugenie Morozov (Sakhalingidromet) and Pavel Truskov (SakhalinNIPImorneft) in 1982. The peculiarity of this method was measuring of ice drift velocity as a vector time series in the fixed points like wind or current measuring. The obtained vector time series of ice drift were analyzed using standard method of current analysis.

The analysis of ice drift data allows obtain some new results relating tide and wind-induced ice movement and ice cover deformation within 12-15 km along shore on the

---

[1] Environmental Company of Sakhalin, LTD, Yuzhno-Sakhalinsk, Russia
[2] Sakhalin Energy Investment Company, LTD, Moscow, Russia
[3] Sakhalin Research Institute of Fisheries and Oceanography, Yuzhno-Sakhalinsk, Russia

northeastern shelf of Sakhalin Island (Shevchenko, Putov, 1999; Tikhonchuk et al, 2001; Tambovsky et al, 2001; Tikhonchuk et al, 2002).

Special ice drift measurements were carried out in the spring of 2003 (May 14 – 21) to estimate ice cover deformations in the area of Molikpaq. Distances and directions passed by the ice-floes were determined on the basis of their trails within 7 fixed circular areas located at a distance of 4 nautical miles from each other at points maximally spaced out within the radar view zone. This enabled direct assessment of ice cover deformations at the drilling platform location. This paper presents the method of ice radar observations and result of analysis of ice drift particularities and deformations of ice cover in the area of drilling platform induced by tides and wind force.

MOLIKPAQ ICE DRIFT OBSERVATIONS

In the spring of 2003, ice drift observations were carried out during one week on the Molikpaq using radar Furuno model. The antenna of radar was deployed on the top of the production module at the 50 meters height from the sea surface and provides the good indication of floating ice within 12 nautical miles (nm) range. The ice observations were fulfilled every hour. The trails of drifting ice were recorded with 20-30 minutes interval and 6 nm monitor range was used. An M-63M anemometer was used to make synchronous wind measurements.

Distance and direction of ice drift was determined by the ice trail on the monitor. Ice drift velocity was calculated using known distance and time of the ice movement. Ice drift was fulfilled within seven circles, which had diameter at 1.5 nm (Fig. 1). These circle areas were located at the distance 4 nm from one to another on the monitor. The value of ice drift velocity and direction were determined within this circle area and were referred to the center of the area for every hour of observations. Using this method, seven time series of ice drift (one for every circle area) were obtained during one week of observations. The method of ice drift observations was analogous to the method of ice observation conducted using coastal radars on the northeastern coast of Sakhalin in 1986-1995 years. Deformation parameters were estimated based on spatial derivatives of drift velocities, obtained from differences between projections of drift vectors on the parallel and meridian at the corners of a square with a side size of 8 miles.
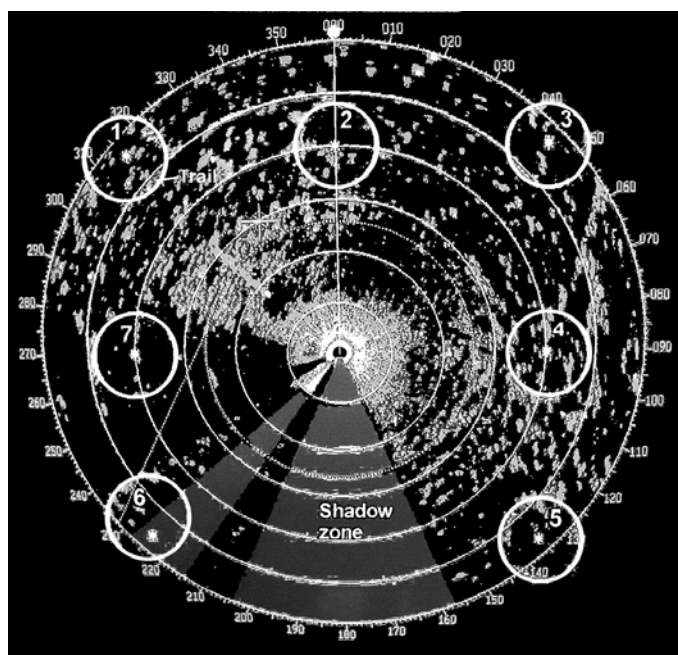

Fig.1. Radar monitor and circle areas of ice drift measurement

TIDAL ICE DRIFT PECULIARITIES

The changes of tidal currents within 10-20 km marine area usually are small. The same small changes are typical for the tidal ice drift too. The other conditions are on the northeastern shelf of Sakhalin. The tidal shelf waves (the variety of Rossby topography shelf wave) take part in diurnal tides formation. These waves are inducing the high tidal currents velocity in the near-shore shallow water zone. One more peculiarity of tidal shelf wave is quick reducing of tidal current velocity with offshore distance and quick change of tidal current phase along the shore (Rabinovich, Zhukov, 1984; Shevchenko, Putov, 1999; Tambovsky et al, 2001).

The northward and eastward components of tidal ice drift vector were estimated for analysis of ice drift changes in accordance with offshore distance. The tidal ice drift was calculated using least square method. The parameters of 4 main tidal waves (two diurnal K_1, O_1, and two semidiurnal M_2, S_2) were calculated. Fig. 2 shows the eastward and northward components of "clear" tidal ice drift in the points 1, 2, 3 that located on the line perpendicular to the shore. The north component has a few variations the most outstanding at the moments of maximum speed of tidal and ebb-tidal current (the minus value indicates the south-directed drift). The east component has more essential variations induced by the semi-diurnal tide, but the contribution of the semi-diurnal tide for the tidal current formation is small.

The significant differences between tidal ice drift in the shallow water area (to the west of the Molikpaq) and deeper water area (to the east of the Molikpaq) are the important conclusion. These differences are the reason of the stretching and compression of the ice cover induced by the tides (Tikhonchuk et al, 2001). The forecast of these phenomena can be useful for the supplies vessels working within the ice near Molikpaq.

Fig.2 also shows the plots of ice cover deformations under the tide influence near Molikpaq. The plots show that the same indexes of deformations are typical for the different phases of tide. Divergence is positive while ebb-tide changes to the tide and the tidal current changes from positive value to negative. This event indicates stretching of the ice cover. Rotor, an index of ice cover rotation, is shifted on half of tidal cycle against divergence and has the maximum negative value (the clockwise rotation is prevailed). The divergence is the positive while the tidal current changes from north to south direction. The divergence is negative and rotor is positive when the tide changes to ebb-tide. The speeds of stretching (e_1) and compression (e_2) reach the highest values when the divergence is highest too. The very close results were obtained from Odoptu radar data analysis (Tikhonchuk et al, 2001).
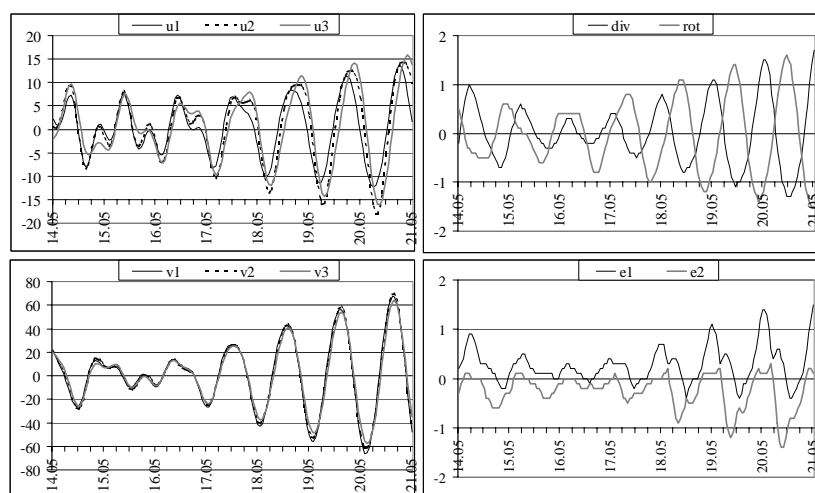

Fig.2. East component (u, cm/s, left, upper picture) and north component (v, cm/s, left, lower) of tidal ice drift in the points 1, 2, 3, located on the perpendicular line to the shore and indexes of tidal deformations – divergence and rotor ($10^{-5}c^{-1}$, right, upper) and velocity of stretching and compression (e1, e2, $10^{-5}c^{-1}$, right, lower)

The identical regularity of tidal ice cover deformations in different areas of northeastern Sakhalin ice mass indicates the possibility of forecast (prediction) of tide-inducing ice cover deformation. The ice drift measurement must be carried out during one month for more exact results.

WIND-INDUSED ICE DRIFT

The investigations of wind-induced ice drift were conducted using Odoptu coastal radar that located at 60 kilometers to the north from Molikpaq. Two-dimensional regression analysis indicated non-isotropic and compound response of ice drift on the wind action (detailed analysis see in the paper of Tikhonckuk and Shevchenko in the present book). The two-dimension matrix transformation can be described by ellipse, which is formed by different directed vectors of outside action. The large axes of "response ellipse" for typical elements of matrix have orientation north-northwest – south-southeast that is parallel to coastline (tidal ellipses have the same orientation). The large semi-axis of ellipse has value of about 4 and the small semi-axis is about 1. The unit of semi-axis is cm/s, or percentages. It means that the wind 10 m/s of "effective direction" induces ice drift velocity 40 cm/s and the same wind of "ineffective directions" induces ice drift velocity10 cm/s only. The northeasterly winds are prevailing over investigation area in February and March and southeasterly winds in May-June. Both are "effective". The parameters of these ellipses that were calculated for different years and months changed insignificant. The results of calculations of Odoptu data obtained in 1992 and 1993 (Tikhonchuk et al, 2002) show that the elements of matrix and consequently the size and orientation of ellipses are identical (see Table 1 and Fig. 3).

Table 1. Matrix elements of "the winds coefficients" calculated on the Odoptu radar data obtained in 1992-1994 years and data observation on Molikpaq in 2001 and 2003 years

	Od-1992	Od-1993	Od-1994	Mol-2001	Mol-2003
A_{11}	1.45	0.95	1.73	1.28	1.27
A_{12}	-0.36	-0.15	-0.44	0.36	1.07
A_{21}	-2.35	-2.75	-0.82	-1.07	-0.51
A_{22}	3.08	2.58	2.87	3.8	3.9

The result of the calculation of matrix coefficients based on the data ice drift measurement on Molikpaq in 2001 and 2003 years also indicated the highly closed result. The elements of large diagonal of matrix responsible for collinear movement have the more stability in contrast to elements of slating diagonal responsible for the normal components. These events appear when the ellipses are most compacted and the most deviation angles happen. It can be as a result of the influence of shore effects to the ice drift and more proved for Odoptu coastal radar.

The result of the ice drift investigation in 2003 year on Molikpaq shows that variance of regression a model was 59% for the east component and 78% for the north component. The north component makes the general impact on dynamic of the ice cover within the area of Molikpaq. This result indicates the high effectiveness of the two-dimension matrix regression model.

Fig.4 shows the plots of distribution of the wind coefficients and the angles of deviation between the wind and drift direction. The wind direction determines in mathematics

coordinate system. The direction of the vector to the east anticlockwise at 90° corresponds to south wind (270° - north wind). The maximum values of wind coefficients correspond to north-south directions of wind. Data obtained in 2001 year confirm this conclusion, but analysis data obtained in 2003 year indicated the deviation in 15°. The angle deviations have a typical asymmetry; the negative value of angle deviation (up to -45°) is more then the positive value (up to 15°). This situation indicates the prevailing clockwise deviation of drift from the wind. The eigen vectors are determine as the vectors with angle deviations that are equal to zero. Ice drift has no deviation from wind because of balance between Coriolis force and coastline influence.
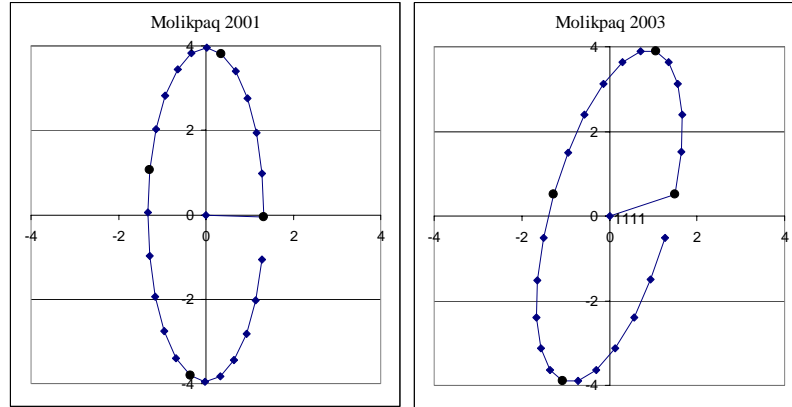
Fig. 3. The ellipses responsible to ice drift-wind interaction (1 m/s speed wind) for all directions in accordance with matrix of wind coefficients calculated on data obtained on Molikpaq in 2001 and 2003 years. The circles indicate the ice drift direction for west (line from the point of origin), south, east, and north directions of wind

The stability of matrix "wind coefficients" allows one to forecast the ice drift velocity and direction using the known wind speed and direction. It is possible to use both tidal ice drift characteristics and matrix of wind coefficients for ice drift forecast for operational and long-term purposes. The operation purpose includes the forecast of movement of personal floe under the wind and tide influence. The purpose of long-term forecasting is to estimate the extremal values of ice drift velocity of low probability.

Fig.5 shows the variations of stretching and compression of ice cover calculated on base of the ice drift data obtained in the points around Molikpaq in 2003 under the wind influence (tidal component was predicted and subtracted from the initial series). The wind direction changed significantly during period range of observation, from north-northeastern to south-southeastern and to northeastern again.
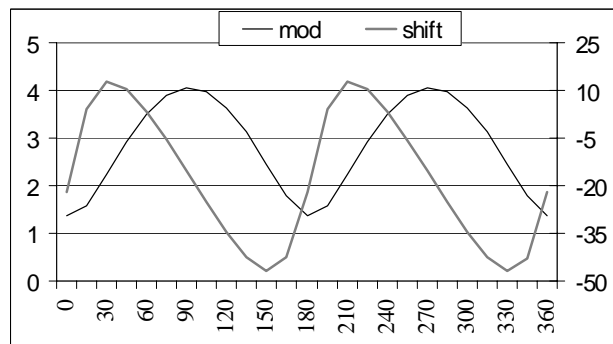

Fig. 4. The wind coefficient (mod, %, the left scale) and angle deviation between the wind and ice drift direction (shift, degree, right scale) depending from wind direction (0°-west wind, 90°-south wind, 180°- east wind, 270°-north wind)
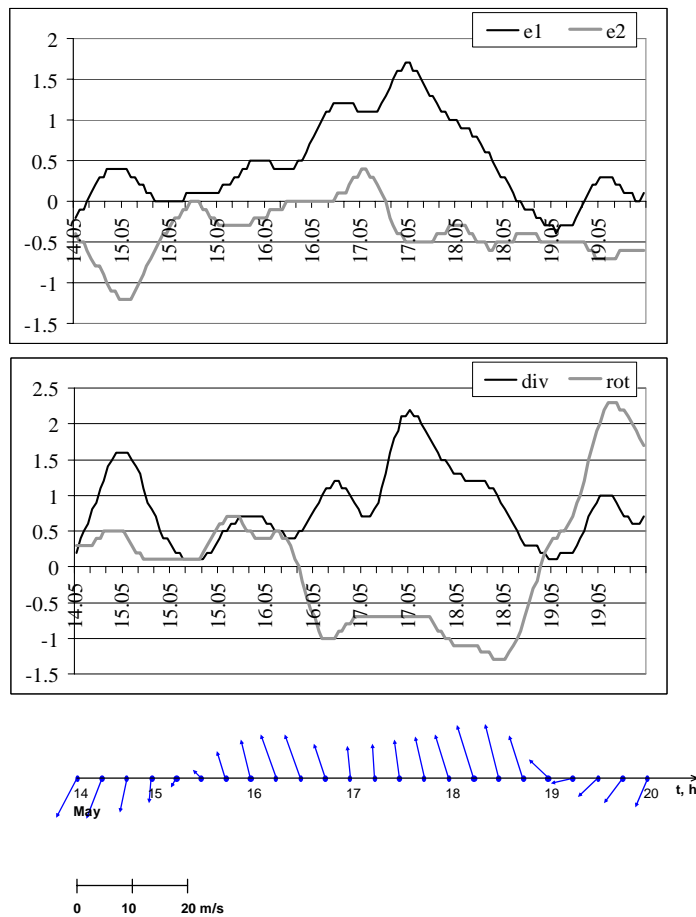
Fig. 5. Variation of deformation parameters: speed of stretching and compressions (e_1, e_2, $10^{-5}c^{-15}$) (upper picture); divergence and rotor (div, rot, c^{-1} 10^{-5}) (middle); the mean vectors of wind speed within 6 hours range

The indexes of ice cover deformations changed significantly too. If wind direction changed (15 and 19 of May), these indexes decreased. If the wind speed increased, the speed of stretching was increased too. Fig.5 shows the typical situation when the stretching was along the one axis and compression along another. There was an exception to this on 17 May when the weak southerly wind induced the stretching along both axes (e_2 was positive too). Opposite situation was observed at 19 of May (the total compression was occurred, e_1 was negative) under influence of easterly shoreward wind. It is impossible to make the final conclusion relating ice cover deformation in the area adjacent to Molikpaq platform under the wind influence because the period of the ice drift observations was too short, only about one week.

CONCLUSION

The measurements of ice drift using Furuno radar deployed on Molikpaq (northeastern shelf of Sakhalin) carried out in May 2003. Interesting results were obtained from the analysis of ice drift data that were measured in 7 points around the platform:

1. The significant differences of tidal ice drift velocities in shallow water (westerly from platform) and deep-water areas (easterly from platform) were found. These differences are a cause of tide-induced ice cover deformations in the area adjacent to Molikpaq.

2. The semidiurnal tides have significant influence on the ice cover deformations, although their role in tidal currents formation is low.

3. Indexes of ice cove deformations changing periodically accordingly to tidal ice drift oscillations, so they can be predicted as tidal ice drift. Dependence of these indexes from tidal ice drift is close to obtained on the base of Odoptu coastal radar data.

4. Two-dimensional regression method was used to determine response of residual ice drift (tides were predicted and subtracted) on wind force. The response matrices are relatively stable – close results were obtained from ice drift data that were measured using Molikpaq (2001) and Odoptu radar (1992-1994).

5. "Response ellipses" were calculated that describe "effective" wind directions with wind coefficients about 4% and "ineffective" wind directions with wind coefficients about 1%. The stability of the results allows one to forecast wind drift using the real wind speed and direction. It is possible to use both tidal ice drift characteristics and matrix of wind coefficients for ice drift forecast for operational and long-term (estimation of maximal ice drift velocities) purposes.

6. The differences of residual ice drift characteristics between coastal and offshore areas were used for estimation of wind-induced stretching and compression of ice cover.

Obtained results show good prospects for this drift observation method to determine such important characteristics as the velocities of ice stretching and compression in order to forecast ice compressions and diffusions in the vicinity of Molikpaq and ensure safe operation of supply vessels around the platform during the ice season.

REFERENCES

Rabinovich, A.B., and A.E. Zhukov. Tidal oscillations on the shelf of Sakhalin Island. *Oceanology*, 24 (2), 184–189. (1984).

Shevchenko G.V., Putov V.F. On wind and tide induced sea-ice drift on the northeastern shelf of Sakhalin Island. *PICES Sci. Rep.* 12 (1999) 11-17.

Tambovsky V., Tikhonchuk E., Shevchenko G. Characteristics of morphometry and dynamics of sea ice on the northeastern shelf of Sakhalin Island. *Intern. Symposium on Okhotsk Sea & Sea Ice,* Mombetsu, Hokkaido, Japan, (2001) 356-390.

Tikhonchuk E., Shevchenko G., Tambovsky V. Tide-induced drift velocities and deformations of ice cover on the northeastern shelf of Sakhalin Island. In *Proceedings of the 11-th ISOPE conference,* Stavanger, Norway - Cupertino, California, USA (2001) 739-743.

Tikhonchuk E., Shevchenko G., Tambovsky V. Ice drift, induced by the wind influence on the northeastern shelf of Sakhalin Island. In *Proceedings of the 12-th ISOPE conference,* Kitakyushu, Japan (2002) 849-852.

MODELING OF LEVEL ICE ACTION ON FLOATING ANCHORED STRUCTURE CONCEPTS FOR THE SHTOKMAN FIELD

Shkhinek, K.N.[1], Bolshev, A.S.[1], Frolov S.A.[1], Malyutin, A.A.[2] and Chernetsov, B.A[2].

ABSTRACT

Between different structures concepts for the Shtockman field the floating anchored structure with downward cone form near the waterline seems to be the most attractive. But anchored systems are very compliant and therefore design of their interaction with ice needs sophisticated methodology. The rough methodology for ice loads on these structures calculation, its calibration and some concrete results of calculation are presented in this paper.

NOMENCLATURE

Ice and water
R_c – unconfined strength;
R_t – tensile strength;
R_f – bending strength;
$\gamma_в$, $\rho_в$ – water specific weight and density;
$\gamma_л$, $\rho_л$ – ice specific weight and density;
E – modulus of elasticity;
f – friction coefficient;
L – initial length if the ice sheet,

Structure
M – mass;
J – moment of inertia in vertical plane;
R – structure radius at waterline
ξ_0 – horizontal displacement from initial position;
ζ_0 – vertical displacement;
θ_y – угол крена;
F_{anch}, M_{anch} – force and moment of an choring system;
F_g, M_g – hydrostatic force and moment;
F_{ij}, M_i – forces and moment due to ice action;
λ_{ij} – added masses;
b_{ij} – drag coefficients

---

[1] St. Petersburg Polytechnics University
[2] Central Design Bureau for Marine Engineering, Rubin

1. INTRODUCTION

Design of a platform for the Shtokmanovskoye field meets many problems because of the great water depth in the place of location and ice action. Apparently the single possible the structure concept in these conditions is anchored structure with the complicated mooring system. Some of these concepts are considered by Ivanov et al, 2003 . For diminishing ice loads the downward cone form in the underwater part of the structure is used in this concept. There are many papers about ice loads on inclined plate or upward cone. But only maximal or average quasi-static load on immovable structure are considered. For example Nevel (1972), Ralston (1978), Croasdale and Cammert (1993), Frederking (1980), Maattanen (1986), Timco et al (1984), Evans and Parmattaer (1985), Frederking and Timco (1985), and many others. Significantly less is number of work or recommendations for ice loads on downward cone or pyramid: API (1988), Frederking and Schwarz (1982), Lau and Williams(1991), Timco et al (1993). Numerical simulation of the Kullul in pack ice conditions was considered by Barker et al, 2000.

The anchored structures have the following peculiarities:

- they are very compliant therefore an action is imposed by mutual ice/structure displacement and velocity;

- it is impossible to use for anchored structure design the load had been determined for immovable structure;

- the position of the contact area changed constantly and should be determined in solution at each time moment during the computation;

- not only amplitude of maximal action but the whole load time history should be determined for structure design. Additionally resonant can arise at some action frequency;

- structure form is complex and ice sheet is subjected to 3D deformation., therefore ice failure has a complicated mechanism.

Only few work: Evans and Parmeter(1985), Maattanen (1986,1994) Shkhinek et al.(1996), Shkhinek and Uvarova (2001), Matskevitch (2002), considered methods of dynamic actions estimation on inclined structure but they refer to upward immovable plane. Only some of peculiarities of process of ice interaction with the flexible structure have been considered in literature e.g.Maattanen (1999) and it is clear that the strict solution of this problem should be extremely sophisticated. Therefore only very approximate numerical solution of the problem can be suggested.

2. THE PROBLEM STATEMENT

A level semi infinite ice sheet moves with the velocity *U* against the floating anchored structure. The underwater part of the structure near the waterline has form of a downward cone. At some depth this cone is connected with a cylinder. In principle the structure has 6 degrees of freedom, but this solution proposes that phenomenon is symmetric in relation to axis of symmetry. So only 3 degrees of freedom are taken into account

The scheme for computation is shown in Figure1. The goal of the work is to determine the actions formed in result of the ice/structure interaction.
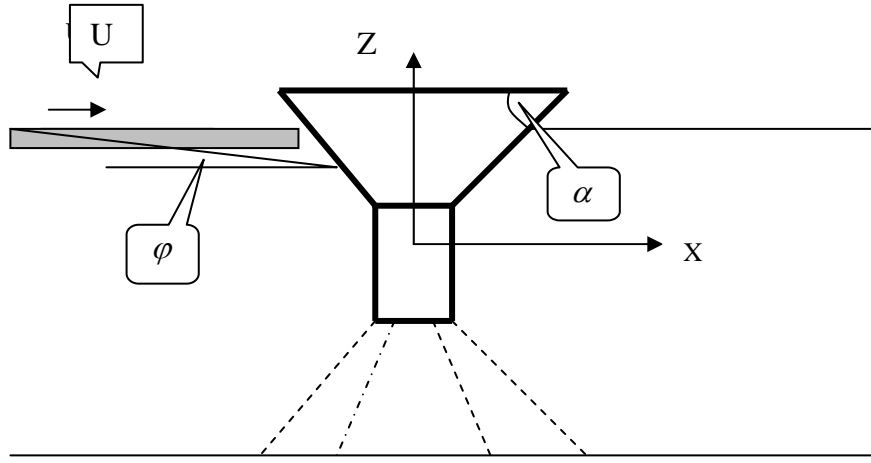
Fig. 1. Scheme for computation

The equations of the structure motion can be written as:

$$\begin{cases} (M + \lambda_{11})\ddot{\xi}_0 + b_{11}\dot{\xi}_0 = F_{anchx} + F_{ix} \\ (M + \lambda_{33})\ddot{\zeta}_0 + b_{33}\dot{\zeta}_0 = -Mg + F_{gz} + F_{anchz} + F_{iz} \\ (J + \lambda_{55})\ddot{\theta}_y + b_{55}\dot{\theta}_y = M_{gy} + M_{anchy} + M_{iy} \end{cases}$$ (1)

An equations of the ice sheet or its part motion have the form:

$$M_j \ddot{X}_j = F_j \ (\text{j=x,z,}\varphi)$$ (2)

where M_j, $\ddot{X}_j$, F_j are the mass and moment of inertia of the ice sheet (or its part), acceleration and forces acting on the ice sheet during its motion in directions j correspondingly. Components F_j will be considered later.

All parameters besides F_{ix}, F_{iz} and M_{iz} (components of ice actions) in Eq (1), and F_j in Eq (2) are known or can be determined beforehand by the existing programs. Our task is to develop methodology of description of dependencies of listed above unknown functions (and their link with structure and ice motion). After that Eq (1) and (2) can be integrated numerically and structure motion, stress in chains, etc can be calculated in the process of integration.

3. A METHODOLOGY OF ICE LOADS CALCULATION

The main assumptions:
Ice sheet has an infinite momentum, so the process of ice/structure interaction can continue as long as we need. The phenomenon has symmetry regarding the longitudinal vertical plane, which coincides with the structure axis of symmetry. The edge of the ice sheet slides along the moving structure surface during the interaction and the sheet itself can be compressed and bend during the interaction. Compressive and flexure stresses and longitudinal deformations in the sheet are considered, but flexure deformations are neglected, i.e. the sheet can move and rotate in vertical plane as a plane plate.

The following forces act on the sheet:
- the structure reaction on ice action (friction, pressure),
- a water reaction on ice motion (inertia, drag and additional buoyancy due to sheet diving),

- an action of an ice rubble which forms during the interaction. This rubble located under the sheet and resists to sheet rotation,
- the sheet inertia during motion and rotation.

Compressive, flexural and shear stresses induced by these factors in any time are determined step by step for each cross-section of the sheet. These stresses are compared with failure criteria. The flexure, compressive and shear failure criteria are taken into consideration.

The process of interaction is divided on several stages.

The stage 1 – intact ice sheet is sliding along the structure surface. Its motion is considered in combination with the structure displacement. Correspondingly the sheet moves, rotates and is. As soon as the failure criterion is reached in some section of the sheet then the sheet in this section is divided on two parts, which are connected with a hinge. The geometry of phenomenon in vertical plane changes: the part nearest to the structure (we shall name it the first part) remains to be in contact with the structure and with the second part of the former sheet. The second part comes to the water surface and takes horizontal position. New position of the contact point between the structure and ice sheet, displacements and velocities in the contact point of ice and structure are recalculated from the current geometry.

The stage 2 – the nearest to structure part of the sheet slides along the structure surface being pushed by the second part. The structure and the sheet velocities and displacements in the end of the first stage are used as initial conditions for the Eq (1,2) integration at the seconds one. The stage 2 continues until failure criterion is reached in the first part of ice sheet or this part lays on the structure surface. Two scenarios can develop later. In the ***first scenario*** the next hinge forms between element of the first part of the sheet, when failure criterion is reached. New position of all parts of the former sheet is determined again, and integration of Eq (1,2) continued. So *stages 2.1, 2.2, etc.* of the first part of the subsequent sheet division are considered. The process of division can be repeated many times until the length of the nearest to structure part of the sheet is more than five ice thickness (Li et al, 2003) The shorter pieces can only slide and rotate. It is proposed in the ***second scenario*** (when part of ice sheet lays on the surface) that nearest to structure portion of ice will dive under the ice sheet and later will be considered as the part of the rubble, which is collected under the sheet. The end of the stage 2 corresponds to situation when all first part is divided on blocks, which have dived.

The next phase of interaction considers motion, sliding and diving of part two of the ice sheet. The stages of interaction considered above will be repeated again for this part of the sheet several times.

The simplified algorithm of ice behavior computation is shown in Fig 2.

Initial conditions

3 types of initial conditions are used during the computation:
- in the beginning of calculation

$I = J = 1, t = 0, \xi_0 = \zeta_0 = 0, \alpha = \alpha_0, \varphi = 0, \theta_y = 0, \dot{\theta}_y = 0, \dot{\xi}_0 = \dot{\zeta}_0 = 0$;

- if piece of ice dives ($\varphi = \alpha$ at time t_1) then the following conditions are used for the next part of ice

$$t = t_1, \ \xi_0 = \xi_0(t_1), \ \zeta_0 = \zeta_0(t_1), \ \alpha = \alpha(t_1), \ \varphi = 0, \ \theta_y = \theta_y(t_1),$$

$$\dot{\theta}_y = \dot{\theta}_y(t_1), \ \dot{\xi}_0 = \dot{\xi}_0(t_1), \dot{\zeta}_0 = \dot{\zeta}_0(t_1) ;$$

- if ice fails in time t_a and correspondingly is divided on two parts then the following initial conditions are used for integration

$$t = t_a, \ \xi_0 = \xi_0(t_a), \ \zeta_0 = \zeta_0(t_a), \ \alpha = \alpha(t_a), \ \theta_y = \theta_y(t_a), \ \dot{\theta}_y = \dot{\theta}_y(t_a), \ \dot{\xi}_0 = \dot{\xi}_0(t_a), \dot{\zeta}_0 = \dot{\zeta}_0(t_a)$$

$$\varphi = \arcsin\left[\frac{b - tg\,\alpha\sqrt{(tg^2\alpha - b + 1)}}{1 + tg^2\alpha}\right], \text{ where b is some constant which depends on}$$

structure and ice position in time t_a
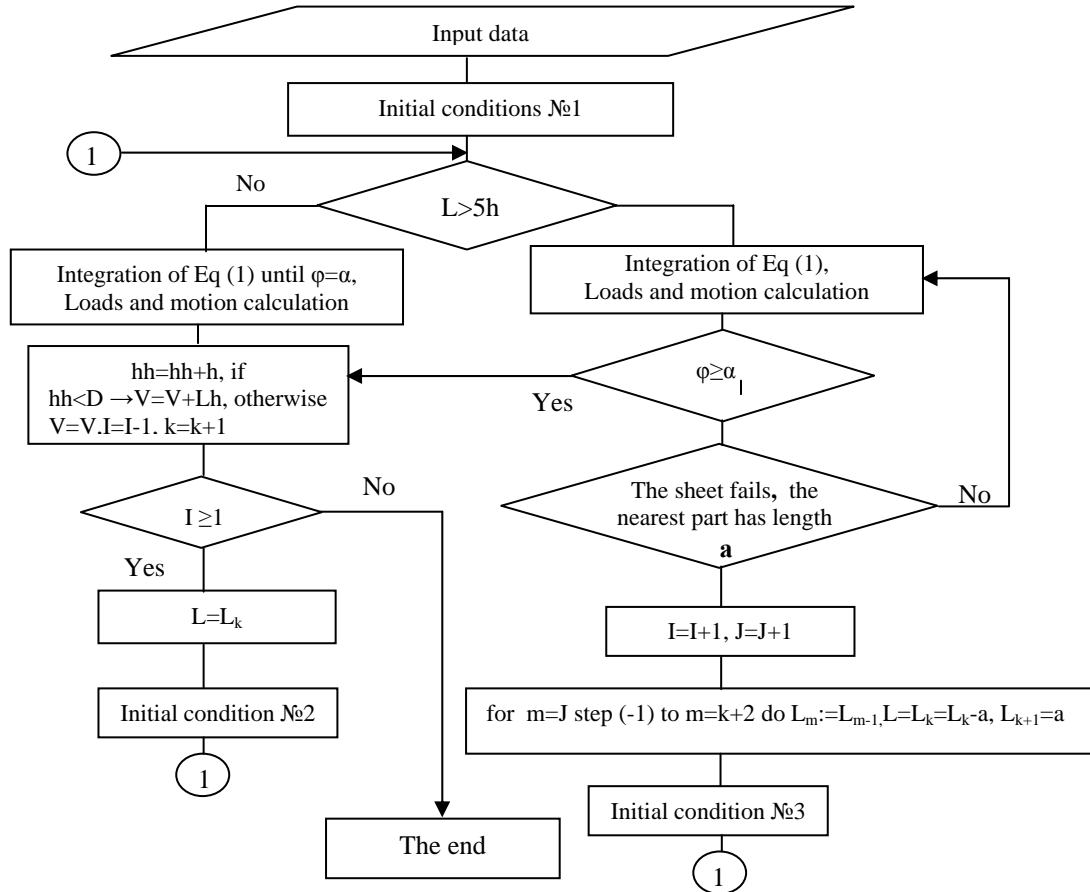
Fig. 2. Algorithm of calculation

4. SOME ASSUMPTIONS AND DETAILS OF THE METHODOLOGY.

The forces

The following forces (and corresponding moments) act on the ice sheet during its interaction with the structure:

- longitudinal F_l and normal to sheet axis F_n forces induced by interaction with structure. These forces produce normal F_N and frictional F_f actions on the structure:
- ice sheet inertia during translational motion F_x and force due to rotation inertia F_j;
- hydrodynamic reaction – inertia $F_{\lambda n}$ and drag F_{gn};
- hydrostatics (extra buoyancy) F_b;

- forces on the border between ice sheets F_c;
- force induced by rubble buoyancy F_r.

The structure:

The structure front side is divided on 9 parts in calculation. The main, central part has a width R, others R/8.Within each parts the structure surface is considered as an inclined plane. The angle of the plane inclination in each part is equal to angle of inclination to horizon of a cone surface in vertical section crossing the center of this part. Within each part ice is considered as a beam, but experimental correction between the utmost moment to beam and plate (Lavrov,1971) is taken into account. The calculations by the program which were done afterward showed that the main part of the mean global pressure is determined by the central part and the others give some additional mean pressure which elongates the period.

The ice sheet/structure contact:

During the interaction structure executes displacement and rotation and ice slides along the structure surface. Problem of determination of ice/ structure contact zone is solved on each time step. The sheet edge can not slide freely due to influence of the sheet inertia, hydrodynamics and friction so its motion will be followed with the sheet longitudinal compressive and flexure stresses.

The ice sheet edge:

To avoid great stress peak at the initial ice/structure hit, it is proposed that ice edge contains some protrusions before the first contact. So the contact area (and correspondingly the longitudinal force F_l in the sheet) arises gradually during the initial ice /structure contact. The problem of longitudinal sheet oscillations due to the ice hitting the structure is solved using an artificial damping, which is proportional to the strain rate. The current strain rate is determined as difference between the sheet longitudinal deformations in the two subsequent times divided on time step.

The ice sheet inertia:

Forces F_{xin}, F_{zin} and $M_{\varphi in}$ are determined as inertia forces of the beam with given width and length executing translational motion and rotation.

The hydrodynamic forces:

The structure added masses and drag coefficients are determined by the special program The hydrodynamic influence is determined as normal forces on the plate which moves with some acceleration.

Appendix

a) drag force and moment, which acts on the moving sheet can be determined as:

$$F_{dn} = -C_{33}W\frac{\rho_B}{2}\int_0^L U_n(l)|U_n(l)|Udl \,,$$

$$M_{dn} = -C_{33}W\frac{\rho_B}{2}\int_0^L U_n(l)|U_n(l)|\left(l-\frac{L}{2}\right)dl \,,$$

where normal to sheet surface velocity is determined by formula:

$$U_n(l) = U_3\cos\varphi + U_1\sin\varphi + U_5l \,,$$

U_I – components of sheet velocity vector, in the i=1,3,5 directions of axis' of coordinate,

89

C_{33} – the drag coefficient of sheet with the length L and the width is taken from hydrodynamics.

b)inertia force and moment are determined by formulas:

$$F_{\lambda n} = -\rho_B \lambda_{33} S^{1/2} W \int_0^L a_n(l) dl ,$$

$$M_{\lambda n} = -\rho_B \lambda_{33} S^{1/2} R \int_0^L a_n(l)\left(l - \frac{L}{2}\right) dl ,$$

$$a_n(l) = A_3 \cos\varphi + A_1 \sin\varphi + A_5 l ,$$

where A_i – components of the sheet acceleration vector, S-the area of the sheet part which is under consideration, λ_{33} – the coefficient of added masses of sheet with dimensions L, W, (S), moving along the direction 3 is taken from hydrodynamics.

The hydrostatic forces:

The current forces and moments due to hydrostatic water pressure attendant on the sheet diving and rotation F_b can be easy determined from geometry.

The forces at the border between separate parts of the ice sheet F_c :

It is assumed that friction, longitudinal and normal forces act at the border between separate parts of ice sheet.

The force induced by rubble buoyancy:

The rubble is collected under the sheet surface as the ice sheet parts sink. This process develops in time and correspondingly rubble volume increases during computation. It is proposed that rubble draught changed linearly under the sheet with maximum near the structure surface and angle of inclination corresponding to the friction angle of the ice blocks (assumed 25°). The maximal possible height of rubble corresponds to the depth where the cone is replaced by cylinder. Porosity of rubble is assumed to be 50%.

The failure criteria:

Ice can fail due to compression, bending or shear. The common employed conditions for sheet which is under compression and bending are used as compressive and shear failure criteria. But a flexure criterion has. some peculiarities. The failure starts when usual condition of flexure failure is reached in some the sheet cross-section :

$$\frac{F_l}{Wh} - \frac{6M}{Wh^2} = R_f , \tag{3}$$

where M is the bending moment. But due to the plastic hinge formation in this section this condition does not signaled that the resistance to bending moment and the ice bearing capacity are exhausted and it can not increase in future.

The following reasons determines formation of this hinge:

- increase of longitudinal compression in the next time moment can prevent development of the crack formed due to bending;

- it is well known that the utmost stresses should spread over the whole cross-section area to lost bearing capacity of the sheet, whereas condition (3) corresponds only to beginning of failure;

- even if the crack develops over the whole cross-section and divides the sheet on two parts, which are compressed longitudinally and are under the action of the turning moment then special conditions realized on the border between these parts. Sodhi (1998) and Peters et al. (1982) considered simpler problem: the bearing capacity under eccentric vertical loading of the ice sheet located between two others (without longitudinal compression). They shoved that the utmost ice bearing capacity is 2-5 times higher than one corresponding to beginning of the flexure crack formation. It happens because local eccentric compression develops at a contact area near the free surfaces of the sheets. These stresses produce additional moment, which resists to bending. The results of Sodhi's experiments are used for the utmost resistance calculation. Additionally the strain rate factor k_c, which takes into account the strength dependence on strain rate is used.

$$k_c = (\frac{\dot{\varepsilon}}{\dot{\varepsilon}_0})^{0.33} \ (0.2 < k_c < 1).$$ Here $\dot{\varepsilon} = \frac{V_n}{L}$; $\dot{\varepsilon}_0 = 10^{-3}$ 1/s; V_n – normal to the sheet end

velocity; L – a current length of the nearest to the structure part of the sheet.

5. CALIBRATION

Comparison with experiments had been conducted by Frederking and Schwarz (1982), Law and Williams (1991), experiments with anchored structure had been performed in the Krylov Institute (2003), and full scale Kulluk measurement were carried out. Some results of calibration are shown in Tables 1 and 2 (The results of the comparison with difference no more than 15% are marked with bold numbers in the tables) and Figures 3,4.

An input data of Frederking and Schwarz (1982) experiments: $\alpha = 45^o$, h=5.4 cm,

$R_f = 63$ kPa, $R_c = 200$ kPa, E = 400 MPa, f = 0.1, D = 1 m.

Table 1. Comparison of the calculated loads with the results of the Frederking and Schwarz (1982) lab tests

U, m/s	F mean (N)			
	Horizontal component F_x		Vertical component F_z	
	Experiment	Calculation	Experiment	Calculation
0.01	**170**	**174**	250	170
0.05	**153**	**185**	296	180
0.1	**191**	**182**	364	185
0.25	**235**	**202**	339	188
0.5	**255**	**240**	276	221

Table 2. Comparison the of the calculated mean loads with the results of Lau and Williams (1991) lab tests

V, m/s	h, cm	R_f, kPa	$F_x$experim N	$F_x$calcul N	$F_z$experim N	$F_z$calcul, N
The model diameter D=1.08m						
0.01	8.51	37.4	**285**	**258**	310	249
0.01	5.46	23.8	80	113	84	110
0.01	3.56	36.1	38	89	56	87
0.05	8.5	36.5	**288**	**260**	314	251
0.05	5.11	28.8	**111**	**125**	**117**	**122**
0.05	3.56	35.2	39	95	56	93
D=1.28						
0.01	8.51	42.9	**324**	**352**	**386**	**345**
0.01	5.46	23.2	99	128	86	126
0.01	3.56	38.6	53	118	73	116
0.05	8.51	41.9	**320**	**358**	**376**	**343**
0.05	5.46	26	118	144	**140**	**141**
0.05	3.35	35	52	97	63.2	95
0.1	8.51	41.5	**382**	**351**	425	339
0.1	5.46	25.6	**142**	**150**	**167**	**145**
0.1	3.56	37.3	66	115	81	111
0.25	3.35	35	**93**	**108**	67	105
0.5	3.35	35	**139**	**124**	26??	118
D=1.48						
0.01	8.51	46.7	**365**	**422**	**460**	**413**
0.01	5.46	25.1	108	160	**144**	**157**
0.01	3.56	41.6	47	137	76	134
0.05	5.46	24.6	119	162	**148**	**158**
0.1	8.51	44.8	**422**	**444**	**508**	**432**
0.1	5.46	24.4	124	163	**141**	**158**
0.1	3.56	40.3	68	153	94	149

One can see very acceptable correlation between the experimental and calculated horizontal components of actions in all Frederking and Schwarz's experiments and for high and average ice thickness in Lau and Williams' experiments. For very low thickness' in the last experiments correlation is worse. Correlation of vertical component for thin ice in Lau and Williams' experiments is better than of horizontal one. It needs to be marked that calculations overestimate vertical load for Law and Williams experiments and underestimate for Frederking and Schwarz's ones. Probably it testifies about some difference in experimental results.

Two types of floating anchored structures were suggested by a Rubin Bereau: a SPAR with a cone collar (SD) and a cone shape TLP (LD). The structures dimensions are as following: SD- the diameter at waterline /minimal cone diameter ratio is 82/55 m, the draft is 58 m. LD- the diameter at waterline/minimal cone diameter is 51/38 m, the draft is 240 m.

Very detailed experiments with two models of considered structures (both immovable and anchored) were carried out by the team of the Krylov Institute (Krylov, 2003). Comparison of calculations with the experiment with the immovable structure is shown in Figure 3.

Comparison of average calculated horizontal loads (denominator) and measured by the Krylov Institute staff is presented in Table 3.
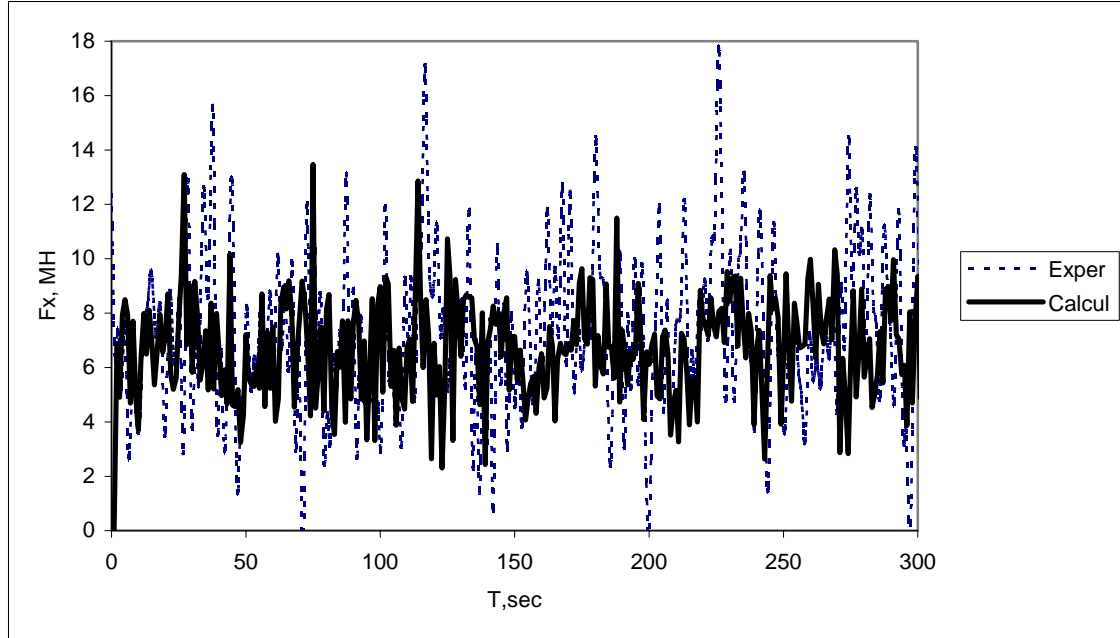

Fig. 3. Comparison of experiments in the Krylov Institute ice tank and calculation results, immovable structure. Experimental results are brought to full-scale conditions

Table 3. Some results of the Krylov Institute experiments and calculations (immovable model)

Model	Velocity м/ s	Rf, MPa	h, м	E, MPa	Fx mean, MN
SD	0.95	0.765	1.3	915	7.52/7.8
SD	0.95	0.765	1.4	915	9.23/8.5
SD	0.31	0.765	1.25	915	5.73/5.7
SD	0.99	2.785	1.05	2140	12.5/13.2
SD	1.15	2.785	1.15	2140	14.9/13.8
SD	0.28	2.785	1.2	265	8.1/10.4
SD	0.96	0.48	0.85	265	4.9/3.85
SD	1.16	0.48	0.9	265	6.0/5.2
SD	0.27	0.48	1	265	4.4/2.9
LD	1.18	0.945	1.65	1580	9.8/8.56
LD	0.27	0.945	2		6.0/7.3

Similar acceptable correlation was seen for the anchored structure.

The real structure which is resemble to considered is the Kulluk platform. Results of measurement of action of ice with different thickness (points, Wright 2000) and calculations (line and points) are presented in Figure 4.

All have been discussed above results indicate that reliability of calculated methodology is not worse than the experimental ones. Good correlation with Kulluk data testifies acceptance of the suggested methodology.

Full Scale Kulluk Loads in Level Unbroken Ice versus thickness
(normalized to a 500 kPa flexural ice strength)
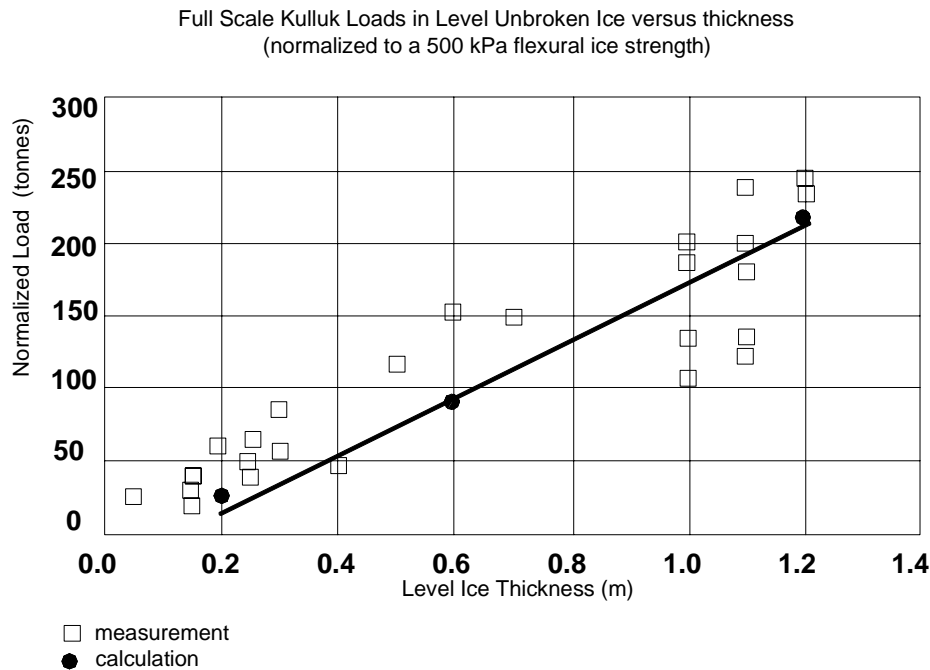
Fig. 4. Comparison of the calculations results with the Kulluk measurements

CONCLUSION

1. An approximate numerical program for calculation of the floating anchored structure behavior under level ice action is worked out. This program gives possibility to determine ice actions, the structure displacement and forces in mooring system during the interaction process.

2. Comparison of the calculation results with different experimental data and full scale measurements (Kulluk) showed their acceptable correlation. Some loads overestimation at thin ice in Lau and Williams experiments testifies that calculation methodology is conservative, but good correlation with Kulluk gives more confidence in possibility of it use.

3. Results of calculations and experiments gave possibility to the Central Design Bureau Rubin to improve design concept.

REFERENCE

API, 1988. American Petroleum Institute. Recommended Practice 2N, Planning, Designing, and Constructing structures and Pipelines for Arctic Conditions.

Barker A, Timco G., Saued M., Wright B., 2000. Numerical Simulation of the "Kulluk in Pack Ice Conditions. *Proceedings of the IAHR Symp*. pp. 65-171.

Croasdale K.R. and Cammert, A.B. (1993). Modified Method of Ice Loads Calculation on Sloping structures. *Proceedings of the RAO Conference*. St. Petersburg, pp. 158-165. (In Russian).

Evans, K, J And Parmeter, R.R., 1985: Ice Forces due to Impact Loading On A Sloping Structure. *Proceedings Of Civil Engineering in the Arctic Offshore*, pp. 220-229.

Frederking R., 1980: Dynamic Ice Forces on an Inclined Structure. 1980, In: *Physics And Mechanics Of Ice*, P.Tryde (Ed.), IUTAM Symp., Copenhagen, pp. 104-116.

Frederking R.M.W. And Timco G.W, 1985 Quantitative Analysis of Ice Sheet Failure Against an Inclined Plane. *Journ. of Energy Resources Technology*, Vol. 107, pp. 381-387.

Frederking, R.M.W. And Schwarz, J., 1982: Model Tests of Ice Forces On Fixed And Oscillating Cones. *Cold Region Science and Technology*, 6. pp. 61-72.

Ivanov A.I., Kitanov Yu.S., Karulin E.B et al. (2003). Development of Experimental Investigations Techniques of Wave and Ice Loading to the Marine Platforms in the Conditions of Shtokmanovskoye Deposit…… *Proceedings of the RAO Conference*, pp. 173-177.

Lavrov, V.V., 1971 Deformation and Strength of Ice, (in Russian) Hydrometeoisdat.

Krylov, 2003. Experimental Investigations of the Andored Platforms Behavior Under Waves and Ice. Actions. Report of the Krylov Institute to Design Rureau Rubin. Vol. I. 235 pp.

Lau, M., And Williams F.M. 1991: Model Ice Forces on A Downward Breaking Cone. *Proceedings Of The POAC Conference*, St. John's, pp 167-184.

Li F., Yue Q., Shkhinek K., Karna T., 2003. A Qualitative Analysis of Breaking Length of Ice Sheet Against Conical Structures. *Proceedings of The POAC Conference*, Trondhein, Vol. II, pp. 293-302.

Li, F., Yue, Q., Shkhinek, K., Karna, T., 2003: A Quantitative Analysis of Breaking Length of Ice Sheet Against Conical Structure. *Proceed. of the POAC Conference*, Trondheim, Vol. II. pp. 293-305.

Maattanen, M., 1999. Numerical Model for Ice-induced vibration Load Lock-in and Synchronisation. *Proceedings of the14[th] IAHR Symposium on Ice*, Vol. 2. pp 923-929.

Maattanen, M., 1986: Ice Sheet Failure Against An Inclined Wall. *Proceed. of the IAHR Ice Symp*.

Maattanen, M., 1994: Ice Load Design and Measurement on a Conical Structure. *Proceedings of the IAHR Ice Symp*. pp 401-410.

Matskevitch, D.G., 2002: Velocity Effects on Conical Structure Ice Loads. *Proceedings of OMAE* 2002-28079, Oslo, Norway.

Nevel, D., 1972, The Ultimate Failure of Floating Ice Sheets. *Proceedings Of IAHR Symposium*, pp. 17-22.

Nevel D.E. 1992. Ice Forces on Cones From Floes. *Proceedings of IAHR Ice Symposium*, St. Petersburg, Vol. 1.

Peters, D.B., Ruser, J.R. And Watt, B.J., 1982: Rational Basis For Design of Floating Ice Roads and Platforms. *Proceedings of OTC*, 4314, pp 153-167.

Ralston T.D. 1977, Ice Force Design Considerations for Conical Offshore Structures. *Proceedings of 4 International Conference POAC*, St.Johns, Newfoundland, Vol. 2, pp.741-752.

Ralston T.D. 1979, Plastic Limit Analysis of Sheet Ice Loads on Conical Structures. In: *Physics and Mechanics of Ice*, Per Tryde (Ed), IUTAM Symp., Copenhagen, pp. 289-308.

Ralston, T.D. 1978 Ice Force Design Considerations for Conical Offshore Structures. *Proceedings of the POAC Conference*, St.John's. Vol. 2, pp. 741-752.

Shkhinek, K., N., and Uvarova E., V., 2001. Dynamics of the Ice Sheet Interaction with the Sloping Structure. *Proceedings of the POAC Conference*, Ottava, Canada, Vol. 1, pp 639-648.

Shkhinek K., Kapustiansky S., Jilenkov A., Blagovidov L. 1996,Ice Loads Onto Sloping Structures. *Proceedings of POLARTECH Conference*, Workshop D, pp. 171-178.

Sodhi D., S. (1998): Wedging Action During Vertical Penetration of Floating Ice Sheets. *Int Journal of Solids and Structures* 35931-32). 427-4294.

Timco, G.W., 1984. Model Test of Ice Forces on a Wide Inclined Structure. *Proceed. Of The IAHR Ice Symp*. pp. 87-94.

Timco, G.W., Irani, M.B., Funke, E.R, English L., Carroll, L.B. And Arrambari, E.1993. Ice Load Distribution on a Faceted Cone Structure. *Proceed. of the POAC 93 Conference*, Vol. 2, pp 607-616, Humburg.

Wright, B. 2000. Full Scale Experience with Kullul Stationkeeping Operations in Pack Ice. *PERD/CHC Report*. pp. 25-44.

A METHOD AND TOOL FOR PREDICTING STATIC ICE LOADS ON DAMS

G. Comfort[1], A. Liddiard[1], R. Abdelnour[1]

ABSTRACT

An 11-year investigation was conducted regarding static ice loads on hydro-electric dams. Field measurements were made at 8 sites over a 9 year period. Algorithms were developed to predict ice loads along the length of the dam; and on stoplogs and gates. An environmental model was developed to predict ice thickness, snow depth, slush, and ice temperature. Ice temperature changes and thermal loading events were hindcasted for 73 stations in Manitoba, Ontario, and Quebec. An Ice Load Design Guide was made that: (a) synthesized the results, and; (b) established a statistical database which allowed loads to be calculated using a computer program for: (a) the long face of dam, and; (b) stoplogs. The measured loads show reasonable agreement with the predicted ones with respect to magnitude and return period.

INTRODUCTION AND SCOPE

Although dams have been built and operated for many years in northern regions, ice loads on them are not well understood. An 11-year investigation was conducted regarding:

(a) ice loads applied over a long face of a dam: large-scale ice loads are important for safety analyses for low-head (around 15 m) dams. Traditional ice load design values for dams are in the range of 150-225 kN/m, or 10-15 kips/ft. The ice load value can materially affect the results of stability analyses and the resulting need for dam rehabilitation works.

(b) the distribution along the dam – this is of concern for gates and stoplogs.

ICE LOAD MEASUREMENT AND ANALYSIS PROGRAM

Field measurements were made over 9 years, beginning in 1991-1992, at 9 sites in central and eastern Canada (Table 1). The highest loads (of 374 kN/m - 25 kips/ft) occurred at Manitoba Hydro's Seven Sisters dam. In addition, the ice loads exerted on piers, gates, and stoplogs were measured at two sites in Quebec and Manitoba for 2 and 3 years, respectively. Analytical work was done in parallel to develop models to calcu-

[1] BMT Fleet Technology Ltd., 311 Legget Drive, Kanata, Ont., Canada, K2K 1Z8
Tel.: 613-592-2830 ; Fax: 613-592-4950 ; email: gcomfort@fleetech.com

late: (a) ice loads on dams, stoplogs, gates, and piers, and; (b) ice environmental parameters.

Table 1. Maximum Ice Loads Measured Along the Dam Face

Case	Owner; Measurement Site & Yrs of Record	Maximum Load
Negligible Water Level Changes : Ice Loads Primarily Thermally- Generated	Hydro-Quebec; Paugan Dam (3 yrs)	70 kN/m (4.8 kips/ft)
	National Research Council; Basin (1 yr)	47 kN/m (3.2 kips/ft)
	Man. Hydro; Seven Sisters (1yr):1996-97	62 kN/m (4.2 kips/ft)
	Man. Hydro; Pine Falls Dam (2 yrs)	61 kN/m (4.1 kips/ft)
	Man. Hydro; McArthur Falls Dam (2 yrs)	85 kN/m (5.8 kips/ft)
Significant Water Level Changes Occur: Ice Loads Generated By Combination Of Ice Temperature And Water Level Changes	Ontario Power Gen.; Arnprior Dam (4 yrs)	210 kN/m (14.3 kips/ft)
	OPG; Otto Holden Dam - Main Reser – 3yrs	52 kN/m (3.5 kips/ft)
	- East Bay – 2 yrs	65 kN/m (4.4 kips/ft)
	Man. Hydro; Seven Sisters (4 yrs):1995-96	324 kN/m (22 kips/ft)
	1998-99	374 kN/m (25.6 kips/ft)
	Lab & Nfld Hydro; Churchill Falls (1yr)	89 kN/m (6.1 kips/ft)

Mechanisms Generating Ice Loads And Predictive Methods

The main load-generating mechanisms were found to be ice temperature and water level changes. This is a major finding of the work as previous methods for calculating ice loads on dams were based on the presumption that ice loads are solely thermally-generated. With distinct (but not excessive) water level changes, ice loads were much larger and more variable than purely thermal loads (Table 1). Separate ice load predictors were developed (e.g., Comfort et al, 2003) for:

(a) negligible water level changes: in this case, ice loads are generated thermally;

(b) "combined" thermal/water level regime: water level changes affect ice loads significantly.

Excessive water level changes constitute another case. However, because they break the ice sheet, which prevents the build-up of significant ice loads, load algorithms were not produced for this.

Another major finding of the work is that ice loads were found to be related to dam operating techniques, and that ice loads could be reduced by several times by a relatively large one-time drop in water level in early winter. This issue is not discussed further here due to page limits.

Environmental Modelling

A general environmental model was produced (Singh and Comfort, 1997; 1998) to predict the ice thickness, the snow cover depth, slush formation and freeze-up, and the ice temperature profile changes for each day of winter starting at freeze-up. The model has the following inputs: (a) the mean daily air temperature for each day of the winter; (b) the reservoir freeze-up date; (c) the accumulated snow on the ground at a nearby station; (d) the daily rainfalls over the winter, and; (e) the snow density over the winter. The model predicted the measured ice thicknesses, snow cover depths, and ice temperature profile changes at the Arnprior, Paugan, and Seven Sisters dams within about 10% on average.

ICE LOAD DESIGN GUIDE

Recently, an Ice Load Design Guide was produced, which is available from CEA Technologies Inc. (Comfort, Gong, Singh, Abdelnour and Liddiard, 2003). The work included hindcasting, probabilistic analyses, and computer program development. The

Design Guide synthesized the results of the project, and it established a statistical database that allowed ice loads to be calculated in a coherent format for:

(a) the long face of a dam for various locations, forebay operational regimes, return periods and confidence levels. These loads would be relevant for dam safety analyses;

(b) stoplogs for various designs (i.e., stoplog span, cross-section, and material, and; pier length) – due to page limits, this aspect of the Guide is not discussed here.

Ice Loads for Dam Safety Analyses: Thermal Loads

Thermal ice loads were hindcasted for 73 stations in Manitoba, Ontario, and Quebec, (Figure 1) for a total record length of 1773 station-years using:

(a) the environmental model produced previously (Singh and Comfort, 1997;1998);

(b) the thermal ice load algorithms produced previously (e.g., Comfort et al, 2003);

(c) input data for the environmental model (item a above) for all of the sites analyzed. The stations used for the analyses were all of the Environment Canada ones that were capable of providing the input data required to run the environmental model.
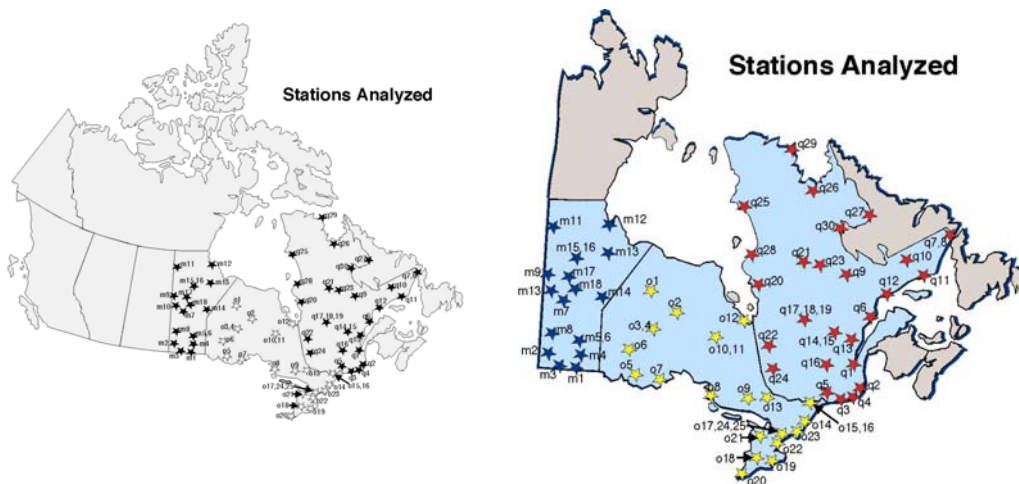
Fig. 1.   Stations Analyzed

The analyses predicted the snow cover, the slush thickness, the ice thickness, and the ice temperature profile area at each station for each day of each winter. Figure 2 shows a sample result for Inukjuak, Quebec, which is a northern site with little snowfall. The peak load occurred in late-winter as the ice warmed up due to the onset of spring.

Figure 3 shows a sample result for Dauphin, in southern Manitoba. It was affected by snowfalls in early-to-mid winter, which accumulated on top of the ice, eventually depressing the ice surface below water level, producing slush. Although the largest ice temperature changes occurred in mid-winter (before slush was formed), this did not produce the maximum load as the ice was thin. (The thermal ice load was found to be strongly related to the ice thickness and also, the change in ice temperature profile area - Comfort et al, 2003). The peak load occurred in late-winter despite lower ice temperature changes then, owing to the thicker ice present at that time.
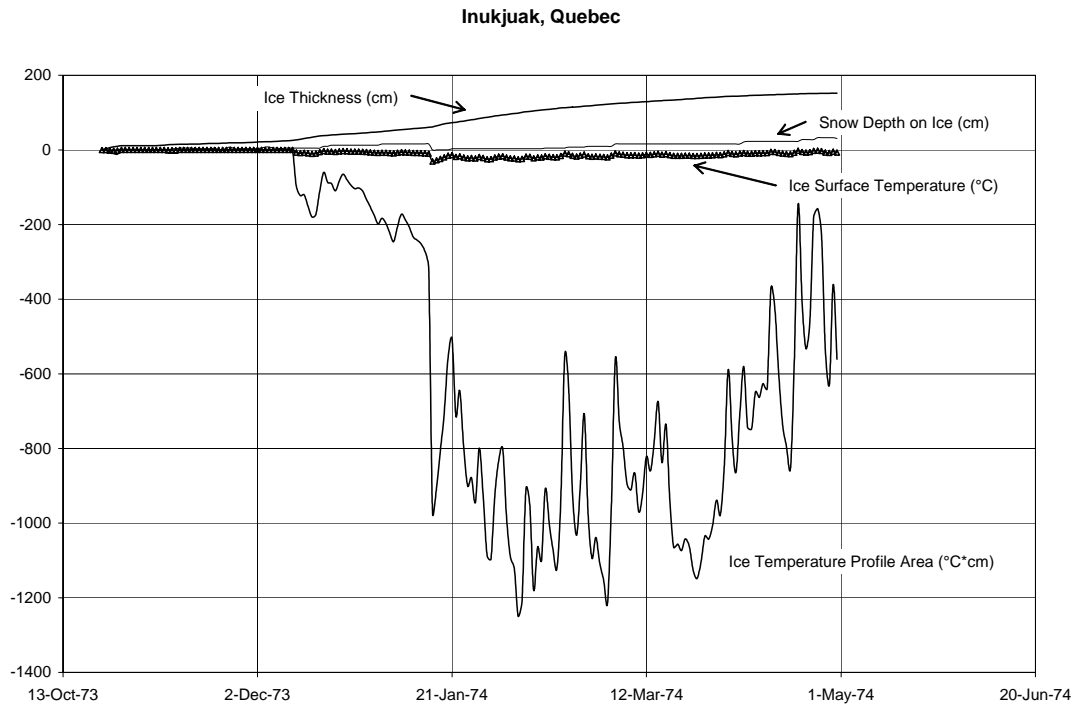
Inukjuak, Quebec

Fig. 2. Sample Hindcasting Result for Inukjuak, Quebec: 1973-1974
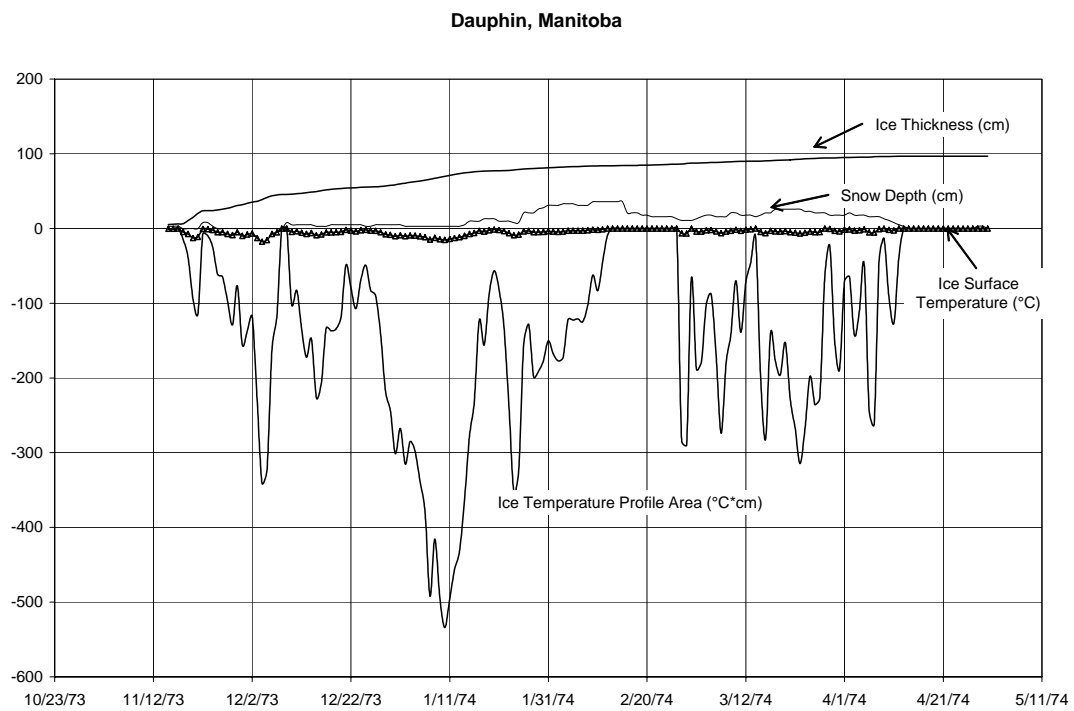
Dauphin, Manitoba

Fig. 3. Sample Hindcasting Result for Dauphin, Manitoba: 1973-1974

The annual maximum thermal ice load was determined for each station and year. These were ranked to form a distribution of annual maxima for each site (Figure 4). The normal, lognormal, Gumbel, and Log-Pearson Type III distributions were then checked for

goodness-of-fit to the hindcasted ice load distribution. A database was established with the best-fit distribution and the fit parameters for each station. This was later used in the Ice Load Calculation Program.

Trend analyses showed that the annual maximum thermal load:

(a) generally increased with the ice thickness and the number of freezing degree days

(b) was affected by the geographic location – although lower ice loads were predicted for more southern locations in general, ice load analyses needed to be as site-specific as possible. Reliable results could not be obtained by, for example, sub-dividing each province into geographic regions, and developing ice load statistics for each region.
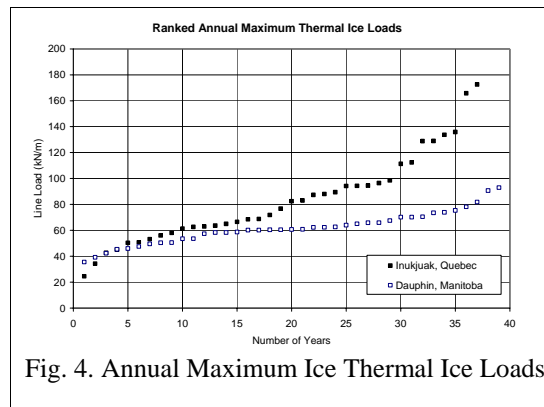
Fig. 4. Annual Maximum Ice Thermal Ice Loads
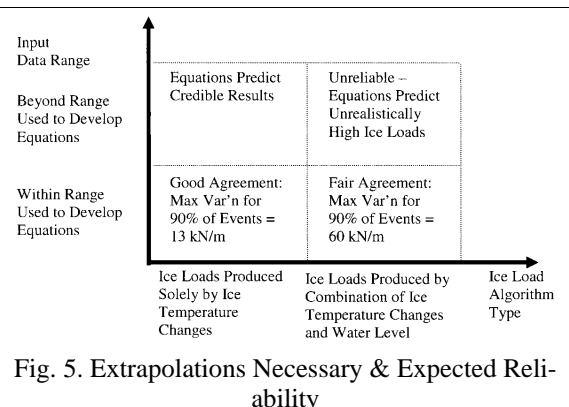
Fig. 5. Extrapolations Necessary & Expected Reliability

The hindcasting exposed the environmental model and the thermal load algorithms to cases beyond the data range used to develop them. It is believed that the thermal algorithms can be reliably extrapolated (Figure 4) as the results were credible over the full range of the hindcasting.

Loads Produced by a Combination of Water Level and Ice Temperature Changes

These loads depend on both the thermal loads (which are controlled by environmental conditions), and on water level change parameters (which are controlled by the dam operator). Previous analyses (e.g., Comfort et al, 2003) showed that "combined" loads were affected by: (a) water level change magnitudes, and; (b) mean water level changes. The distribution of annual maximum ice loads was determined for twelve cases of water level change amplitude and mean level change for all 73 stations.

The hindcasting analyses exposed the ice load algorithms to cases that were beyond the range of the available field data (which were used as a basis for developing them), and that the ice load algorithms predicted unrealistically high loads in these cases. It was concluded that the ice load algorithms for the "combined" case could not be reliably extrapolated beyond their development range (Figure 5). As a result, the dataset of annual maxima used for probabilistic analyses for "combined" loads was limited to years where all of the input parameters were within the development range of the ice load equations. This reduced the data set of annual maxima for "combined" loads, compared to purely thermal loads, which caused the predicted "combined" loads to be less reliable. Nevertheless, the analyses allowed "combined" ice loads to be determined for all 73 stations. As was done for the purely thermal loads, a database was established that contained the best-fit distribution and the fit parameters for each station. This database was later used in the Ice Loads Calculation Computer Program.

Trend analyses were conducted with respect to geographic location. As for the purely thermal loads, the ice load for the combined case increased with the ice thickness. The combined loads correlated well among stations in Manitoba, Ontario and Quebec on the basis of ice thickness.

As expected, alternative treatments of outliers produced ice load variations. The method used in the model resulted in less variation among stations with similar ice thickness for the larger loads.

LOAD CALCULATIONS FOR DAM SAFETY ANALYSES

Operating zones were mapped where water level changes are, and are not, significant (Figure 6):

(a) thermal regime – loads produced solely by ice temperature changes;

(b) combined regime – loads produced by a combination of water level and ice temp. changes;

(c) transition regime (between the thermal and the "combined" regimes).

To maintain consistency, loads were never allowed to fall below the "pure" thermal value, even though large water level changes would break the ice and produce hinge cracks, causing lower loads. The analyses did not include the effects of: (a) reservoir geometry; (b) a one-time water level drop; (c) a steady reservoir drawdown, and; (d) unsteady forebay fluctuations. Despite this, the method produced credible results in relation to the data (described subsequently).

The analyses showed that high ice loads are only generated in a relatively small zone of water level change parameters (Figures 7 to 9), as follows: (a) water level change amplitude: about 10-20 cm; (b) change in mean water level: nil, and; (c) time required for the water level to go from a minimum to a maximum value: about 0.5 – 1 day. The ice loads diminished rapidly for larger amplitudes, changes in mean level, and time periods.

DETAILED COMPARISONS WITH THE MEASURED LOADS

It is of interest to compare the loads predicted by the model with the measured values. The model was run for the following stations, which are closest to the respective measurement sites:

(a) Gimli, Manitoba – presumed to be representative of the Seven Sisters dam, the Pine Falls dam, and the MacArthur Falls dam;

(b) North Bay, Ontario - presumed to be representative of the Otto Holden dam;

(c) Ottawa, Ontario - presumed to be representative of the Paugan and Arnprior dams.

There is reasonable correlation between the predicted and measured values (i.e., load magnitudes and return periods) in relation to the length of record obtained at each dam site (Table 2). The model tended to indicate that the measured loads were slightly extreme as the predicted return periods for the maximum measured loads usually exceed the actual length of record. However, the model indicated that the maximum measured loads at Seven Sisters (which were the highest in the whole project) were quite extreme in relation to the record length (Table 2).
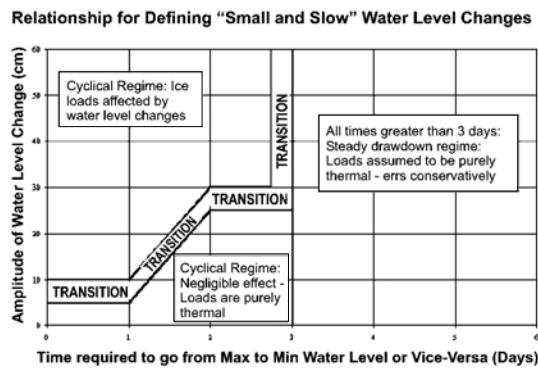
Fig. 6. Definition for Significant Water Level Changes
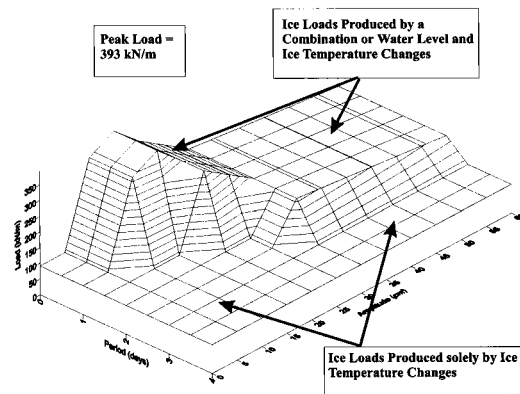
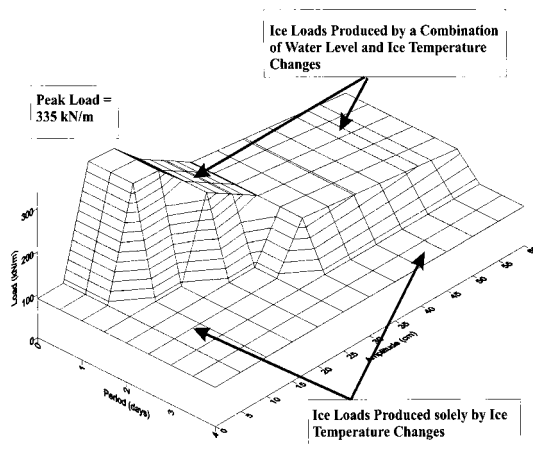Fig. 7. 1000-Year Ice Loads for North Bay, Ont.: No Change in Mean Water Level

Fig. 8. 1000-Year Loads for North Bay, Ont.: Mean Water Level Change = 20 cm
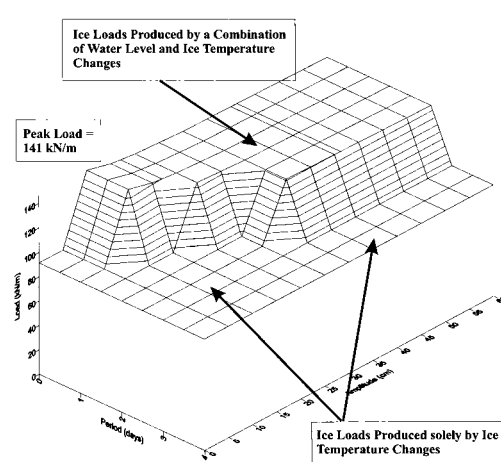

Fig. 9. 1000-Year Loads for North Bay, Ont.: Mean Water Level Change = 40 cm

COMPUTER PROGRAM DEVELOPMENT

An Ice Load Calculation Program was developed in MS Excel (Figure 10). It operates as a database program using the station locations and the fitted load distributions for each one. The Program outputs ice loads for user-specified: (a) locations in Manitoba, Ontario, and Quebec; (b) "zones" of interest for which stations are expected to provide ice load information that is relevant to the site location under consideration; (c) water level change parameters, and; (d) return periods and confidence levels.

102

Table 2. Detailed Comparisons with the Measured Loads

Case: Ice Loads Generated By Ice Temperature Changes Only					
Dam	Maximum Measured Load (kN/m)	Years of Monitoring	Predicted Return Period (yrs) for Maximum Measured Load	Predicted 100-Year Ice Load (kN/m)	Predicted 1000-Year Ice Load (kN/m)
Paugan	70	3	20	81	95
Pine Falls	61	2	2	105	117
MacArthur Falls	85	2	7	105	117
Seven Sisters	62	1	2	105	117
Case: Ice Loads Generated by Both Ice Temperature and Water Level Changes					
Dam	Maximum Measured Load (kN/m)	Years of Monitoring	Predicted Return Period (yrs) for Maximum Measured Load	Predicted 100-Year Ice Load (kN/m)	Predicted 1000-Year Ice Load (kN/m)
Arnprior	210	4	43	264	382
7 Sisters (98-99)	374	4	97	393[1]	494[1]
7 Sisters (95-96)	324	4	24	397[1]	499[1]
Otto Holden	62	3	2	140	182

1: The 100-yr & 1000-yr loads for 98-99 & 95-96 differ due to variations in the water level amplitude and mean water level change for each year.

Fig. 10. Ice Loads Calculation Program: Input Screen for Calculating Ice Loads
for Dam Safety Analyses

103

CONCLUSIONS

Progress has been made towards understanding ice loads on dams. An extensive set of field data has been obtained. Equations have been developed to predict ice loads. The project has shown that water level changes affect ice loads significantly. Distinct (but not excessive) water level changes produced loads that were much larger and more variable than "pure" thermal loads.

An Ice Load Design Guide was produced that synthesized the results of the project, and established a method for calculating ice loads for: (a) the long face of a dam for various locations, water level change operational regimes, return periods and confidence levels, and; (b) stoplogs for various designs. The predicted loads compare reasonably with the measured ones.

REFERENCES

Comfort, G., Gong, Y. and Liddiard, A., 2003, Static Ice Loads on Dams, *Proc. ICOLD*, Montreal.

Comfort, G., Gong, Y., Singh, S., Abdelnour, R. and Liddiard, A., 2003, Static Ice Loads On Hydro-Electric Structures: *Summary Report; Ice Load Design Guide*, and; Ice Load Prediction Computer Program, *CEATI Report*. T002700-0206.

Singh, S., and Comfort, G., 1997, Static Ice Loads on Hydro-Electric Structures: Environmental and Probabilistic Analyses of Thermal Loads, CEA EG 910012.

Singh, S., and Comfort, G., 1998, Expected Thermal Ice Load in Reservoirs, *IAHR Conference*, Potsdam, NY.

DYNAMICS OF ELEMENTS OF HYDROTECHNICAL STRUCTURES (HTS) INTERACTING WITH ICE COVERING

Kozlov D.V., Sabodash P.F.[1]

ABSTRACT

Mathematical models of physical processes showing interaction of the ice cover with HTS elements have been built. Succession of stages of the work is as the following chain: physical representations – mathematical models – their realization.

The following is considered as HTS elements:

1. The vertically located circular cylinder frozen into the ice cover on the side surface of which the plane front of the monochromatical flexural wave falls spreading in the ice cover.

2. The immersed into water vertical pile the lower end of which is rigidly fixed into the ground foundation perceiving a side impact of the ice floe floating on the water surface.

3. The slope of the ground dam on the inclined surface of which a floating ice floe surges.

The impact dynamic ice load values necessary for exact prediction of strength, stability and reliability of HTS elements are rounded off.

1. WAVE ICE LOADING ON THE VERTICAL CYLINDER FROZEN INTO ICE

Let's consider the task concerning deformation of the ice cover frozen to the rigid cylinder surface. Ice movement in the vicinity of the structure surface leads to the appearance of moments of flexure and transverse forces acting from the ice cover side on the cylinder surface.

In the work the linear mathematical model is built for rounding off values of ice wave loading on the side surface of the hard circular cylinder of radius R to the surface of which the ice field not limited in the plan is frozen and which lies on the water surface in deep depths. Water properties are determined by the density ρ_w and transmission speed of wave compression $\tilde{N}_w$ in it.

Let's suppose that in the ice cover from "infinity" a plane monochromatic wave of transverse flexure is transmitting due to the action of impact or blast loading on ice far from the structure. Propagating along the axis *X* in the ice cover the plane front of the flexural wave is parallel to the generatrix of the cylindrical structure (Fig.1). After reaching the side surface the process of flowing around the structure begins – diffraction of elastic wave in the ice cover. As the cylinder is frozen into ice, the transverse movement of the frozen-in field causes transverse forces and flexural moments affecting from the side of the ice floe on the cylinder surface.
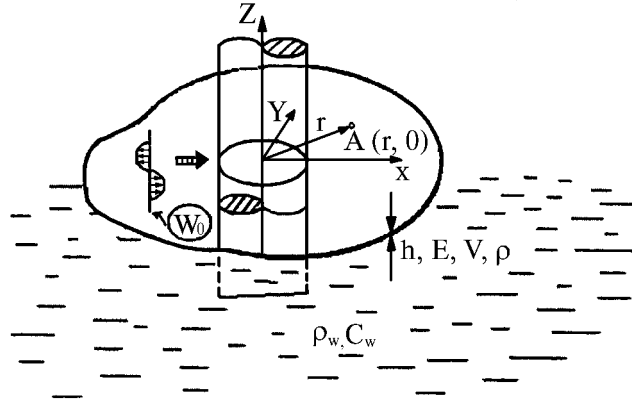
Fig. 1.

The ice cover of large sizes in the plan is modeled by a thin elastic plate the material properties of which are characterized by density ρ, coefficient of elasticity *E*, Poison's ratio v, *h* – constant thickness of the plate (visco-plastic properties of ice are not taken into consideration).

Transverse (flexural) oscillations of the ice plate supposing that the wave length of flexure λ is much longer than its thickness ($\lambda \gg h$) in variables *x, y, t* are described accurately enough by the linear homogenous quartic equation with constant coefficients

$$D\left[\frac{\partial^4 W(x,y,t)}{\partial x^4} + 2\frac{\partial^4 W(x,y,t)}{\partial x^2 \partial y^2} + \frac{\partial^4 W(x,y,t)}{\partial y^4}\right] + \rho h\frac{\partial^2 W(x,y,t)}{\partial t^2} + \rho_w C_w\frac{\partial W(x,y,t)}{\partial t} = 0,$$

$$-\infty < x, y < +\infty, D = Eh^3 \Big/ 12(1-v^2)$$

(1)

In this equation the influence of water under ice is taken into consideration in the left part. As a matter of fact this influence is equivalent to the external viscosity. It is supposed that deformation of the ice plate proceeds in such a way that the continuous contact with the water surface remains even under the plate bulging.

For ice cover prevention the following condition of dynamic strength is used

$$\sigma_i \leq \sigma_B,$$

(2)

where σ_i means the intensity of stresses in the plate $\sigma_i = \sqrt{\sigma_x^2 + \sigma_y^2 - \sigma_x\sigma_y + 3\tau^2_{xy}}$ and σ_B – breaking strength of the ice plate (it is determined experimentally).

The equation $\sigma_i = \sigma_B$ means the marginal state of the ice cover.

Let's suppose that in the ice plate a plane monochromatic wave of the transversal flexure (Fig.1) is spreading. Let's assign an amplitude of transverse movements of ice particles in this wave by the following dependence

$$W' = W_{dec} = W_0 e^{i(\alpha x - \omega t)} = W_0 e^{-i(\omega t - \alpha x)}, i = \sqrt{-1} , \tag{3}$$

where W_0 – the amplitude of the flexural wave transmitting in the plate, ω – the frequency of oscillations, α – meanwhile the arbitrary parameter.

The last expression shall meet the equation of transverse oscillations of the ice plate from here we can find the following expression parameter α

$$\alpha = \left[\left(\rho h \omega^2 + i \rho_w \tilde{N}_w \omega\right) D^{-1}\right]^{1/4} . \tag{4}$$

The internal force factors in the plate are expressed as follows

$$M'_x = -D \frac{\partial^2 W'}{\partial x^2} = M_0 e^{i(\alpha x - \omega t)}, M_0 = DW_0 \alpha^2 ,$$

$$Q'_x = Q_0 e^{i(\alpha x - \omega t)}, \quad Q_y \equiv 0; \quad Q_0 = i\alpha M_0 ,$$

$$M'_y = -Dv \frac{\partial^2 W'}{\partial y^2} = -v M'_x, \quad M'_{xy} \equiv 0, \quad Q'_x \equiv -D \frac{\partial^3 W'}{\partial x^3} = -i\alpha^3 Dv_0 e^{i(\alpha x - \omega t)}. \tag{5}$$

Here M_0 and Q_0 are maximal values of the flexural moment and lateral force in the ice plate caused by the passing flexural wave in the plate when there is no hydrotechnical structure in the ice cover. In the explicit way parameter α is calculated as follows

$$\sqrt[n]{a + ib} = \sqrt[n]{a^2 + b^2} \left[\cos\left(\frac{\varphi + 2k\pi}{n}\right) + \sin\left(\frac{\varphi + 2k\pi}{n}\right) \right], k = 0,1,2...; n = 4,$$

$$\varphi = arctg\left(\frac{\rho_w \tilde{N}_w}{\rho h \omega}\right),$$

$$\alpha = D^{-1/4}\left(\rho h \omega^2 + i \rho_w \tilde{N}_w \omega\right)^{1/4} = D^{-1/4} \sqrt[4]{\left(\rho h \omega^2\right) + \left(\rho_w \tilde{N}_w \omega\right)^2} \cdot \left[\cos\left(\frac{\varphi}{4}\right) + i\sin\left(\frac{\varphi}{4}\right)\right],$$

$$\beta_1 = D^{-1/4} \sqrt[4]{\left(\rho h \omega^2\right)^2 + \left(\rho_w \tilde{N}_w \omega\right)^2} \cos\left(\frac{\varphi}{4}\right),$$

$$\beta_2 = D^{-1/4} \sqrt{\left(\rho h \omega^2\right)^2 + \left(\rho_w \tilde{N}_w \omega\right)^2} \sin\left(\frac{\varphi}{4}\right). \tag{6}$$

Taking into account the above results the amplitude of the damped incident flexural wave can be presented as follows:

$$W' = W_0 e^{-\beta_2 x} e^{i(\beta_1 x - \omega t)}. \tag{7}$$

The analysis of the last dependence visually demonstrates the role of water as a factor damping oscillations in the process of their spreading. Absence of water ($\rho_w \tilde{N}_w = 0$) means, that $\beta_2 = D^{-1/4}(\rho_w \tilde{N}_w \omega^2)^{1/2}$, $\varphi \equiv 0, \beta_2 \equiv 0$. In this case the flexural wave is transmitting without damping and under $\omega = 0$ we receive a static task. The front of the incident flexural wave reaches the cylinder generatrix at the moment of time $t_0 = \alpha R / \omega$.

Then at $t > t_0$ there a process of the wave repulse from the curvilinear surface of the obstacle takes place.

Deformation of the ice plate in the repulsed wave should be described in the polar coordinates r, θ (Fig. 1). These coordinates are connected with certain Cartesian

dependencies $x = r\cos\theta$, $y = r\sin\theta$, $R < r < \infty$, $0 < \theta \le 2\pi$, $\pi = 3,14$. In polar coordinates linear transverse oscillations of the ice plate are described by the following differential quatic equation with floating factors:

$$D\left(\frac{\partial^4 W}{\partial r^4} + \frac{1}{r^4}\frac{\partial^4 W}{\partial \theta^4} + \frac{2}{r^2}\frac{\partial^4 W}{\partial r^2 \partial \theta^2} - \frac{2}{r^3}\frac{\partial^3 W}{\partial r \partial \theta^2} + \frac{2}{r}\frac{\partial^3 W}{\partial r^3} + \frac{4}{r^4}\frac{\partial^2 W}{\partial \theta^2} - \frac{1}{r^2}\frac{\partial^2 W}{\partial r^2} + \frac{1}{r^3}\frac{\partial W}{\partial r}\right) +$$

$$+ \rho h \frac{\partial^2 W}{\partial t^2} + \rho_w \tilde{N}_w \frac{\partial W}{\partial t} = 0. \qquad (8)$$

In a special case when derivatives on the angular coordinate are absent, from the equation (8) we receive a differential equation of neo-axis-symmetrical transverse oscillations of the ice plate.

Internal force factors in sections $r = const, \theta = const$ are expressed by the following formulas:

$$M_r = -D\left[v\nabla^2 W + (1-v)\frac{\partial^2 W}{\partial r^2}\right], \; M_\theta = -D(1+v)\nabla^2 W - M_r,$$

$$M_{r\theta} = D\left[(1-v)\frac{1}{z}\frac{\partial}{\partial \theta}\frac{\partial W}{r} - \frac{W}{r}\right], \; Q_r = -D\frac{\partial}{\partial r}(\nabla^2 W), \; Q_\theta = -D\frac{1}{r}\frac{\partial}{\partial \theta}(\nabla^2 W),$$

$$\sigma_r = \frac{6M_r}{h^2}; \; \sigma_\theta = \frac{6M_\theta}{h^2}, \; \tau_{r\theta} = \frac{6M_{r\theta}}{h^2}, \; (9) \qquad \sigma_i = \sqrt{\sigma_r^2 + \sigma_\theta^2 - \sigma_{r\theta} + 3\tau_{r\theta}^2}. \qquad (9)$$

The equation $\sigma_i = \sigma_B$ gives the condition of failure of the ice plate.

When formulating boundary conditions we proceed from the fact that various regimes of contact interaction of the moving ice cover are possible from the side surface of the cylindrical structure. Let's consider the case when the structure is inside a circular cutting of R radius in the ice cover and regelation of the side surface with the ice edge has taken place (fast ice). In this case on the contact surface boundary conditions of rigid fixing are fulfilled

$$W(r,\theta,t) = 0, \; \frac{\partial W(r,\theta,t)}{\partial r} = 0, \; r = R, 0 < \theta < 2\pi. \qquad (10)$$

On the infinity at $r \to \infty$ parameters of the scattered elastic field in the ice plate satisfy the conditions of "radiation".

$$W \to 0, \qquad \partial W/\partial r \to 0, \quad r \to \infty. \qquad (11)$$

Besides, the solution of the edge neo-axis-symmetrical task should have a property of periodicity on the angular coordinate

$$W(r,\theta,t) = W(r,\theta + 2\pi, t), \qquad R < r < \infty. \qquad (12)$$

If the lateral contour of the structure is free from connections with the ice cover the boundary conditions on the free contour are presented in the following way:

$$M_r = 0, \qquad Q + \frac{\partial M_{r\theta}}{r\partial \theta} = 0, \qquad r = R \qquad 0 < \theta < 2\pi. \qquad (13)$$

After repulsing the flexural wave from the structure additional elastic stresses are created in the ice cover. Diffraction flexural waves are described by the differential equation (8). The general solution of this equation (Arfken, 1970) expressed through

four arbitrary constants of integration A_n, B_n, C_n and D_n is expressed as the following infinite series on the cylindrical functions

$$W''(r,\theta,t) = \sum_{n=0}^{\infty}\left[A_n H_n^{(1)}(\alpha r) + B_n N_n(\alpha r) + C_n I_n(\alpha r) + D_n K_n(\alpha r)\right]\cdot\cos(n\theta)e^{-i\omega t}, \quad (14)$$

where $H_n^{(1)}(\alpha r) \equiv I_n(\alpha r) + N_n(\alpha r)$ -Hankel function, $N_n(\alpha r)$ -Neiman function, $I_n(\alpha r), K_n(\alpha r)$ - Bessel functions of imaginary argument. Owing to the condition of amplitudes damping at $r \to \infty$ the constants B_n, C_n should be taken as equal to zero. Two constants of integration A_n, D_n are determined from two boundary conditions (10). First for their determination let's break the field of the incident plane wave into infinite series on Bessel functions

$$e^{i\beta x} = e^{i\beta r\cos\theta} = \sum_{n=0}^{\infty}E_n(i)^n I_n(\beta r)\cos(n\theta), \; E_n = \begin{cases} 1 \; npu \; n = 0 \\ 2 \; npu \; n > 0 \end{cases}. \quad (15)$$

Let's write the expression for the incident flexural wave in the plane in the following form

$$W' = W_0 \cdot \sum_{n=0}^{\infty}E_n(i)^n I_n(\alpha r)\cos(n\theta)e^{-i\omega t}, \qquad i = \sqrt{-1}. \quad (16)$$

Due to the linearity of the hydraulic elastic task full transversal displacement of the circular plane points is determined by means of the superposition in the incident and repulsed wave.

$$W(r,\theta,t) = W'(r,\theta,t) + W''(r,\theta,t), R < r < \infty, 0 < \theta \leq 2\pi. \quad (17)$$

The full field of flexural displacements in the ice plate is expressed by the following formula:

$$W(r,\theta,t) = \left\{W_0\sum_{n=0}^{\infty}E_n(i)^n I_n(\alpha r) + \sum_{n=0}^{\infty}\left[A_n H_n^{(1)}(\alpha r) + D_n K_n(\alpha r)\right]\right\}\cos(n\theta)e^{-i\omega t}. \quad (18)$$

The turning angle of the cross section $r = const$ is expressed by the dependence

$$\frac{\partial W}{\partial r} = \alpha\left\{W_0\sum_{n=0}^{\infty}E_n(i)^n I_n'(\alpha r) + \sum_{n=0}^{\infty}\left[A_n H_n'^{(1)}(\alpha r) + D_n K_n'(\alpha r)\right]\right\}\cos(n\theta)e^{-i\omega t}. \quad (19)$$

The boundary conditions of the rigid joint on the side surface of the cylinder (10) result in the system of two linear algebraic equations for finding two target coefficients A_n and D_n

$$A_n H_n^{(1)}(y) + D_n K_n(y) = -W_0 E_n(i)^n I_n(y), \qquad y = \alpha R$$

$$A_n H_n'^{(1)}(y) + D_n K_n'(y) = -W_0 E_n(i)^n I_n(y), \qquad n = 0,1,2\ldots \quad (20)$$

The explicit formulas which determine the coefficients A_n and D_n assume the following form

$$A_n = \frac{\beta_n\left[I_n'(y)K_n(y) - I_n(y)K_n'(y)\right]}{\Delta_n(y)}, \quad D_n = \frac{\beta_n\left[H_n'^{(1)}(y)I_n(y) - H_n^{(1)}(y)I_n'(y)\right]}{\Delta_n(y)}$$

$$\Delta_n(y) \equiv H_n^{(1)}(y)K_n'(y) - H_n'^{(1)}(y)K_n(y). \quad (21)$$

Equality to zero of the identifier $\Delta_n(y)$ leads to the frequency equation determining resonant frequencies of oscillations of the ice plate. The transcendental equation $\Delta_n(y) = 0$ has an endless spectrum of frequencies of own oscillations.

As an example let's consider the following initial data of the hydraulic elastic system:

$$\rho = 900 \frac{kg}{m^3}, \quad \rho_w = 1000 \frac{kg}{m^3}, \quad E = 52 \cdot 10^3 \, P\grave{a} \text{ at the temperature } -10^\circ \, C, \, v = 0.3, \, h = 0.5m,$$

$$C_w = 1500 \frac{m}{s}, \quad \sigma_\rho = 198 \cdot 10^4 \, Pa, \omega = 0.1s^{-1}.$$

Then in the frontal point $\theta = \pi$ of the circular contour $r = R$ we receive the following ice loading on the cylinder surface $\left| \dfrac{M_r(R, \theta = \pi)}{M_0} \right| = 1.87$, $\left| \dfrac{Q_r(R, \theta = \pi)}{Q_0} \right| = 1.23$. (22)

The results expressed by these dependencies show that for prevention from destruction of HTS frozen into ice it is necessary first of all to take into consideration the moments acting on the structure surface from the ice cover side (when ice is rigidly fasted to the cylinder surface). The longitudinal efforts Q_r on the surface $r = R$ are of less importance. The dynamic strength of the ice cover is determined by the strength condition $\sigma_i \leq \sigma_B \quad R = 0, \; 0 < \theta < 2\pi$.

A more complicated task of determination of ice loading on side surfaces of the system of the vertically located cylinders frozen into the ice field when it is necessary to take into consideration conditions of interaction of all cylinders on the surface of the given one is decided similarly how it was done with the single cylinder.

2. THE FLOATING ICE FLOE TRANSVERSE IMPACT ON THE END OF A SEPARATELY LOCATED PILE

A linear mathematical model has been built on determination of the stress - deformed state (SDS) of a detached reinforced concrete tubular pile vertically located in the plane – parallel water layer. The ice floe floating on the surface strikes a blow on the upper part of the pile (Fig. 2). The logically substantiated assumption is assumed that the impact speed of the ice floe V_0 coincides with the flow current on the water surface.

The proposed linear hydraulic elastic model on the impact interaction of the floating ice floe with a part of the reinforced concrete pile comes to integration of the linear differential quartic equation

$$EI \frac{\partial^4 W}{\partial Z^4} + H\rho_w \tilde{N}_w \frac{\partial W}{\partial t} + \rho A_0 \frac{\partial^2 W}{\partial t^2} = 0 \ldots\ldots 0 < Z < H, t > 0. \quad (23)$$

Here $W(Z, t)$ – horizontal movement of the pile points, E – modulus of elasticity of its material, ρ – its density, H – pile height, A_0 – square of the pile cross section. I – moments of inertia of the pile cross section square, ρ_w – water density, C_w – sound speed in it.

The current time $t > 0$ will be calculated from the moment $t = 0$ of the first touching of the striking floe on the pile end $Z = H$. In the points of the lower squeezed end usual boundary conditions of rigid finishing are carried out there.

$$W(Z,t)\big|_{Z=0} = 0; \qquad \frac{\partial W(Z,t)}{\partial Z}\bigg|_{Z=0} = 0, \qquad \forall t \geq 0. \qquad (24)$$
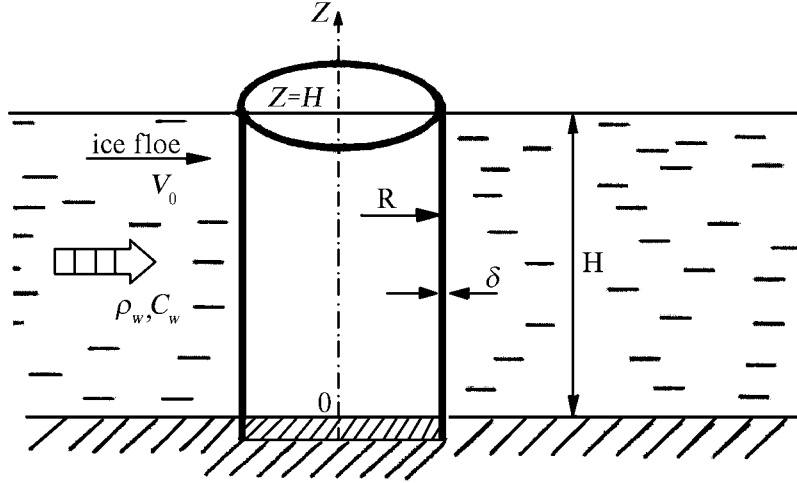

Fig. 2.

The striking floe is under continuous contact with the pile during a small interval of time $0 < t < \tau$; under $t > \tau$ there happens separation (rebound) of the ice floe from the pile surface. At the initial stage the upper end of the cylindrical pile $Z=H$ and the adherent floe of mass M move jointly which is described by the differential equation of the Newton second law (the ice floe is modeled by the point mass)

$$M\frac{\partial^2 W}{\partial t^2}\bigg|_{Z=H} = -Q, \qquad Q = EI\frac{\partial^3 W}{\partial Z^3}, \quad 0 < t < \tau, \qquad (25)$$

where Q – transverse force in the pile at $Z=H$. The second boundary condition on the end $Z=H$ comes to the equality to zero of the flexural moment in the pile.

$$M(Z,t)\big|_{Z=H} = 0, \qquad M(Z,t) \equiv EI\frac{\partial^2 W}{\partial Z^2}, \quad 0 < t < \tau, \qquad (26)$$

After the ice floe rebounding the top end $Z=H$ remains free i.e. the boundary conditions will be equations $Q = M = 0$ on the end $Z=H$. The following initial conditions are true

$$W(Z,t)\big|_{t=0} = 0, \quad 0 \leq Z \leq H \,; \frac{\partial W(Z,t)}{\partial t}\bigg|_{t=0} = 0, \quad 0 \leq Z < H;$$

$$\frac{\partial W(Z,t)}{\partial t}\bigg|_{t=0} = V_0, \quad Z = H \,. \qquad (27)$$

The linear edge task will be decided by the method of one-sided Laplace transformation on the time t with the parameter s:

$$\bar{f}(s) = \int_0^\infty f(t)e^{-st}dt, \operatorname{Re}s > 0. \qquad (28)$$

In the space of images according to Laplace we receive an edge task for the ordinary differential quartic equation with constant coefficients

$$EI\frac{d^4\overline{W}}{dZ^4} + s\left(H\rho_w\tilde{N}_w + \rho A_0 s\right), \overline{W} = 0......0 < Z < H \,, \qquad (29)$$

111

under following edge conditions

$$\overline{W}(Z,s)\big|_{Z=H} = 0, \quad \frac{d\overline{W}}{dZ}\big|_{Z=0} = 0, \quad \varepsilon = M(\rho A_0 H)^{-1},$$

$$\frac{d^2\overline{W}}{dZ^2}\big|_{Z=H} = 0; \quad \left[\frac{d^3\overline{W}(Z,s)}{dZ^3} + s^2\overline{W}(Z,s)\frac{\varepsilon}{EI}\right] = \frac{\varepsilon}{EI}V, \tag{30}$$

where the non-dimensional parameter ε $(\varepsilon > 0)$ means a relation of the striking ice floe mass M to the pile mass $\rho A_0 H$.

Let's write the equation (29) in a more compact form

$$\frac{d^4\overline{W}}{dZ^4} + 4k^4\overline{W} = 0, \quad k = \left[\frac{s}{4}(H\rho_w\tilde{N}_w + \rho A_0 s)(EI)^{-1}\right]^{1/4}. \tag{31}$$

The system of fundamental solutions of the last equation assumes the following form

$$\varphi_1(Z) = ch(kZ)\cos(kZ); \qquad \varphi_2(Z) = ch(kZ)\sin(kZ)$$
$$\varphi_3(Z) = sh(kZ)\cos(kZ); \qquad \varphi_4(Z) = sh(kZ)\sin(kZ), \tag{32}$$

here $ch(kZ)$, $sh(kZ)$ – hyperbolic cosines and sinus.

Due to the linearity of the task the general decision of the homogenous equation (31) can be presented in the form of superposition of particular solutions $\varphi_i(Z)$, $i = 1,4$

$$\overline{W}(Z,s) = C_1\varphi_1(Z) + C_2\varphi_2(Z) + C_3\varphi_3(Z) + C_4\varphi_4(Z) = \sum_{i=1}^{4} C_i\varphi_i(Z). \tag{33}$$

Satisfying the boundary conditions on the pile ends $Z=0$ and $Z=H$ we receive the following system of four algebraic equations for determination of four constants C_i

$$AX = B, \quad A = a_{ij}, \quad X = (C_1, C_2, C_3, C_4)^{tz}, \quad B = (b_1, b_2, b_3, b_4)^{tz}. \tag{34}$$

The solution for arbitrary constants is received in the explicit form $C_i = \Delta_i(\Delta)^{-1}$, $\Delta = |a_{ij}|$. Thus in the space of images the exact solution has been built.

Inversion on s we will carry out numerically (Krylov and Skoblja, 1974) under high values s $(s \to \infty)$ Such solution is of great interest in impact-wave tasks as impact processes are quite short in time $0 \le t \le (10^{-2} \div 10^{-3})c$. Particular cases $\varepsilon \ll 1$; $\varepsilon \gg 1$, $\varepsilon = 1$ are considered separately. If in the determinant $K = i\omega$, the equality $\Delta = 0$ represents a transcendental equation relative to the frequency of the pile oscillations in water.

$$M\omega^2[sh(kH)\cos(kH) - ch(kH)\sin(kH)] - k^3EI[1 + ch(kH)\sin(kH)] = 0. \tag{35}$$

After the striking floe separation from the pile, the latter fulfills free oscillations and the frequency equation (35) is significantly simplified $(M = 0)$: $ch(kH)\sin(kH) + 1 = 0$. The roots of this equation are a numerical succession $k_1H = 1,875$; $k_2H = 4,694$;

$$k_nH = \frac{2n-1}{2}\pi.$$

For frequencies of free oscillations of the console pile in water we receive the following values

$$\omega_1 = \lambda \left(\frac{1,875}{H}\right)^2, \ \omega_2 = \lambda \left(\frac{4,694}{H}\right)^2, \ \lambda = \left(\frac{EI}{\rho A_0 + x}\right)^{1/2}, \ x = \frac{\rho_w \tilde{N}_w}{\rho C}, \ C = \sqrt{E/\rho}. \quad (36)$$

Water availability decreases frequencies of the pile oscillations; at $\rho_w \ C_w = 0$ we receive frequencies of the pile oscillations in air. Numerical results were received for the following values of the initial data $V_0 = 2.5 m/s$, $H = 10 m$, $M = 1000 kg$, $\delta = 0.2 m$ (the wall thickness of the tubular pile), $\rho = 1800 kg$, $\rho_w = 1000 kg$, $C_w = 1500 m/s$, $E = 3.4 MPa$. The curves in Fig.3 show the forms of transverse oscillations of the pile at the fixed moment of time for frequencies cases a), b) and c) relatively. Figure 1 illustrates oscillations in water; oscillations in air are marked by figure 2.
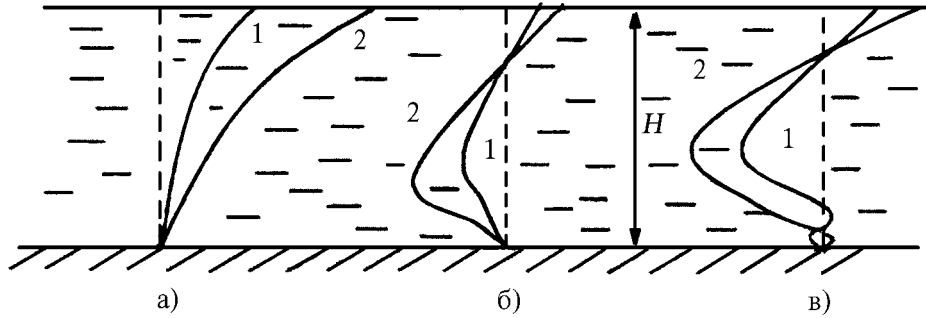
Fig. 3.

The dynamic stability of the pile to overturning is estimated on the basis of the expression for the overturning moment calculated relatively to the lower end squeezed into the ground $Z=0$.

Changing of the impact contact ice load on the pile in time is shown by the curve in Fig.4. The ice load achieves its maximal value at the moment of time $t=0.08s$; the duration of impact $t=0.15s$ (after that there happens rebound of the ice floe). Forced and free oscillations of the pile end $Z=H$ are illustrated by the curve in Fig.5; after rebound of the ice flow the amplitude of free oscillations of the upper end of the pile increases greatly.
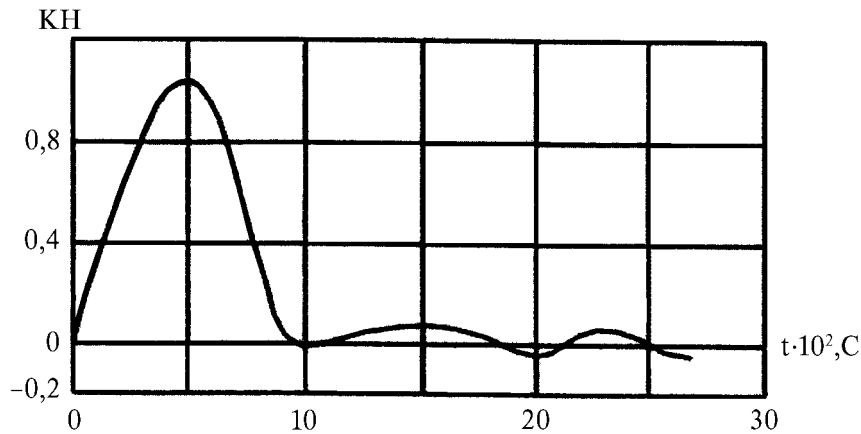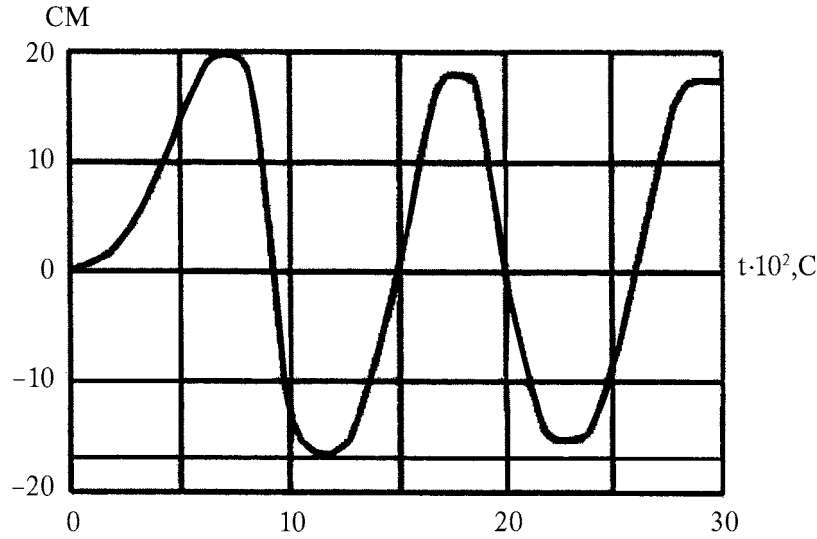

Fig. 4.

113

Fig. 5.

3. THE IMPACT INTERACTION OF THE ICE COVER WITH THE INCLINED SURFACE OF LAND SLOPES

Let's suppose that the ice floe floating on the water surface at the initial moment of time collides with an inclined plane of the land slope (slope angle γ). It is required to determine an ice load on the slope surface.

We will design the striking ice floe as an elastic column of the alternate cross section $A(x) = A_0(1 + bx)$, $0 < x < l$, l – length of the column, A_0, b– positive constants. The stored kinetic energy of the traveling floe $T = 0,5MV_0^2$ (M – floe mass) is spent on deformation (destruction) of the floe and deformation of the pliable slope.

The proposal is accepted that the maximal value of the impact speed of the ice floe V_0 is much more less than the spreading speed of the longitudinal elastic wave in the floe $V_0/C \ll 1$. We are ignoring the dissipative properties of ice. In the field of $0 < x < l, t > 0$ it is necessary to integrate the linear second-degree differential equation with floating factors

$$\frac{\partial}{\partial x}\left[A(x)E\frac{\partial u}{\partial x}\right] = \rho A(x)\frac{\partial^2 u}{\partial t^2}, \qquad 0 < x < l, \quad t > 0, \tag{37}$$

where $u(x,t)$ - longitudinal (axial) movement of the floe cross sections, x - geometric coordinate coinciding with the column axis, t – the current time (it is calculated from the moment of the first contact of the left floe end with the inclined slope surface).

In our case the obstacle (slope) is in a quiescent state while the ice floe is traveling, thus the initial conditions become as follows

$$u(x,t) = 0; \ \frac{\partial u(x,t)}{\partial t} = -V_0, t \le 0, 0 < x < l. \tag{38}$$

Let's formulate the boundary conditions of the task on the ends of the floe-striker. On the struck end $x = 0$ the elastic pliancy of the land slope is taken into consideration;

114

therefore it is assumed that its reaction is proportional to the end movement $x = 0$ in the process of its braking. The right end $x = l$ of the ice column is free from stresses. These boundary conditions are analytically written as follows

$$\sigma_x(x,t) \cdot A(x) = -K_0 u , \quad x = 0, t \geq 0 ; \quad \sigma_x(x,t) \equiv E \frac{\partial u}{\partial x} = 0 , \quad x = l, t \geq 0 . \quad (39)$$

With the help of parameter K_0 the deformation pliancy of the ground slope is taken into consideration. For the linear law of changing of the floe cross section the equation of its longitudinal oscillations is written in the following way

$$\frac{\partial^2 u}{\partial x^2} + \frac{b}{1+bx} \cdot \frac{\partial u}{\partial x} = \frac{1}{c^2} \frac{\partial^2 u}{\partial t^2} , \qquad 0 < x < l, t > 0 . \qquad (40)$$

After replacement of the variable according to the formula $Z = 1 + bx$

$$\frac{\partial^2 u}{\partial Z^2} + \frac{1}{Z} \cdot \frac{\partial u}{\partial Z} = \frac{1}{(bc)^2} \frac{\partial^2 u}{\partial t^2} , \qquad 1 < Z < bl . \qquad (41)$$

By applying the Laplace transformation to this equation, boundary and initial conditions we receive the following edge task in the image space

$$\frac{d^2 \bar{u}}{dZ^2} + \frac{1}{Z} \cdot \frac{d\bar{u}}{dZ} - \left(\frac{s}{bc}\right) \bar{u} = V_0 , \qquad \begin{array}{l} \bar{\sigma}_x \cdot A_{0Z} = -k_0 \bar{u}(Z), \quad Z = 1, \\ \\ \dfrac{d\bar{u}}{dZ} = 0, \quad Z = 1 + bl. \end{array} \qquad (42)$$

The general solution of the homogenous ordinary differential equation (42) expressed through two arbitrary constants of integration B, D becomes

$$\bar{u}(Z,s) = B I_0 \left(\frac{sZ}{bc}\right) + D K_0 \left(\frac{sZ}{bc}\right), \quad 1 < Z < 1 + bl, \qquad (43)$$

where I_0 and K_0 – Bessel functions of the imaginary argument of the zeroth order.

The particular solution of the heterogeneous equation (42) is expressed as follows

$$\bar{U}^* = -V_0 \left(\frac{bc}{s}\right)^2 . \qquad (44)$$

The general solution in the image space according to Laplace is presented in the following way

$$\bar{u}(Z,s) = B I_0 \left(\frac{sZ}{bc}\right) + D K_0 \left(\frac{sZ}{bc}\right) - V_0 \left(\frac{bc}{s}\right)^2 . \qquad (45)$$

The arbitrary constants B and D are determined from the boundary conditions.

Built in this way this solution of the initially edge task is a superposition of plane straight lines and reflected from ends waves. (Fig. 6) The numeric results are received for the following values of the initial data: $A_0 = 0,25 m^2$, $b = 0,1 m^{-1}$, $l = 4m$, $\rho = 950 kg/m^3$, $E = 10 MPa$, $V_0 = 1,5 m/s$. It is possible to expand vector $\bar{V}_0$ into a constituent directed along the slope equal to V', and a normal constituent V'', equal to $V'' = V_0 \sin \gamma$, where γ – angle of slope, $0 \leq \gamma \leq 90°$. If $\gamma = 0$, there is no slope and the ice floe strikes a tangent blow

along the horizontal plane; at $\gamma = 90°$ the slope transforms into a vertical wall (the floe blows into the vertical wall). Let $\gamma = 45°$. The curves in Fig. 7 show dependencies of the ice load (contact force) from time t/τ, $\tau = l/c$, for different values of the compliance coefficient of the slope K_0. Curve 1 relates to compliance $K_0 = 0.1$ kn/m; the value $K_0 = 0,8$ kn/m is marked by figure 2; figure 3 relates to the value of parameter K_0 equal to 1.5 kn/m. The analysis of these results shows that with the growth of rigidity of the land slope the amplitude of the ice load on it increases reaching the maximum value during the time $t/\tau = 15$; rebound can be observed at the moment of time $t/\tau = 28$. On the contrary at small values of pliancy the impulse of the ice load is stretching in the time; the duration of the contact of the ice column with the slope significantly increases.
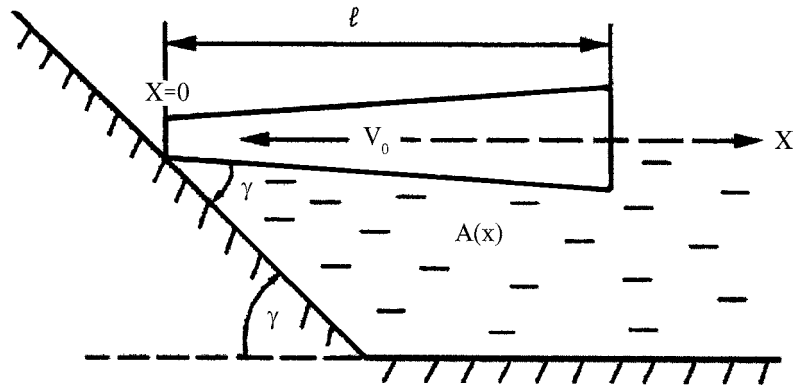
Fig. 6.
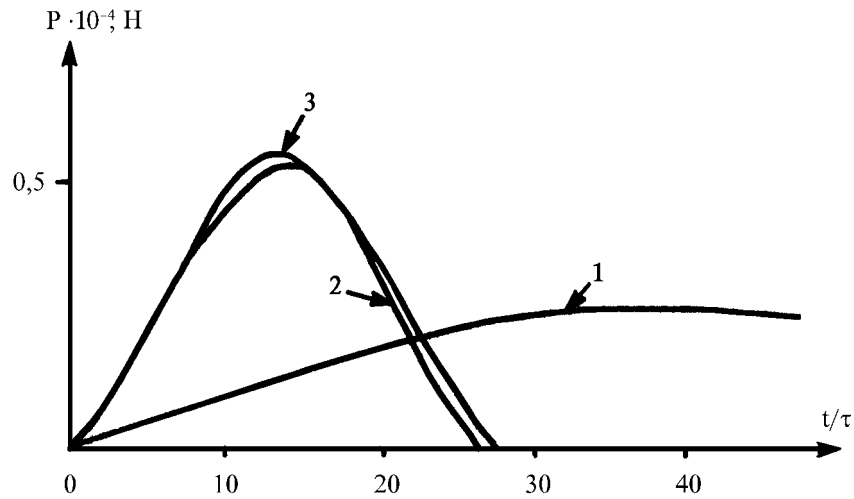
Fig. 7.

The general conclusion: during the interaction of the striking ice floe with the land slope surface there arises a possibility of the floe destruction in the vicinity of the struck end due to the bearing deformation; the other place of destruction can be a zone around the free end of the ice column. When repulsing from the free end $x = l$ of the compression wave in this zone tensile stresses are formed. If their level exceeds the allowable tensile stresses of ice in this area destruction can happen through breaking off. For elongated

floes the impact bend can be dangerous as well when the ice (contact) force *P* exceeds the critical Eiler force for the column $F_{kr} = \pi^2 EIL^{-2}$. For all that the elongated ice column can fail to withstand the dynamic load and break (in several places simultaneously). Number *n* of the column fractures equals to the whole number

$$n = \left[\sqrt{\frac{P}{2F_{kr}}}\right].$$

REFERENCES

Kozlov D.V. Wave processes in reservoirs and waterways with ice cover. *MSU of Environmental Engineering*, Moscow (2001) 223 p.

Arfken G. Mathematical methods in physics. *Atomizdat*, Moscow (1970) 712 p.

Krylov V.I., Skoblja N.S. Methods of approximate Fourie transformation and inversion of Laplace transformation. *Nauka*, Moscow (1974) 223 p.

PROTECTION OF MARITIME POWER STRUCTURES AGAINST ICE IMPACT IN RUSSIA

I.N.Usachev[1]

The necessity of special measures on protection of maritime power structures against ice impact in Russia firstly arose during construction of pioneer tidal power plant (TPP) – Kislogubskaya TPP on the Arctic sea coast of the Barents Sea (Fig. 1) [1].
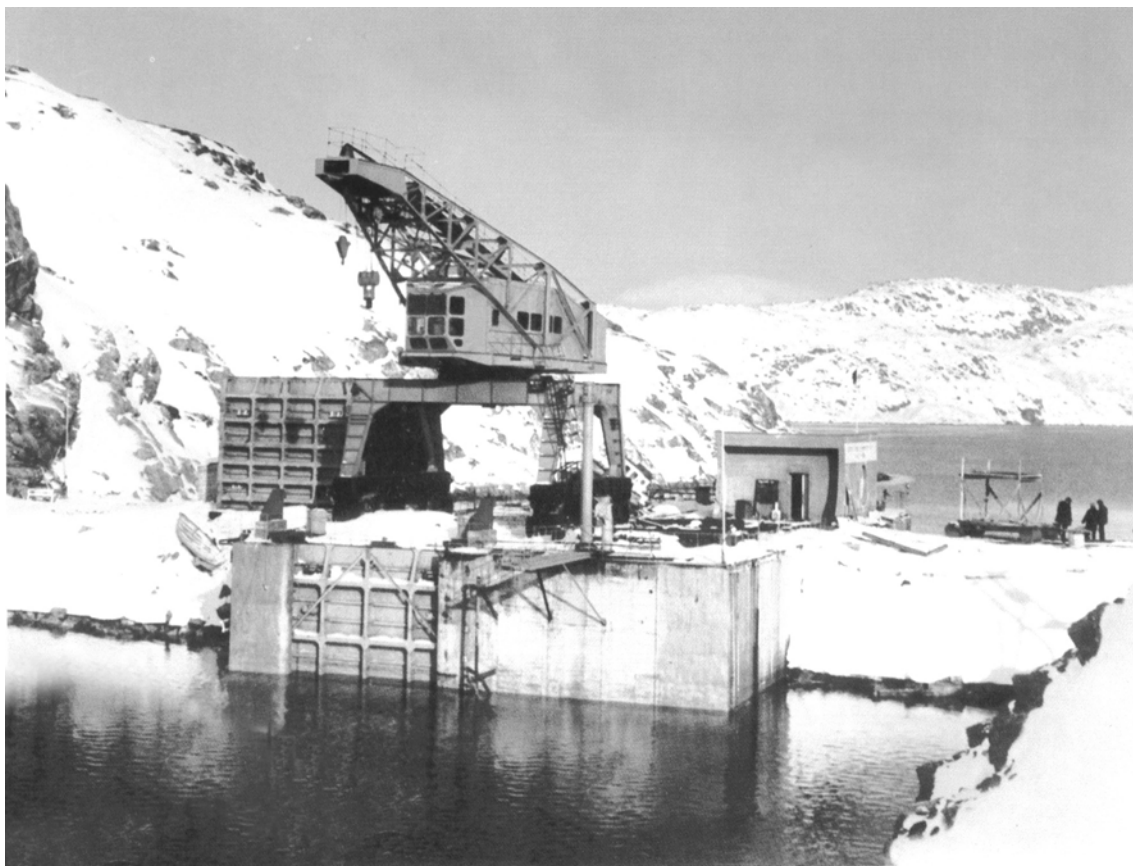

Fig. 1. The Kislogubskaya TPP on the Arctic sea coast of the Barents Sea

[1] JSC "Scientific Research Institute of Energy Structures" (JSC "NIIES"), Moscow, Russia.

The "ice" problems have being solved during development of the Kislogubskaya TPP and simultaneously for powerful Russian TPPs, perspective in XXI century: Mezenskaya TPP with capacity to 19,2 GW on the White Sea (Fig. 2), 8,0 GW Tugurskaya TPP in the south of the Sea of Okhotst and Pengynskaya TPP near the coast of Chukotst with fantastic now capacity of 87,0 GW.

Fig. 2. General view of water area at the Mezenskaya TPP dam site in winter

During the last decades the experience of TPP designing has been utilized for ice studies and for developing of the Arctic and Far East oil and gas deposits [2].

The ice studies (expeditions to the dam sites and project developments) have been fulfilled in the Hydroproject in cooperation with its branch institutes (VNIIG, NIIES) and special organizations of the Russian Academy of Science and regional hydrometeological service administrations from 1989.

The following problems concerning ice impact on the TPP have been solved during this period: creation of durable ice-proof construction materials, determination of possible pressure and influence of ice mass on the structures, examination of local ice formation in tidal zone and working out of measures to ensure ice protection for plant water conduits.

Ice-proof materials. Construction of ice-proof structures for oil and gas production on the northern shelf of the country as well as tidal plants on the coast of the White Sea and the Sea of Okhotst mostly depends on the creation of construction materials resistant to long-term ice abrasion impact.

Preliminary research of the Arctic coast shows that designing of power structures with operation time till 120 years will resist to long-term ice abrasion with 1,5-2,0 m thickness and 2-3 strength MPa in tidal and wave zones during a long winter period.

119

In practice of hydro construction there were no materials suitable for these natural conditions, for this reason, on the base of the experemental Kislogubskaya TPP, the scientific-research works for creation of ice-resistant concrete and coating for developments of the Mezenskaya TPP, Pengynskaya TPP and Tugurskaya TPP have been begun [3].

The studies have been executed on the basis of ice stand made in the TPP basin. The practical constant vertical mobility of ice with 80 cm thickness and 2,5 MPa strength take place in basin during ice standing period from October to May (Fig. 3).

Fig. 3. Ice stand for field tests on ice abrasion of materials and fragments of structures in Kislogubskaya TPP basin.

During 40-year period the field tests of samples and fragments of fine-wall concrete structures (samples with strength to 85 MPa, water impermeability >14, frost resistance >1000), polymer concrete, epoxy compositions with fillers and metals of different marks (on the stand of marine atmosphere), proposed by specialized organizations, have been carried out [4].

It is perspective to use concrete with microsilica admixtures (MS), which experimental samples were developed by NIIGB and NIIES, and since 1994 have been tested in tidal zone on marine stands with ocean water saltiness (by 35 ‰), atmospheric temperature to -40° C and water temperature from –1,75 to +10,5° C in winter, and also at yearly 450 cycles of freezing-defrosting. Intermediate results of tests show that all MS samples did not have traces of abrasion, mass diminution and strength degradation for 10-year period. The tests are continuing.

It is necessary to note that reinforced concrete fine-wall (only 15-30 cm) building of the Kislogubskaya TPP after 35-year operation is estimated by specialists FIP as only durable large concrete structure in the Arctic regions [1].

Ice regime influence on the structures. At the end of mathematical modelling of currents in Mezenskaya TPP and Tugurskaya TPP gulfs and basins, the reliable initial data for calculations, forecast of ice regime and determination of ice loads were obtained, that allow to make the following conclusions.

Ice formation in the TPP basin begins a little earlier than in natural conditions, owing to intense water desalination due to river flow. Solid ice cover forms in November. Its hummockness is less than the one in natural conditions. The reason is that no ice, drifting in gulf, comes into the basin, that results in less force interaction of ice masses and less amount of ice in basin and also a slightly more ice strength, caused by desalination due to river flow. Ice thickness reaches 2 m in winter. There is a sludge layer under ice coating. Polynia is formed near the TPP in basin, its length decreases to 500 m during a winter. Sludge volume in basin, according to a forecast, reaches 1-2 km² during a winter period at the total ice volume in basin of 3-5 km². Ice destruction begins in basin central part in the middle of May, destruction zone and following melting will look like stripe of 20-30 km width, situated along the way of river floods. The ice melts at the remaining part of water area through heat exchange with air. Full clearing of basin from ice occurs in June.

The ice TPP regime beyond polynia from sea side is similar to one in natural conditions. The range of polynia lengths is 10-15 km in winter. Sludge formation in this polynia will be at water discharge exceeding 550 000 m³/s and current speeds over 0.3 m/s. Sludge discharges in polynia from sea side change from 38 to 171 m³/s for Mezenskaya TPP. When the total units is 400, sludge discharge for each unit is 0,40 m³/s, that is less than 0,2 % of water discharge through the unit, and is not dangerous for unit operation. Maximal sludge volumes which can approach the TPP from sea side are $2.6 \cdot 10^5$ m³ for tidal cycle. At TPP stop, the ice fields and breaking ice, drifting in gulfs, will approach the TPP and fall on the structures during 1.5-3 hours.

Analysis of TPP regimes shows that its principal characteristics are: seasonal behavior (duration of ice period 6-8 months), big ice mass mobility, intensive interaction between ice masses, absence of narrow stripe of developed fast ice zone, contraction and discharge zones constantly appearing in ice coating.

In Mezensky gulf, according to the data of 989 measurements, there are 71-72 % ice blocks of oval form, 11-20 % of elongated form and 9-17 % of rounded form.

At the TPP dam site maximal ice block area was 5.17 km². Ice drift in water area well conforms with tidal flows. Maximum ice drift speed was 1.6 m/s during spring tide period and -1.3 m/s during quadrature period.

According to the radiolocation aerophotography (487 measurements), in the Pengynsky inlet the ice blocks of rounded and oval shape are prevailing and decreasing while drift into inlet. At the dam site maximal ice block area was km². Maximum speeds of ice block displacements were 2.6 and 1.3 m/s during high and low tides respectively.

The stripe extent of accreted hummocked ice near the blank dams and the TPP building from sea side reaches 0,5 km by the end of winter. Maximum value of hummocked ice near TPP building doesn't exceed 7 m.

Calculated (normative) ice load on the vertical upstream face of TPP building during tidal period will make 22360 MN, equal to 1MN/m (~100 ts/m), on pier ~33 ts/m and on gate ~39 ts/m (according to VNIIG data for Mezenskaya TPP). Recommended thickness of upstream face for reinforced concrete TPP building is not lesser 1.5 m to resist to these loads.

Ice protection of water conduits. For ice protection of turbine and spillway conduits, the conduit visor beams are designed at 1.5-5.0 m below the minimal water level (at the 99% supply). For prevention of air hole provoking ice plunging into bottom water conduits it was proposed to dispose ice-protective shields on visor beams. The hydraulic model of unit for the Mezenskaya TPP building was created to solve problems of ice approach to water conduit in the presence of (absence) equipment preventing water conduits and also for shied design (Fig. 4) [5].
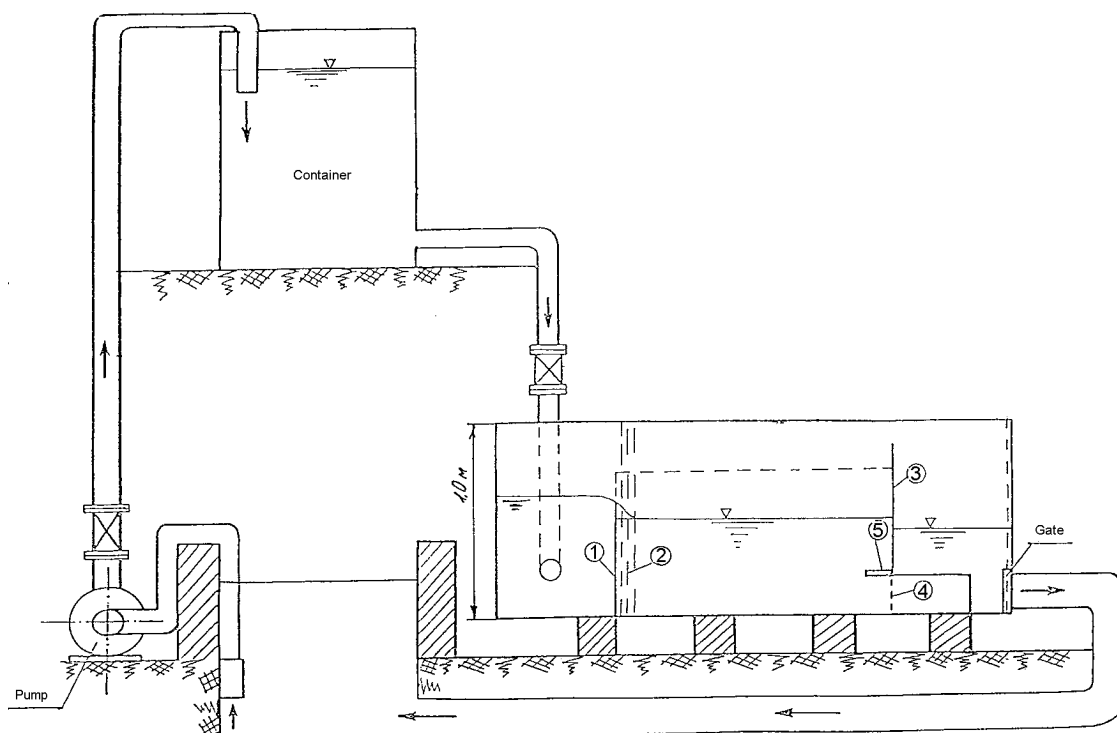
Fig. 4. Diagram of VNIIG experimental unit on modelling of prevention of ice plunging into TPP water conduits: 1 – spillway; 2 – grate; 3 – upstream face; 4 – water conduit; 5 – shield

The hydraulic modelling is executed in 1:75 scale. The ice was simulated by paraffin wax.

Result analysis of laboratory experimental studies showed that proposed ice protection structure which comprises turbine water conduit extended to 16.6 m to sea side and ice-protective shield of 2 m length, will block conduits if levels of ice approach the TPP structure are at least no less 1.5 m higher than visor beam elevation [6].

The proposed structure permits to protect turbine conduits from sea side against ice and to drop an idea of high-priced holding ground construction.

The holding ground installation is not necessary from basin side, since the ice, taking away by the Mezen and Kula rivers, is retained in the gulf narrowing, but in the TPP basin practically all winter period the solid ice field will be existing, not separeted fields. This field is separated from the coast fast ice by tidal crack. It rises and falls together with water level and doesn't press into turbine conduits.

The recommended ice-protective shield for the Mezenskaya TPP (for the Tugurskaya TPP), at minimal possible excess of ice level above visor beam, reduces relative possi-

ble amount of ice getting into conduits to 3.2 %. In case of water conduit extent to sea side not less than 16.6 m, the possible ice coming into it will be reduced to 0.4 %, and practically will not affect power plant operation in ice conditions.

Ice freezing to structure. The 35-year monitoring of ice influence on the Kislogubskaya TPP permitted to establish that in 4 m tidal zone from sea side, on vertical reinforced concrete surface the ice freezing shape reminds Gauss curve (curve of normal mistake distribution law), when Y-axis coincides with average sea level. The biggest fixed thickness of freezing is 1.63 m.

The ice cantilever freezing to the structure serve as a damper between the structure and ice field affected it. However, in case of cantilever destruction the possibility of plunging of large ice fragments into turbine conduits and spillway holes can arise.

MAIN CONCLUSIONS

1. The main marine fuel-power projects in Russia (at the dam sites of TPP and at oil and gas deposits) are situated on the Arctic and Far East sea coasts, exposed to severe ice regime.

2. Durable operation of hydraulic structures is only possible in case of utilization of high-stable materials, resistant to electrochemical and biological corrosive impact of sea-water with ocean water saltiness as well as to ice abrasion impact during operation period. Now monitoring results of Kislogubskaya TPP allow to propose unabradable concrete compositions with microsilica admixtures, strength to 85 MPa, water impermeability >14 and frost resistance >1000.

3. For reliable ice protection at Mezenskaya TPP on the White Sea and Tugurskaya TPP on the Sea of Okhotst constructions, perspective in XXI century, it is proposed to build out of plant manufactured floatable units with visor beam disposition lower than minimal ice level 1.5 m and below, to use ice protective shield with length not less than 2 m above water conduits, and to extent water conduits towards sea side on the distance not less than 16.6 m.

4. For resistance of ice field pressing onto structures it is recommended to make sea side upstream faces of 1.5 m thick, in the same time taking into account supplementary loads of freezing ice in tidal zone, which thickness can reach 2 m.

REFERENCES

1. Bernshtein L.B., Silakov V.N., Usachev I.N. and other, Tidal Power Plants, Moscow, *Hydroproject*; 1994.

2. Usachev I.N., Braude V.M., Gavrilov V.G., Rozental N.K., Ice-proof marine oil-gas trade stationary structures, reinforced concrete, Code of rules SPZZ -101-00, Moscow, *Lukoil*; 2003.

3. Usachev I.N., Research on creation of materials for ice-proof floatable structures, Ice-83, *Minenergo USSR*, Murmansk; 1983.

4. Usachev I.N., Researche on creation of materials materials resistant to long term ice abrasion impact, Ice difficultie control on the rivers and water reservoirs at construction and operation of hydraulic structures, Leningrad, *Energoatomizdat* ; 1984.

5. Karnovich V.I., Vasilevsky A.G., Usachev I.N., Tregub G.A., Engineering measures on security of tidal power plant reliable operation in severe ice conditions, *Hydraulic construction*, 1998.

6. Karnovich V.I., Tregub G.A., Usachev I.N. and other, Water intake, Certificate of the Russian Federation on useful model № 15897, Gosreestr of the Russian Federation of the 20th September, 2000.

DESIGN AND MODEL TESTING OF ICE BARRIERS FOR THE PROTECTION OF OFFSHORE STRUCTURES IN SHALLOW WATERS IN WINTER

Karl-Ulrich Evers[1], Alexandra Weihrauch[2]

ABSTRACT

In order to increase the safety of platforms in shallow water, ice barriers are designed to take main loads from floating ice sheets. Platforms and equipment protected by ice barriers can be dimensioned and constructed more economically, when ice barriers are present. Several concepts were investigated and for promising concepts ice model tests were carried out in the Large Ice Model Basin of the Hamburgische Schiffbau-Versuchsanstalt (HSVA) in order to establish the design ice loads and to prove that the design force for offshore structures can be reduced significantly by using ice barriers. Model tests were conducted in different ice conditions in order to investigate the ice rubble formation process, to evaluate the design alternatives and to establish design loads. The measured ice loads were analysed and compared to loads theoretically derived by use of existing methods. The analysis comprises a statistical evaluation of the ice loads related to site conditions in the North Caspian Sea.

INTRODUCTION

Existing ice barriers which are designed to withstand ice loads without the stabilizing effect of the ice itself have to be anchored in the sea bottom or must have extremely high weight to transfer forces to the sea bottom through bottom friction. Different concepts of ice barrier types for shallow water areas are developed by IMPaC Offshore Engineering, HSVA and the shipyard Lindenau GmbH. The main objective of this study is to design economic and simplified ice barriers, which can be installed on site easily in order to initiate an ice rubble pile up in the vicinity of the offshore structure. The presence of such an ice rubble pile up may protect an offshore structure (e.g. exploration platform, drilling rig, etc.) with respect to ice load reduction. The idea of the research project is to design modular ice rubble generators (IRGs), which are able to catch early thin broken ice, stabilize themselves due to the added weight and can withstand thicker ice later in the winter season. The IRGs can be removed during ice free seasons and shall fulfill the criteria: self-floating for transport, self stabilizing during rubble forma-

---

[1] Hamburgische Schiffbau-Versuchsanstalt GmbH, Hamburg, Germany ; Email: evers@hsva.de
[2] IMPaC Offshore Engineering, Hamburg, Germany; Email: alexandra.weihrauch@impac.de

tion, fast and environmentally sound installation and deinstallation, cost efficiency regarding fabrication, transport and maintenance, flexibility, safety and reliability, sufficient availability of construction material and participation of local fabrication facilities. The design of different IRGs is verified by ice model tests in the Large Ice Model Basin at HSVA.

ICE MODEL TESTS

The ice model tests are carried out at a model scale of $\lambda = 16$ with different types of shallow water ice barriers in the Large Ice Model Basin at the Hamburgische Schiffbau-Versuchsanstalt GmbH (HSVA) in two experimental phases. According to ice conditions typical for the North Caspian Sea, the ice thickness varies from 0.1 m to 1.3 m (full scale = f.s.), and the ice bending strength is about 750 kPa (f.s.). Ice drift angles (90°, 60° and 30°) and the configuration of ice barriers are varied during the tests. The design water level in the model tests is about 4 m (f.s.).

The main objectives of the tests are:

- to determine ice loads acting on individual piles and barges with ice rubble generators, and

- to investigate the formation of ice rubble along the ice barriers.

MODEL TEST SET – UP

Phase I – Vertical and inclined ice protection piles

Groups of vertical and inclined protection piles of about 480 mm diameter (f.s.) are installed in a row. The pile distance , i.e. the center to center distance varies from 2 times diameter to 8 times diameter, i.e. 2*d to 8*d (Fig.1). At least one pile of each pile group is instrumented with a triaxial load cell (KISTLER type) in order to measure the ice force on this individual pile.
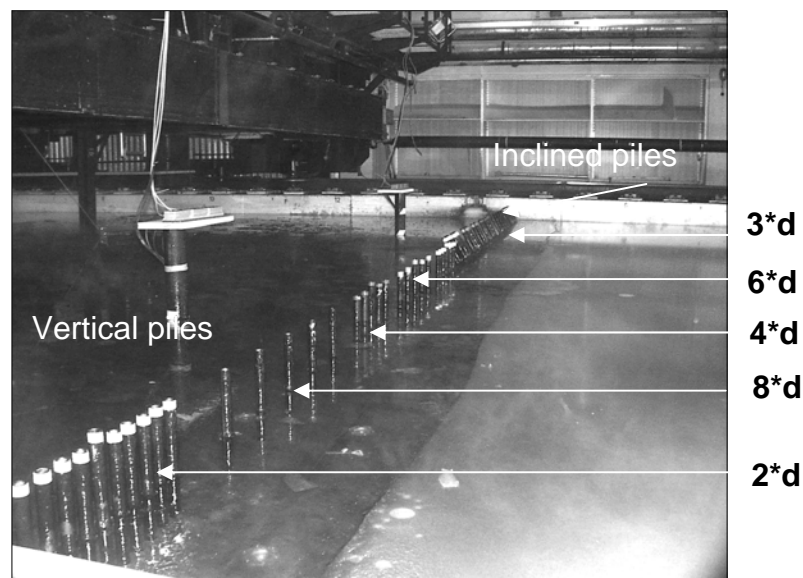

Fig. 1. Arrangement of vertical and inclined protection piles

The vertical ice protection piles cut the 0.1 m (f.s.) thick ice sheet into strips which pass the structure downstream. No ice rubble formation is observed along the vertical piles and at the end of the test run only some ice rubble is observed along the inclined piles. For the 0.5 m (f.s.) thick ice sheet the ice fails by upward bending along the inclined piles with a small pile to pile spacing. In the transition area between inclined and vertical piles ice rubble starts with subsequent ice bridging to both sides. At the end of the test ice rubble is grounded to some extent.

Phase I – Inclined ice protection piles and barges

As a result of previous tests the vertical ice protection piles do not seem to be efficient with respect to rubble formation, thus these piles are replaced by barges. Three barges with two parallel vertical pile rows (structure A), two inclined pile rows (structure B) and two parallel inclined sidewalls (structure C) are investigated (Fig.2). The angle of inclination in all cases is 60° to the horizontal. Each individual barge is instrumented with one triaxial load cell KISTLER type) and two uniaxial load cells (U9b type).

Besides the barges inclined protection piles of about 480 mm diameter (f.s.) are installed in a row. A 60°-inclination of the piles is chosen to initiate downward bending failure of the ice sheet.
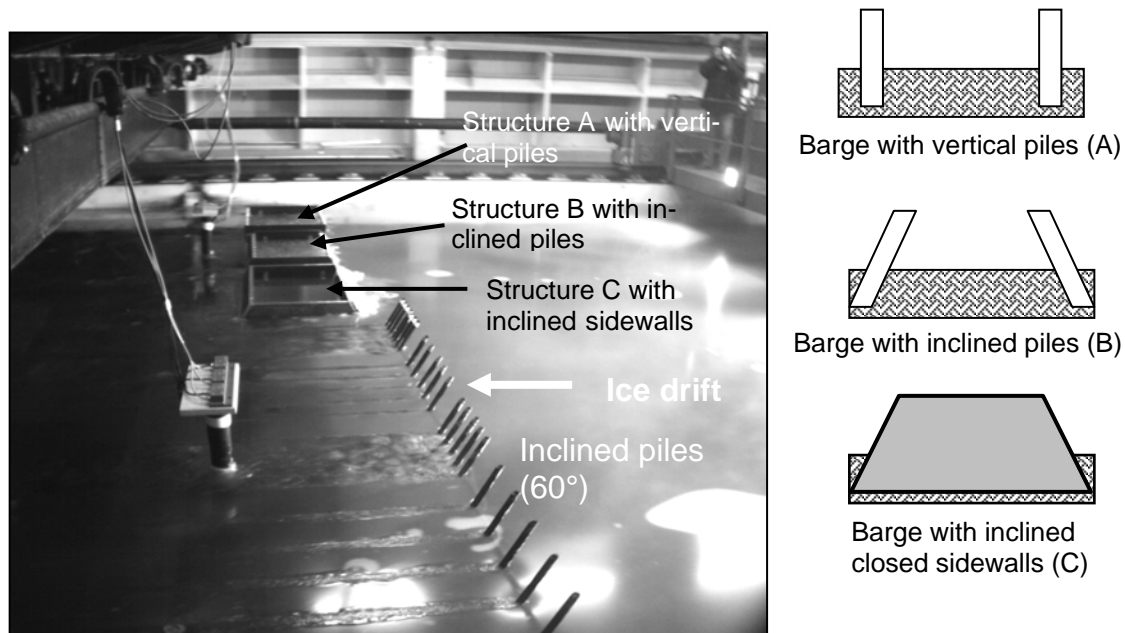
Fig. 2. Inclined ice protection piles and barges to initiate ice rubble formation

In the 0.1 m (f.s.) thin ice sheet ice rubble occurs at first on the barge with inclined sidewalls, however no ride-up is observed. In front of the barges with installed piles (B an C) ice rubble occurs and broken ice blocks are caught. Along the row of inclined piles the ice is cut into strips and drifts downstream without any accumulation (Fig. 3). In the 0.5 m (f.s.) thick ice sheet ice ride up is observed simultaneously on all barges. At the beginning the broken ice is cleared downstream between the barges until ice bridging starts and the space between the barges is subsequently filled with broken ice. The extent of ice rubble towards the upstream side of the barge is slightly higher than the ice rubble collected in the barges (Fig. 4).
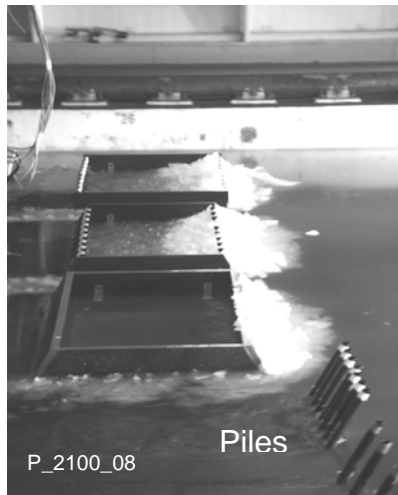
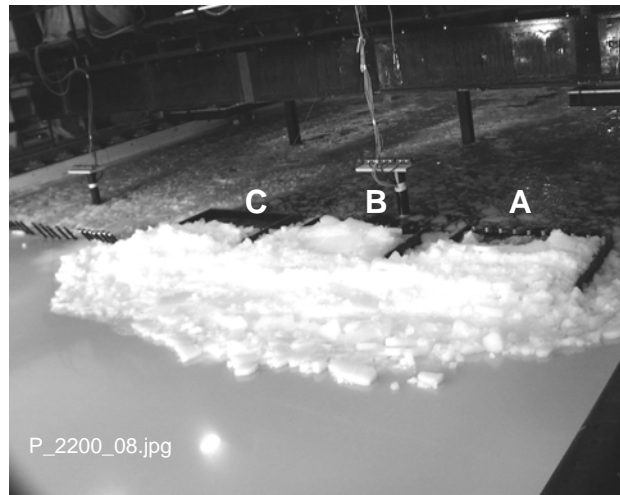Fig. 3. Ice rubble on barges,
ice thickness is 0.1 m (f.s.)

Fig. 4. Ice rubble on barges, ice thickness is 0.5 m (f.s.)

Phase II - Ice rubble generators (IRGs)

From the results achieved in Phase I the use of barges in combination with IRGs seems to be very efficient with respect to ice rubble formation.

The IRGs are installed on barges, which can be moved to a certain location and then lowered to the seafloor. The barges are instrumented with triaxial (KISTLER type) and two uniaxial load cells (U 9b type) in order to measure the entire ice force on each barge. The test set-up consists of a configuration of three different IRGs. Two parallel rows of 30° inclined piles with a pile distance of 4*diameter are installed. The inclined piles initiate upward bending ice failure. One row of vertical piles with pile distance of 4*diameter is installed as well as a 'roof structure'. The latter consists of a pleated steel sheet mounted on piles. Between the piles an 'ice catcher' consisting of a Nylon® net of about 0.3 m (f.s.) mesh width is stretched in order to keep the broken ice floes inside the 'roof structure' (Fig.5). A schematic of the 'roof structure' which is fixed on the barge is shown in Fig. 6.

The 'roof structure' elements are arranged as shown in Fig. 7. The ice sheet encounters with an oblique angle of 60°. Three components of the 'ice catcher' are instrumented (A, B and C) with two triaxial load cells each, whilst additional 'roof structure elements' (D, E and F) are installed without instrumentation. Between 'roof structure' elements D and F a bulkhead is installed, in order to avoid that broken ice floes drift downstream. Fig. 8 shows the IRGs filled with broken ice blocks after a test.
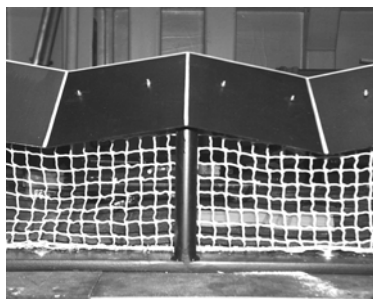

Fig. 5. 'Roof type' structure
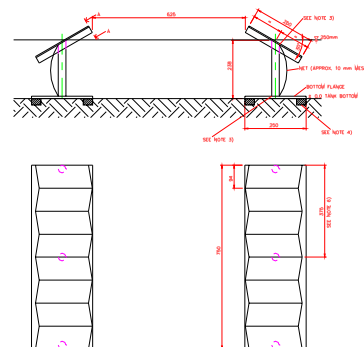with a net between vertical piles
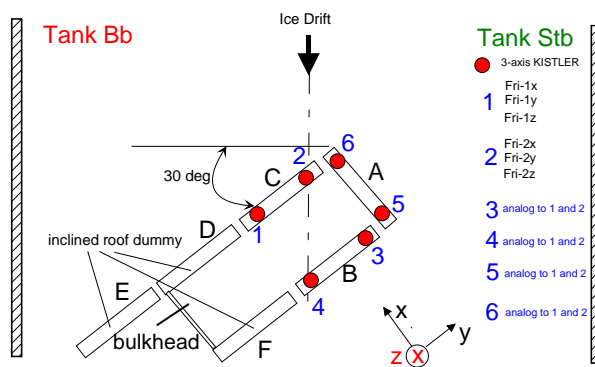

Fig. 6. Schematic of the 'roof type' structure

127

Fig. 7. Schematic of 'roof type" structure arrangement and instrumentation a net between vertical piles
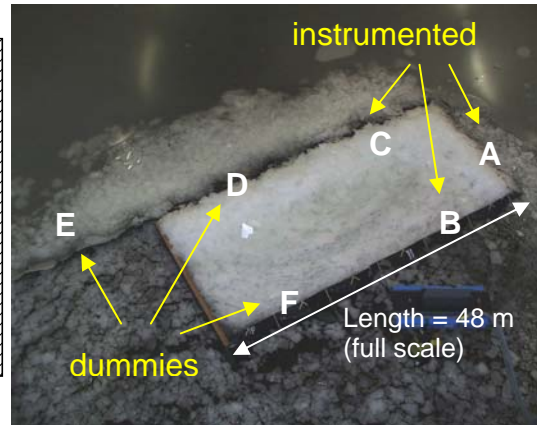
Fig. 8. 'Roof type" structure filled with broken ice a net between vertical piles

When the ice drift angle is 60°, the 0.1m (f.s.) thick ice sheet fails along the short and long side of the structure by bending and the broken ice floes ride up on the inclined roof and fill its inner part. After a steady state is achieved, the filling process stops and ice rubble formation starts at the long side of the structure. When the ice drift angle is 30°, the ice rubble formation process is similar.

When a 0.5 m thick ice sheet encounters under 60° drift angle, the IRGs are filled with ice blocks and an existing rubble is in front of the structure, the ice fails by bending on the existing rubble without ice over-ride. During the ice breaking process the ice rubble extends in upstream direction. When the ice drift angle is 30°, the ice rubble formation process on an existing rubble starts and a subsequent ice over-ride occurs. The structure is completely filled with ice blocks and without accumulation of broken ice along the sides of the structure. No grounded ice rubble is observed.

DESIGN ICE FORCES

The following processes of the ice-structure interaction can be observed for all IRGs resulting in different calculation approaches for the design loads:

- filling of IRG with ice blocks,

- ice rubble formation in front of IRG; pushing of ice sheets through rubble pile,

- random rubble forming process.

The horizontal forces at the very beginning of the ice-structure interaction are expected to give the ruling load case because the structure has not yet been self-stabilized at that time. The forces were calculated by an analytical model for the 0.1 m thick ice and for the 0.5 m thick ice and compared to the measured values. The results for the inclined roof structure are shown in Fig. 9.
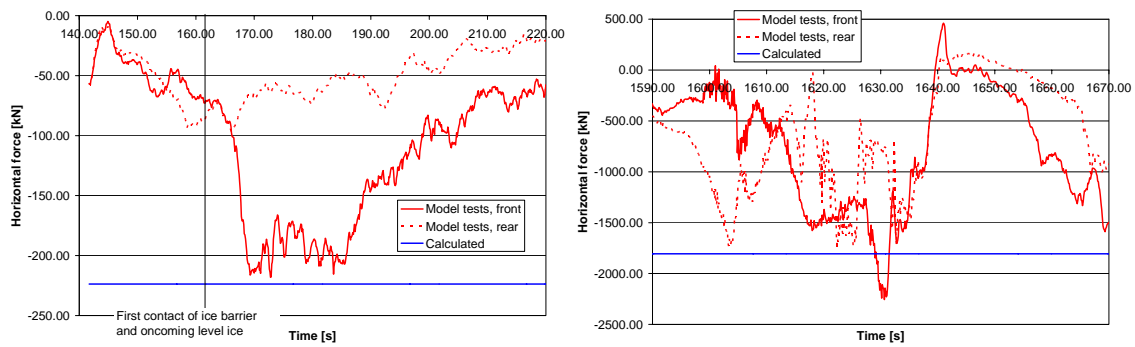
Fig. 9. Horizontal forces on inclined roof at the beginning of the model tests

The calculated forces agree with the measured forces in the order of magnitude. Once a rubble pile starts to form in front of the structure, ice sheets may still be able to push through. Even though the structure has already started to self-stabilize, the extremely high horizontal forces resulting from the ice sheet being pushed through the ice rubble may also become the ruling load case for the stability analysis. The result of the calculation with the analytical model is, however, very sensitive to a variation of the rubble pile inclination angle and of the rubble pile height (CROASDALE et al., 1994).

With further growth of the ice rubble in front of the structure, other failure modes may become significant. The loads applied to the structure during this phase may even result from a multimodal failure (simultaneous bending, crushing and shearing) occurring over multiple zones (CAMMAERT, MUGGERIDGE, 1988). The forces are not completely transmitted to the structure, but are reduced due to the energy-absorption capacity of the ice rubble (ALLYN, CARPENTIER, 1982). An example of measured the loads for the IRG with inclined roof is shown in Fig. 10.
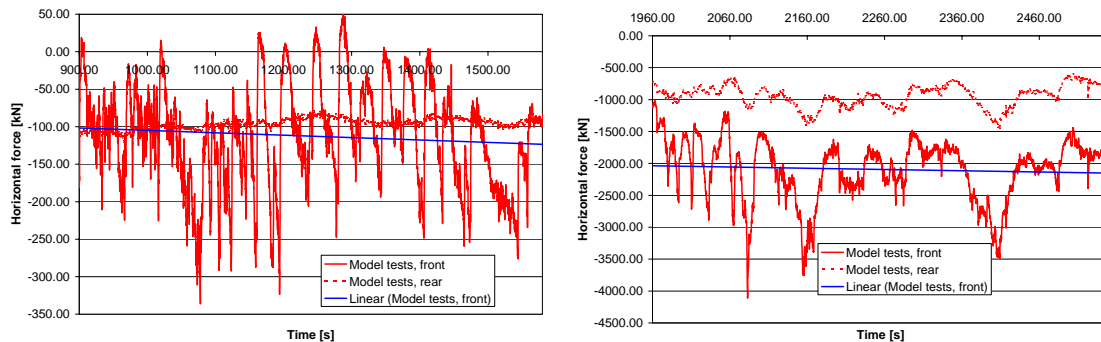

Fig. 10. Horizontal forces after a rubble pile has formed in front of the structure

From Fig. 10 it can be seen that the horizontal force in front of the structure increases significantly when compared to the initial forces applied by bending failure and ride up. It is yet much lower than the force applied by the ice sheet being pushed through the rubble pile. The trend curves in Fig. 10 show slightly increasing loads while the maximum values decrease and the minimum values also increase. This behaviour shows the damping effect of the ice rubble on the loads applied to the structure. The measured forces were statistically evaluated. Fig. 11 shows the quantiles of the load distribution.
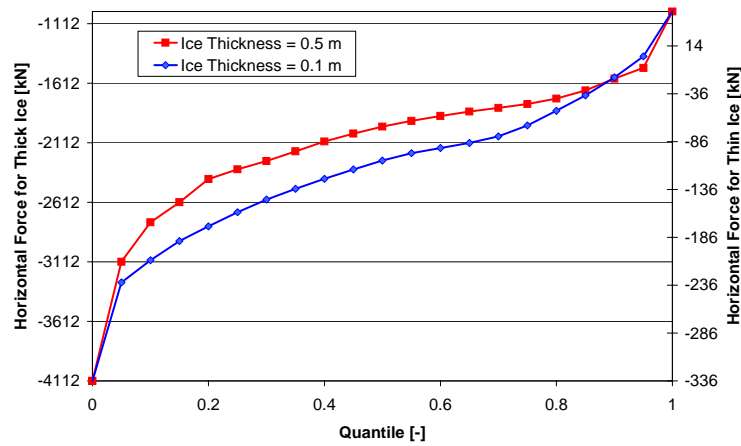
129

Fig. 11. Quantiles of the horizontal forces for 0.1 m thick ice and for 0.5 m thick ice

Fig. 11 can be used to derive design loads for a specific safety level. The load distribution may be described statistically e.g. by a GUMBEL-distribution.

SAFETY ASPECTS

The stability analysis was carried out for the structure with inclined roof. For the first contact of ice and structure at the beginning of the ice season when the structure has not yet been self-stabilized the sliding stability is guaranteed for ice thicknesses up to 0.5 m if skirts are arranged. Without skirts, the structure can still withstand force from ice not thicker than 0.3 m. The ruling load case results from ice pieces being pushed through the rubble pile in front of the structure leading to high peaks of the horizontal loads. The stabilizing effect of the ice rubbles inside the structure and in front of the structure (upstream) has to be taken into consideration in this case. The weight of the rubble sail that is not compensated by the buoyant forces on the keel generates a frictional force that must be exceeded before the rubble can be moved. The rubble piles apply a significant stabilizing vertical force which is much greater than the weight of the structure.

The dimensions of the rubble piles are derived from measurements at the end of the model tests and from volume balance considerations (see Fig. 12). The sliding resistance of the structure is compared to the measured horizontal forces applied to the structure. The displacement of the structure can approximately be quantified by a dynamic load balance. The results are shown in Fig. 13.
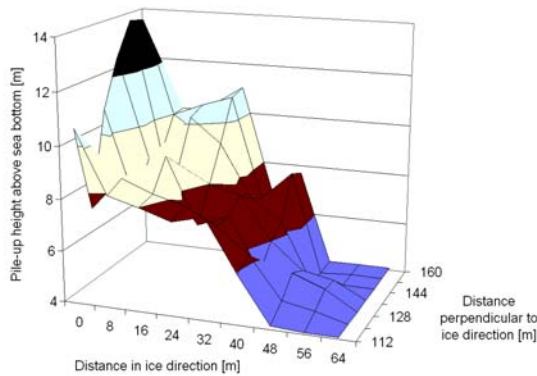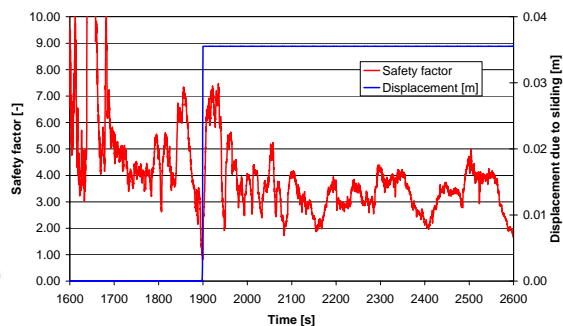

Fig. 12. Shape of rubble pile

Fig. 13. Safety factor against sliding

130

Fig. 13 shows that the safety factor is below 1.0 only for the peak load which is applied to the structure over 1.6 s. The load balance gives a displacement of 3.5 cm. This value seems to be acceptable. Also, it is necessary in most cases to arrange several ice barriers around the structure to be protected. The ice barriers can be interconnected and therewith have a higher overall sliding resistance.

CONCLUSIONS

From the results of the model tests design criteria for IRGs can be derived. The investigations on ice loads and stability show that the IRG with inclined roof is suitable to protect offshore structures from high loads caused by floating ice. The forces acting on the structure are caused by bending of the ice sheet applying much lower loads than it would be the case if the ice failed by crushing. Once rubble piles have built-up inside and in front of the structure, other failure modes may occur. Due to the self-stabilizing effect of the rubble piles, these loads do not put the stability of the structure at risk. Only for very high peak loads resulting from an ice sheet being pushed through the rubble pile, the structure starts to slide. If several ice barriers are arranged and connected, displacements can probably be avoided.

ACKNOWLEDGEMENT

REFERENCES

Allyn, N, Charpentier, K. (1982). Modelling Ice Rubble Fields Around Arctic Offshore Structures. *Proceedings OTC*, Houston, pp. 501-508.

Cammaert, A. B., Muggeridge, D. B. (1988). Ice Interaction with Offshore Structures. *Van Nostrand Reinhold,* New York.

Croasdale, K. R., Cammaert, A. B., Metge, M. (1994): A Method for the Calculation of Sheet Ice Loads on Sloping Structures. *IAHR Ice Symposium 1994, Trondheim,* Norway.

Evers, K.-U., Kühnlein, W. (2001). Model Tests of Ice Barriers in Shallow Water. *HSVA-Report E 311-01 (unpublished).*

Jochmann, P., Evers, K.-U., Kühnlein, W. (2003). Model Testing of Ice Barriers used for Reduction of Design Ice Loads. *Proceedings of OMAE'03 , 22nd International Conference on Offshore Mechanics and Arctic Engineering,* Cancun, Mexico, June 8-13, 2003, OMAE2003-37385.

Lengkeek, H.J., Croasdale, K.R. (2003): Design of Ice Protection Barrier in Caspian Sea. *Proceedings of OMAE'03 , 22nd International Conference on Offshore Mechanics and Arctic Engineering*, Cancun, Mexico, June 8-13, 2003, OMAE2003-37411.

Weihrauch,A., Berger, J., Bartels, M. (2003): Design of Self-stabilizing Ice Barrier. *Proceedings of OMAE'03 , 22nd International Conference on Offshore Mechanics and Arctic Engineering*, Cancun, Mexico, June 8-13, 2003, OMAE2003-37163.

OSCILLATIONS OF A DRILLING PLATFORM CAUSED BY THE ICE COVER AND WIND IMPACT

Smirnov V. N., Korostelev V. G.[1], Shibakin S. I.[2]

ABSTRACT

The vibrations and oscillations of the floating drilling platform in the Ob Bay during winter were studied. The four supports of the platform were raised at the winter period. The oscillations were caused by action of ice at the construction and by wind at the supports. The oscillations are divided in two classes: oscillations with frequency corresponding external forces and oscillations at the impulse of the external forces characterizing the self oscillations of the platform.

INTRODUCTION

The reaction study if the constructions to the impacts of wind, waves and ice allows to understand better the interaction mechanism of the construction with natural forces and to take in account it during designing, installation and exploitation. In some cases the measurements of parameters in nature help to determine the magnitudes of existing loadings. The attempts of such approach were made for a long time.

THE DEVICES AND THE METHODS OF STUDY

The oscillations of the platform and the ice cover were registered in directions X, Y, Z. The relative analysis included the comparison of the spectra of the platform and ice cover oscillation. The X direction was selected parallel to the long side of the platform (50 m parallel to the shore) and the Y to the short one (37 m perpendicular to the shore) (Figure 1). The sensors situated on the ice surface were oriented the same way. The mutual spectral analysis of the recordings allowed to find out presence of interconnected terms in the spectra of ice and platform oscillations .

RESULTS AND DICCUSSION

The oscillations may be divided in two classes:

- oscillations with frequency corresponding external forces,

- oscillations at the impulse of the external forces characterizing the self oscillations of the platform etc.

---

[1] Arctic and Antarctic Research Institute, Bering Str., 38, 199397, St-Petersburg, Russia
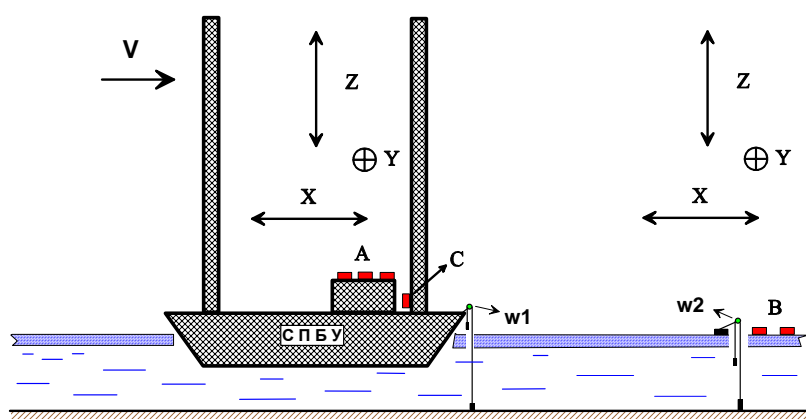[2] VNIIGAZ, settlement Razvilka, Leninsky district, 142717, Moscow region

Fig. 1. The scheme of reaction measurements of the platform to the external impact:
A – seismometers (X,Y,Z) and tiltmeter; B – seismometers (X,Y) and tiltmeter,
C – tensometer; W1 and W2 – wavemeters

The oscillations caused by water level change must be related to the forced oscillations. The floating installation simultaneously with surrounding it ice cover made oscillations relatively to a basin bottom. The fluctuations of the sea level primarily are caused by semidiurnal tide. The Figure 2 shows a fragment of the simultaneous recording of the two devices installed on the ice cover surface and the platform deck. Low-frequency oscillations of the 12-hour period are well distinguished. The magnitudes of semidiurnal level fluctuations and the platform are practically the same.
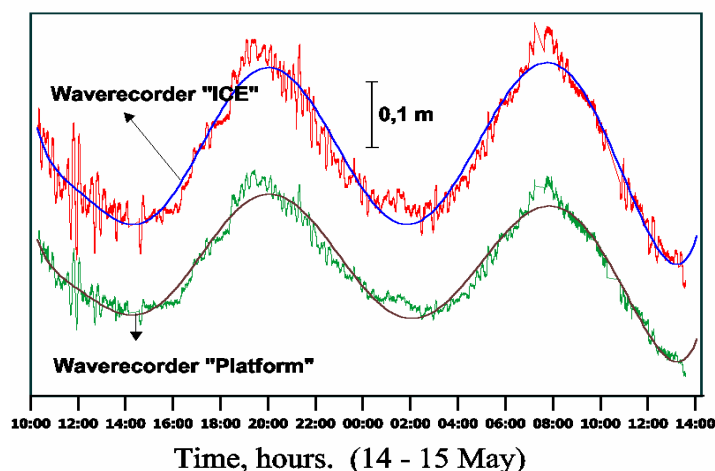

Fig. 2. The simultaneous recordings of the devices on the ice surface and on the platform deck

The oscillations of the 12-15 minutes period of the level, ice cover tilts and the platform were fixed incidentally. Their intensivity depended on the tide phase and the meteorological conditions. They are well noticed on the Figure 2 as more high-frequency oscillations compared with the tide oscillation frequency. We assume that they are seiche or standing waves arising in closed or particularly closed basin (gulf, bay). The figure 3 shows the fragment of simultaneous record of two devices installed on the surface of ice cover.

133

The recording fragment presented on the Figure 3 characterizes changes in time of the platform tilt at the decreasing of the sea level during the low-tide.
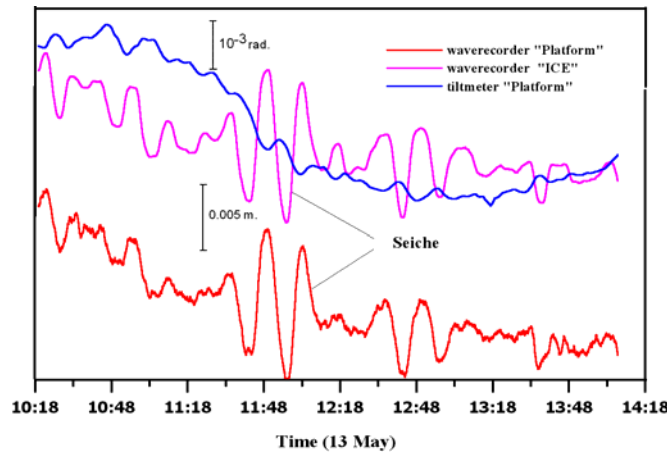

Fig. 3. The fragment of the platform tilt and of the oscillations of ice

The results of the spectral density of the oscillations are shown on the Figure 4.

The comparison of the three spectra finds out energy term at the frequencies 0.0011 Hz (T_1=15.1 min), 0.0013 Hz (T_2=12.8 min) and 0.0022 Hz (T_3=7.6 min).

The construction of three mutual spectra to determine the connection between the components of time series spectrum was performed.

The appearance in the oscillations spectra of the terms (T_1 and T_3) at multiple frequencies (0.0011 Hz and 0.0022 Hz) testifies about their interrelation.

The presence of the phase connection between two terms of the oscillation process confirms its nonlineratity or an existence of several modes of the free environment oscillations. This can be seiches or standing waves arising in the closed or particularly closed basin. Here can be created the free oscillations with some period depending of horizontal sizes and depth. Seiches arise under wind, difference of atmosphere pressure, tides or water oscillations in the adjacent basin. Compared weak actions of the external forces can cause series of damped seiche oscillations, which will be significantly amplified, if the action period approaches to the free oscillations period of the basin.

If the wavelength is small compared with the basin's depth the seiche behavior is described by long wave's theory according to which the phase velocity of the wave is $\sqrt{gh}$, where g is gravity acceleration, h is basin depth. The period of the free oscillations in the particularly closed basin is *4L/(2n-1)* $\sqrt{gh}$, (*L* –length basin, *n* – nodes quantity). The lines of the nodes and beams are located on the open and closed ends correspondingly. The Figure 5 shows scheme illustrating one-noded seiche realization in a rectangular basin.

The wave motion in the semi-closed channels or harbors is usually excited at their entrance.
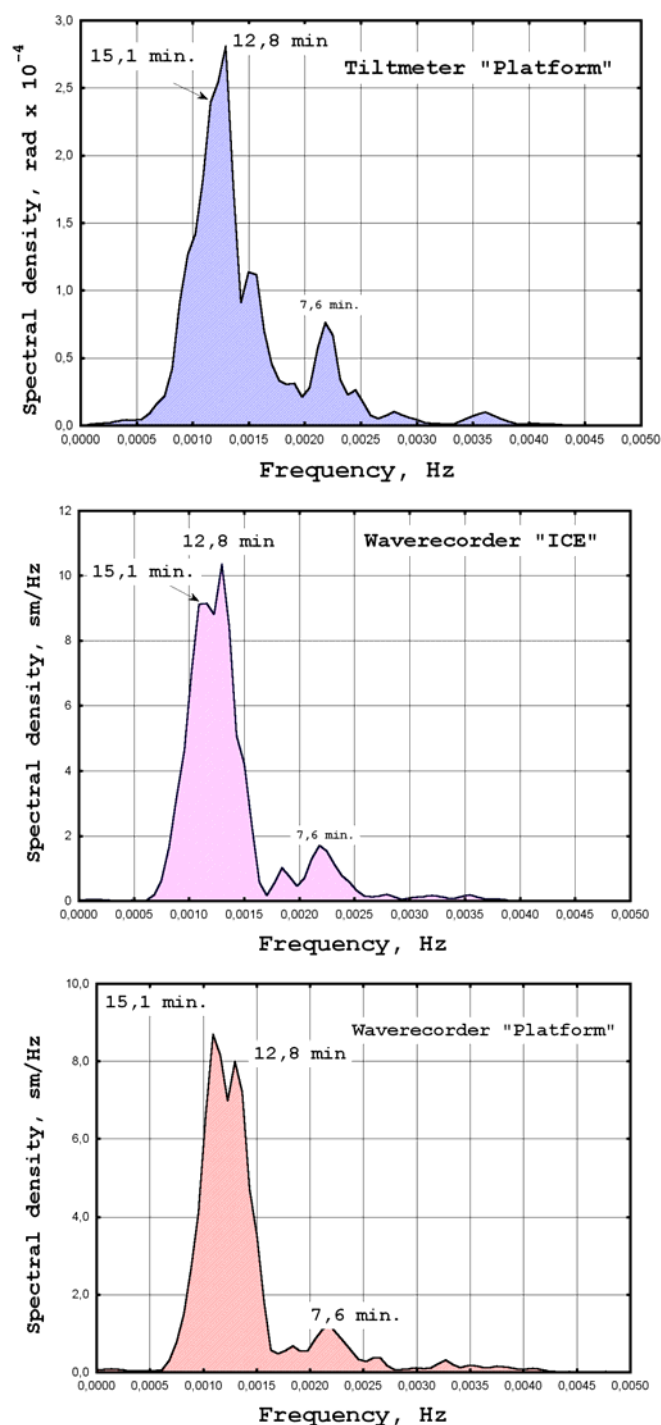
Fig. 4. The spectral density of the dynamic platform tilts and the level oscillations

The channel response at this action, which can be defined as relation of maximum amplitude in the channel at its entrance in it in general, depends both on the channel shape and the excitation frequency. The simplest example of the resonance response is a channel in the quarter wavelength. In such channels the entrance corresponds to node line for the free oscillations, the sea level fluctuation being final at the entrance into the harbor or canal becomes essential in the rest part of the basin. In this resonance dissipative forces limit the amplitude of the oscillations on the external excitation.
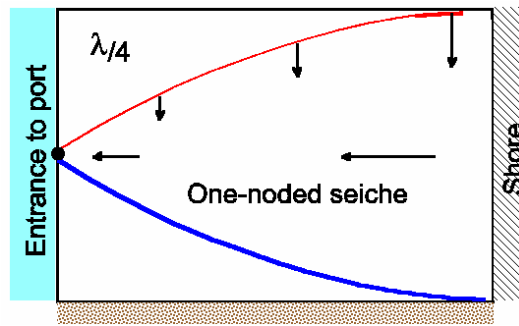
Fig. 5. Scheme of one-noded seiche generation in a particularly closed rectangular basin

The result of the calculation is well coordinated with a real value of the channel length. The obtained result confirms the fact of mechanism realization of the quarter wave resonance in the water area of the port. The spectral term with 6.7 minutes period (double frequency of the main period) is obviously connected with seiche energy dissipation caused by friction on the rough bottom, lateral waterway boundaries and the coastal line. The friction is a square-law nonlinearity, which leads to appearing in the oscillation spectra of the spectral terms connected by phase.

The wind action changes sharply the oscillations features. The spectrum of the vibrations becomes low-frequency, especially the oscillations excited intensively in the narrow frequency band below 1 Hz. In this case the spectral composition depends essentially on the wind velocity. It is connected with the features of the platform construction including 4 raised high supports.

The Figure 6 shows spectral densities of the tilts and accelerations of the ice cover (Y), deformations of the support, horizontal (Y) and vertical (Z) terms of the platform oscillations. The term with frequency 0.32 Hz (T = 3.1 sec.) is present on the all spectra. The tilt spectrum and the horizontal accelerations of the ice cover show the term of 0.34 Hz (T = 2.9 sec). The harmonic at the 0.34 Hz is weakly marked in (X) and (Y) spectrum oscillations. At that time in the spectrum of support deformation a term at the frequency 0.43 Hz (T = 2.3 sec.) is present. It is not practically found out in the spectra of ice and the platform oscillations.
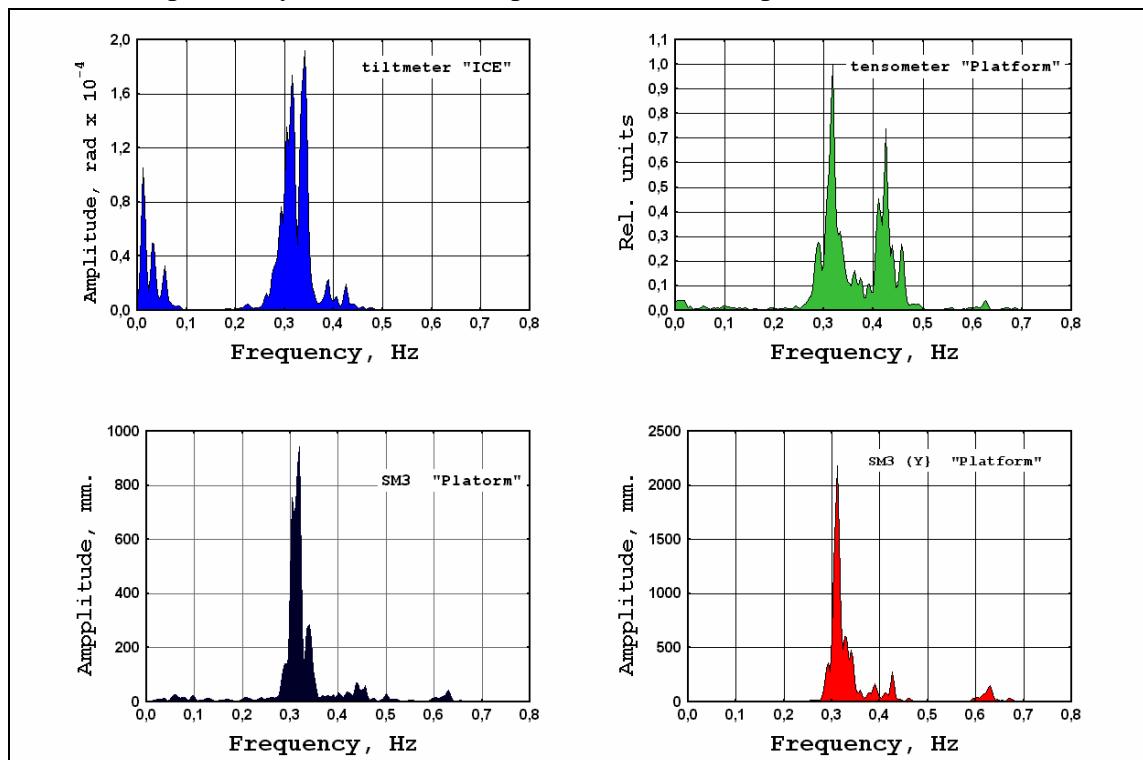

Fig. 6. The oscillations of ice and the platform

The mutual spectrum densities for the corresponding pairs demonstrate the harmonic at the frequency 0.32 Hz. This means that sensors registered the oscillations from the same source. The dynamic tilts of the platform under wind action can be such source.

In the spectra the fission/disintegration of the harmonics in the frequency about 0.32 and 0.34 Hz. is noticed. The spectrum of the ice cover demonstrates it well.

With increase of the wind velocity (to 10-13 m/sec) in the spectra of the platform oscillations appeared the additional harmonics multiples to the main frequency of the oscillations. The presence of terms in the oscillations spectra at the frequencies in 1, 2, 3 etc. times exceeding the main frequency of the oscillations shows a nonlinearity of a corresponding process. As an example the Figures 7 and 8 show the spectra of platform oscillations (in the horizontal (Y) and in the vertical (Z) planes). The registration of the oscillations is performed on May 27 (00:02 – 01:40) at the time when average wind velocity was 9.8 m/sec and at /in the squalls to 14 m/sec. In the period of the substantial wind velocities the connection the ice cover and the platform was well notified.
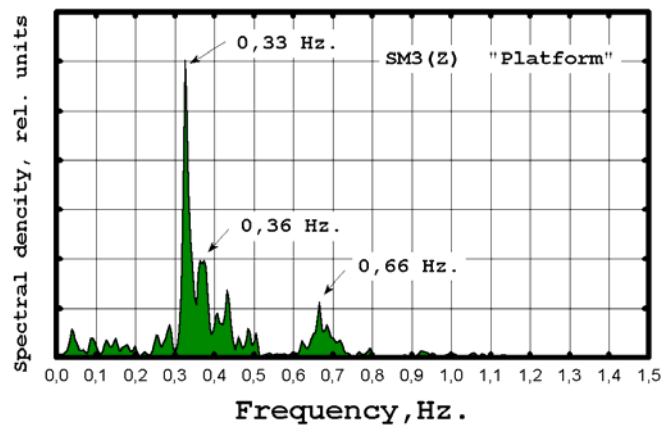

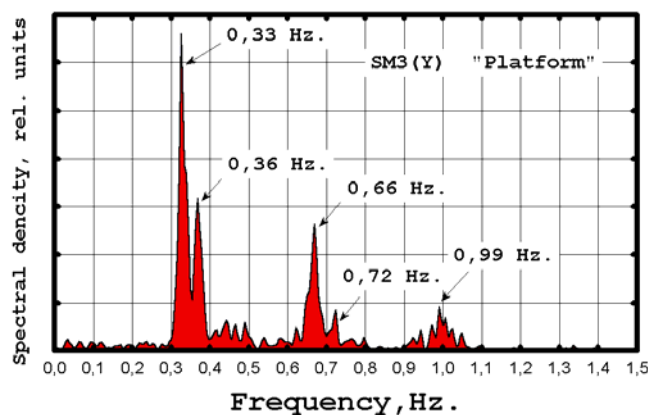Fig. 7. Spectrum of the platform oscillations in the vertical plane (Z)

Fig. 8. Spectrum of the platform oscillations in the horizontal plane (Y)

CONCLUSION

During the winter the wind and ice action at the drilling platform was accompanied by oscillations of all platform and its supports in the gulf of the Ob Bay. The analysis of the sensors installed on the platform found out a spectrum of oscillations and vibrations. The oscillations are divided in two types depending on the character and the nature of the external forces. The oscillations of the first type are the oscillations with the frequency of the external action and the oscillations of the second type are the free oscillations at the impulse action of the wind.

The mutual oscillations of ice and the platform with a period of 12-15 minutes are found out. Their intensivity depended on tide phase and meteorological conditions. The spectral analysis found out terms at the periods T1=15.1 min, T2 = 12.8 min and T3 = 7.6 min. Seiche in the gulf is the main cause of these oscillations.

ACKNOWLEDGEMENTS

FULL-SCALE TESTS OF DYNAMIC ICE FORCE IN BOHAI BAY

Qianjin Yue, Xiangjun Bi, Feng Li and Yan Qu[1]

ABSTRACT

Comprehensive full-scale measurements of ice force and ice induced vibrations have been performed in Bohai Bay over a number of years. Five narrow compliant ice-resist offshore structures, of which three are circular cylinder structures and two are conical structures, have been equipped with sensors. The ice load panels were mounted on cylinder as well as on cone to direct measure ice forces. Meantime accelerometers and the video cameras were used to measure structure responses, velocity and failure behavior of ice. Large-scale test data have been collected. The present paper briefly introduces the test arrangements on these structures and concentrate to discuss the results of dynamic forces and ice induced vibrations on cylindrical and conical structures.

INTRODUCTION

The offshore oil development activity in Bohai Bay started in 1960's. Yue and Liu (2003) reviewed the ice condition and ice caused problems on oil exploitation in this area. At early stage, because the harmfulness of sea ice was no seriously considered and lack of knowledge of designing ice resist structure, two offshore structures designed in 1960's were damaged by sea ice. From 1980's, as several new oil fields were found in north part of the gulf, where the ice condition is heavier than other part of the gulf, the extensive studies of ice-structure interaction including full-scale ice force measurements were carried out. From 1988 to now, five structures, which contain multi-leg and monopod structures with narrow cylindrical or conical legs, have been adopted to measure ice force and ice induced vibrations. In present paper, the tests on each of the structures are introduced.

TESTS OF JZ202-MS PLATFORM

JZ202 oil field, located in north part of Bohai Bay, as shown in Fig.1, consist of four drill platforms at present. All of them have been used to perform full-scale test. JZ202 MS is the first constructed platform in 1988. It was not put into production but specially

---

[1] Dalian University of Technology, China, 116023

used to determine ice forces. A cooperative research project was undertaken by China National Offshore Oil Corporation (CNOOC) and HSVA of German (Wessels and Jochmann, 1991). Direct ice force measurements were conducted. Five load panels of 1.5 m high and 0.6 m wide were mounted on one of the jacket legs. Mean time, several accelerometers were set on the platform. The aim of the project is to determine the peak force of the cylinder and data were used to support the low-level ice force formula (Schwarz, 1994). The accelerometers deployed in top of the structure recorded strongly vibration induced by ice, some times steady state vibrations were also observed. The issue of ice-induced vibrations was no fully investigated in this project, but it evoked much concern for the oil company.
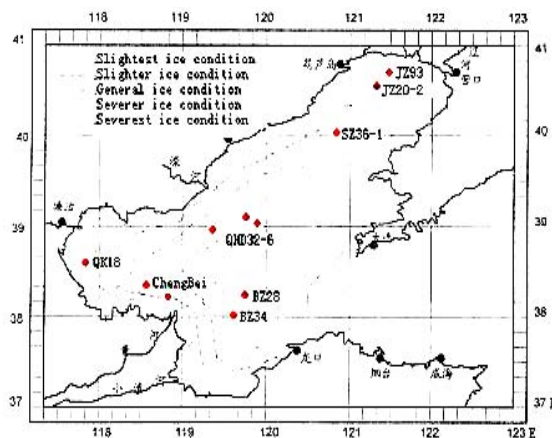

Fig. 1. Bohai Bay and oil field distribution

Fig. 2. JZ202 MW platform

TESTS ON JZ202 MUQ AND MNW PLATFORM

MUQ is the center process platform of JZ202 oil field. MNW is a drilling platform nearby MUQ as shown in Fig.3. They were constructed in 1991 and initially designed as cylindrical structures. Considering the severe vibration observed on JZ202 MW platform, double side (up-ward and downward) ice breaking cones were mounted on each of the legs of these two platforms as well as JZ202MS platform aiming to mitigate vibrations and reduce ice force. But after these platform get into operation, staff on the platform complained about the vibrations when ice acting on the platforms. In order to investigate the ice induced vibration on conical structures, field tests carried out on MUQ and MNW platform since 1995(Yue and Bi, 1996). The test set up is shown in Fig.4.

Specially designed the ice load panels with same surface feature of the cone were mounted on the up-ward cone (Fig.5) to measure ice force (Fig.6). One panel covers 8º and a total 48º of the cone surface was covered by the panels. Accelerometers and video cameras were also set to record the dynamic response and failure behavior of ice sheet. Systematic studies of dynamic ice force of conical structure achieved based on these test data.
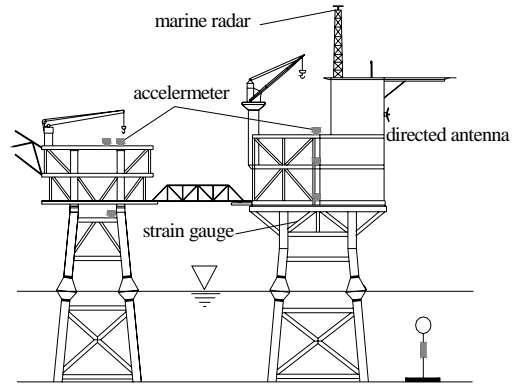
Fig. 3. JZ202 MUQ and MNW platforms

Fig. 4. The test set up on MUQ and MNW

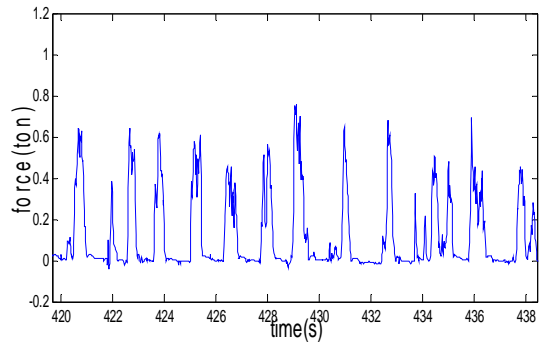Fig. 5. Ice load panels of conical structure

Fig. 6. Ice force variations of conical structure

Yue et al (1998) reported that when ice acting on up-ward cone the breaking length of ice sheet is approximately 7 times of ice thickness. At high ice speed, the resonant vibration may appear. Based on direct measured ice force and ice failure process analysis, a triangle-shape load function was developed as follows:

$$F(t) = \begin{cases} F_0\left(1 - \dfrac{t}{\tau}\right) & (0 \le t < \tau) \\ 0 & (\tau \le t < T) \end{cases} \tag{1}$$

Where F_0 is amplitude of total horizontal ice force on the cone. T represents the period of the ice breaks along circumferential direction, and τ is the acting time of ice sheet against the cone.
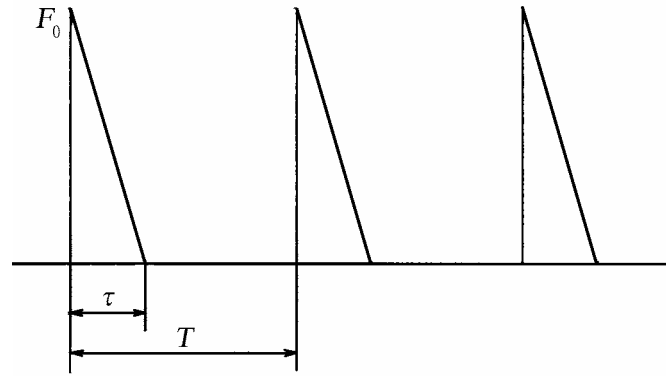
Fig. 7. Ice load functions for conical structures

Li and Yue (2002) analyzed the breaking length when ice fails in wedged beam failure. Li et al (2003) reported that there exist two failure modes when ice acting on up-ward cone: wedged beam bending failure and plate bending failure. It is confirmed that for wedged beam bending failure, the breaking length is about 7 times ice thickness, but for plate bending failure is about 4 times ice thickness. They also analyzed the transition condition for ice sheet failure modes from wedged beam to plate. Qu et al (2003) studied the random ice force of narrow conical structure. They presented the random distributions of ice force amplitude and period for two kind failure modes.

TESTS OF JZ202 MSW PLATFORM

JZ202 MSW platform is a three-leg jacket structure built in 1997 as shown in Fig. 8.

Fig. 8. JZ202MSW platform
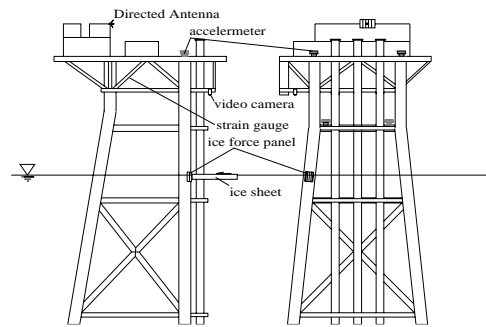
Fig. 9. The test set up of JZ202MSW

At first three years, it was not added with ice breaking cones so that it was used to investigate the ice induced vibrations of cylindrical structure. The accelerometers, video camera and ice load panels were deployed on the structure as shown Fig.9. Yue and Bi (2000) reported the test results that when ice fails in crushing two types of vibrations were observed. At high ice speed ice induces random vibrations and in an intermediate ice speed steady state vibrations were recorded.

142

Fig. 10. Ice induced steady state vibrations

Fig. 11. Ice induced random vibrations

The maximum acceleration appeared in steady state vibrations nearly 0.2g which have caused severe accidents. A natural gas pipeline on the platform was broken because of the strong vibrations. Unfortunately, the load panels did not work then and no directly measured ice force data were obtain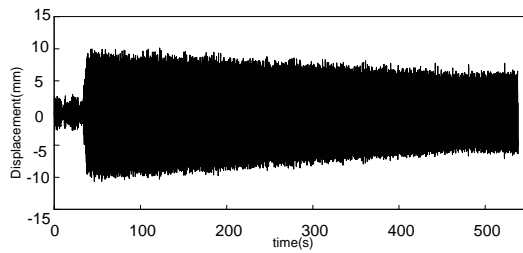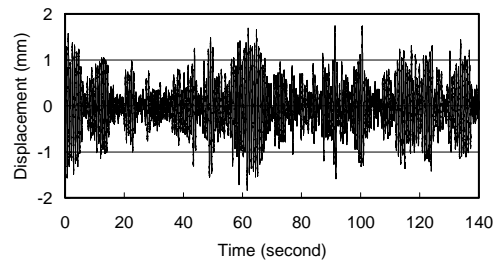ed. In 1998, the ice breaking cones were mounted on each leg of the structure. After that, the phenomenon of ice induced steady state vibrations had never been found again.

TEST OF JZ93 MDP-1 PLATFORM

JZ93 MDP-1 is a monopod structure for mooring oil tanker. It was used to measure ice force since 2001.The test arrangement is shown in Fig. 12. A mosaic ice load panel composed with 18 panels (shown in Fig.13) was mounted on the ice contacting area of the structure and dynamic response and ice speed were recorded simultaneously. The dynamic ice forces and responses of the structure in crushing failure of ice sheet were strictly recorded.
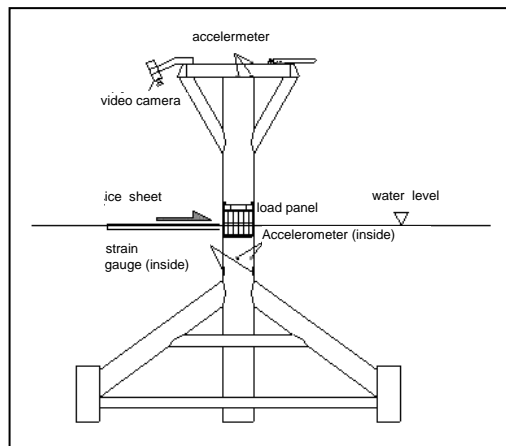
Fig. 12. The tests of JZ93MDP-1 platform

Fig. 13. The mosaic ice load panels

Yue et al (2002) reported the tests results. The tests displayed three ice force modes distinguished by ice speed, which cause structure quasi-static, steady state or random vibrations. Analysis showed that the mechanism of each ice force mode takes place in ductile, ductile-brittle transition and brittle failure, respectively. The failure processes of each ice force mode during the loading and unloading phases are analyzed.

143
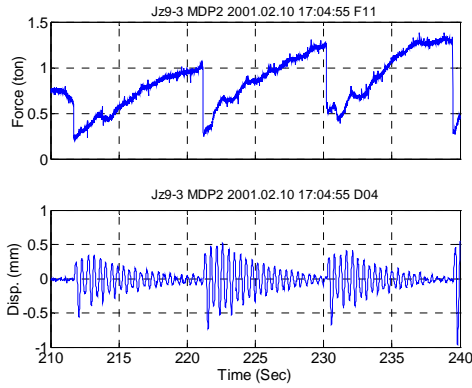
Fig. 14. Quasi-static ice force and the response of structure.
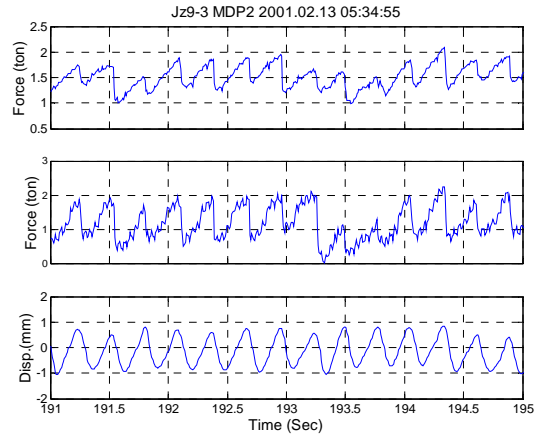
Fig. 15. Steady state vibrations of structure and ice forces.

Quasi-static vibration means force periods much longer than the structure period. This phenomenon takes place when the speed was very slow (below than 2 cm/s). The ice force period is about 20 times the structure nature period. It is supposed that during quasi-static ice force the ice fails simultaneously around the circumference and ice fails in ductile stage.

The steady state vibration took place when ice speed between 2-4cm/s. The further analysis confirms that during steady state vibration ice fails in the transition zone of ductile and brittle failure of ice. Ice load panels display the simultaneous failure behaviour. The test data also disclose that frequency lock-in phenomenon (as shown in Fig. 16) during the steady state vibration that may support the theory of self-excitation. The mechanism of ice induced the steady state vibration were analyzed. The micro-cracks activities of ice in the ductile-brittle transition zone play the key role in the formation of steady-state vibrations. When structure moves forwards, the loading rate of the ice just slows down, but near the ductile-brittle transition point dense steady micro cracks are formed. When micro-cracks reach to saturate the structure move back and the formed micro-cracks propagate unsteady (Fig. 17).
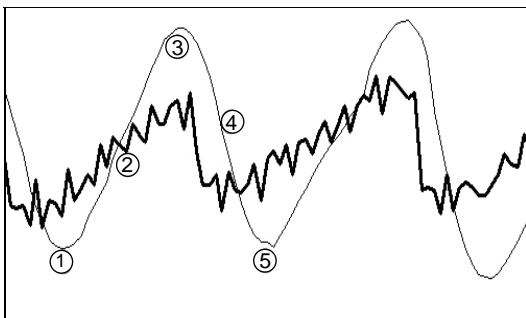

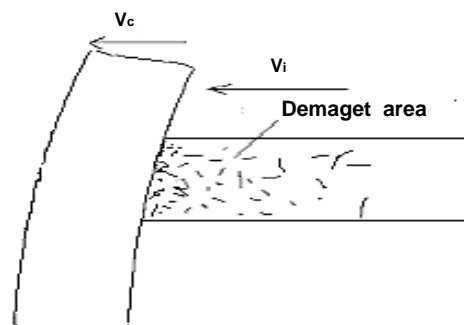Fig. 16. The phenomenon of frequency lock-in

Fig. 17. The failure mechanism of ice induced steady state vibration

When ice speed is faster than 4 cm/s, the ice forces and response are random. It is because of ice failure in brittle. And ice load panel shows the non-simultaneous failure

behaviour. Fig 18 shows the ice failure in crushing at fast speed and Fig. 19 is the ice force variations at fast ice speed.

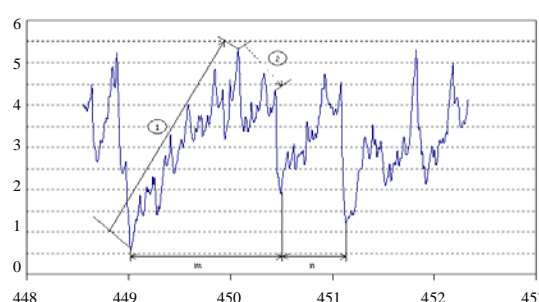Fig. 18. Ice acting on cylinder in crushing

Fig. 19. Random ice force in fast ice speed

CONCLUSION

The full-scale tests conducted in Bohai Bay are reported. The object of tests is focused on dynamic ice forces of narrow compliant structures with cylindrical structure in crushing failure and conical structure in bending failure. Five structures have been deployed sensors and quite a lot infield data are obtained. From JZ202 MUQ and MNW platform, the dynamic ice forces of conical structure are comprehensively studied. Based on direct ice force measurement and failure process analysis a simplified load function is developed.

From JZ202 MS, JZ202 MSW and JZ93 MDP-1 platforms the dynamic ice force of cylindrical structure in crushing failure are investigated. The test displayed that when ice interacts with compliant cylindrical structure three types of ice force would appear. With the ice speed changing from slow to fast, ice would induce structure quasi-static vibration, steady-state vibration and random vibration. This supports the supposing of Engelbrekston (1977) and Karna (1990). Then the physical mechanism of the dynamic ice force formation is discussed but the theoretic model for predicting structure response needs further research work.

REFERENCE

Engelbrektson, A. Dynamic ice loads on lighthouse structures. In Proceedings of the 4th International Conference on Port and Ocean Engineering under Arctic Conditions, St. John's, Canada (1977), 2.

Li F., Yue Q. J. An analysis of amplitude and period of alternating ice loads on conical structures. In Proceedings of the 16th International symposium on ice. International Association for Hydraulic Research, Dunedin, New Zealand (2002). Vol.III, 87-93.

Li,F.,Yue Q.J Shkinek,K,K and Karna,T A qualitative analysis of Breaking length of sheet ice against conical structure. In Proceedings of the 17th International conference on Port and Ocean Engineering under Arctic Conditions. Trondeim, Norway (2003). Vol.I. 293-302.

Karna, t. and Turnunen, R. A straightforward technique for analyzing structural response to dynamic ice action. In Proceedings of the 9th International Offshore Mechanics And Arctic Engineering conference. Houston (1990). Vol.IV, 135-142.

Maattanen, M. Ice-induced vibrations of structures – Self-excitation. In Proceedings of the 9th International symposium on ice. International Association for Hydraulic Research, Sapporo (1988). Vol.2, 658-665.

Schwarz.J Low level ice forces Proc. In Proceedings of the 12th International symposium on ice. International Association for Hydraulic Research, Trodheim, Norway (1994) Vol.III. 1040-1050.

Wessels.E and Jochmenn, P. Model/full scale correlation of ice forces on a jacket platform in Bohai Bay. In Proceedings of the 11th International conference on Port and Ocean Engineering under Arctic Conditions. St. John's, Canada (1991) 198-212.

QU, Y, Yue, Q.J., Bi,X.J and Karna,T, Random Ice force on conical structure, In Proceedings of the 17th International conference on Port and Ocean Engineering under Arctic Conditions. Trondeim, Norway (2003) Vol.I P. 259-271.

Yue, Q.J., Zheng, R.T. and Bi, X.J. "Observations of Ice Cracks under Compression tests." In Proceedings of the 13th International symposium on ice. International Association for Hydraulic Research, Beijing, China (1996), Vol.3, 932-937.

Yue, Q.J. and Bi, X.J. Full-scale tests and analysis of dynamic interaction between ice sheet and conical structures. In Proceedings of the 14th International symposium on ice. International Association for Hydraulic Research, Vol. II, Symposium on Ice, Potsdam (1998).

Yue, Q.J. and Bi, X.J. Ice-induced jacket structure vibrations in Bohai Sea. *J. of Cold Regions Engineering 14J*(C2): 81-92 (2000).

Yue,Q.,J., Zhang, X., Bi. X., and Shi Z,. 2001, Measurement and analysis of ice induced steady-state vibrations. In *Proceedings of the 16ᵗʰ International conference on Port and Ocean Engineering under Arctic Conditions*. Ottawa, Canada (2001) Vol.1. 413-420.

Yue Q,J, Bi X, T. Karna. Dynamic ice forces caused by crushing failure. In Proceedings of the 14th International symposium on ice. International Association for Hydraulic Research, Dunedin, New Zealand (2002). Vol.III, 231-237.

Yue Q.J and Liu. L. Ice problems in Bohai Sea oil exploitation. In Proceedings of the 17th International conference on Port and Ocean Engineering under Arctic Conditions. Trondeim, Norway (2003) Vol.I P. 151-164.

APPLICATION OF A BOREHOLE JACK FOR DETERMINING THE LOCAL STRENGHT OF FRESH AND SEA ICE

Kovalev S.M., Korostelev V.G., Nikitin V.A., Smirnov V.N., Shushlebin A.I.[1]

ABSTRACT

Results of the tests of practically fresh ice with a borehole jack in the north-west part of the Caspian Sea in February 2003 and of fresh ice in the middle part of the Ob Bay in May 2003 are discussed. The deformation and failure mechanisms of ice by indentor at the different stages of loading in the borehole are studied. The local strength exceeded uniaxial compressive strength of ice samples in 3.8 times for the Caspian Sea and in 4.6 times for the Ob Bay. It is suggested to use a borehole jack for anisotropy determination of ice strength in azimuthal plane. The control of cracking processes in ice cover was carried out with seismoacoustic devices. The configuration and crushing zones sizes, friction angles and cohesion of these zones with ice cover are determined.

INTRODUCTION

In the papers about borehole jack tests the principal attention is paid to the next problems;
– of the test results interpretation on the basis of theoretical analysis of deformation and failure;
– comparison of local strength of ice cover by indentor loading with uniaxial compressive strength of ice sample;
– obtaining of full scale strength of ice cover dependence on temperature and ice salinity in conditions of confined compression;
– seasonal variation of local strength and its correlation with calculated ice flexural strength;
– strength index distribution of thickness for ice features and boundary estimation of refrozen layer in ridge.

In Masterson (1992) it is shown that as a result of indentor introduction in the ice three zones of deformed ice are generated remote of borehole jack wall. Their boundaries are also determined: crushing zone, radial crack zone and the zone of elastic ice behavior.

Predicted in this paper value of the upper limit of correlation between local strength and the uniaxial compressive strength was confirmed in Masterson et al. (1997). The sea ice strength in confined conditions compression at the diameter of indentor about 9 cm has exceeded strength of cylindrical samples of 7.5 cm diameter approximately in 4 times.

---

[1] Arctic and Antarctic Research Institute, St-Petersburg, Russia

Empirical dependence of ice cover strength in borehole of deformation velocity and the brine volume is presented in Spencer et al. (2001).

In Johnston et al. (2002), Timco et al. (2001) the data about seasonal variation of local strength of first year sea ice cover are presented. They are compared with flexural strength of ice cover, calculated by formula from the Timco, O'Brien (1994).

The results of ridge investigations and level ice during the spring in the region of Sakhalin Island are presented in Smirnov et al. (2000). The possibilities of borehole jack for determination of thickness of refrozen ridge layer are shown.

The selected review of studies describing the results of ice cover study with borehole jack shows that this method is a multi-functional. Excepting obtained during the tests values of local ice strength and the distribution of strength index by thickness of ice formations the method allows to determine full-scale compressive and flexural strength of ice cover and without sample tests estimate uniaxual compressive strength of standard ice samples.

In this paper the results of local ice strength determination in the north-west part of the Caspian Sea in February 2003 and in the middle part of the Ob Bay in May 2003 are discussed. Attention was paid to the mechanisms of deformation and failure of ice as it was loaded by an indentor. Acoustic emissions were monitored with seismic devices. The possibility of estimation of anisotropy of ice strength in azimuthal plane was found out and the crush zone was studied by special experiments.

THE DEVICES AND THE METHODS USED IN THIS STUDY

The local in situ ice strength in the borehole was measured with a hydraulic jack with replaceable indentors of diameter 3, 6, 9 and 12 cm and suitable configurations of their surfaces providing closely adjoining of the indentor to the borehole wall was used. The indentor was installed into the ice in one direction and the base displacement of the indentor was limited by a support, its surface area exceeded the surface area of the indentor in many times. The maximum pressure in the hydrosystem was 70 MPa, the maximum force – 350 kN, the papering stroke of the indentor reached 6.5 cm. The boreholes were drilled with ring drill of 22 cm diameter. During the tests the time of loading, indentor displacement and pressure in the hydrosystem were fixed.

The in situ stress applied by the borehole jack indentor was determined from the formula:

$$\sigma_i = \frac{S_p}{S_i} P, \tag{1}$$

where S_p – paper area of piston in probe; P – pressure in the hydrosystem; S_i – surface area of the indentor.

The diameter of indentor of the borehole jack sets tests discreteness of the level ice cover and the refrozen ridge layer at vertical. It is determined by the ice zone sizes in which the irreversible deformation processes at loading of ice are developed. The distance between the layers of the performed test had approximately 3 indentor diameters according to the methodic suggested in Smirnov et al. (2000), Spencer et al. (2001).

The tests of samples for uniaxial compression were performed in field conditions on hydraulic press develop with maximum force 100 kN and ensuring samples deformation

velocity 10^{-4} – 10^{-3} m/s. The failure of samples was plastic and plastic-brittle depending on physical state of ice. The prismatic samples had a cross sectional area that was close to the surface area of the indentor used in these tests.

The rate anisotropy studies of ice strength were performed at the same depth of the jack immersing into the borehole at of the indentor at 90°. The 3 cm diameter indentor was used. The experiments were performed on the warm ice of the Caspian Sea.

The crack formation processes and arising in this case acoustical emission were fixed with seismic acoustic receivers and CB-5 which were frozen into or screwed into the surface ice cover layer at the distance about 1 m from the borehole wall.

To find the crush zone configuration, its cohesion with ice cover and the friction angle particularly destroyed ice volume was squeezed out into the cut, sawed out at the distance 6-10 cm from the borehole wall. 16 experiments were performed on Caspian Sea ice, the indentor diameter was 3 cm.

THICKNESS, TEMPERATURE, SALINITY AND ICE CONSTRUCTION FEATURES

The tests of ice cover in north-west part of the Caspian Sea were performed in the first ten days of February 2003. The works performed on the level and rafted ice, the thickness of which varied from 24 to 84 cm. The average ice temperature was –1.5 °C. Minimum ice salinity was 0.1 ppt and the maximum ice salinity was 0.8 ppt. The ice in general was of columnar structure with layers of air inclusions.

The works in the middle part of the Ob Bay were performed on the fast ice in the first 10 days of May 2003. The fresh ice thickness varied from 102 to 188 cm. The general results were obtained in the temperature range –2.9°C to –6.2°C. The tested fast ice had highly expressed pyramid structure. The characteristic of ice crystals growth is usual highly expressed in the geometric selection law. Therefore their vertical sizes reached some tens of centimeters. In the bottom layer of the ice cover the cross sizes of crystals were 10–12 cm.

RESULTS AND DICCUSSION

The local strength

The most typical dependences between stress which is created by the indentor in the ice cover (introduction stress) at the approximately constant velocity of loading and the time of the loading are shown on the Fig. 1. The analysis of the obtained dependences, visual observations and fixing of cracks in the ice cover with seismic devices allow to represent the interaction process of the indentor with ice as following. The three stages of borehole loading are observed.

The first stage is completed by arising of a surface crack and characterizes the initial moment of indentor introduction that means surface ice strength. The second stage of the loading is completed by the particular failure of some ice volume at the peak stress (local strength) leading to crush zone formation and possible to radial cracks. Their formation is caused first of all the physical state of ice (warm, cold). The formation of the crush zone is spontaneous.
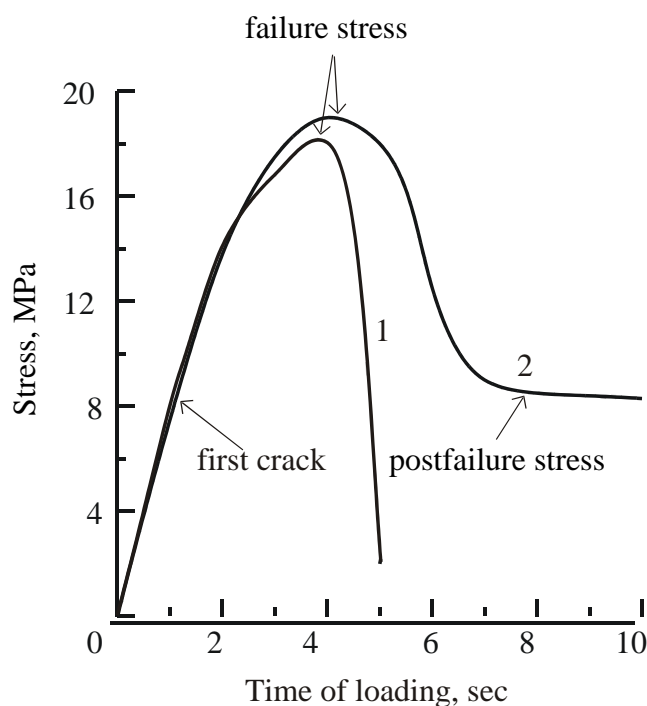
Fig. 1. Stresses in ice vs time by indentor loading

At the third stage of the loading in general two types of indentor interaction with ice are observed. The first type (Fig. 1, curve 2) was characterized by the penetration of the indentor through crush zone at the practically constant post-failure (post-peak) stress which was less than the failure at 20-60% for the Caspian Sea ice and at 20-30% for the Ob Bay fast ice. According to Masterson (1992) one half the post-peak stress corresponds to ice cover strength at the shear or cohesion at internal friction angle, which is equal 0 at the conditions of confined compression.

The second type of the interactions of indentor with ice at the third stage of loading was characterized the one of the radial cracks turned into magisterial after it reaches the peak stress (Fig. 1, curve 1). It leaded to spalling of some ice volume at top or bottom surfaces depending of indentor immerging depth.

In the Table 1 some results of static treatment of ice strength values are shown. The indentor diameter was 9 cm.

Table 1. The results of ice strength determination

Paper area	Caspian Sea		Ob Bay	
Average ice temperature or range of its changes, ºC	-1.5		-2.9 … -6.2	
Fixed parameter	σ_l	σ_c	σ_l	σ_c
Numbers of measurements	78	63	67	58
Mean, MPa	11.0	2.9	24.1	5.2
Standard deviation, MPa	0.9	1.2	2.5	1.6
Coefficient of variation	0.1	0.4	0.1	0.3

Comments:

σ_l – failure (peak) introduction stress;

σ_c – uniaxial compressive strength of the ice sample.

The low values of coefficient of variation for σ_l are caused uniform distribution of the local strength by the thickness of the ice cover which is determined by its temperature regime, texture and structure features. Essentially higher values of the coefficient of variation for σ_c (0.3, 0.4) may be caused both the natural variation of physic-mechanical properties of ice samples and the influence of external factors on its physical state after the extraction onto the surface ice cover bores and preparation during some time the samples and performing tests series in the field conditions.

The local strength of the ice cover exceeded uniaxial compressive strength of ice samples at the in 3.8 times for the Caspian Sea and in 4.6 times for the Ob Bay. These values of the correlations between σ_l and σ_c are closed to the data from Masterson (1992), Masterson et al. (1997), which again confirms a possibility of data obtaining about uniaxial compressive strength of ice samples using borehole jack.

The strength anisotropy

The strength anisotropy of the ice cover in the horizontal plane was primarily caused by under ice currents. According to experimental data obtained on first-year samples of sea ice Borodkin et al. (1992) the largest uniaxial compressive strength was observed at the force application along dominating C-axis orientation (azimuthal angle is 0º). The lowest strength corresponds 45º, and at the angle 90º the second maximum (lower the first) of the ice strength is obtained. The maximum anisotropy reached 50%. At the change of loading application direction the mechanism of failure of samples is also different. At 45º relating C-axis the sliding of the crystals occurs along each other and from here is the minimal strength. In this case the shear deformations are accompanied by acoustic emission which is perceived as «rustling». At the 0º and 90º the mechanism of crystals failure dominates which has an «explosion» character.

For the middle ice layers of the Caspian Sea the local strength anisotropy reached 30-40%. The anisotropy rate investigations with borehole jack can find out the directions of the maximum or minimum ice strength in the horizontal plane.
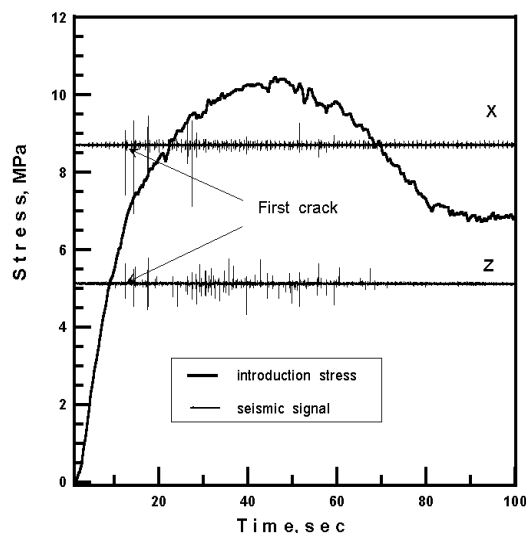
Acoustic emission

Fig. 2. An example of ice load recording with seismic signal by the borehole jack

151

The example of ice loading record by the borehole jack with acoustic emission recording is shown on the Figure 2. The seismic devices fixed accurately the moment of first crack arising, characterizing the surface ice strength in the borehole.

The crush zone

The crush zone configuration, its cohesion with ice cover and friction angle were determined as results of extrusion particularly destroyed ice volumes into the cut which had shape closed to truncated cone (Fig. 3). The calculations of the surface area of the truncated cone S, cohesion C and friction angle φ_0 according to Fig. 4, were made by formulas:

$$S = \pi r_1 \sqrt{r_1^2 + (h_1 + h_2)^2} - \pi r_2 \sqrt{r_2^2 + h_2^2} \; ;$$

$$C = \frac{S_p P}{S} \; ; \quad tg\,\varphi_0 = \frac{r_1 - r_2}{h_1} \; ; \quad h_2 = \frac{r_2}{tg\,\varphi_0} \; .$$

The means, standard deviations and coefficients of variation for φ_0 were 43°, 8°, 0.2, for cohesion C – 0.3, MPa, 0.1 MPa and 0.4, correspondingly.

Fig. 3. Ice volumes particularly failed by borehole jack
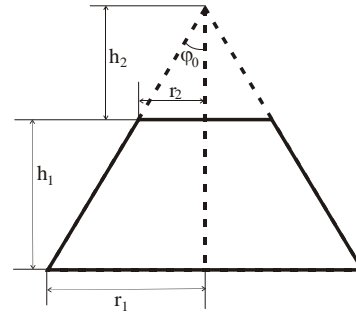
Fig. 4. Scheme calculation of surface area of truncated cone, cohesion and friction angle for crush zone

The suggested methods of tests performing and obtained with its results can be used for:

– estimation of load of particularly destroyed ice volume on construction elements of the hydrotechnical constructions;

– modeling and interpolation of the large scale experiments of refrozen layer ridge loading on its keel to determine the friction angle and cohesion weakly connected ice fragments making the ridge keel.

CONCLUSION

The local strength data of practically fresh ice in the north-west part of the Caspian Sea in February 2003 and the middle part of the Ob Bay in May 2003 are presented. The mean of local strength for ice of the columnar structure were 11.0 MPa at its temperature -1.5ºC (Caspian Sea) and 24.1 MPa for temperature change range from -2.9ºC to -6.2ºC (Ob Bay).

The local strength exceeded the uniaxual compressive strength of ice samples at in 3.8 times for the Caspian Sea and in 4.6 times for the Ob Bay. The possibility to estimate

the uniaxual compressive strength of ice samples with borehole jack in situ is confirmed.

It is suggested to use the borehole jack for determination of ice cover mechanical anisotropy in the horizontal plane. The investigations of the anisotropy range with borehole jack can find out directions of maximum or minimum ice strength in the horizontal plane.

The seismic devices fix the moment of arising of the first crack characterizing the surface ice strength in the borehole.

It is determined with special experiments that the crush zone has shape like a truncated cone. The means and standard deviations were 0.3 and 0.1 MPa, for cohesion particularly destroyed ice volumes with undestroyed ice cover for the friction angle – 43 and 8°, correspondingly. The suggested methods of experiments with extrusion particularly destroyed ice volumes into the cut the crush zone and obtained with it results can be used for the estimation loading of the particularly destroyed ice volumes on construction elements.

REFERENCES

Borodkin, V.A., Gavrilo, V.P., Kovalev, S.M., Pasynkov, V.V. and Lebedev, G.A. 1992. Influence of structural anisotropy of sea ice on the mechanical and electrical properties. *The proc. of the second int. offshore and polar engineering conference*, San Francisko, USA, Vol. 2, pp 670-674.

Johnston, M., Frederking, R. and Timco, G. 2002. Properties of decaying first year sea ice: two seasons of field measurements. 17th *Int. Symposium on Okhotsk sea and sea ice*, Mombetsu, Hokkaido, Japan, pp 303-311.

Masterson, D.M. 1992. Interpretation of in situ borehole ice strength measurement tests. *IAHR Ice Symposium, Proceedings*, Vol. 3, Banff, Alberta, pp 802–815.

Masterson, D.M., Graham, W.P., Jones, S.J. and Childs, G.R. 1997. A comparison of uniaxial and borehole jack tests at fort Providence ice crossing, 1995. *Can. Geotech. J., 34*, pp 471–475.

Smirnov, V., Sheikin, I., Shushlebin, A., Kharitonov, V., Croasdale, K., Metge, M., Ritch, R., Polomoshnov, A., Surkov, G., Wang, A., Beketsky, S. and Weaver, J. 2000. Large scale strength measurements of ice ridges; Sakhalin 1998. *Proc. ICETECH-2000*, St.Petersburg, pp 512-520.

Spenser, P.A., Masterson, D.M. and Yockey, K.E. 2001. Floating sea ice road strength from borehole jack date: Northstar 2000. – *Proc. of the 16th Int. Conf. on Port and Ocean Eng. under Arctic Conditions, POAC'01,* Ottawa, Ontario, Canada, pp 183–192.

Timco, G.W. and O'Brien, S. 1994. Flexural strength equation for sea ice. *Cold Regions Science and Technology, Vol. 22*, pp 285-298.

Timco, G.W., Johnston, M. and Kubat, I. 2001. Ice decay and the ice regime system. *Canadian hydraulics center, Technical report HYD-TR-070*, December 2001, 28 pp.

FEATURES OF THE ICE DRIFT RESPONSE TO THE WIND INFLUENCE ON THE NORTHEASTERN SHELF OF SAKHALIN ISLAND

Elena Tikhonchuk[1] and George Shevchenko[2]

ABSTRACT

Vector series of ice drift and wind velocities were analyzed. The analysis shows a high correlation between the wind series and the residual component of ice drift. Values of "wind coefficient" are calculated using two-dimensional linear regression. A matrix of linear transformation is found to represent the relationship between the vector series of wind and drift by a response ellipse.

INTRODUCTION

The development of oil and gas deposits on the northeastern shelf of Sakhalin Island is carried out in severe ice conditions. Sea-ice is one of the major factors affecting the operation of drilling platforms, pipelines, servicing vessels and tankers during the ice period. Significant values of drift velocity, caused by the tide and wind influence, are the distinctive feature of this area.

Velocities of tidal drift reach significant values (1 m/s and more) in given area, it is caused by the influence of diurnal shelf waves. The features of tidal drift are in detail considered in paper Shevchenko et al., (2001). In the given work we shall concentrate the attention on features of the response of an ice cover to the influence of a wind.

When deep cyclones are passing over the investigated region, wind velocities reach great values (18-22 m/s) (Kato A. et al., 2001). Accordingly, the velocity of wind drift can reach the significant values. It is shown in paper Tambovsky et al, (2001), that wind induced ice drift velocities can exceed 100 cm/s, and can create significant loads on objects of oil and gas complex located on the shelf.

The character of the response of ice drift to the influence of a wind in the open sea is well-investigated and as a whole is satisfactory described by the Ekman theory. However, near to coast, the reaction of drift to influence of a wind gets rather specific features because of change of the sea depth and presence of reflecting coastal border. First

---

[1] Institute of Marine Geology and Geophysics, Russian Academy of Sciences, Yuzhno-Sakhalinsk, Russia
[2] Sakhalin Institute of Fisheries & Oceanography, Yuzhno-Sakhalinsk, Russia

of all this reaction becomes not isotropic - value of «wind factor», describing velocity of drift in relation to the wind velocity, will obviously depend on a direction of external influence. Similarly, it is possible to say about the deviation of ice drift direction from a direction of external force action.

We applied method of the two-dimensional (matrix) regression analysis to research the features of the response of drift to the influence of a wind for conditions of the north-eastern shelf of Sakhalin. As it will be shown below, this simple method has appeared to be rather effective for definition of many important features of ice drift reaction to the influence of a wind. It is possible to attribute to these features directions at which the greatest and least values of wind factor are observed, so it is possible to find "effective" and "inefficient" directions of a wind, respectively. The second important moment is the definition of eigen directions, at which the direction of drift coincides with direction of external force. These directions divide areas with a various deviation of ice drift direction from direction of a wind (clockwise or counter-clockwise). It is possible also to estimate directions, at which such angular shift will reach the greatest value.

The purpose of this study is to estimate these peculiarities of the ice drift response to the wind influence in the offshore Sakhalin region on the base of coastal radar data.

MEASUREMENTS OF ICE DRIFT

Measurements of ice drift using radar stations on the northeastern coast of Sakhalin island were carried out at the beginning of 1990 years. The recognition of ice blocks and observation of their drift was made on defined typical features of geometric forms, giving clear signal on indicator. Data of measurements from two radar stations Odoptu and Komrvo in 1993-1993 [should this be 1992-1993] were used. Vector series for 1992-1993 were used to determine the nature of interaction between wind and corresponding residual component of ice drift.

Velocity and direction of ice drift were observed every hour in the fixed 9 points with distance of 4 km between them. The depth of the sea in the most close to the coast points was10-15 m, in the most distant - about 50 meters. Wind velocity was measured synchronously at height of 10 m (Tambovsky et al., 2001).

The tidal component was subtracted from the initial data of ice drift to define components of drift connected with the wind influence. Obtained residual series were smoothed using a 25-hours running mean to eliminate the high-frequency oscillations of drift. The similar smoothing was applied to the wind velocity series.

CALCULATION OF THE REGRESSION MATRIX

Regression model was used for the analysis of synchronous hourly series of the wind and ice drift. The calculation of a matrix A, corresponding to transformation in Eq.(1), gives "wind coefficients":

$$(u,v) = A * (wu,wv) + (\varepsilon u, \varepsilon v), \qquad (1)$$

where (u,v) are vector series of the residual component of ice drift, (wu,wv) are the synchronous series of wind velocity vectors, and $(\varepsilon u, \varepsilon v)$ are the residual variations of drift, which cannot be determined by a linear transformation of the matrix A. The matrix A has the elements:

$$\begin{pmatrix} a_{11} & a_{12} \\ a_{21} & a_{22} \end{pmatrix}. \tag{2}$$

Calculations of matrix elements were made using the method of least squares:

$$(u - a_{11}\, wu - a_{12}\, wv\,)2 \rightarrow min$$

$$(v - a_{21}\, wu - a_{22}\, wv\,)2 \rightarrow min\,. \tag{3}$$

Minimization is produced on the result characteristic (drift velocity). Here, coefficient a_{11} represents the response of the eastward component of drift due to a similar component of wind. The element a_{22} corresponds to the meridian component. Two other elements reflect the influence of wind components on the opposite components of drift: a_{12} - corresponds to the response of the eastward component of drift to the northward component of wind, and a_{21} corresponds to the response of the northward drift to the eastward component of wind (Shevchenko et al., 2001). The calculations were made for each month series apart, as well as on full series for each year.

Table 1 presents regression coefficients for wind and ice drift velocity at coastal radar stations Komrvo and Odoptu (1993, 1994) [should this be 1992, 1993] for two off-shore ice observation distances: 4 km (S1) for both sites, and 12 km (S3) for Komrvo and [should this be 16] km (S4) for Odoptu. The main diagonal ("co-linear") elements of the regression matrix are positive for all cases, indicating that winds generate drift currents in the general direction of the wind. In contrast, the off-diagonal elements are negative, indicating that current vector is related at significant angle to the wind vector.

Table 1. Regression matrix, calculated on full series 1992, 1993
for CRS Komrvo and Odoptu, for two off-shore ice observation distances:
4 km (S1) for both sites, and 12 km (S3) for Komrvo
and 16 km (S4) for Odoptu

Year Station		Regression matrix	
		1992	1993
K o m r v o	S_1	$\begin{pmatrix} 3.07 & -0.51 \\ -4.71 & 5.34 \end{pmatrix}$	$\begin{pmatrix} 0.9 & -0.4 \\ -3.06 & 2.24 \end{pmatrix}$
	S_3	$\begin{pmatrix} 2.27 & -0.67 \\ -4.32 & 4.84 \end{pmatrix}$	$\begin{pmatrix} 1.4 & -0.64 \\ -4.45 & 3.91 \end{pmatrix}$
O d o p t u	S_1	$\begin{pmatrix} 1.9 & -0.15 \\ -2.68 & 3.12 \end{pmatrix}$	$\begin{pmatrix} 1.04 & -0.26 \\ -2.18 & 2.18 \end{pmatrix}$
	S_4	$\begin{pmatrix} 1.14 & -0.36 \\ -2.16 & 3.31 \end{pmatrix}$	$\begin{pmatrix} 0.95 & -0.15 \\ -2.75 & 2.58 \end{pmatrix}$

This model shows from 60% to 80% scatter of ice drift velocities. Moreover, prediction of the northward component is more exact. Maybe, that the northward component is only slightly influenced by the coast line because of the topography of the region.

Eigen values of the regression matrix were estimated from characteristic equation of the matrix:

$$\left| \begin{pmatrix} a_{11} & a_{12} \\ a_{21} & a_{22} \end{pmatrix} - \lambda \times \begin{pmatrix} 1 & 0 \\ 0 & 1 \end{pmatrix} \right| = 0, \qquad (4)$$

or, this is the same:

$$(a_{11} - \lambda) \times (a_{22} - \lambda) - a_{12} \times a_{21} = 0, \qquad (5)$$

$$\lambda^2 - (a_{11} + a_{22})\lambda + (a_{11} \times a_{22} - a_{12} \times a_{21}) = 0. \qquad (6)$$

Substituting

$$I_1 = a_{11} + a_{22}, \qquad (7)$$

$$I_2 = a_{11} \times a_{22} - a_{12} \times a_{21}. \qquad (8)$$

We get

$$\lambda_{1,2} = \frac{I_1 \pm \sqrt{I_1^2 - 4I_2}}{2}. \qquad (9)$$

Eigen vectors change only the length and keep orientation of the initial vector. Eigen values of the most calculated regression matrixes are positive (table 2), so there are wind directions, that induce ice drift in the same directions.

Table 2. Eigen values of the regression matrix for CRS Komrvo and Odoptu,
for two off-shore ice observation distances: 4 km (S1) for both sites,
and 12 km (S3) for Komrvo and 16 km (S4) for Odoptu

		Eigen values			
Year		1992		1993	
Station		λ_1	λ_2	λ_1	λ_2
Komrvo	S_1	6,13	2,28	2.86	0.28
	S_3	5.69	1.42	4.76	0.55
Odoptu	S_1	3.39	1.63	2.55	0.66
	S_4	3.62	0.83	2.8	0.73

CALCULATION OF THE "WIND COEFFICIENTS"

It is possible to describe the transformation corresponding to the calculated matrix by an ellipse.

$$u = a_{11} \cos\varphi + a_{12} \sin\varphi$$

$$v = a_{21} \cos\varphi + a_{22} \sin\varphi. \tag{10}$$

The "response ellipse" is traced by the tip of the ice drift velocity response vector during one complete rotation of the uniform unity wind vector. For an isotropic response, this ellipse becomes a circle.

Eigen directions are defined:

$$\lambda_1 \cos\varphi = a_{11} \cos\varphi + a_{12} \sin\varphi, \tag{11}$$

$$tg\,\varphi_1 = \frac{\lambda_1 - a_{11}}{a_{12}}. \tag{12}$$

For the second eigen value:

$$tg\,\varphi_2 = \frac{\lambda_2 - a_{11}}{a_{12}}. \tag{13}$$

Calculated angles of eigen vectors show high stability at the both stations for different periods of observations. At stations Komrvo and Odoptu in 1992,1993 values of φ_1 changed from 184° up to 191°, φ_2 changed from 311° up to 330°. These values answer to the south-southeastern and the north-eastern directions (in our case the northward direction corresponds to the angle of 0°). Winds of these directions induce ice drift in the same direction without any deviation.

Definition of the wind direction, corresponding to maximum and minimum drift velocity is of interest. Square module of the response vector

$$u^2 + v^2 = (a_{11} \cos\varphi + a_{12} \sin\varphi)^2 + (a_{21} \cos\varphi + a_{22} \sin\varphi)^2, \tag{14}$$

accordingly, extreme response values will be defined from this equation:

$$[(a_{11}^2 + a_{21}^2)\cos^2\varphi + (a_{12}^2 + a_{22}^2)\sin^2\varphi + \sin\varphi \cos\varphi \, (a_{11}a_{12} + a_{21}a_{22})]' = 0, \tag{15}$$

[what is the ' at the end of the square bracket in equation 15]

$$tg\,2\varphi = \frac{2(a_{11}a_{12} + a_{21}a_{22})}{a_{21}^2 + a_{11}^2 - a_{22}^2 - a_{12}^2}, \tag{16}$$

$$\varphi_m = \frac{1}{2} arctg\left(\frac{2(a_{11}a_{12} + a_{21}a_{22})}{a_{21}^2 + a_{11}^2 - a_{22}^2 - a_{12}^2} \right) + \frac{\pi}{2}, \tag{17}$$

Angles of maximum and minimum response differ on 90°, so it is necessary to find one of them. These directions form "efficient" and "inefficient" winds, which induce maximum or minimum drift velocity.

It is important to estimate maximum deviation of drift directions from directions of the wind force. Angle of the result vector is defined using Eq. 10,

$$\beta = arctg \frac{u}{v} = arctg \frac{a_{11} \cos \varphi + a_{12} \sin \varphi}{a_{21} \cos \varphi + a_{22} \sin \varphi} \, . \tag{18}$$

Purpose of the study is to find values φ, when difference $\beta\text{-}\varphi$ reaches maximum (minimum) values. To define these conditions we will calculate derivative on φ and equate it with zero. As a result we obtain

$$tg\varphi_m = \frac{-(a_{11}a_{12} + a_{21}a_{22}) \pm \sqrt{(a_{11}a_{12} + a_{21}a_{22})^2 - (a_{21}^2 + a_{22}^2 + a_{12}a_{21} - a_{11}a_{22})(a_{11}^2 + a_{21}^2 + a_{12}a_{21} - a_{11}a_{22})}}{a_{21}^2 + a_{22}^2 + a_{12}a_{21} - a_{11}a_{22}} \tag{19}$$

and accordingly

$$\beta_m = arctg \frac{a_{11} + a_{12}tg\varphi_m}{a_{21} + a_{22}tg\varphi_m} \, . \tag{20}$$

It is clear seen from the fig.1, that difference between drift and wind directions changes with variations of wind directions. Maximal deviations of drift directions from the wind reach 16° counter clockwise and -70,4° clockwise at Komrvo station *(a)*, and 21,7° counter clockwise, -65,7° clockwise – at CRS Odoptu *(b)*. Maximal shift falls to angles of wind direction φ =15° and 195° at Komrvo and to the same angles φ =15° and 195° at Odoptu. When difference is equal to 0, these moments correspond to eigen values λ_1, λ_2, so ice drift and wind velocities have identical directions.

Module of the response vector at Komrvo station has maximum 6,8 m/s when the wind direction φ is equal to 135° and 315° shift of the wind and drift directions at this moment is about -27°. At Odoptu station module of the response vector has maximum 4,04 m/s when the wind direction φ is equal to 120° and 300°, angle between the wind and drift directions is about -17°.

Maximum of the module does not correspond to moments when difference of directions is equal to 0, that is meaning that eigen vectors do not coincide with directions of semi-axes of the response ellipse. Such concurrence is observed for the symmetric matrixes, at the same time designed matrixes for various stations and various intervals of time were asymmetrical, that reflects general prevalence of clockwise turn. The observable asymmetry of deviations is caused, obviously, by influence of the Earth rotation. Probably, in process of removal from the coast this asymmetry will amplify, and the eigen vectors will be absent since some distance (mathematically, eigen numbers will be complex). Presence of the real eigen numbers, and accordingly presence of wind directions at which the drift has the same direction, grows out of the balance between influence of coastal topography and rotation.

At CRS Komrvo value of the shift is more than at station Odoptu. Probably, it is connected that first of stations concerns to more deep-water area, and the influence of a ground relief is slight here. CRS Odoptu is located in area of Piltun shallow-water, that, probably, has an effect for value of «wind factor».

For typical values of the matrix elements the major axis of the ellipse is oriented towards the north-northwest - south-southeast, which coincides with the orientation of the coast line (the tidal ellipses are oriented at approximately the same direction). The major axis of all ellipses is larger than the minor axis by a factor of 5-6 at Odoptu station. At Komrvo station their difference is significantly greater. It is clearly seen, that north-northwest and south-southeast winds produce the largest ice drift.
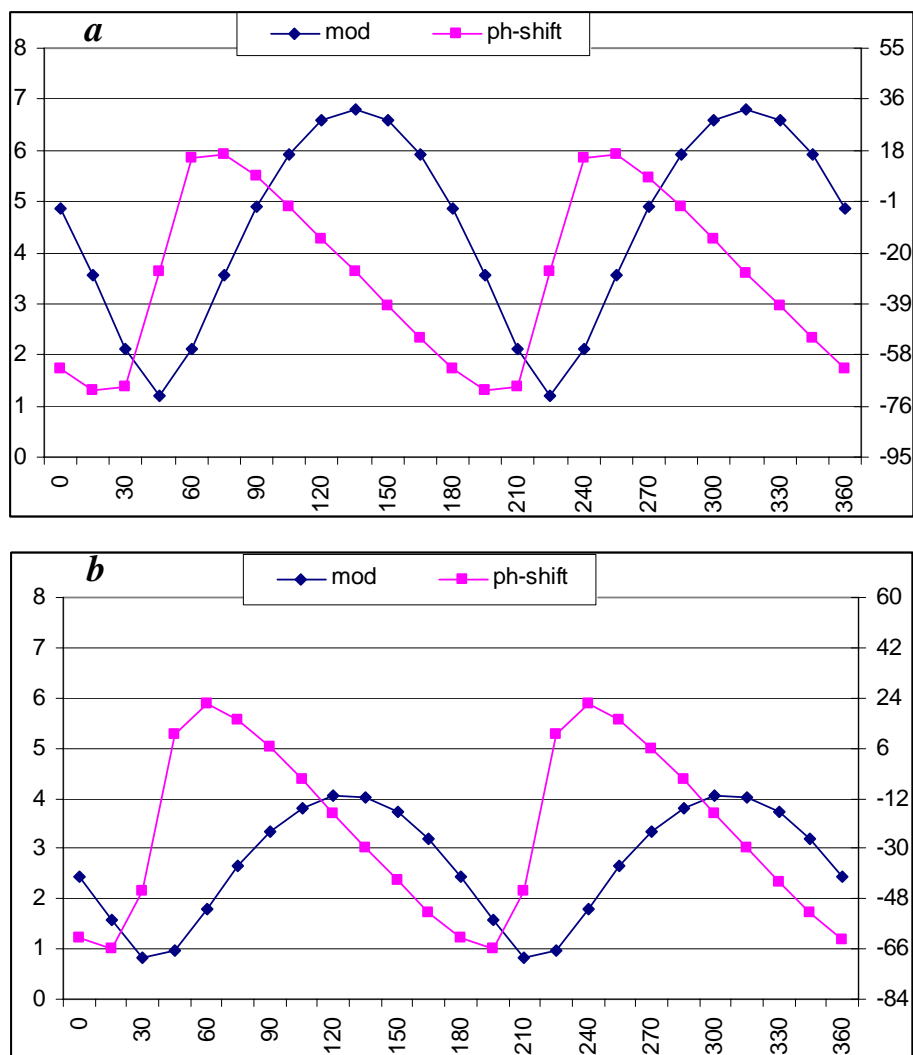
Fig. 1. Module of the response vector (mod), *m/s* and difference between drift and wind directions *β-φ* (ph-shift), *degree*. Direction of the wind velocity changes from 0° up to 360°. The response matrix is calculated for full 1992 series at station Komrvo *(a)* and Odoptu *(b)*

"Wind coefficients" have value of semi-axes and are expressed in %. For example, if the major semi-axis has value 4, "wind coefficient" will be about 4%. It means, that wind velocity 10 m/s will induce ice drift velocity about 4% of wind velocity, or 0.4 m/s.

The major semi-axis has values close to 4, but the small – about 0.5 at Odoptu station in1993. Value of the major semi-axis decreases to 2 in April – May. A similar picture exists at Komrvo station. The value of the major semi-axis decreases by the end of spring. The major semi-axis has a value about 10 in February, and 6 in May.

Ellipses, calculated for stations Odoptu and Komrvo using full series of 1992 and 1993, are shown in fig.2. The major semi-axis reaches a value of about 7.5 at Komrvo (1992), and the minor semi-axis of about 1 (Fig. 2*a*). This means that for the "most efficient" directions of wind velocity, wind about 10 m/s induces an ice drift velocity of about 0.75 m/s. However, for "inefficient direction, the drift velocity is only 0.1 m/s. Wind with the same velocity about 10 m/s will induce ice drift velocity 0.45 m/s in efficient direction at Odoptu station (1992) (Fig. 2*c*). As it can be seen from the Fig. 2, the

northwest and south-east winds fall into the category of "efficient". The major axis of the ellipse of Komrvo exceeds that of Odoptu by a factor of 1.5-2.

CRS Komrvo, 1992
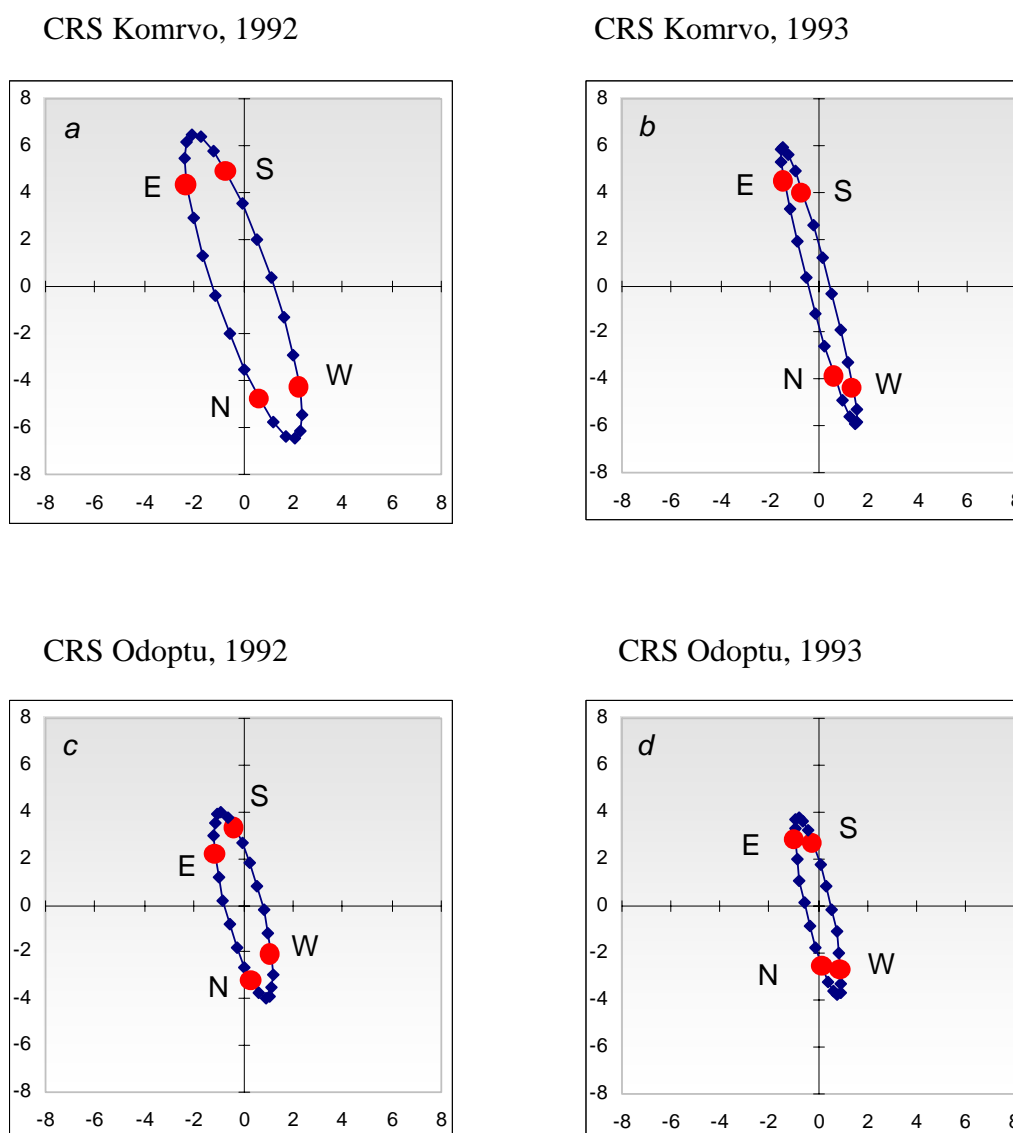
CRS Komrvo, 1993

CRS Odoptu, 1992

CRS Odoptu, 1993

Fig. 2. Ellipses, corresponding to values of ice drift for wind velocity 1 m/s from different directions, calculated using "wind coefficients" matrix. Ellipses are calculated for full 1992 and 1993 year series at stations Komrvo *(a)* – 1992, *(b)* – 1993 and Odoptu *(c)* – 1992, *(d)* – 1993. Letters "W", "N", "E" and "S" give the observed speed and direction of the ice drift in response to winds blowing toward the west, north, east and south, respectively

This correlation is true for monthly calculations, and for full year series. Possibly, topography at Odoptu station is responsible for this effect. For results, corresponding to different years and months, parameters of ellipses undergo only small changes.

CONCLUSIONS

Data sets of ice drift velocity, which were measured using coastal radar stations installed on the northeastern Sakhalin, were analyzed.

Matrix of regression was obtained. It shows ice drift velocity and deviation from the wind direction depending on direction of compelling force. Deviations are absent at

some directions (eigen directions) that, probably, grows out of balance between coastal effects and rotation of the Earth.

From components of wind and drift, values of "wind coefficient" are obtained, using linear regression. The computed elements of the matrix of linear transformation, which relate the vector series of wind and drift, can be represented by an ellipse with orientation approximately along a north-northwest and south-southeast directions. Values of wind coefficients at Komrvo (1992) for "efficient wind directions" are about 7.5 and about 1 for "inefficient wind directions". At Odoptu (1992) station, the corresponding values are 4.5 and 1. In 1993 wind coefficients for Komrvo are about 7 for "efficient directions" and 0.5 for "inefficient directions". For Odoptu (1993) coefficients are about 4 and 0.5.

The drift response to the wind influence strongly varies depending on direction of a wind - there are "effective" and "inefficient" directions. Northwest and southeast directions are effective directions in this area -, northeast and southwest directions are inefficient, accordingly.

The results of calculations for various years at the same radar station are well coordinated, that speaks about stability of results and their applicability for the purposes of the forecast of ice drift.

REFERENCES

Kato A., Savelyev V., Shevchenko G. (2001). Regime features of wind for Sakhalin Island, obtained on the base of instrumental data, *Dynamic processes on the shelf of Sakhalin and the Kuril Islands /* Ed. Shevchenko G. V. – Institute of Marine Geology & Geophysics, Sakhalin Science Centre, FEB RAS, Yuzhno-Sakhalinsk, Russia, pp. 177-194.

Shevchenko G., Tambovsky V., Tikhonchuk E., Putov V. (2001). Morphometry and dynamics of ice in the zone of the northeastern shelf of Sakhalin Island, Environmental monitoring and facilities on the Sakhalin shelf, Sakhalin publishing house, Yuzhno-Sakhalinsk, Russia, pp. 123-142.

Tambovsky V., Tikhonchuk E., Shevchenko G. (2001). Characteristics of morphometry and dynamics of sea ice on the northeastern shelf of Sakhalin island, *International Symposium on Okhotsk Sea & Sea Ice*, MOMBETSU-2001, Mombetsu, Hokkaido, Japan, pp. 356-390.

Thorndike, A.S., and R. Colony, 1982: Sea ice motion response to geostrophic winds. *J. Geophys. Res.*, vol. 87 (C8), pp. 5845-5852.

Thorndike, A.S., 1986: Kinematics of the sea ice, in: The Geophysics of Sea Ice, edited by N. Untersteiner, Plenum, New York, 489-549.

Fissel, D.B. and C.L. Tang, 1991: Response of sea ice drift to wind forcing on the northeastern Newfoundland shelf. *J. Geophys. Res.*, vol. 96 (C10), 18,397-18,409.

Hibler, W.D. III, 1986: Ice dynamics, in: The Geophysics of Sea Ice, edited by N. Untersteiner, Plenum, New York, 577-640.

ON THE ACCURACY OF THE ICE-SPECIFIC DESIGN VALUES DERIVED FROM LONG-TERM OBSERVATIONS

Dmitry A. Onishchenko[1] and Sergey I. Shibakin[1]

ABSTRACT

The paper deals with the question on the accuracy and reliability of ice feature thickness and ice load design values which are statistically derived from the field observation data covering short time periods, e.g. a few years in duration. A procedure of probability modelling is suggested which make it possible to find analytically a) the probability that the sampling design value of ice thickness is less than the 'true' value by quantity δ, and b) the probability that the load generated by an ice feature will exceed the calculated sampling value by $\varepsilon\%$ at least once during the nearest L years. As an example, model calculations are performed for the case of the Korzhavin type equation for sheet ice action. The calculation results for the case of five-year survey show that the reliability of the design values (for $L = 50$) obtained using the corresponding field data might be insufficient for such critical constructions as sea platforms in ice conditions.

MODEL OUTLINES

In most cases the interaction of sea platforms with ice features of different types is the governing factor for platform design in the Russian shelf conditions. The problem of determining the design ice load on a platform is very complicated. The results of numerous studies of different aspects of the problem are widely presented in relevant publications (e.g., RAO, 1993-2003 and references incide). One of the problems arising is the choice of the characteristic/design value of the specific ice feature thickness for the point of platform installation. Ice loads on a platform depend on a variety of factors which are random values in their nature. In general case these values can be determined on the basis of the statistical processing of corresponding field data only. The question is how long the period of field observation should be to provide sufficient reliability for the design values derived from the field data sample.

In the paper, taking as an example the year maximal level ice thickness which is one of the most important element of ice regime, the question on the accuracy and reliability of ice feature thickness and corresponding ice load design values is analysed provided they

---

[1] VNIIGAZ Ltd, Pos. Razvilka, Leninsky District, Moscow Region, 142717, Russia E-mail:
  D_Onishchenko@vniigaz.gazprom.ru

are statistically derived from the field observation data covering relatively short time periods, e.g. about a few years in duration. A general procedure is proposed that models a sequence of data of a random variable which is ice thickness in the problem under consideration and evaluates the confidence level for the derived characteristic and design values of ice loads (or the seek of simplification, all other parameters of the ice feature are considered to be deterministic):

- as an initial step, a hypothesis of the probability distribution of the random variable is adopted. For example, this could be the Gumbel distribution or the normal distribution. It should be noted that the justified choice of the real distribution and values of its parameters can be only done on the basis of large data series and relevant physical and mathematical arguments; this problem is not treated in the paper;

- then a design formula (procedure in general case) is chosen that allows one to calculate the ice load for any fixed value assigned to the random parameter under investigation. Within the model presented, the quantity found further with the help of this design formula will be called as the "true" design value of the ice load;

- finally, a sampling of data for the random parameter is simulated using the adopted distribution. The standard statistical processing of the sample gives a so-called sampling value for the parameter under investigation. The found sampling value is a model estimate for the design value of the parameter.

The sampling value is, in turn, a random quantity, because it depends on the field data series which should be reasonably treated as a random object. Hence, within the model constructed one can find deterministic "true" value and random sampling value for the design ice load. The probability of the sampling value deflection from the "true" design value by the given quantity may serve as one of the possible characteristics reflecting the reliability of the sampling value.

It is known that in many ice-laden areas ice ridges, rubble fields or rafted ice are those ice features that govern the structure design but not level ice. The model constructed can be equally employed in all the cases. However, the last is chosen in the paper for the model presentation due to the most clearness from the methodological point of view.

MODEL ANALYSIS

As an example, perform model calculations for the ice load on a wide structure with vertical walls, using a general design formula of the Korzhavin type for level ice action. More concretely, let us suppose that the maximal value of the load arising from an ice sheet cutting through by the structure is given by the following relation

$$Q = p_{eff} h W , \tag{1}$$

where h is the ice sheet thickness, W is the construction width, and p_{eff} is the effective ice pressure under ice failure against the structure. Similar relationships are recommended, in particular, by the USA and Canada codes. To calculate the value p_{eff}, take advantage of the power type formula which is frequently encountered in literature recent time (e.g., Masterson and Spencer, 2001)

$$p_{eff} = p_0 h^{-\alpha} \ (0 < \alpha < 1), \tag{2}$$

with p_0 as a specific value of ice effective pressure corresponding to ice thickness of 1 m. Note that Korzhavin himself (Korzhavin, 1962) used the combination kR_c (in-

stead of the quantity p_{eff}), where R_c stands for ice sample compression strength and k is the indentation factor. An analogous approach is realised in Russian codes for ice loads. In the following model calculations relation (2) will be used.

Introduce the conventional notation $w_t(x)$ and $F_t(x)$ for the probability density and cumulative functions correspondingly, which will be used in the further presentation. Usually ice codes prescribe to calculate the characteristic value of ice load by formula (1) using 1% fractile for ice thickness in the totality of year maxima. It is possible to assume that the ice sheet with thickness equal or more than such value may be encountered in average 1 time for 100 year period at the platform installation point. For simplicity, we disregard here the factor of year-by-year changeability and adopt the normal law hypothesis for distribution of ice thickness year maximum values, $F_h(x) \equiv \Phi(x; M_h, S_h)$, with the mean value M_h and variance $S_h{}^2$ (see Conclusion for some argumentation). It follows that the "true" ice thickness design value, $h_{1\%}$, corresponding to 1% fractile in the upper end of the maximum ice thickness distribution, can be found from the relation $\Phi(h_{1\%}; M_h, S_h) = 0.99$ and equals

$$h_{1\%} = M_h + 2.33 S_h. \tag{3}$$

Consider further a field data series $h_1, h_2, \ldots, h_n$ of year maximal values for ice thickness at the point of platform location for n-year period. By analogy with relation (3), let the sample design value $\tilde{h}_{1\%}$ for ice thickness be calculated by the formula

$$\tilde{h}_{1\%} = \tilde{M}_h + 2.33\, \tilde{S}_h. \tag{4}$$

Here the sample mean value and variance are found through the field data series in the ordinary way:

$$\tilde{M}_h = \tfrac{1}{n} \sum_i h_i, \qquad \tilde{S}_h^2 = \tfrac{1}{n-1} \sum_i \left(h_i - \tilde{M}_h \right)^2. \tag{5}$$

Emphasise that the quantity $\tilde{h}_{1\%}$ is random due to its deducing from the field data which constitute a random sample. Denote its distribution function as $F_1(x)$.

Then using the statistical sample property in the normal law case, when the quantities $u = \dfrac{\tilde{M}_h - M_h}{S_h / \sqrt{n}}$ and $v = \dfrac{(n-1)\tilde{S}_h^2}{S_h^2}$ are mutually independent and are described by standard normal distribution and χ^2-distribution with n–1 degrees of freedom correspondingly (Manual, 1978), one can derive analytical formulae for calculating different quantities that characterise sampling values, for instance,

a) the probability that the sampling ice thickness design value, obtained through the filed data, turn out to be underestimated at least by the quantity δ with respect to the "true" value (which is a deterministic one):

$$p_\delta = \mathbf{P}\left\{ \tilde{h}_{1\%} < h_{1\%} - \delta \right\};$$

b) the probability that in practice the level ice sheet load Q exceed the sampling design load value $\tilde{Q}_d$, derived through the field ice thickness observation, by value ε (in percentage) at least one time for the L-years period of platform operation:

$$p_\varepsilon = \mathbf{P}\left\{ Q > (1 + 0.01\varepsilon)\tilde{Q}_d \,\middle|\, L \text{ years} \right\}.$$

Here, due to relations (1) and (2), the ice load design value is defined by the formula

$$\tilde{Q}_d = \gamma\, p_0 \left(\tilde{h}_{1\%}\right)^{1-\alpha} W\,,$$

with γ as the load factor for ice loading. It can be shown that

$$p_\delta = \int_{-\infty}^{\infty} w_u(x) F_r(c-x)\,dx\,, \qquad (6)$$

$$c = \left(2.33 - \delta/S_h\right)\sqrt{n}\,, \quad F_r(y) = F_v\left(\left(1-\tfrac{1}{n}\right)\!\left(\tfrac{y}{2.33}\right)^2\right);$$

$$p_\varepsilon = 1 - \left[1 - \int_0^{\infty} w_h(x)\, F_1\!\left(x\big(\gamma(1+0.01\varepsilon)\big)^{-1/(1-\alpha)}\right)dx\right]^{L}\,, \qquad (7)$$

where $w_h(x)$ is the density function for the random variable h which is normally distributed with known parameters accordingly to the above-mentioned, and

$$F_1(y) = \int_{-\infty}^{\infty} w_u(z) F_r\!\left(\frac{y - M_h}{S_h/\sqrt{n}} - z\right)dz\,.$$

NUMERICAL RESULTS

The following parameter values were taken for model calculations: $\alpha = 0.174$, $p_0 = 1.5$ MPa (the values are adopted from the paper of Masterson and Spencer (2001)); in addition, the value $\alpha = 0.3$ is also analyzed for comparison), $\gamma = 1.1$ (the load factor for ice loading stated in Russian codes (SNiP, 1995)), $M_h = 1.0$ m and $S_h = 0.2$ m (the values are assumed for this study only, however, they are related in a sense to the Barents Sea conditions (Mironov et al., 1993; Gudoshnikov et al., 2003)), $L = 50$ years (the design period for platform operation). The computed results for probabilities p_δ are given in Table 1 (they do not depend on the parameter α), while those for probabilities p_ε are shown in Table 2, with n being the duration of field observations (in years).

Table 1. Probabilities p_δ of optimistic error by quantity δ for ice thickness design value

δ, m	0		0.05		0.1		0.2	
n, years	3	5	3	5	3	5	3	5
	0.613	0.578	0.536	0.471	0.455	0.362	0.294	0.175

Table 2. Probabilities p_ε of exceeding sampling ice load design value for period $L=50$

ε, %	0		5		10		20	
n, years	3	5	3	5	3	5	3	5
$\alpha=0.174$	0.827	0.494	0.622	0.263	0.407	0.122	0.131	0.021
$\alpha=0.3$	0.762	0.405	0.500	0.174	0.273	0.063	0.058	0.006

The results obtained show that if the record length is equal to or less than 5 years, then the reliability of the design values obtained using the corresponding field data might be insufficient for such critical constructions as sea platforms in ice conditions. Indeed, for $n = 5$ the probability of exceeding design ice thickness value by 10 cm during period $L = 50$ years is equal to 0.362; the probability of exceeding design ice load value by 10% for the same period is equal to 0.122 for $\alpha = 0.174$ and 0.063 (this is much better) for $\alpha = 0.3$. For the case of extra short observation period with $n = 3$ years, the design values of ice thickness and corresponding ice load associated with 1% fractile turn out to be much more unreliable, as it is expected. Note that within the framework of the constructed model the sampling ice load design value could not be considered as sufficiently reliable for $n \le 5$ even with the account for the load factor $\gamma = 1.1$.

Further using the computer simulation method we give an illustration to practical technique for finding design ice thickness values by formulae (4) and (5). Consider again the case of normal distribution with mean value $M = 1,0$ m and quadratic deviation $S = 0,2$ m. Table 3 displays three computer generated samples of 5 values each, corresponding to observation period of $n = 5$ years (all sample values are in metres). For each sample, the sampling values $\widetilde{M}$ and $\widetilde{S}$ are found with the help of formulae (5). These values are estimates for the "true" mean value M and deviation $S,$ which are, of course, unknown in practice. Also the design ice thickness value is calculated by formula (4). In accordance with relation (4), the "true" design ice thickness value $h_{1\%}$ equals 1.466 m.

Table 3. Examples of the statistical processing of field data samples

No. of sample	Sample (ordered)					Sampling values		
	h_1	h_2	h_3	h_4	h_5	$\widetilde{M}$	$\widetilde{S}$	$\widetilde{h}_{1\%}$
1	0.738	0.749	0.868	0.915	1.126	0.879	0.157	1.246
2	0.813	1.171	1.262	1.274	1.339	1.172	0.209	1.660
3	0.920	0.926	0.992	1.091	1.144	1.015	0.100	1.248

It is seen that the scattering of the values obtained is rather big, to both sides of smaller and larger values, which is in conjunction with the above theoretical studies.

For comparison, similar analysis have been performed using the least-squares method, which results are presented in Fig. 1 using the probability paper. Marked are five points corresponding to the sample $h_1,\ldots, h_5$, the x-coordinate of the ith point is equal to $\Phi_0^{-1}(i/5)$, where Φ_0 is the standard normal distribution, and the y-coordinate of the same point is equal to $h_i - \widetilde{M}$. The slope of the line drawn by the least-squares method gives certain estimate for the standard deviation of random variable h, that is of year maximal ice thickness. One can see that the sampling deviations obtained with the help of the least-squares method (see equations in Fig. 1) are somewhat smaller than those obtained above (quantities $\widetilde{S}$ in Table 3). This lead to lower and therefore less reliable values for sampling design ice thickness.
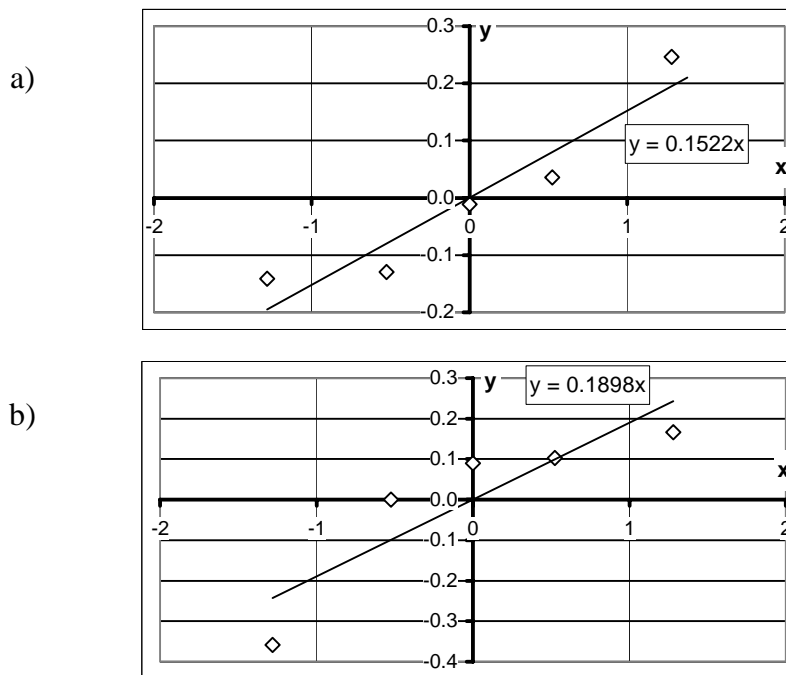
a)

b)

Fig. 1 Sample processing by the least-squares method (samples 1 and 2, Table 3)

IMPORTANCE OF THE RECORD LENGTH

Using the presented model, it is possible to analyse the influence of the record length on the reliability level of the sampling ice thickness and load design values. The graphs plotting in Fig. 2 illustrate the corresponding reliability increasing of the sampling design load values (decreasing of the exceedance probabilities p_ε (7)). The model predicts the probability of order 0.02 that the ice load exceed the sampling design value by 10% or more at least once during the 50 year period of platform operation provided the preceding observation period equals to 10 years. It seems that in such a situation the value 0.02 could be considered as quite admissible.
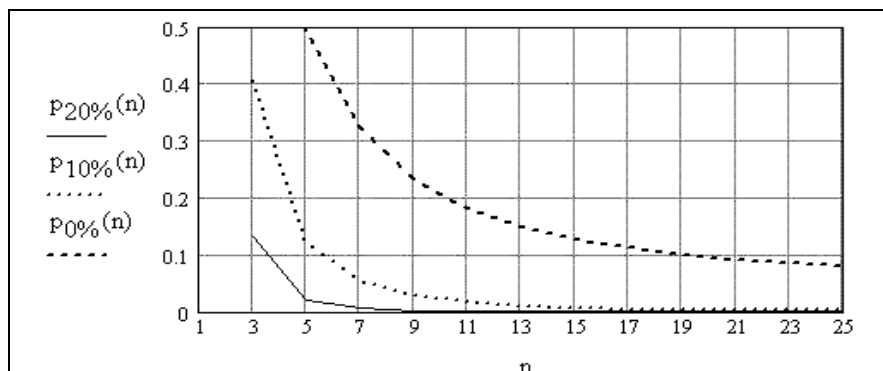

Fig. 2. Exceeding probabilities for the design ice load by ε% ($\varepsilon = 0, 10, 20$) during platform operation period ($L = 50$ years)

The 95% confidence intervals for sampling design ice thickness (in relative terms) are shown in Fig. 3, and those for sampling design loads with confidence level of 90, 95 and 95% in dimensional and comparative form with respect to "true" design value are displayed in Fig. 4 and 5. It seems that under model assumptions the use of the data re-

168

cords with length less then 10-15 years could be risky, if the load factor $\gamma_f = 1,1$ is approved in a platform project.
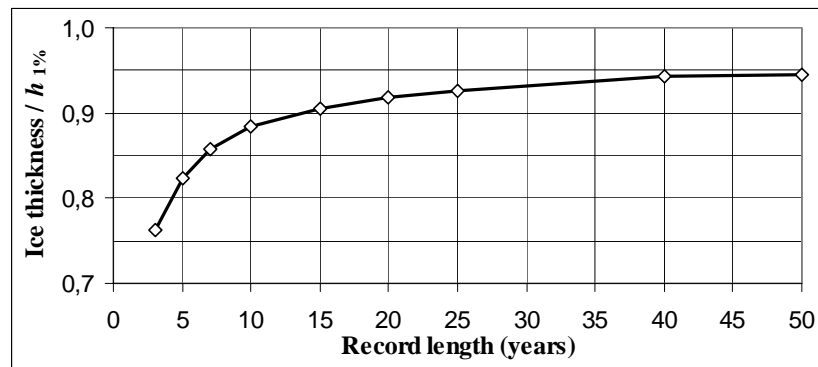

Fig. 3. Lower 5%-fractiles for sampling design ice thickness (comparative values)
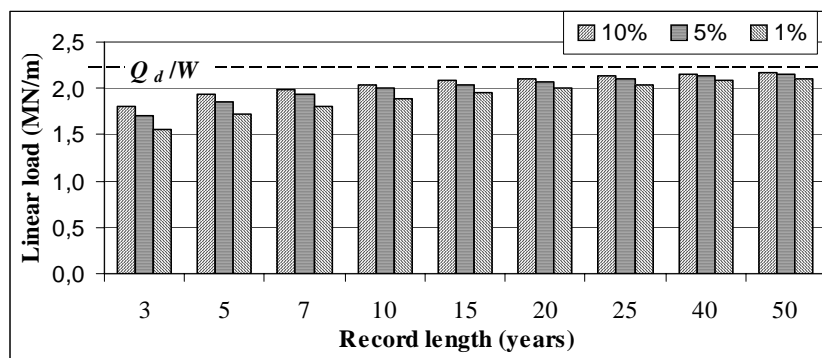

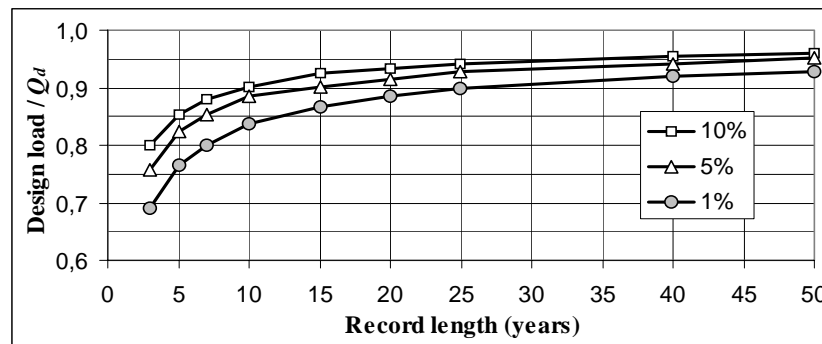Fig. 4. Sampling design loads (dimension values)

Fig. 5. Sampling design loads (b – comparative values)

CONCLUSION

The analysis similar to that presented in the paper can be realised also for other hypotheses about year maximal ice thickness distribution and relations for ice load calculation, and can be applied to other governing parameters as well. However, additional analytical difficulties can arise, e.g. the sampling random quantities $\tilde{M}$ and $\tilde{S}$, or above introduced variables u and v might be statistically dependent.

In addition, the use of the normal law for the annual maxima in the problem of the ice thickness design value setting can be supported with the following argument. It is the

ice thickness averaged over rather extensive area within an ice feature that determines the load on the platform but not the point thickness. The annual maxima of averaged ice thickness, being in general smaller than those of point measurements, should not obey the extreme values distributions. The theory of ordered statistics (David, 1981) predicts the asymptotically normal behaviour for non-maximal values instead of specific extreme distributions arising in the case of maximal values.

The method presented in the paper could be useful for the sea platform design in regions where detailed field data on ice thickness are unavailable or are obtained for the short-time observation period. In particular, the enlarged value for the load factor can be recommended in some circumstances.

REFERENCES

David, H.A. Order statistics. *Wiley Publ.*, New-York (1981).

Gudoshnikov, Yu.P., Zubakin, G.K. and Naumov, A.K. Morphometric characteristics of ice features of the Pechora Sea based on multiyear expedition data. In *Proc. RAO* (2003) 295-299.

Korzhavin K.N. Ice impact on engineering constructions. Novosibirsk, 1962.

Manual on the probability theory and mathematical statistics. *Naukova Dumka Publ.*, Kiev (1978) 584 p.

Masterson, D.M. and Spencer, P.A. Ice Force Versus Aspect Ratio. In *Scaling Laws in Ice Mechanics and Ice Dynamics*. Kluwer Academic Publishers, Dordrecht etc. (2001) 31-42.

Mironov, Ye.U., Spichkin, V.A. and Yegorov, A.G. Seasonal and annual sea variations in the Russian Arctic offshore: Barents and Kara Seas. In *Proc. RAO* (1993) 119-126.

RAO. Proc. Int. Conf. "Development of the Russian Arctic Offshore" (*RAO'93 – RAO'03*). St. Petersburg, Russia (1993-2003).

SNiP 2.06.01-86. Hydrotechnical structures. Basic design provisions. *Minstroy Publ.* Moscow, Russia (1995) 32 p.

PRESSURE/AREA MEASUREMENTS FROM THE GRAPPLING ISLAND ICEBERG IMPACT EXPERIMENT

Freeman Ralph[1], Richard McKenna[1], Greg Crocker[2], Ken Croasdale[3]

ABSTRACT

In 1995, an ambitious program was undertaken to measure for the first time, full-scale forces and pressures resulting from iceberg impacts with an engineered structure. The C-CORE Iceberg Impact Experiment was conducted on Grappling Island in southern Labrador. Impact forces and pressures were measured on a 6 m × 6 m instrumented panel mounted on a nearly vertical cliff face. Bergy bit and growler sized ice masses were towed into the panel by an ocean-going tug. Twenty-eight impacts were recorded, 22 of which were used in the analysis of pressure/area relationships. The measured crushing pressures were typically lower than values obtained from other medium scale tests at corresponding contact areas. However, they were generally not outside the extreme range of values obtained from other sources. The Grappling Island data are compared to pressure/area data from other sea ice and iceberg experiments, including Sanderson (1988), Masterson and Frederking (1993), and the Pond Inlet indentor data documented by Masterson *et al.* (1992). The use of actual versus nominal contact areas is discussed with respect to the relationship between ice pressure and contact area determined from the experiments.

INTRODUCTION

In 1995, C-CORE carried out an iceberg impact experiment on Grappling Island near Packs Harbour, southern Labrador. A 6 m x 6 m panel containing 36 instrumented triangular sub-panels was mounted to a rock face and icebergs were towed into the panel, as illustrated in Figure 1, to achieve realistic impact dynamics.

While many experiments have been conducted to study the pressure-area relationship associated with ice-structure interactions, the 1995 iceberg impact experiment was the best representation of iceberg impacts on offshore structures. It yielded the most comprehensive data set of the full scale iceberg impacts prior to the bergy bit impact experiment in 2001 where forces and pressures were measured from collisions with a Canadian Coast Guard icebreaker (Gagnon *et al*, 2002).

---

[1] C-CORE, St. John's, NL, Canada
[2] Ballicater Consulting Ltd., Kingston, ON, Canada
[3] K.R. Croasdale and Associates Ltd., Calgary, AB, Canada

At the time of the C-CORE iceberg impact experiment, there existed few ice load data for large contact areas, and a near absence of information on iceberg impact pressures at large contact areas. Furthermore, the only medium scale data for iceberg ice were derived from highly confined, cold Arctic ice, which may not represent normal conditions at the impact interface. It was suspected that this lack of 'real world' experience with iceberg/structure interactions was leading to conservative parameterizations of crushing pressures, especially for floating platforms.

The overall purpose of the field program was to identify the relationship between iceberg crushing pressure, contact area, and shape, and to advance the understanding of the kinematics involved in iceberg collisions with structures.

EXPERIMENT SETUP

The load panel consisted of a sub-frame of "I" beams with feet contacting the cliff at 16 points (on a 2 m grid) as illustrated in Figure 2. Each sub-panel, made of triangular steel plates, had a surface area of 1 m^2 and was connected to the frame via a 75-ton capacity load cell under each corner of the triangle. In total, there were 108 load cells in the panel. In addition each impact was recorded with both the overhead video camera (mounted on a jib boom 11 m above the water, looking down on the panel) and a hand-held video camera. The video record provided quantities such as iceberg size, impact speed, and impact angle, in addition to qualitative information on each impact.
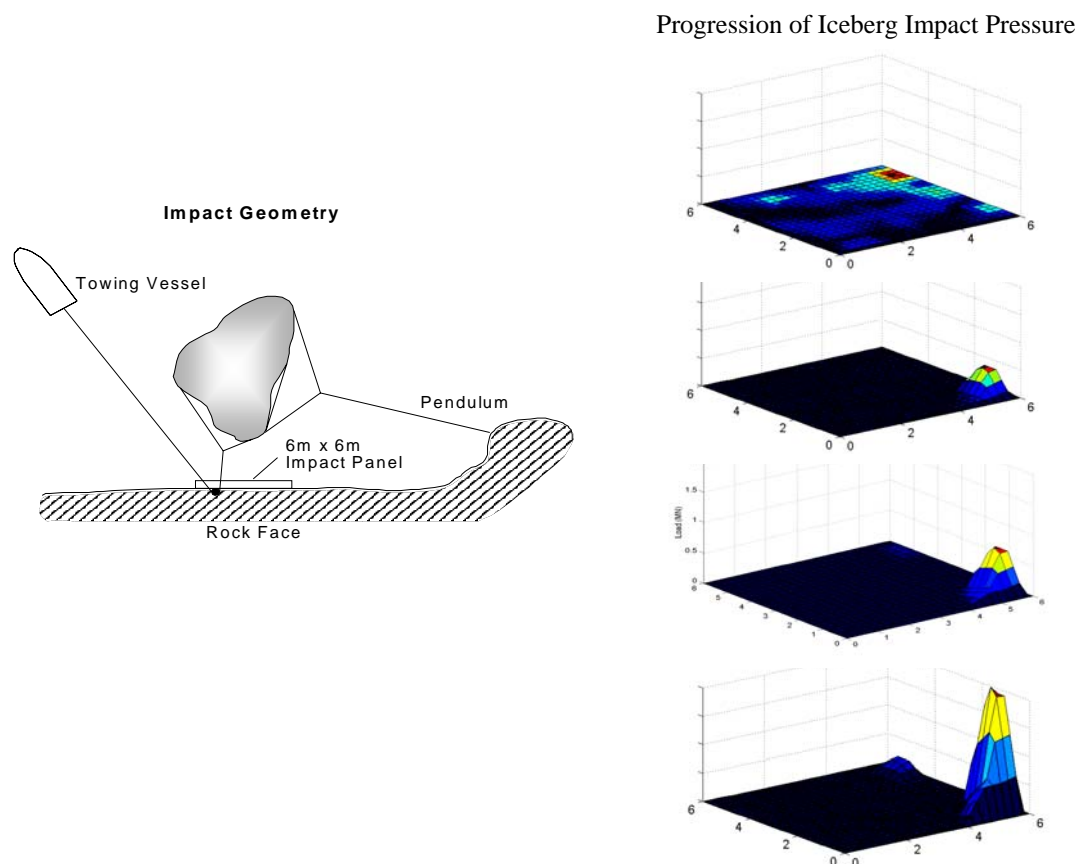

Fig. 1. Illustration of 1995 Iceberg Impact Experiment set-up and distribution of pressures on load panel as impact progresses
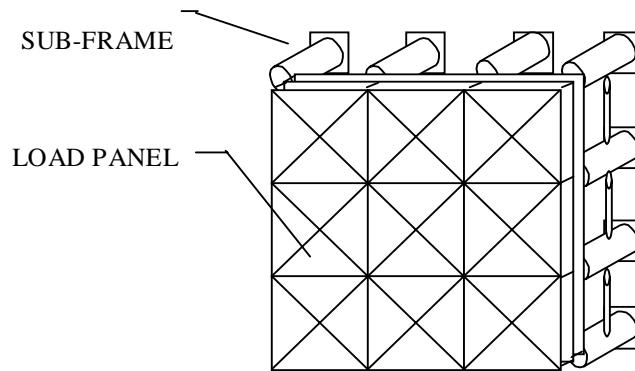
Fig. 2. Instrumented load panel

DATA ATTRIBUTES

Twenty-eight iceberg impact events were recorded. One of the impacts was not considered in the analysis because the registered load was too low. An additional five impacts were not considered because the icebergs struck the side of the panel. Twenty-two events were considered good impacts.

For each impact, the forces on the 108 load cells were sampled at a rate of 100 Hz and filtered at 50 Hz over a 20-second duration. The duration of the impacts ranged from 0.23 to 2.29 seconds. Estimated masses ranged from 180 to 1000 tonnes and impact speeds ranged from 0.36 to 1.89 m/s. Peak forces ranged from 0.09 to 2.09 MN and contact areas ranged from 0.02 to 2.17 m^2.

Time series for global force, contact area, and local pressure for each impact were deduced from the force data from each load cell. Several collisions only impacted a single panel indicating the contact area was $1m^2$ or less throughout the crushing process. In order to get a better representation of the contact area, a triangle method, using the distribution of load on the three load cells of the individual panel, was used to identify the loaded sub-region on each triangular panel for each instant sampled in time. The local pressure was evaluated based on global force and the actual contact area. Fig. 3 shows processed data from a typical impact. The graphical display includes:

- a view of the collision from an overhead camera;

- total load vs. time traces measured by the load cells;

- changes in the distribution of impact loads over the area of panel as impacts progressed; and

- additional information including mass of the berg, initial contact velocity, force, pressure and calculated contact area.

IMPACT CONDITIONS AND LOADS

The Grappling Island icebergs were relatively warm at the surface (compared with Pond Inlet data) resulting in a steep temperature gradient. Penetrations were typically small and most crushing was into the softer surface layer of ice. When repeated impacts were carried out on the same iceberg, the forces and pressures tended to increase for the later impacts, suggesting that crushing into colder isothermal ice may have led to increased pressure.

173

PRESSURE-AREA RESULTS

Examples of the changes in pressure, force, and contact area during two selected impacts are given in Figures 4 and 5. For clarity, only selected portions of the impact are shown in these figures, but they all include the portion of the impact where the peak force occurred. In some of the impacts (e.g. impact #28 in Fig. 4) the variations in contact area and pressure are quite smooth. In others (e.g. impact #31 in Fig. 5), there are abrupt fluctuations in area. Although the "nominal" contact area might be expected to increase rather steadily during an impact, the estimated contact area from the impact panel is derived from the applied load, and spalling events will result in rapid reductions in actual, as opposed to nominal, contact area.
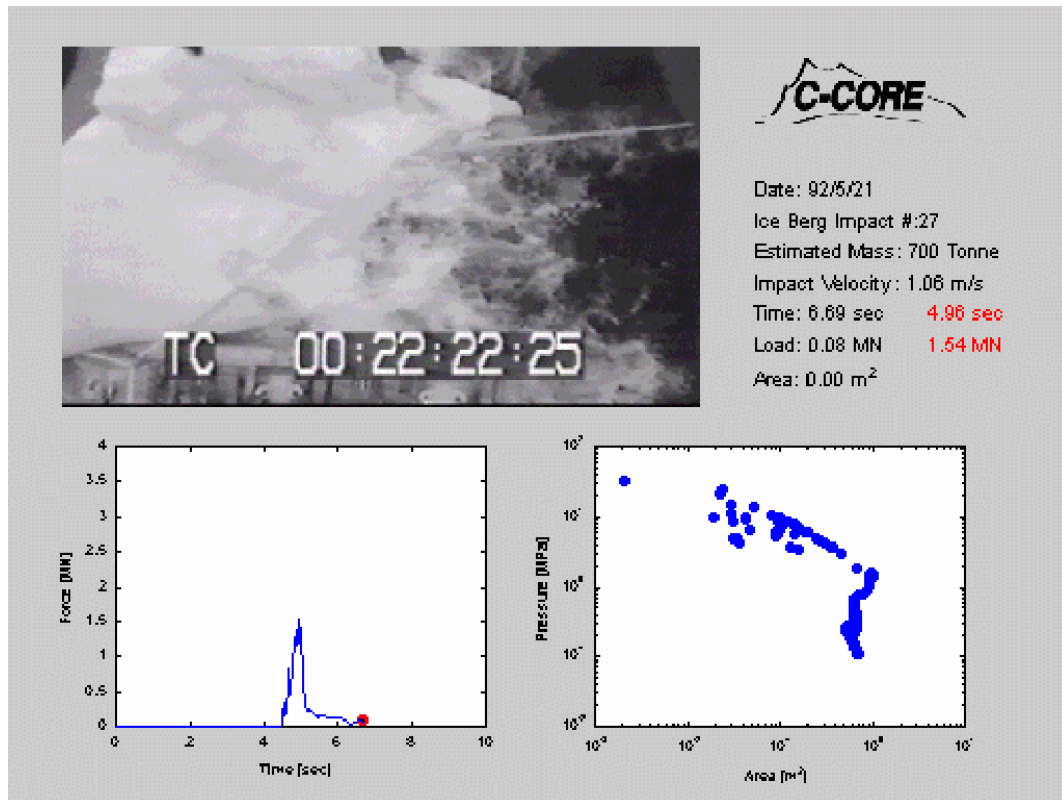

Fig. 3. Graphical display of digital image sequence for iceberg impact #27

The contact area based on applied force may underestimate the nominal contact area, and result in an overestimate of the pressure, as defined in previous pressure/area analyses.

A pressure - area relationship was evaluated based on maximum forces and corresponding areas encountered for the 22 iceberg impacts with the panel (Crocker *et al*, 1997). The evaluated pressure - area relationship was given as

$$P = 0.73A^{-0.65},$$ (1)

where P is the pressure and A is the contact area.

Additional analyses were carried out including a reworking of the contact area estimates using the triangle method as well as a sensitivity assessment of Equation (1) based on the following conditions including:

- impact velocities greater than 0.5 m/s;

- measured impact force greater than 0.4 MN;

- direct hits (minimal rotations induced due to towing); and

- no contact with the side of the panel.

Ten impact conditions satisfied the above conditions and the resultant pressure-area relationship was re-evaluated to be

$$P = 1.55A^{-0.70} \quad \text{(See Figure 6).} \tag{2}$$

COMPARISONS TO OTHER DATA

To compare The Grappling Island data to other pressure/area data from other sea ice and iceberg experiments, (i.e. Masterson and Frederking (1993), Masterson *et al* (1992) and Sanderson (1988), the 1995 iceberg impact experiment data have been placed in the context of medium-scale indentation and ship ram data as illustrated in Fig. 6. The most directly comparable results for pressure – crushed area relationship for larger contact areas was the Pond Inlet tests. These data yielded the relationship

$$P = 3.22A^{-0.38}. \tag{3}$$

The derived constant 0.73 from Equation (1) is considerably lower than values from other experiments and is believed to be a product of shallow penetrations, which resulted in crushing only in the warm near-surface ice and low confinement. Extensive analysis of ship ram trials on multi-year sea ice (Carter *et al*. 1995 and Jordaan *et al*. 1996), which has mechanical properties similar to iceberg ice, yielded the average relationship

$$P = 3.0A^{-0.4} \quad \text{(See Figure 6).} \tag{4}$$

This is fairly close to the Pond Inlet data and provides an upper bound to iceberg impact pressures. However, the 1995 iceberg impact data indicate a steeper slope than other data in this range. It is recognized that the slope is influenced by a small number of pressures on small contact areas, which are more difficult to estimate from the load cell data. Because of the small dataset, recognition of the associated uncertainty should be considered in their application to design for iceberg loads.

NUMERICAL SUMULATIONS

Some general conclusions can be drawn from the experiment based on numerical simulations. It was previously noted that impact forces increased with consecutive collisions of the same iceberg having the same impact conditions including contact location and estimated impact velocities even though iceberg mass was lost after each impact.

Previous analytical work suggested that softer ice layers on the surface may have been removed with each impact thus leaving stronger ice for the next impact, resulting in larger measured forces (Muggeridge *et al*, 1996). This effect was modeled to account for mass reduction with each collision. It was verified that increasing the strength term (first coefficient) in the pressure-area relationship increased the resultant force for decreasing mass such that the results were comparable to the experimental results. This helped to validate the assumption that a harder surface was exposed after each impact resulting in higher impact loads for consecutive collisions.
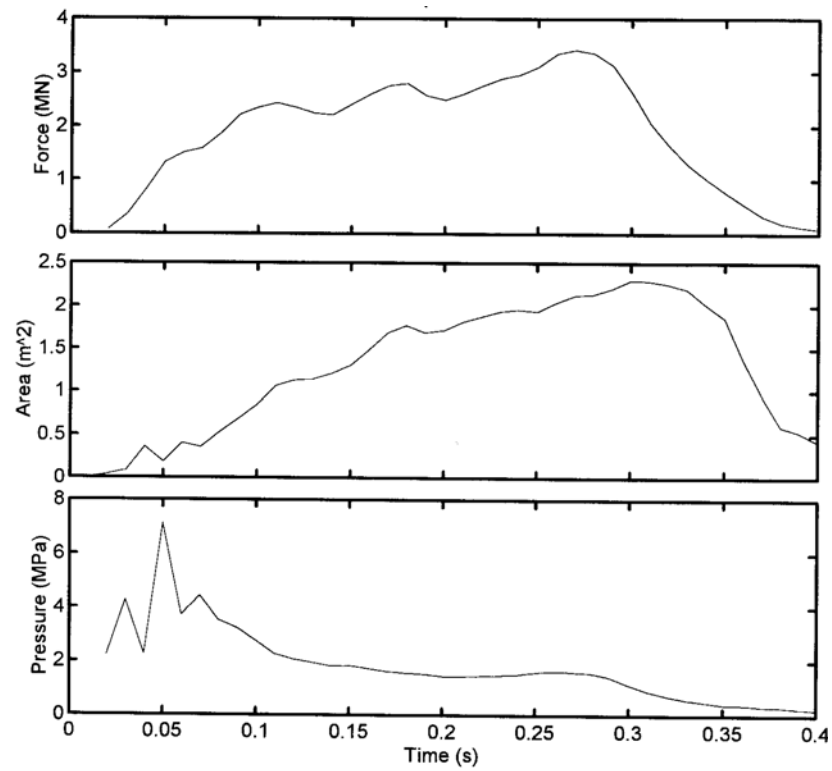
Fig. 4. Example of time series data for iceberg impact #28 showing global load, local pressure, and the associated contact area
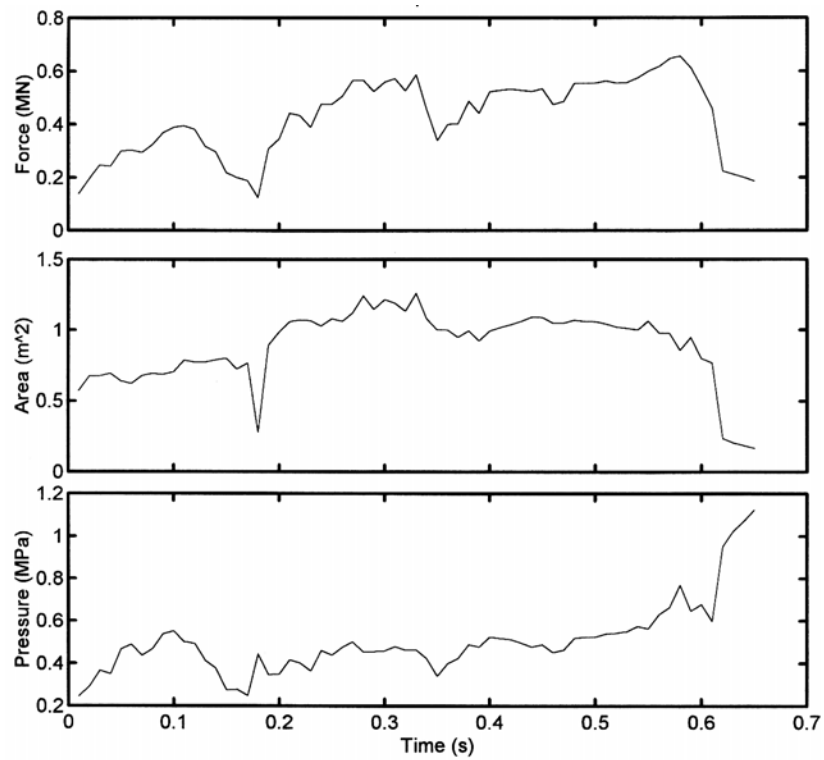

Fig. 5. Example of time series data for iceberg impact #31 showing global load, local pressure, and the associated contact area
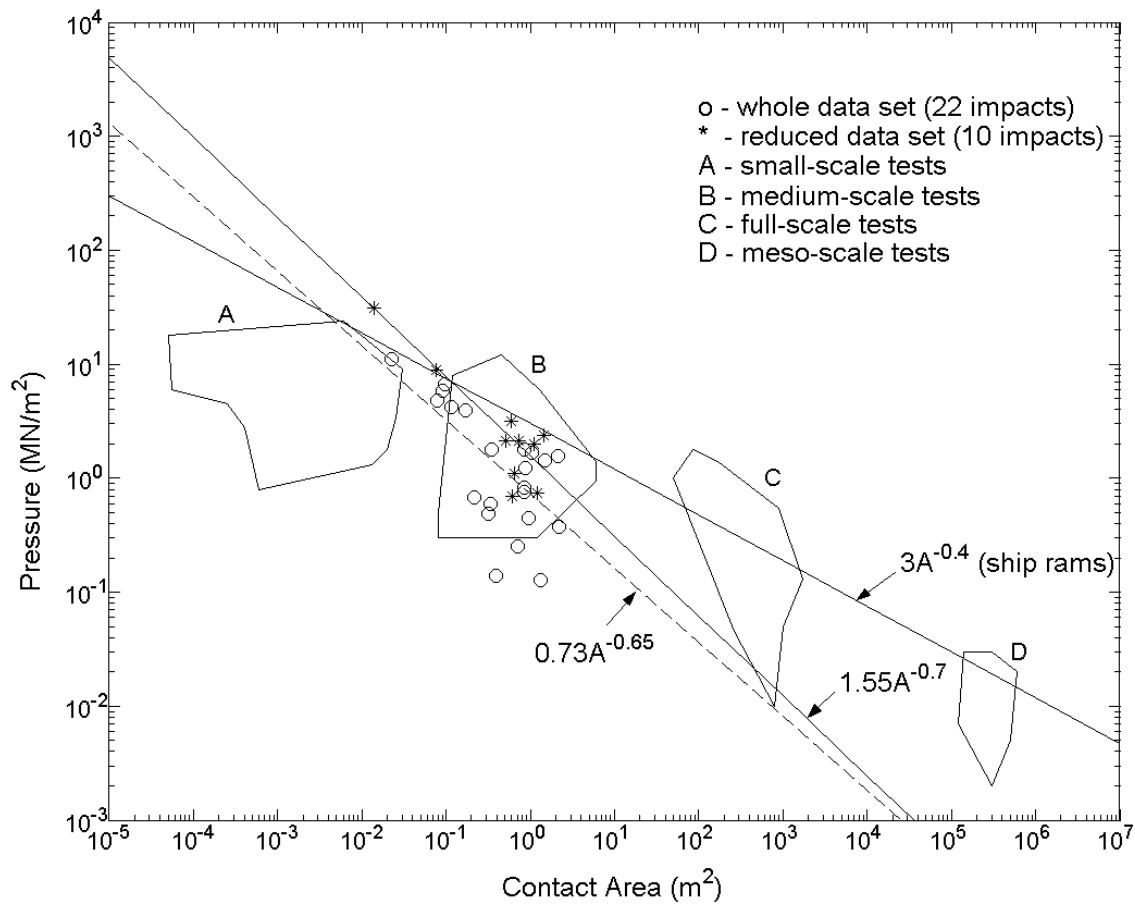
Fig. 6. Grappling Island impact data in context of other pressure-area data

RELEVANCE TO LOCAL ICE LOADS

Actual contact areas were estimated for the 1995 iceberg impact experiments. In practice, nominal contact areas are used for design and nominal areas have been estimated based on correlation with the above-mentioned sources. The triangle method of contact area estimation gives reasonable results. However, it is well known that the pressure distribution within the contact area is far from constant. Numerous indentor and ship ramming tests have shown that much of the force is applied through relatively small zones within the nominal contact area. The accuracy of the derived pressure/area relationship is a function of the accuracy of the technique used to estimate contact area. Analysis of these techniques indicate that both the constant and exponent in the pressure/area relationship are fairly insensitive to the estimation technique used, although there is considerable uncertainty for small contact areas, particularly those less than 0.5 m^2.

CONCLUSIONS

The iceberg loads measured in this experiment yielded the most comprehensive data set documenting the iceberg impact process. The mechanical behaviour of the Grappling Island ice is representative of conditions during real iceberg/structure interactions. However, the penetration depths in the Grappling Island tests (the distance into the ice to which ice was crushed) were not large, and most of the crushing occurred in the warm ice near the surface. If larger penetration depths had been obtained, the crushing of cold, isothermal ice may have led to increased pressures. This is an important consid-

177

eration if the pressure/area relationship from the Grappling Island data is extrapolated to larger contact areas corresponding to greater penetration depths.

ACKNOWLEGEMENTS

REFERENCES

Carter, J.E., Daley, C., Fuglem, M., Jordaan, I.J., Keinonen, A., Revill, C., Butler, T., Muggeridge, M. and Zou, B. Maximum Bow Force for Arctic Shipping Pollution Prevention Regulations - Phase II. *Memorial University of Newfoundland, Ocean Engineering Research Centre, Submitted for Canadian Coast Guard Arctic Ship Safety*, pp 247, 1995.

Crocker, G., Croasdale, K., McKenna, R., English, G., Guzzwell, J., and Bruneau, S., C-CORE Iceberg Impact Experiment – Phase 2 Final Report, Contract Report for Petro-Canada Resources Limited, Mobil Research and Development Corporation, Chevron Petroleum Technology Company, Husky Oil, and the National Energy Board of Canada, *C-CORE Publication* 96-C16, 1997.

Gagnon, R., Cumming, D., Ritch, R., Browne, R., Johnston, M., Frederking, R. and Ralph, F., Overview of Bergy Bit Impact Trials, *IAHR 16th International Symposium on Ice*, Dunedin, New Zealand, 2002.

Jordaan, I.J., Fuglem M. and Matskevitch, D.G., Pressure-area relationships and the calculation of global ice forces. Proceedings, *IAHR Symposium on Ice*, Beijing, China, Vol. 1, pp. 166-175, 1996.

Muggeridge, K., Matskevitch, D., and Jordaan, I. Contact Zone Mechanics. *Contract Report for National Energy Board of Canada*. 1996.

Masterson, D. M., and Frederking, R.M.W. Local Contact Pressures in Ship/Ice and Structure/Ice Interactions. *Cold Regions Science and Technology* 21: 169-185, 1993.

Masterson, D., Nevel, D., Johnson, R., Kenny, J., and Spenser, P. The medium scale iceberg impact test program. *IAHR Ice Symposium, Banff*, Alberta, Vol. 2, pp 930-966, 1992.

Sanderson, T. Ice Mechanics: Risks to Offshore Structures, 1988.

CONFEDERATION BRIDGE – THE RELATION BETWEEN MODEL AND REALITY

Thomas G. Brown[1]

ABSTRACT

After 6 winters, much has been learnt about the interaction between ice cover and the piers of Confederation Bridge. Some of this has been surprising and some predictable, but the results, in terms of ice forces on the piers, suggest that the original modeling placed undue emphasis on the strength of first-year ridge keels, and the homogeneity of consolidated layers. In contrast, the frequency and extent of rubble pile-ups on the piers was under-predicted in the modeling. The interaction between an interacting ice sheet and the rubble pile is, however, not as obvious as was first thought, and there remain unanswered questions regarding the mechanics associated with these interactions. Nevertheless, much has been learnt, and certainly, the importance of pier shape has been borne out in the interactions that have been observed to date. The paper will describe these observations in detail, in comparing the full-scale performance with the predicted performance used in the probabilistic modeling. The paper will discuss the interactions between first-year ridges and the piers, and the role of the keel, and the pier shape, in the determinations of the total load. The paper will also discuss interactions involving sheet ice, where flexural behaviour was predicted to dominate the interaction, but where the rubble pile has become the dominant feature. To what extent this affects the original failure of the ice sheet is not known, although some clues are presented.

INTRODUCTION

This paper presents comparisons between observations of ice interactions, and measured ice forces, on the Confederation Bridge piers and the corresponding assumptions made during the design of the bridge. In many instances, the differences are dramatic and therefore some of the statements in this paper may seem provocative. I hope that, as a minimum, they will provoke discussion and reassessment of how we model ice interactions with conical structures and the behaviour of unconsolidated rubble.

The bridge, instrumentation system, and ice conditions in Northumberland Strait, have been described many times previously (Tadros, 1997; Brown, 1997; Brown, 2001). Because it is important to the understanding of some of the behaviour described in this paper, Figure 1 illustrates a typical main pier. The two piers that are fully instrumented are P31, in 20 m of water, and P32 in 18 m of water. However, because the main piers are all founded on rock, the actual pier heights are different; P31 is founded 27m below mean sea level, P32 22 m below mean sea level.

---

[1] University of Calgary, 2500 University Drive NW, Calgary, Alberta, Canada, T2N 1N4.
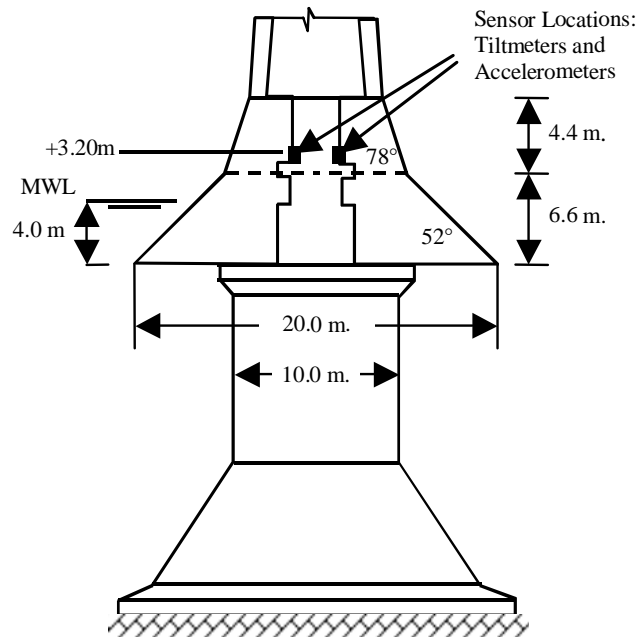
Fig. 1. Pier Layout

The observation and measurements that are discussed in the paper are derived from the output of the instrumentation system over the six years since the bridge opened. This output includes video sequences, sonar measurements, ice pressures, current recordings, wind data, and ice forces derived from the bridge response.

ICE FORCE DESIGN PROCESS

During the design process for the piers, it quickly became apparent that the accurate prediction of ice forces was crucial and, indeed, that ice forces would constitute the design lateral load conditions for the Bridge (Tadros, 1997; Brown et al 2001). As a result, much effort was expended in the determination of the ice forces and on the assessment of the data needed for this determination. In the end, there remained considerable uncertainty, and wide divergence in the estimates of ice loads expected over the 100 year lifetime of the Bridge (Brown et al, 2001).

The ice features that resulted in the maximum loads, and which therefore received the most attention, were first-year ridges. These occur frequently in Northumberland Strait and each pier encounters something like 5000 ridges, with keel depths of 4 m or greater, every year. Ridge keels in the vicinity of the Bridge can potentially reach a depth of 18 m and keels in excess of 16 m have been observed. The maximum keel depth is somewhat limited by the bathymetry to the west (upstream) of the Bridge. While the keels are largely unconsolidated, a consolidated layer at the water-line does develop and this layer could reach a thickness of 3 m in extreme winters, although, to date, only 2 m consolidated layers have been observed.

The loads resulting from ridge interactions with the piers were assumed to result from two components: failure of the consolidated layer in flexure, analogous to ice sheet failure; and failure of the keel. The sail was ignored. The two failures were assumed to be independent and the resulting maximum loads were added. The rationale for this was that, with large ridges, the consolidated layer is of such an extent that multiple flexural

180

failures will occur during a single ridge interaction, and that one such failure is likely to be coincident with the maximum keel failure load. Keel loads were determined by considering both local and global failures and latterly used a cross-over model.

Flexural failure loads were determined using the Croasdale two-dimensional model (Croasdale, 1980) modified to account for three-dimensional effects from the initial failure of the ice sheet (consolidated layer), subsequent ride-up of the broken layer, and the rubble accumulation on the cone (Croasdale et al, 1994). The model assumes interaction between the components, and adds the loads from all components to obtain the total load. In comparison with measured loads for flexural failure of ice sheets (Mayne and Brown, 2000b) the Croasdale model has been shown to give the best results (Figure 2), although, as seen, the linear correlation has a slope of 0.43, and a low correlation coefficient (R^2) of 0.12. This suggests that simple analytic models such as this cannot adequately model the complex mechanics of ice interacting with conical structures.
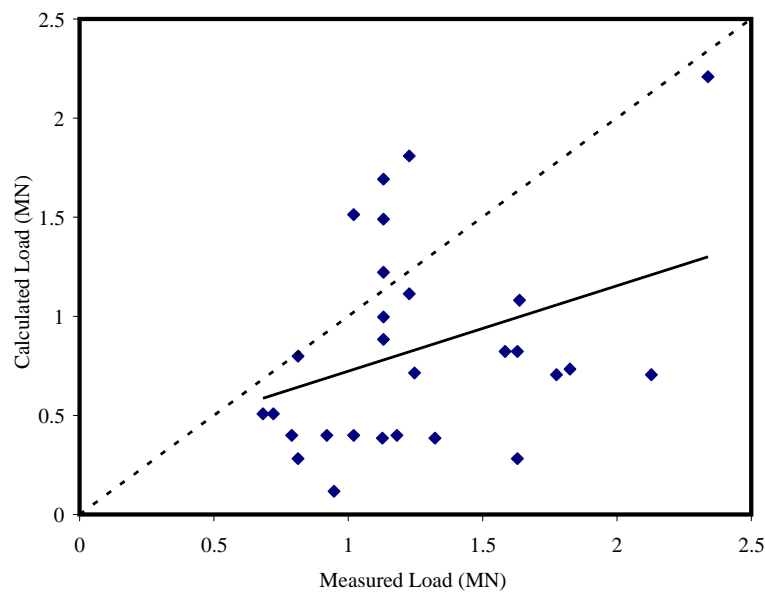

Fig. 2. Comparison Between Measured and Calculated Loads

Keel failure loads were determined on the basis that the keel rubble behaved as a Mohr-Coulomb material. As indicated above, the loads were based on either a local failure (e.g. Dolgopolov, 1975) or a global failure (Croasdale, 1980). The ridge interaction model also included the effects of oblique impacts and the inertial effects of decelerating the ridge keel. There was considerable debate as to the appropriate values of c and φ to be used with the keel models, and indeed, whether the material should be considered either cohesive or frictional, but not both. It was concluded that rate of loading would be a major determinant of this (Weaver, 1994).

The Dolgopolov model is based on passive failure of a wedge of rubble adjacent to the pier. The model accommodates a surcharge of rubble material below the keel and against the pier caused by previous indentation - as some function of the pier diameter. Using the Mohr-Coulomb model for ice rubble shear strength, this assumption can result in a significant strength increase in the keel. As the pier indents the keel, this local

keel load increases rapidly, until a complete plug failure of the keel becomes the lower failure load. The plug failure occurs through the formation of a shear plane along the underside of the consolidated layer and two vertical planes commencing at the sides of the indenting pier. These planes may diverge from the direction of motion of the ridge relative to the pier, and depending on the normal stress state on the vertical planes.

It is clear from this brief description of the models used in the determination of the loads on the piers, that the mechanics of the ice interaction process with the piers are complex. The failure of ridges involves a number of independent processes depending on relative deformation of the consolidated layer and the keel but does not consider interaction between the two. At the time of the load determinations for the design of the piers, it is the author's belief that the modeling used was the best available approach to the determination of these loads. The following points characterize the load models used:

- independence of keel and consolidated layer failures;
- superposition of maximum loads from these two failures;
- ride-up occurs for every interaction;
- rubble pile-up does not occur for every interaction, and is accompanied by ride-up;
- flexural failure geometry (location of circumferential crack) is not influenced by rubble pile, but depends only on characteristic length;
- circumferential cracks are circular;
- rubble pile and ride-up heights are independent of ice conditions and velocity;
- ice conditions do not affect failure loads, except in as much as providing driving forces;
- keel rubble is in full contact with the structure;
- keel rubble fails on clearly defined failure planes;
- keel rubble behaves as a Mohr-Coulomb material;
- keel rubble is not affected by velocity and hydrodynamic effects;
- the consolidated layer is homogeneous.

OBSERVATIONS

Since the Bridge opened in 1997, there has been continuous monitoring of ice forces and ice interactions with two piers of the Bridge (e.g. Brown, 2001), as well as measurement of forces and pier response on two other piers (Kubat and Frederking, 2001). For piers P31 and P32 the ice forces for well in excess of 6000 interactions have been measured and for many thousands of these, there is accompanying video, sonar, wind and local ice pressure information. The information has provided considerable insight into what actually happens when first-year ridges encounter the Confederation Bridge piers. The loads themselves provide interesting information in themselves, but the added information provides better understanding of the actual behaviour that occurs.

It is the author's view that many of the assumptions made in the analysis of ice loads on the piers, properly held at the time, were wrong. This may partly result from the unique shape of the Confederation Bridge piers, but there is enough evidence to suggest that many of the commonly held beliefs related to failure of ice on conical structures of all types need to be rethought. Some observations, on reflection, might now seem obvious, others though, are less so. Undoubtedly, as more, and better information is gathered, the

conclusions will be refined. The following provides summaries of the observations, as they relate to the assumptions made in the modeling:

Rubble Piles: Rubble piles occur virtually 100% of the time during continuous ice failure (Figure 3). The few exceptions that might result in the absence of rubble piles are: the complete absence of snow on a wet ice upper surface; occasions when the rubble pile breaks downward through the supporting sheet (consolidated layer); and when significant ride-up occurs with thick consolidated ice. These omnipresent rubble piles are associated with the complete absence of ride-up, suggesting that the two phenomena are mutually exclusive. Maximum rubble pile height depends on ice thickness (Mayne and Brown 2000a; Maattanen and Hoikkanen, 1990) but the average rubble pile height is significantly less than the maximum (Figure 4). Maximum rubble pile height also depends on the velocity of the interacting ice, with the height reducing at higher velocities, due to more effective clearing of the rubble at higher velocities (Figure 5). The rubble pile is very dynamic with continuous motion of ice blocks within the masses of the pile up. There have also been some observations of stationary behaviour of blocks at the apex of the rubble pile during continuous flexural failure of sheet ice. Generally, the rubble pile does not have a linear profile, but is more often bi-linear, with a quite distinct kink in the profile. The blocks are small in lateral extent and very variable in size – the maximum block size seldom exceeds twice the ice thickness. The frequency of rubble piles was unexpected, as was their characteristics, and the concurrent absence of ride-up.

Ride-Up: As indicated above, this is a rare event (Figure 6) and usually only occurs when thick consolidated ice interacts with the piers. The maximum ride-up can be very high, reaching the neck of the pier, but is very unstable, and is never
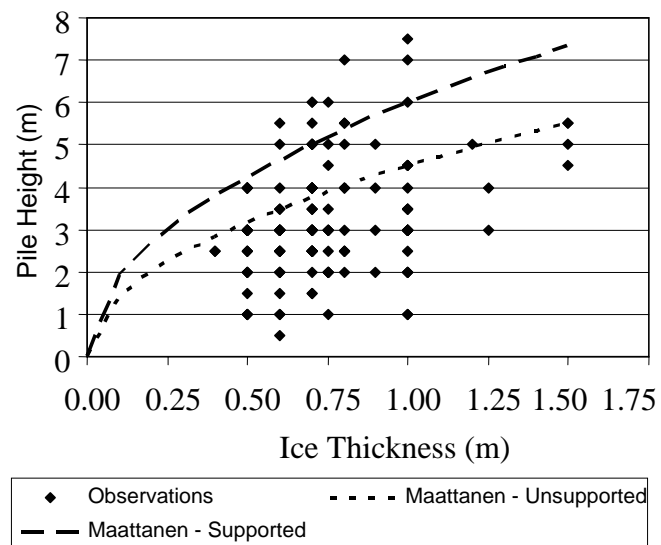

Fig. 3. Typical Rubble Pile
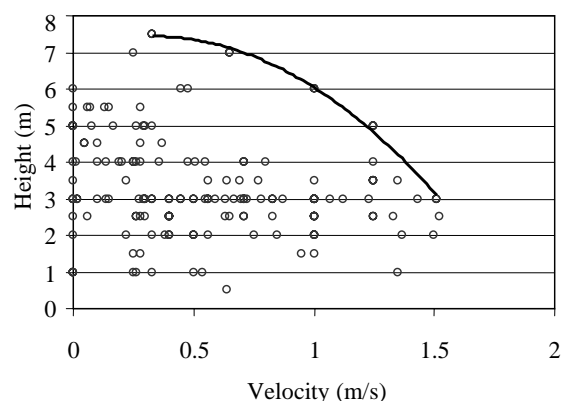

Fig. 4. Rubble Height Variance

Fig. 5. Rubble Pile Height vs Ice Velocity

183

more than a single block. This is clearly related to the geometry of the piers. The water line diameter of 14 m, and a neck width of 8 m at a height of 7 m mitigates against the ride-up of large pieces of ice that may be 6 m long by 3 m wide. However the ride-up of these pieces of ice provides a very effective clearing mechanism for rubble piles. The virtually complete absence of ride-up is surprising and indicative of the importance of the rubble pile in defining the failure mechanisms of the ice sheet or consolidated layer.

Fig. 6. Typical Ride-Up

Interaction between Keel and Consolidated Layer: On reflection, this interaction, on any conical surface, should have been obvious. Any keel rubble, and particularly the keel rubble immediately below the consolidated layer, which itself will be partially consolidated, when trapped between the cone and the consolidated layer, will cause an uplift force on the consolidated layer, accentuating the upward breaking force. The keel also has the effect of changing the effective foundation modulus as it provides additional upward buoyancy to the consolidated layer. This effect also occurs from rubble that is trapped under an advancing ice sheet as a result of previous sheet failures.

As the consolidated layer fails, it removes the upper boundary of the keel, thus causing a loss of buoyant equilibrium to the keel. It may be argued that this effect is localized – only applying to that piece of the consolidated layer between the circumferential crack and the cone. However the extreme lack of homogeneity of the consolidated layer means that this effect is more extensive than just the circumferential crack.

Consolidated Layer: Consolidated layers are extremely inhomogeneous features. Given the previous observation of the non-uniformity of sheet ice thickness, this should not be surprising. Ridges are not uniform features, ridge sails and keels have highly non-uniform geometry so the heat transfer process that

Consolidated layer failure
In front of rubble pile

Fig. 7. Instability of Consolidated Layer

leads to the consolidation is not one-dimensional. Consequently, the consolidation layer is also highly non-uniform. This may be a function of the Gulf of St. Lawrence climate where the Freezing Degree-Day total over the winter is less than 1000°C-D. However, consolidated layer thicknesses of up to 2 m have been observed and this suggests that very significant consolidation does occur. The lack of homogeneity has several effects: classical flexural failure seldom occurs; out-of-plane instability of the consolidated layer is common (Figure 7), and the implied boundary condition provided by the consolidated

184

layer for plug failure of the keel may not be present. For the large ridges with extensive regions of consolidation, the consolidated layer often fails by shear in the horizontal plane. This is discussed in more detail in the discussion on keel failure. One result of this is that, although several failures of consolidated layers can occur in a single ridge interaction, the interactions are seldom classical flexural failure, and the loads are correspondingly less.

Keel Failure: The importance of the keels of first-year ridges in contributing to total loads was dramatically over-estimated (Lemee and Brown, 2002). There is no doubt that the shape of the piers is an important factor in this over-estimation, but there are other factors that may be relevant in other ice regimes and different structures. For the keel load determination, the pier was modeled as a uniform diameter pier where the diameter was averaged over the height of the pier, without regard to the shape. In this regard, the pier shape and specifically, the leading edge provided by the ice-breaking cone (Figure 1), is a major contributor to the disintegration of the keel rubble. Together with the breaking of the consolidated layer, this results in additional instability of the rubble in the keel. Occurring in the tidal flow regime prevailing at the Bridge site, the instability leads to rapid disintegration of the keel into discrete ice blocks which do not apply force to the piers (Lemee and Brown, 2002). Pressure panels that were installed on the pier shaft below the ice-breaking cone, have experienced far fewer pressures than would be predicted on the basis of the number of ridge interactions and the interaction behaviour previously understood. This is a major departure from the understanding that was in place during the ice load design process and it suggests that careful design of piers and structures for deployment in similar ice regimes (no multi-year ice, current flow) can strongly mitigate keel forces.

Lemee (2003) was able to identify two general forms of ridge failure: a bow failure (Krankkala and Maattanen, 1984) and a plug failure. However, in this case, the plug failure often includes plug failure of the consolidated layer so that effectively only two vertical failure planes through the ridge are formed. Based on observations of the surface track of these planes, they diverge as arcs from both sides of the piers (Lemee 2003). The theories used at time, and still being postulated (Karna et al, 2001, Croasdale and Cammaert, 1993) include the deviation angle, ω. In theory, an increase in this angle increases the resulting load. In practice, the failure plane is associated with the lowest force necessary to fail the ridge, so, adhering to the Mohr-Coulomb model, normal pressure on the vertical failure planes, must be closer to the active state, than neutral or passive states. The bow failure involves the development of a prow of ice against the pier with local failure of the consolidated layer and, possibly the keel, taking place at the front of the prow.

Sheet Ice Failure: Failure of level ice sheets, while not resulting in loads as high as those associated with ridge failures, has also resulted in certain new insights into their behaviour. As with ridges, pile-ups against the pier always occur without the presence of ride-up. The circumferential crack is not circular, but elliptical with the shape depending to some extent, on the presence of the rubble pile. In the absence of a rubble pile, occurring either at the initial contact, or after collapse of the rubble pile, the crack is closest to the cone on the axis of motion; with a rubble pile, the crack appears closest at the peripheries. On the axis of motion, this crack is seldom visible beyond the extent of the rubble pile. Figure 8 shows one example of an exception to this where thick, level, ice is failing against P31. Collapse of the rubble pile, which is a common occur-

rence during continuous failure, seems to be as a result of this crack approaching the end of the rubble pile. Rubble has also been seen below the ice sheet, suggesting that there is never "clean" contact between the ice sheet and the cone but rather that contact takes place at points round the circumference of the cone which are constantly changing as the ice fails. This failure mode would allow blocks to slide down below the ice sheet as well as being pushed up into the rubble pile. This conclusion is supported by the pressures observed on the cone – these indicate significant non-simultaneity of pressure round that portion of the cone covered by the panels, 10 m of circumference at the water-line.
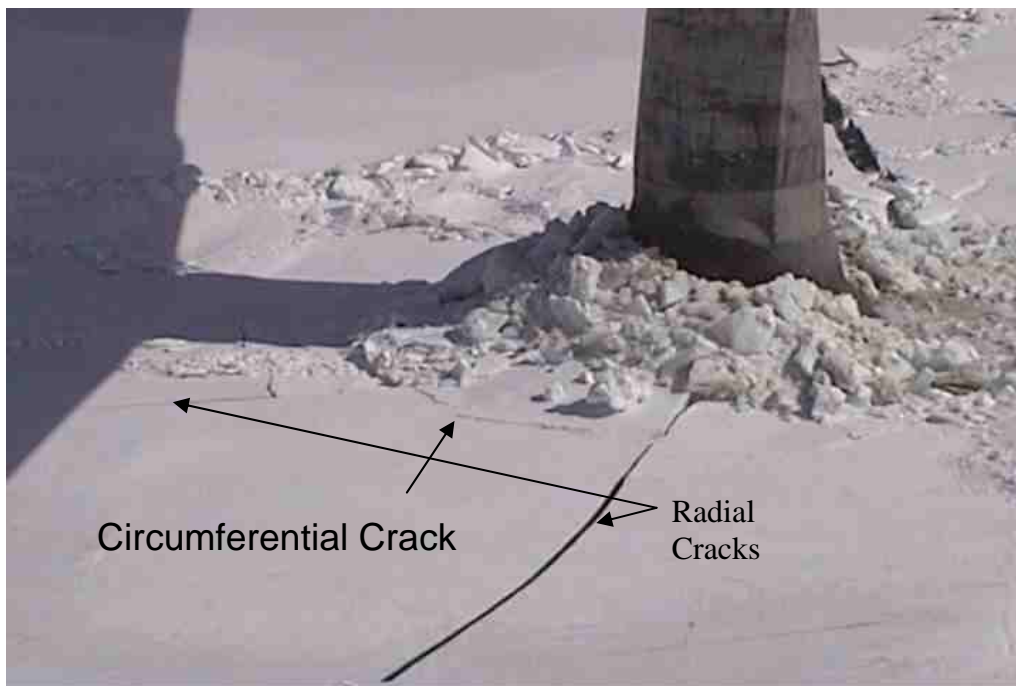

Fig. 8. Circumferential Crack

Pack Pressure. One element that was not considered, except in relation to the determination of driving forces, was the continuity of the ice cover during interactions. Once again, this has been found to be a major mitigating element in reducing ice forces, primarily because a lack of continuity allows cracks to run to the sides of floes, and these cracks provide relief of forces. Even when very large floes (of the order of 500 m or more in extent, and therefore interacting with two or more piers) encounter a pier, the load is often reduced by cracks. The interaction of large floes with the piers results in a deceleration of the floe, and frequently in cracking across the floe between piers, as the drag forces tend to accentuate Type I fracture. Figure 8 shows the initiation of one of these cracks. Early analyses did not consider the sieving effect of the piers on the floe size distribution. Later analyses showed, however, that, because of the tidal flow at the bridge, much of the ice seen by the bridge has already passed the bridge at least once, and therefore floe sizes are smaller, and the pack effect is reduced.

Summary. The observations obtained from the performance monitoring of the Confederation Bridge ice cones has provided significant insight into the behaviour of ice interacting with conical structures. These have provided information on the behaviour of

both first-year ridges, and sheet ice. While many of the observations relate to the inherent inhomogeneity of the ice cover, some are new. However, the measured forces are lower, for a given interacting ice feature, than was predicted by the algorithms used during the design process, and has led to re-assessment of how ice interactions with conical structures are considered. Particularly striking has been the absence of keel pressures on the pier shafts, which has occasioned a major re-assessment of the local behaviour of ridge keels.

Seven years of observations do not make a lifetime, and there continues to be uncertainty about the nature of the interactions, and the resulting loads. In April 2003, the largest load measured since the bridge opened was encountered. This load was almost twice the previously measured highest load and has given pause for thought. Table 1 summarizes the maximum loads measured on the two instrumented piers over the 7 years of observations, and gives the corresponding winter severity. The performance assessment of the piers is continuing, with the focus currently on discerning trends that are not obvious from the data, in particular with relation to the effects of speed.

Table 1. Annual Load Maxima

Year	Freezing Degree-Days	Maximum Load (MN)
1997	~570	4.0
1998	411	4.3
1999	436	4.8
2000	489	4.1
2001	551	4.6
2002	463	4.3
2003	720	7.3

ACKNOWLEDGEMENT

REFERENCES

Brown, T.G, 1997. The Confederation Bridge – early results from ice monitoring program. In *Proc. CSCE Annual Conference*, Vol. 1, Sherbrooke, Canada, 177–186.

Brown, T.G., Jordaan, I., and Croasdale, K.R., 2001, A Probabilistic Approach to Analysis of Ice Loads for The Confederation Bridge. *Canadian Journal of civil Engineering*, Volume 28, No. 4, August, pp562-573.

Brown, T., 2001, Four Years of Ice Force Observations on the Confederation Bridge. In *Proceedings of 16th Conference on Port and Ocean Engineering Under Arctic Conditions POAC*, Ottawa, Canada, pp285–298.

Croasdale, K. R., 1980, Ice Forces on Fixed, Rigid Structures. U.S. Army, *Cold Regions Research and Engineering Laboratory*, Special Report No. 80-26.

Croasdale, K. and Cammaert, A, 1993. An improved method for the calculation of ice loads on sloping structures in first-year ice. In *Proc. First International Conference on Development of the Russian Arctic Offshore*. St. Petersburg, Russia.

Croasdale, K.R., Cammaert, A.B. and Metge, M. 1994. A Method for the Calculation of Sheet Ice Loads on Sloping Structures. *Proceedings of the IAHR '94 Symposium on Ice*, Vol. 2, pp874-875, Trondheim, Norway.

Dolgopolov, Y., Afanasiev, V., Korenkov, V. and Panfilof, D., 1975. Effect of hummocked ice on the piers of marine hydraulic structures. In *Proc. IAHR Symposium on Ice*, Hanover, NH, USA, 469–478.

Kärnä, T., Rim, C.W., Shkinek K.N., 2001. Global loads to first-year ice ridges. In *Proceedings of 16th Conference on Port and Ocean Engineering Under Arctic Conditions POAC*, Vol. 2, Ottawa Canada, pp627-638.

Krankkala, T. and Maattanen, M., 1984. Methods for Determining Ice Forces due to First- and Multi-Year Ridges. *Proceedings of the IAHR '94 Symposium on Ice*, Vol. IV, Hamburg, Germany, pp263-288.

Kubat, I. and Frederking, R., 2001. Response of confederation Bridge to Ice Forces: Winter 2000 Season. In *Proceedings of 16th Conference on Port and Ocean Engineering Under Arctic Conditions POAC*, Vol. 1, Ottawa, Canada, pp319–328.

Lemee, E., 2003. Ridge Interaction with Bridge Piers. Thesis submitted in Partial fulfillment of the Requirements for a Master of Science in Civil Engineering, University of Calgary, Calgary, Alberta.

Lemee, E. and Brown, T.G, 2002. Review of ridge failure theories after analyzing results from Confederation Bridge. In *Proceedings 16th IAHR International Symposium on Ice*, Volume 2, Dunedin, NZ, pp8-15.

Määttänen, M. and Hoikkanen, J, 1990. The effect of ice pile-up on the ice force of a conical structure. In *Proc. IAHR Symposium on Ice 1990*, Vol. 2, Helsinki University of Technology, Espoo, Finland, 1010–1021.

Mayne, D.C. and Brown, T.G., 2000a, Rubble pile observations. In *Proc. 10th International Offshore and Polar Engineering Conference,* Vol. I, Seattle, USA 596–599.

Mayne, D.C. and Brown, T.G., 2000b, Comparison of Flexural Failure Ice-Force Models. In *Proc. Of ETCE/OMAE Joint Conference,* New Orleans, USA, OMAE/P&A-1009, 7p.

Tadros, G., 1997, The Confederation Bridge – an Overview. *Canadian Journal of civil Engineering*, Volume 24, No. 6, December, pp850-866.

Weaver, J., 1994, Review of Ice Rubble Strengths and Failure Modes for the PEI Bridge Piers. *Report to Canatec Consultants Ltd.*, Calgary, Alberta, Canada.

FRACTURE OF THE ICE COVER IN A CONVERGING CHANNEL

Sergei E. Alexandrov, Robert V. Goldstein, Nikolai M. Osipenko[1]

ABSTRACT

Modeling of ice flow in the converging channel was performed taking in mind in particular ice flow in the zones of narrowing the river-bed and in the sea straits. The governing equations for the rigid plastic medium and fracture criteria for the rigid fracturing medium were used to describe ice cover deformation and fracture. The arching formation in the converging channel was modeled and the characteristic parameters of the limit states accompanied by arc formation as well as sizes and location of the arcs were determined.

INTRODUCTION

Among the problems on ice and ice cover dynamics one can separate the specific problems on drifting ice cover motion in straits (converging channels) and ice flow in the zone of narrowing the river-bed often accompanied by jam formation.

Satellite monitoring shows that one of the characteristic schemes of ice cover fracture in the strait zones is related to arc formation. In particular, some data on ice arching in the zone of the Bering strait and Amundsen gulf were given in [1] where a model of arc formation at the motion of fragmented ice cover was suggested. An analysis of the possibilities and conditions of arc formation at the motion of the continuous ice cover was performed in [2]. The strait was modeled as a converging channel and ice cover fracture under the sea current was considered.

The paper is devoted to modeling the ice flow in the converging channel which in particular can be considered as a model of the jam zone. The approach given in [2] is used.

ICE FRACTURE IN A CONVERGING CHANNEL

Following [2] let us model ice medium as a rigid plastic one. The strength of the ice cover will be described within the framework of the theory of rigidly fracturing body [3].

---

[1] Institute for Problems in Mechanics Russian Academy of Sciences

The fracture condition has the following form

$$\left|\sigma_i - \sigma_j\right| \le k, \quad \sigma_i \le d \ (i \ne j, i, j = 1,2,3) \tag{1}$$

where σ_i are the main stresses, k and d are the constants characterizing the medium resistance to shear and tension, respectively. The ice cover is considered in the plane stress state, $\sigma_3 = 0$. Then condition (1) is transformed at $d < k$

$$\left|\sigma_1 - \sigma_2\right| \le k, \quad -\sigma_1 \le k, \quad -\sigma_2 \le k, \quad \sigma_1 \le d, \quad \sigma_2 \le d. \tag{2}$$

Fracture is possible if at least one of inequalities (2) becomes the equality. Condition (2) is represented by an improper hexagon in the plane $\sigma_1\sigma_2$ (Fig. 1). Lines AB and BC correspond to tensile fracture. In other cases shear fracture occurs.

Consider a converging channel covered by ice (Fig. 2, 1 is the shore line, 2 the open water (such that the stresses are absent along line AB), ABCD is the region of possible fracture; (xy), (rθ) – the Cartesian and polar coordinate systems, respectively). For the sake of simplicity assume that the channel is symmetric relative to the x – axis, shore lines AC and BD being straight, the line AB – an arc with the center O, friction is absent along lines AC and BD. Ice cover is loaded by shear loads.
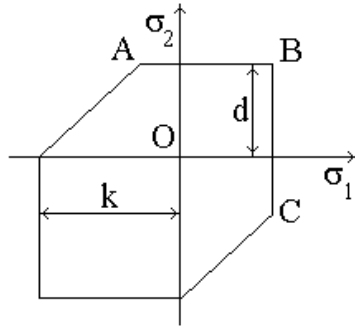

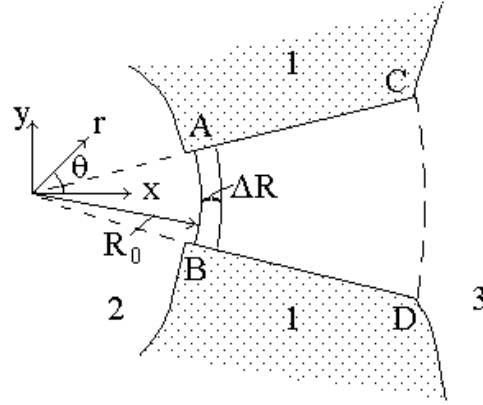Fig. 1. Fracture condition in the plane
of main stresses

Fig. 2. Geometric scheme of the problem

Note, that if the shear loads at the ice cover surfaces are caused by the hydrodynamics resistance to the moving stream, then the value of the shear load (τ) is a function of the stream width. In particular, for the radial converging configuration of the channel one can write

$$\tau \sim \tau_0 \left(\frac{R_0}{r}\right)^2; \quad r > R_0, \tag{3}$$

where τ_0 is the load in the section R_0.

Eq. (1) can easily be obtained within the following assumptions

$$\tau \sim c\upsilon^2, \upsilon \sim \upsilon_0 \cdot \frac{R_0}{r}, \quad \rho c\upsilon_0^2 = \tau_0, \tag{4}$$

where c is the coefficient of the hydrodynamic resistance.

The specific shear load τ = const [2] is related to the wind loading in a slightly converging channel.

The equilibrium equation has the following form in the plane problem

$$\frac{\partial \sigma_r}{\partial r} + \frac{\sigma_r - \sigma_\theta}{r} = \frac{\tau_0}{2H}\left(\frac{R_0}{r}\right)^2 \tag{5}$$

and

$$\sigma_r - \sigma_\theta = k \, ; \sigma_r = 0 \quad at \quad r = R_0 \, , \tag{6}$$

H is the ice thickness.

The solution of Eq. (3) with the condition (4) has the form

$$\sigma_r = \frac{\tau_0 R_0^2}{2H}\left(\frac{1}{R_0} - \frac{1}{r}\right) + k \ln \frac{R_0}{r} \tag{7}$$

$$\sigma_\theta = \frac{\tau_0 R_0^2}{2H}\left(\frac{1}{R_0} - \frac{1}{r}\right) + k \ln \frac{R_0}{r} - k \; . \tag{8}$$

Tensile fracture occurs along the arc r = R_1 at σ_r = p. Using the parameter $\rho = \frac{R_1}{R_0} \ge 1$, we can rewrite Eq. (5) as follows

$$\frac{\tau_0 R_0}{2kH} = \frac{\rho}{\rho - 1}\left(p/k + \ln\rho\right). \tag{9}$$

Remind that the similar relation for the case τ_0 = const has the form [2]

$$\frac{\tau_0 R_0}{2kH} = \frac{\left(p/k + \ln\rho\right)}{\rho - 1} \; . \tag{10}$$

Eqs (7) and (8) determine the interrelation between the problem parameters in the limit equilibrium state and, in particular, the interrelation between R_0 and ρ.

The systems of loading considered in the present paper, equation (3), and in [2] may lead to quantitatively different fracture modes. In fact, equation (9) shows that $\tau_0 \to \infty$ as $\rho \to \infty$, and equation (10) that $\tau_0 \to 0$ as $\rho \to \infty$. Also, it follows from (10) that τ_0 is a monotonically decreasing function of ρ at given values of p and R_0. The latter means that fracture occurs at the maximum possible radius R_1 and thus the position of the fracture surface is completely determined by the geometry of a strait [2]. On the other hand, the right hand side of equation (9) attains a minimum at $\rho=\rho_{cr}$. The value of ρ_{cr} can be found from the following equation

$$\rho_{cr} - \ln\rho_{cr} = 1/pk \tag{11}$$

The corresponding value of $\frac{\tau_0 R_0}{2kH} = t_{cr}$ can be obtained upon the substitution of (11) into (9). It results in

$$t_{cr} = \rho_{cr} \; . \tag{12}$$

The solution to equation (11) is illustrated in Fig. 3. Due to (12), the same curve demonstrates the variation of t_{cr} with p/k. The existence of the aforementioned minimum in the case of the system of loading described by (3) means that the mode of fracture depends on the geometry of a strait and the magnitude of p/k, a material property. If $\rho_{cr} \geq R_1/R_0$, the mode of fracture is the same as that found for the case of the system of loading considered in [2] and the fracture surface is located at r=R₁.

If $\rho_{cr} < R_1/R_0$, the fracture surface is located within the strait at $r = \rho_{cr}R_0$.

If an annular sector of width $(R_1 - R_0)$ is separated then the unloading occurs at the contour of the rest part of the ice cover

Fig. 3. Interrelation between ρ_{cr} and p/k

such that the system returns to the initial state with the new value R_0 (the new $R_0 = R_1$ of the former problem).

It is interesting to evaluate the width of the separated annular sector in dependence on the value R_0.

Denote $R_1 - R_0 = \Delta R$. Let us write (7) and (8) for two variants of loading, respectively:

$$\frac{p}{k} = \frac{\tau_0 R_0}{2kH}\left(\frac{\Delta R}{R_0 + \Delta R}\right) + \ln\left(\frac{R_0}{\Delta R + R_0}\right) , \tag{13}$$

$$\frac{p}{k} = \frac{\tau_0}{2kH}\Delta R + \ln\left(\frac{R_0}{\Delta R + R_0}\right) \quad at \quad \tau_0 = \text{const} . \tag{14}$$

For the real conditions $\Delta R \ll R_0$ and the right sides of Eqs (9) and (10) can be represented in the form of the expansion with respect to the small parameter $\Delta R/R_0$. Retain the first terms, then in both cases we obtain

$$\Delta R \sim \frac{pR_0}{k}\left(\frac{\tau_0 R_0}{2kH} - 1\right)^{-1} . \tag{15}$$

Hence, the width of the separated annular sector is independent on the distribution of shear loads (τ) for relatively small sizes of the parameter $\Delta R/R_0$.

The value ΔR in Eq. (13) tends to the asymptotics

$$\Delta R \Rightarrow \frac{2pH}{\tau_0} , \tag{16}$$

as R_0 grows (and $\Delta R/R_0$ remains constant).

The asymptotic formula (14) can be used to estimate the system parameters (p - values) at the known values ΔR and τ_0.
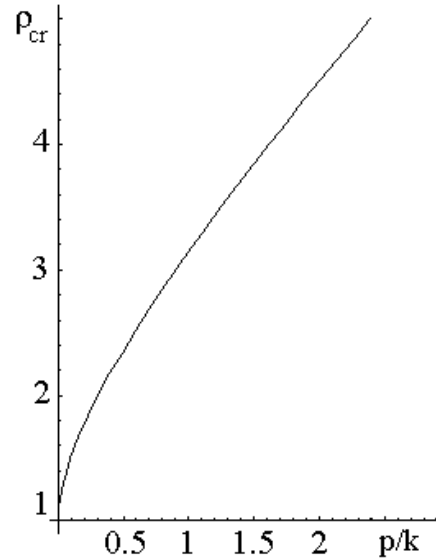
Note, that the faults distribution along the channel widths depends on the loading type at $\Delta R / R_0 \neq 0$. For instance, we obtain from Eqs (9), (10)

$$\frac{\tau_0 R_0}{2kH} = \ln\left(1 + \frac{\Delta R}{R_0}\right)\left(\frac{R_0}{\Delta R}\right) = 1 - \frac{\Delta R}{2R_0} + \frac{1}{3}\left(\frac{\Delta R}{R_0}\right)^2 + \dots$$

$$\frac{\tau_0 R_0}{2kH} = \ln\left(1 + \frac{\Delta R}{R_0}\right)\left(1 + \frac{R_0}{\Delta R}\right) = 1 + \frac{\Delta R}{2R_0} - \frac{1}{2}\left(\frac{\Delta R}{R_0}\right)^2 + \dots$$

at $p \Rightarrow 0$. The difference between the system parameters for to variants of shear loading increases as the parameter $\Delta R / R_0$ grows. The interrelation between $\Delta R / R_0$ and R_0 is given in Fig. 4 for the ice properties under consideration.
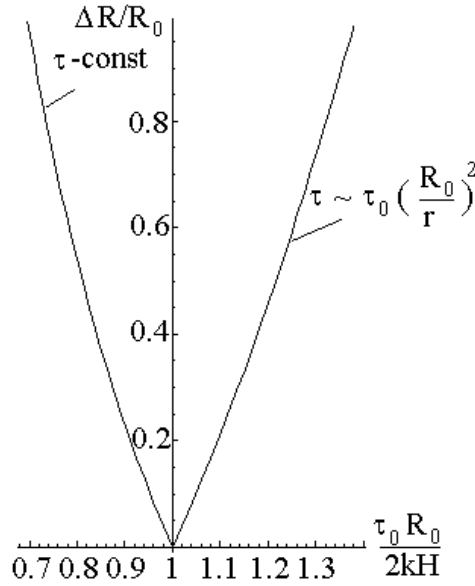

Fig. 4. Interrelation between the size of separated
annular sector and initial radius R_0

Note, that generally another fracture mechanism can be realized in the described loading scheme of the medium in the converging channel (in particular, the mechanism related to ice ridging, i.e. attaining a limit value of compressive stresses σ_θ).

The faults in the peripheral direction can be formed both under the action of global tensile stresses (σ_r) and under the action of local wedging effects at mutual slipping of ice floes at combined loading (σ_r and σ_θ).

Let us study the evolution of the separated annular sector. The loading scheme is changed after its separation. The fault grows is accompanied by unloading for the main part of the ice cover. The unloading leads to redistribution of forces and reactions from the shore (i.e., leads to changing the stresses σ_θ in the annular sector). Assume that the annular sector is thin (i.e., the ratio of its width to its length is small). Then the stress changing can be taken into account within the beam approach. Further, the shear load $\tau(r)$ is assumed to be constant within each annular sector. Hence, in case of friction absence on the piles the difference of the stresses (σ_r) along the separation line equals the

tensile strength (p). This redundant load is perceived by the arc as the external pressure. The additional compressive stresses $\Delta\sigma_\theta$ (average through the annular sector width) are equal to

$$\Delta\sigma_\theta \sim \frac{pR_0}{\Delta R}; \quad \Delta R = R_1 - R_0 . \tag{17}$$

According to Eqs (6) and (15) we obtain for the thin annular sector

$$\sigma_\theta = \sigma_{\theta_0} + \Delta\sigma_\theta \approx \frac{\tau_0 R_0^2}{2H}\left(\frac{1}{R_0} - \frac{1}{R_1}\right) - k\left(1 + \ln\left(1 + \frac{\Delta R}{R_0}\right)\right) - \frac{pR_0}{\Delta R} \tag{18}$$

or at $\Delta R \ll R_0$

$$\sigma_\theta \approx \frac{\tau_0}{2H}\Delta R - k\left(1 + \frac{\Delta R}{R_0}\right) - \frac{pR_0}{\Delta R} . \tag{19}$$

One can believe that two basic variants of deformation of the annular sector exist. If the stresses σ_θ in this sector do not exceed the yield stress, then the annular sector is separated (preserving integrity and elastic state) from the rest massive under the action of additional compressive stresses. The size of the occuring gap is evaluated by the following relation

$$\delta \sim \varepsilon \cdot R_0, \quad \text{where} \quad \varepsilon \sim \frac{\Delta\sigma_\theta}{E} . \tag{20}$$

By incorporating Eqs (15) and (13) we obtain

$$\delta \sim \frac{pR_0^2}{E\Delta R} \approx \frac{R_0}{E}\left(\frac{\tau_0 R_0}{2H} - k\right) \tag{21}$$

If the gap value (δ) is known than using Eq. (19) one can evaluate, e.g., an effective elastic modulus of the ice massive or ice strength (p) at known characteristics of the flow (τ_0) and the fault geometry.

The limit condition of the retaining the integrity of the annular sector is related to the condition of the plastic equilibrium. Then for a thin annular sector one can assume that $\sigma_r \sim 0$.

Hence, by incorporating Eq. (17) we obtain the equilibrium condition

$$\sigma_r - \sigma_\theta \approx k ,$$

i.e.

$$\Delta R\left(\frac{\tau_0}{2H} - \frac{k}{R_0}\right) - \frac{pR_0}{\Delta R} \approx 0 . \tag{22}$$

Eq. (20) enables to search for the limit radius of the inner contour R_0 such that the fracture of separated annular sectors under the action of the longitudinal stresses stops at $R = R_0$. This condition determine the contour of the stable arc shaped configuration of the ice edge at the entrance in the narrow strait (channel). From Eqs (20) and (13) we obtain

$$R_0^* \approx \frac{2H}{\tau_0}(k + p). \tag{23}$$

CONCLUSION

A model of ice fracture at the motion in a converging channel was suggested which enables to analyze the main parameters of motion and fracture of the ice cover related to the observed morphology of ice cover deformation and fracture in narrow straits.

An ice cover medium is modeled by a rigidplastic one in a converging channel loaded by distributed loads caused by the wind and flow.

Within the framework the model we obtained the relations which characterize the limit state of the ice cover, arching conditions and sizes of the arcs, as well as location of the boundary separating the regions stable arching and fractured ice.

The suggested model can be used for solving the problem on limit equilibrium and fracture of ice mass in jams forming at converging zones of rivers.

The model can also be used for evaluation the effective properties of the ice cover on the basis of observed structures of faults.

REFERENCES

Sodhi, D.S. Ice arching and the drift of pack ice through restricted channels. *CRREL Report* 77-18 (1977) 11p.

Alexandrov, S.E. and Goldstein, R.V. Ice cover fracture in a narrow converging channel. *Reports of the Russian Academy of Sciences* 365 (3): 343-345 (1999).

Ivlev, D.D. To the theory of fracture of solids. *Applied Mathematics and Mechanics* 23 (3): 618-624 (1959).

THETIS SPRAY/CHIP ICE ISLANDS FOR HARRISON BAY, ALASKA

D. M. Masterson[1], R. Cooper[2], P. A. Spencer[1], W. P. Graham[1]

INTRODUCTION

Pioneer Natural Resources drilled three exploratory wells from grounded ice islands during the winter of 2003 in 3m (10 ft.) of water in Harrison Bay Alaska, located west of Prudhoe Bay on in the southern Beaufort Sea. The islands were built using sprayed ice for the main bulk of the material and were finished using ice chips mined from the local sea ice near shore. As well, 32 km (20 miles) of grounded ice road was constructed using ice chips. The road was used to transport two drilling rigs to the islands, one rig weighing 680 tonnes (1,500,000 lbs.) and the other 1140 tonnes (2,500,000 lbs.). Drilling from the first island started in mid-February 2003 and all drilling was completed by end March 2003. Ice build-up rates, chip haul rates, ice strength and density and seabed subgrade modulus were measured to substantiate the engineering assumptions made during design of the islands and roads. The ice islands and surrounding pack ice were monitored for movement during drilling using DGPS. Vertical settlement of the islands was also monitored. Extensive monitoring of the rig moves over the ice roads was conducted, where minor breakthroughs were encountered for the heavier rig.

Figure 1 shows a map of the well sites and the roads leading to the islands.

ISLAND DESIGN

Design Water Depth

According to chart datum, the sites have water depths of 2.3m to 3.7m. 0.6m was added to the design depth to account for surge.

Seabed Mechanical Properties

The seabed is alluvial and consists of silts and sand, possibly with some organics. After consolidation from the island surcharge, it is a frictional material with an internal friction angle (ϕ) of 33 degrees and zero cohesion.

---

[1] Sandwell Engineering Inc., Calgary, Canada
[2] Pioneer Natural Resources Canada Inc., Calgary, Canada

Fig. 1. Site Map

Design Ice Thickness

The natural sea ice grows over the winter and reaches a maximum thickness in spring. Only first-year ice is encountered in the region of the wells. While drilling had to be finished by March 31, other operations could continue past this date, and 2m is normally considered an appropriate design thickness. In early January of 2003, it was know that the average ice thickness at the sites was 0.7m. According to the accepted equations the ice thickness should have been 0.95m and a thickness of 0.7m would have been reached 30 days prior to the time of measurement. The natural ice cover thickness on February 10 was 1m. Using the historical projection for design, the ice could only reach 1.5m by April 20 and consequently the design ice thickness was reduced to this amount.

Design Ice Load

The design ice load per meter width of the ice island at the end of the winter season was determined by multiplying the design thickness of 1.5m times the ice pressure. The effective ice pressure is presented in [1]. For the design ice thickness at the present sites, the global ice pressure was 1.38 MPa. The pressures were generally obtained from crushing on vertically sided structures. The ice sheet would likely fail in flexure at the island boundary at pressures less than the crushing pressure. The value of 1.5 MPa is above the envelope containing the highest recorded ice pressure and thus represents a conservative value.

Spray Ice Material Properties Below the Waterline

In determining the sliding resistance of spray ice islands, the shear strength of the spray ice itself must also be considered since, depending on the bottom soil conditions, a shear failure could develop on a plane through the island itself.

There is limited data on the shear strength of spray ice below waterline. Available sources are presented in [2], [3] and [4].

197

The available information suggests that the spray ice below water line is also a plastic, low friction material. An extensive series of cone penetrometer tests was conducted at the Karluk Island during the verification program [5]. The average bearing pressure below the waterline was 3.8 MPa. The range was:

$$1.6 \text{ MPa} < \text{Bearing Capacity} < 6.3 \text{ MPa} .\qquad(1)$$

Assuming, as is standard practice, [6] that the shear strength is 1/6 of this, then the Karluk Island had the following bounds on shear strength below waterline.

$$267 \text{ kPa} < C < 1{,}050 \text{ kPa} .\qquad(2)$$

The lack of voids and general continuity of the ice at Karluk, plus the high cone test results indicate a high shear strength. A weighted mean shear strength using all of the above data is 75 kPa. The range in the shear strength was used to estimate the weight of the value. The spray ice has considerably higher shear strength than the seabed

Spray Ice Properties Above the Waterline

Information from spray ice platforms and islands suggests that the spray ice behaves as a Mohr-Coulomb material such that the shear strength, τ, is given by [7].

$$\tau = C + N\tan\phi .\qquad(3)$$

Where: C = 283 kPa; $\phi = 0.85^{\circ}$; N = normal pressure (kPa).

Island Geometry

The idealized island geometry for the islands is given in Figure 2. The grounded portion of the island forms the core of the island while beyond is the sacrificial edge which, in the event of a major ice movement, would be subject to shear type failure. All critical, non-relocatable facilities, such as the drilling rig and any camp, had to be located within the core radius.
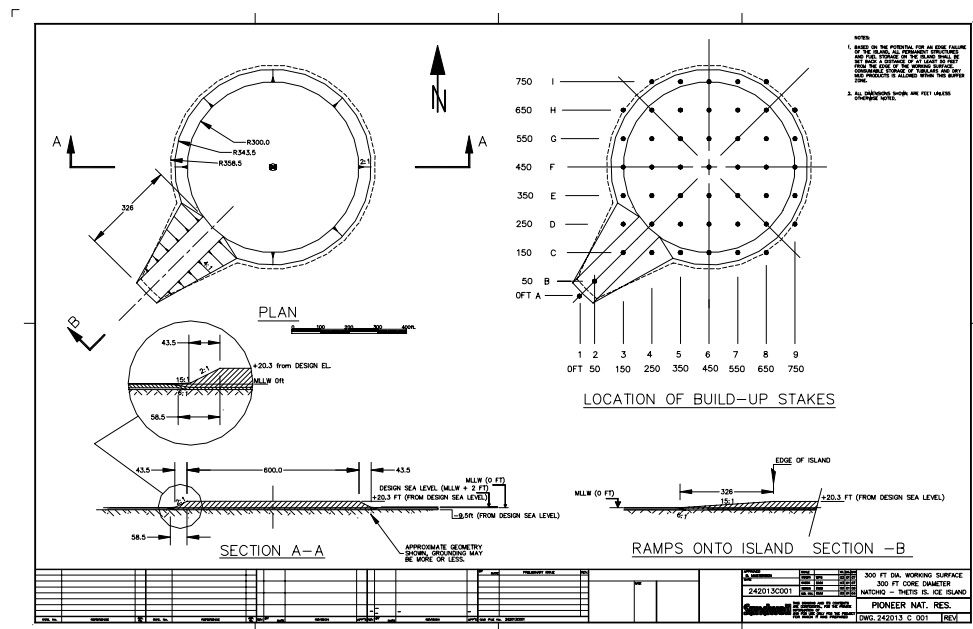

Fig. 2. Geometry of Ice Island – All dimensions in feet

ICE ISLAND STABILITY

Core Resistance of the Island to Sliding

The equation describing the resistance to sliding from forces due to moving ice is given as:

$$\text{Resistance} = \frac{\pi D_c^2}{4}\left[c + \{\gamma_i h + (\gamma_{si} - \gamma_w)H\}\tan(\varphi)\right] \qquad (4)$$

Where:

D_c	= core diameter (ft.)
γ_i = above water spray ice density	= 40 lb/ft^3
γ_{si} = below water spray ice density	= 57.8 lb/ft^3
γ_w = sea water density	= 64 lb/ft^3
h	= island freeboard (ft.)
H	= water depth (ft.)
φ	= bottom material friction angle = 33°
c	= bottom material cohesion = 0.

The lateral ice force from the pack surrounding pack ice and the resisting forces are shown on Figure 3. The Resistance/Lateral Ice Force = Factor of Safety.

As of February 11, the first island (Ivik) had been completed to a height above water of 3m. The remainder of the island was completed using chipped ice hauled from a separate location which was then soaked with water after being placed on the island. Measurements on the ice roads being built showed that the placed chipped ice had a density of 0.83 t/m^3 vs. the spray ice density of 0.61 t/m^3. Thus the required net weight on bottom to produce a shear force sufficient to resist the ice force with a factor of safety of 1.35 could be produced with less ice freeboard or volume.

The required ice island freeboard, considering both the reduced design natural ice cover thickness of 1.5m and the increased density of the placed ice chips, was 5.1m.
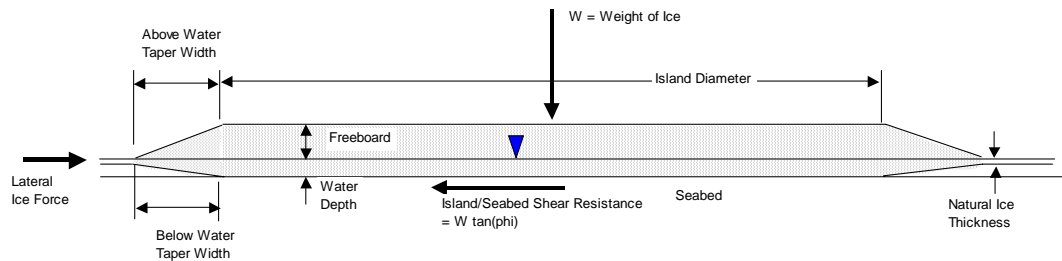

Fig. 3. Spray Ice Island Cross Section – Environmental and Gravity Forces

Island Bearing Capacity

When properly constructed, spray ice has proven to be a material very capable of supporting its own load when set down on the seabed and of supporting heavy surface loads such as drilling rigs.

Below Water Capacity

Observed behavior indicates spray ice to generally be a cohesive material. From foundation theory for a circular plate [8] the bearing capacity is:

$$q = 1.2\, c\, N_c. \qquad (5)$$

Where: c – shear strength of the material; N_c – 5.14.

Above Water Capacity

Previously, the shear strength of the above water ice was given as 283 kPa. Thus the bearing capacity above water is 6 x 283 kPa =1.7 MPa.

Creep Settlement

The short duration of this project's wells resulted in small creep settlement and thus it was not a key design consideration.

Well Conductor and Cellar

Use of the standard North Slope gel/diesel filled annulus between the surface casing and the conductor was sufficient to contain ice melt during drilling and testing of the holes.

The cellar was formed of a standard corrugated steel pipe, 1.8m in diameter, commonly used for drainage and road crossings. Insulation was not required because of the short duration of the drilling.

Access Road

The location of the ice access road is shown in Figure 1. This road was grounded. However, where the bottom support was weak and questionable, the ice thickness required to support the heaviest load in a floating mode was required.

The heaviest planned load was the Nabors Rig 27E substructure which had a weight of 682 t. Using an allowable flexural stress in the ice of 500 kPa, the ice thickness required to transport this load configuration in a floating mode was 3.8m. This ice was grounded on between 0.3 to 0.6 m of softer material, which overlay the stiff soil.

Spraying

Large, 14. MPa pumps were used to spray water to form ice. Pumps for spraying the islands were supplied by CATCO and AIC. CATCO used one 12 m^3/min. pump and three 20 m^3/min. pumps and AIC used two 12 m^3/min. pumps. The pumps sprayed for a pre-determined length of time and then shut down so that the ice could cure and harden. The cycles usually consisted of half an hour of spray and then half an hour of curing but the cycle depended on the temperature.

Chips and Water Hauling

Once the spraying was completed, Cats were used to level the island tops. The chip hauling process began by creating chips at sites away from the ice islands and roads using a chipper, which is a converted asphalt stripper. Once the ice had been disaggregated it was loaded into trucks and transported to the ice islands and roads. The chips of ice were dumped on the ice and levelled and water was poured over the chips so that the voids were filled with water which quickly froze because of the available heat sink.

The benefit of using chips in the building of ice islands and roads is that the temperature does not need to be as low as required with spraying. This is due to the fact that the ice chips absorb the latent heat of freezing and less water has to be frozen. Because of the outflow of the Colville River ice borrow sites for the chipped ice were found that had a salinity much lower than first year sea ice. For most of the access road construction, fresh water was used. One section of offshore road did use a pumping unit to provide an initial layer of sea water for the chips.

IVIK ICE ISLAND

Construction

Spraying of Ivik Ice Island was started on January 24 2003. Three pumps were used for the spraying: one 12 m^3/min. pump and two 20 m^3/min. pumps. Patterns of 15 minutes of spraying followed by 1 hour of curing. On January 28, the island was drilled and the average ice thickness over the core was measured to be 2m, a build up rate of 0.23 m/day.

From February 2 to 7, spraying continued at a lower frequency and duration because of warmer weather. On February 11, spraying was discontinued and the hauling of chips and water to the Ivik ramp area started in preparation to build up the surface of the island to the final height. From February 12 to 16, hauling of chips and water onto Ivik continued. As of February 17, the island was ready for the rig, with a final density of 0.80 t/m³. 73,584 m^3 of chips and 37,606 m^3 of water were hauled onto the island. By comparison, approximately 250,000 m^3 of spray ice was made. On February 19, Rig 27E was mobilized to the island for drilling.

Drilling

Rig 27E started drilling on February 25 and the ice temperature profile in the island indicated satisfactory temperatures. Rig 27E continued drilling on Ivik until March 13, when it was moved to Oooguruk Island. Testing on the island continued after all Sandwell personnel had left the field on April 2.

OOOGURUK ICE ISLAND

Construction

Spraying of Oooguruk Ice Island started at the same time as Ivik Ice Island on January 24 2003. Spraying had to be stopped on January 26 as there was a significant amount of wet, unfrozen material. On January 28, difficulties arose because very wet material had been put down and not given the chance to cure before the next layer was applied. For this reason, there was as much as 1m of unfrozen material with a 25 to 40 mm crust. This was solved by changing the size of the pump nozzle which produced a drier material.

On February 3, an elevation survey was conducted, showing an average ice thickness of 2.5m. After a brief warm period, on February 17 intense spraying and levelling with 2 Cats continued on Oooguruk. The island had an average density of 0.63 t/m³. Spraying continued until February 26, when levelling and the hauling of chips began.

Drilling

The island was ready on March 7, and Rig 27E was brought onto Oooguruk on March 13. The drilling and logging began on March 18 and was completed on March 27.

NATCHIQ ICE ISLAND

Construction

Natchiq Ice Island was started On February 11. The duration of each spray period on Natchiq was increased since temperatures were in the range of -7°C and -9°C. Cure times were 20 minutes. From February 12 to 25, spraying and levelling continued on the

island, which had an average density of 38.9 lb/ft³. Levelling and chip hauling started on February 26 and continued to March 4. March 6 miscellaneous supplies and the Rig 3 camp were brought onto the island.

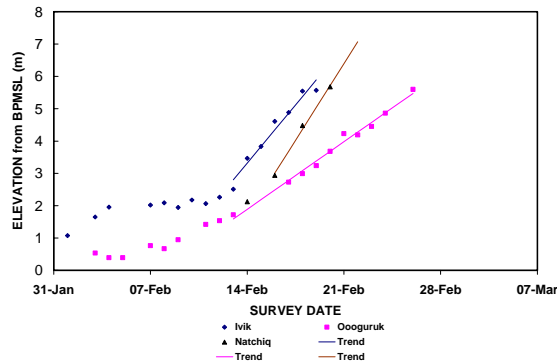Figure 4 contains surface elevations of the ice islands over time, a direct measurement of ice build-up.

Fig. 4. Ice Islands Surface Elevation vs. Time

Fig. 4a. Spraying with 20 m3/min. pump

Drilling

Rig 3 reached the island on March 15. The rig started drilling and logging on March 18 and stopped on March 28.

Ivik Ice Road

Construction of the ice road to Ivik along the shore started on January 26. On February 10 the road to Ivik was completed. Drilling showed there was a 1.2 to 1.8m cap on top of spray ice next to Ivik's perimeter. The ice was continuous from surface to seabed. Structurally, the approach road and ramp to Ivik were ready for the rig.

Oooguruk Ice Road

On January 31, chips were being used to build the road to Oooguruk. On February 10 Ivik ice island was reached and construction continued towards Oooguruk. The construction of the road to Oooguruk finished March 2 when it was surveyed for thickness and quality.

Natchiq Ice Road

On February 19, construction continued on the road. The road was deemed well grounded on March 3, having a thickness of approximately 9.7m. Rig 3 was moved onto Natchiq Island on March 7. All the roads were constantly maintained and repaired until the rigs were moved of the island and back onto shore.

The height above water level to which the grounded ice roads were constructed ensured that they would not refloat during drilling. Water levels from the West Dock STP (seawater treatment plant) was used to establish this height.
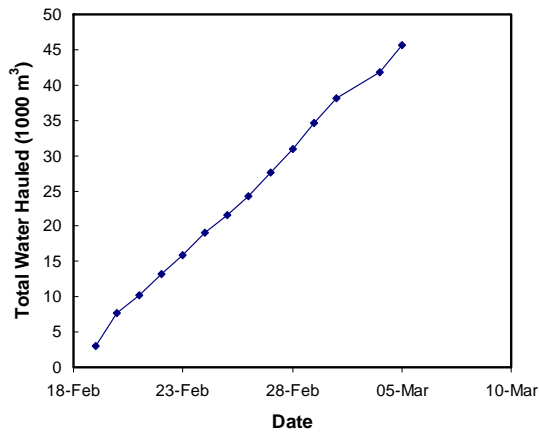
Fig. 5. Cumulative Water Haul
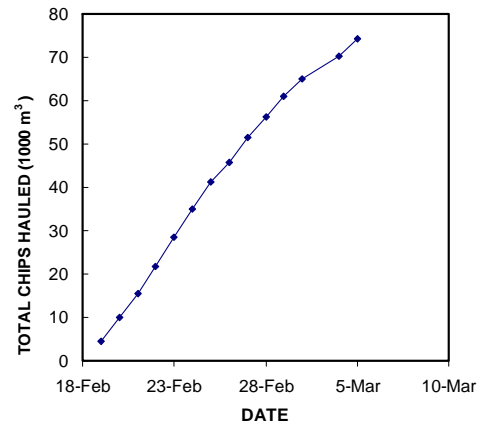on Natchiq Ice Road

Fig. 6. Cumulative Chip Haul
on Natchiq Ice Road

Fig. 6a. Dumping, Watering and Grading Ice Chips

Verification

Once the construction was completed, the safety and strength of the islands and roads had to be verified. In this case, the thickness of the ice was measured at definite points. The ice continuity was evaluated whereby the islands and roads were inspected to ensure that no cracks or other unconformities were present to hamper the transportation of the rigs. The density of the islands and roads was measured. Figures 7 and 8 contain a plot of the spray ice densities collected from all three islands and the Oooguruk Core Density taken on March 17. In Figure 7 the blue (light) bars represent the collected data and the purple bars (dark) represent a Gaussian fit. As can be seen from Figure 7 the histogram is slightly skewed with a tail on the high density side. The scatter is from two major sources, differences in actual material density and errors in the actual density measurement, where the source density variation dominates.

PERFORMANCE

Roads

The shore roads worked well for the transportation of the Rigs. The offshore roads, however, did present a problem for Rig 3. This was due to the fact that Rig 3 was far heavier than Rig 27E, rig 27E being approximately 680t while Rig 3 was approximately 1140t.
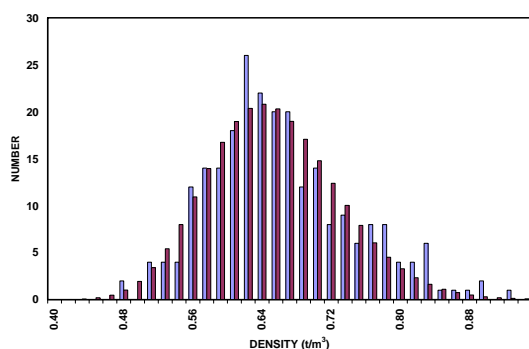
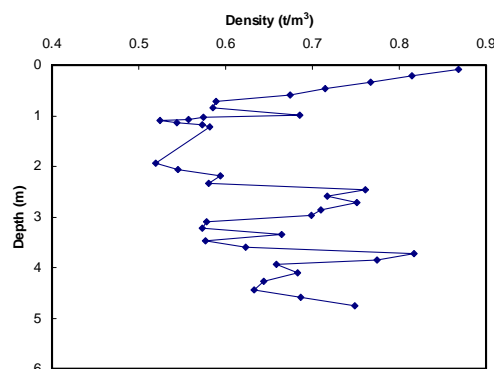Fig. 7. Spray Ice Density Histogram for the Three Islands

Fig. 8. Oooguruk Spray Ice Density Profile

The ice road could not support Rig 3 and the wheels broke through several times on the route offshore to Natchiq. This was due to the fact that the ice was underlain by a layer of soft surficial material between 200 to 300 mm thick. As the rig moved, the ice deflected down through the soft material until it reached stiffer material. By this point, however, the ice had flexed beyond its limit of elasticity and frequently failed.

Islands

Over the course of the period that work was done on the Islands and Roads, the movement of the islands was recorded with the use of differential GPS measurements. Figures 9 and 10 show the Net Ice Motion and the Net Movement Vectors. Note that the movements are obtained from monuments placed on the floating level ice adjacent to the islands. These monuments were typically 800m from the island centers. Post construction measurements showed negligible horizontal movement of the islands themselves. The trend lines in Figure 9 are based on the net movement being proportional to the square root of time. Figure 10 shows that that the movement direction as well as the magnitude was different at each site. At the termination of monitoring the pack ice movements near the islands were 0.95, 0.42 and 0.40m for Ivik, Oooguruk and Natchiq respectively.
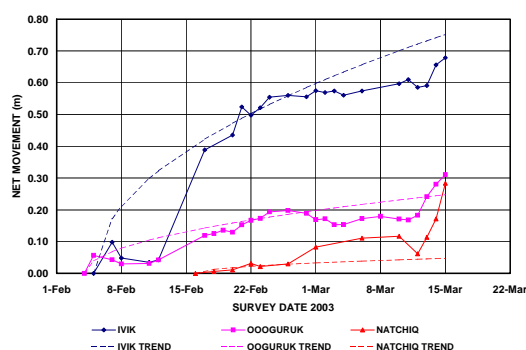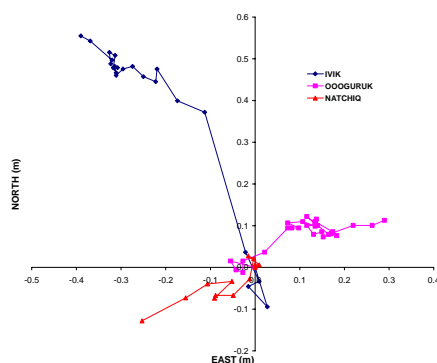

Fig. 9. Pack Ice Motion vs. Time

Fig. 10. Net Ice Motion Vector Plot

Island Settlement During Drilling

Creep settlement of the ice islands during drilling is of a concern to the drilling operation. Excessive settlement will lead to misalignment of the drilling rig and require adjustment, especially if there is appreciable differential settlement between support points. Figure 11 contains island surface elevation measurements taken at Ivik ice island

between February 20 and March 1, 2003. The measurements were taken at two separate stations and the total settlement at each station were 0.25m and 0.18m respectively. These settlements are within the normal range for spray ice structures [9]. At no time during the drilling and subsequent well testing and logging program were island settlements of a concern and no adjustments for them had to be made.
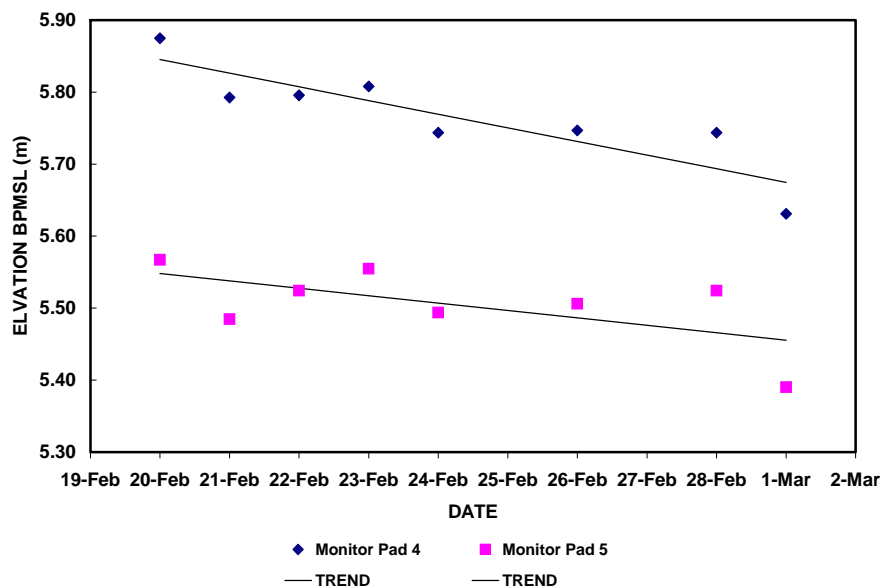

Fig. 11. Ivik Settlement Survey

Ice Temperature Near the Cellars

Thermistor strings were installed in the ice islands and the ice temperature was closely monitored during the drilling and well testing program. The ice near the well cellars is always subject to heating and melting as a result of mud circulation during drilling. The temperature profiles close to the cellars at Oooguruk and Natchiq ice islands are shown on Figures 12 and 13. The temperatures at both cellars remained below 0 °C and there was no melting of ice.

CONCLUSION

The Thetis ice island wells were drilled successfully during February and March of 2003 from grounded spray ice/chip ice islands. The islands were built by spraying of seawater and chip hauling and, although the winter season was late, were finished on time for the drilling and well testing to be completed before the islands had to be abandoned. The islands all had a core diameter of 180m (600 ft.), were located in water depths between 2.3 and 3.7m. 1.4 MPa pressure spray pumps with capacities of 20 m3/min. and 12 m3/min. were used to construct the islands. Ice chips were mined from the natural ice near shore and trucked to the islands where they were deposited, soaked with water and allowed to freeze. 32 km of grounded ice road was constructed using ice chips soaked with water. 73,584 m3 of chips and 37,606 m3 of water were hauled onto Ivik, the first island constructed. Approximately 250,000 m3 of spray ice was built at Ivik. Similar quantities were produced a the other islands.
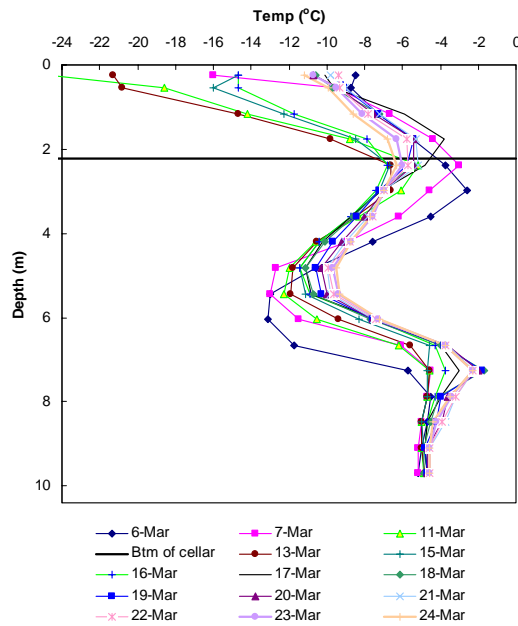
Fig. 12. Ice Temperature Profile
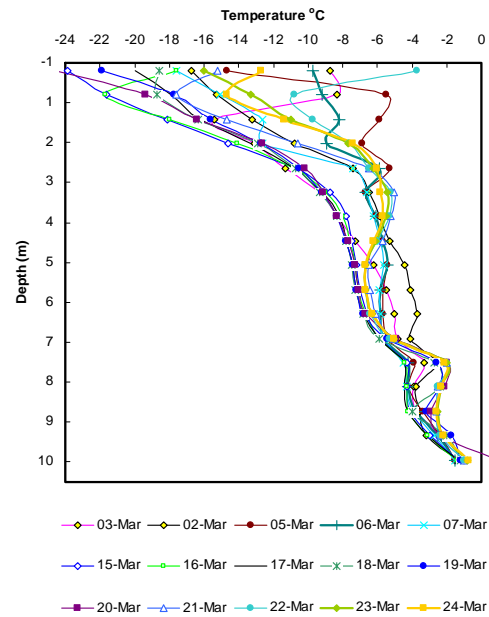at Oooguruk Cellar

Fig. 13. Ice Temperature Profile
at Natchiq Cellar

Two rigs weighing 680 and 1140 tonnes were transported over the grounded ice roads to the islands. Because of the soft surficial seabed material overlaying dense material, the 1140 t rig broke through the offshore road en route to Natchiq island. After matting and levelling the rig could proceed and did reach the island to drill the well. There was no damage to the rig.

− Built-up ice densities for the three islands had a mean of 0.66 t/m3 with a standard deviation of 0.08 t/m3

− Surface settlements of the islands were 0.18m to 0.25m during drilling and well testing and were within acceptable limits.

− Ice temperatures near the cellars remained below 0 °C.

− Island movement was negligible or zero after full grounding with the design freeboard.

− The surrounding pack ice did move and near Ivik island it moved 0.95m.

All drilling was completed before the March 31 deadline.

ACKNOWLEDGEMENT

REFERENCES

Masterson, Daniel M. and Paul A. Spencer (2000), Ice Force Versus Aspect Ratio, *IUTAM Symposium "Scaling Laws in Ice Mechanics and Ice Dynamics"*, Fairbanks, AK, USA, June 2000.

Geotech/Golder Associates (1985), Report on *Construction, Testing & Monitoring of Sohio et al Spray Ice Island*, Prudhoe Bay, Alaska, September, 1985.

Goff R.D., Masterson D. M. (1986), Construction of a Sprayed Ice Island for Exploration, OMAE 1986.

Masterson, D.M., Baudais, D.J., Pare, A. and Bourns, M., Drilling of a Well From a Sprayed Floating Ice Platform - Cape Allison C-47. OMAE `87, Houston, Texas, Paper No. 162.

I.C.E. 1989, Chevron Karluk Ice Island Project Report, *Report for Chevron by I.C.E.*, September, 1989.

Terzaghi, Karl, Ralph B. Peck and Gholamreza Mesri, 1996, Soil Mechanics in Engineering Practice, John Wiley & Sons, Inc.

Geotech (1988), Chevron Karluk Ice Island – Design Basis, November 1988.

Terzaghi, Karl, Ralph B. Peck and Gholamreza Mesri, 1996, Soil Mechanics in Engineering Practice, John Wiley & Sons, Inc.

Bugno W., Masterson D. M., Kenny J., Gamble R. (1990), Karluk Ice Island, OMAE 1990, Vol. 4.

SLIDING RESISTANCE OF GROUNDED SPRAY ICE ISLANDS

A. Barker[1] and G.W. Timco[1]

ABSTRACT

In the 1970's and 1980's, a number of grounded ice islands were used as drilling platforms in the Beaufort Sea. These islands were constructed by spraying sea water into the air to form ice, gradually building up a large platform area that eventually grounded on the seabed. One important factor in the feasibility of using ice in such a manner concerns the sliding resistance of the grounded spray ice. Reports and papers from four sites (Mars, Angasak, Karluk and Nipterk ice islands) were studied in detail. This study provides both qualitative and quantitative knowledge on the sliding resistance of ice pads. It illustrates that these structures were very stable with respect to seabed sliding.

INTRODUCTION

During the exploration drilling for oil and gas in the Canadian and US Beaufort Seas in the 1970s and 1980s, several different types of structures were used to support the drilling activities. These structures included artificial islands, drill ships, gravity caisson structures, and spray ice islands. Different structures were used depending upon the ice conditions and water depth. Initially, gravel islands were constructed in shallow waters (up to 12 m). For these islands, the ice surrounding them was landfast, first-year ice and had little movement during the winter months. The cost of this type of construction was quite high. For many years, ice has been used as a construction material to construct bridges, roads and aircraft runways, and it was used in the form of thickened ice platforms to support drilling activities in the high Arctic. The first spray ice structure to be constructed was the Sohio test island (Goff and Masterson, 1986). This structure was built as a grounded, sprayed test island. In the mid-1980s, innovative technology was developed to use spray ice to construct a drilling platform. Four spray ice islands were successfully constructed and used as drilling platforms – two in the Canadian Beaufort Sea and two in the US Beaufort Sea. These types of islands are formed by spraying sea water into the cold air which would then freeze the water into spray ice. Eventually, the ice is of sufficient thickness and weight that it grounds on the sea bottom. Further spray-

---

[1] Canadian Hydraulics Centre, National Research Council of Canada, Ottawa, ON, K1A 0R6 Canada

ing yields a higher-freeboard ice pad that is used to support the rig and the attendant equipment used for exploration drilling.

One of the key factors for using this type of technology is the stability of the ice pad. It is essential that the ice pad not move by any appreciable amount due to loading by the surrounding ice sheet. That is, the ice pad should have sufficiently high sliding resistance to withstand the imposed ice loads. At first glance, the sliding resistance of a spray ice pad appears to be quite a simple physics problem to solve. The design engineer must design the size and shape of the ice pad to resist the advancing ice sheet. The ice pad should remain stationary if the ice pad is large enough to overcome the environmental driving forces.

There are, however, a large number of issues and uncertainties faced by the design engineer that must be addressed, as summarized in Table 1. These make the task of determining the stability of an ice island a difficult exercise. With this large number of uncertainties, an ice pad cannot be designed in the traditional manner of designing a structure or building. The first ice pads were developed conceptually and field trials were performed to test the design. Subsequent ice pads were built using information gained from each previous ice pad. In this paper, the salient features of four Beaufort Sea ice islands are summarized, and a sliding stability analysis is carried out to provide both qualitative and quantitative knowledge of their sliding resistance.

Table 1. Factors Affecting the Stability of Ice Pads

Vertical Load	Horizontal load	Friction and cohesion/adhesion
Height of ice pad	Environmental driving force	Local/global failure of rubble
Diameter of ice pad	Ice sheet thickness	Seabed cohesion
Waterline location	Ice velocity	Seabed friction angle
Porosity of spray ice	Failure mode at the edge of pad	Nature of the ice/seabed interface
Porosity of ice rubble	Compressibility of ice rubble	
Compressibility of ice rubble	Ice rubble cohesion	
Drainage channels	Ice rubble friction angle	

ICE ISLAND DETAILS

Mars Ice Island

The Mars ice island was the first use of grounded spray ice as a drilling platform. It was constructed in western Harrison Bay in Alaska in early 1986. Amoco was the operator of the well. Most of the information on the Mars Island was found in Funegard et al. (1987). The seabed was clay with an undrained shear strength of 48 kPa (Masterson, personal communication). The water depth was 8 m. The total logged pumping hours for the construction were 892 hours over a 46 day period with over 1 million m³ of water pumped. The as-built island consisted of a 215 m diameter drill rig area with a waterline width of 290 m, and a freeboard of +8 m. Figure 1 shows a photograph of the completed ice island.

Fig. 1. Photograph of Mars Ice Island

The monitoring of movement was done in a real time environment to provide immediate warning if the stability of the island was threatened. Details of the results of the monitoring are confidential and are not publicly available. However, Funegard et al (1987) indicated that there were no large scale movements of the ice island during its use as a drilling platform. Details of the local ice conditions were not provided, so it was only possible to calculate an estimate of the grounding stability of this ice pad.

Angasak Ice Island

The Angasak spray ice island was located in the Canadian Beaufort Sea near Cape Dalhousie and it was constructed in 1986. Esso Resources Canada Limited was the operator of the well. Information for the Angasak Ice Island was found in Weaver and Gregor (1988), Weaver (1987), Golder and Associates (1986) and Weaver and Foster (1986). Angasak Ice Island was constructed in 5.5 m of water, approximately 1 km from shore. The seabed consisted of a silty sand, with an internal angle of friction of 30° and an undrained shear strength of 18 kPa at the island-seabed interface. As a result of unusually warm weather, the spray ice density was higher, creating a stronger pad. In total, 398 000 m³ of water was pumped, over a period of 58 days.

The design normal force for the Angasak spray ice island was 912 MN, with a design global load of 300 MN. The final grounded diameter was 203 m. The island top diameter was 157 m, while the waterline diameter was 214 m. The freeboard was 6.1 m. The projected design ice thickness for the beginning of May was 2.0 m. A factor of safety of 1.5 and a maximum ice load of 1.5 MN/m were the minimum requirements for horizontal shear failure at the seabed. However, the maximum observed ice load was less than 0.2 MN/m. The minimum spray ice strength appeared to be greater than 23 kPa. The performance monitoring program at Angasak for monitoring horizontal island movement used three slope indicators, three in-place inclinometers and trigonometric surveys. The data was collected in real time in order to evaluate island stability as part of an alert program. Global shear failures in the order of 0.15 m were determined to be unacceptable. No horizontal movement was mentioned in the reports or papers.

Karluk Ice Island

Karluk Ice Island, located in the American Beaufort Sea near Prudhoe Bay, Alaska, was constructed in 1988. The well operator was Chevron U.S.A. Inc., with Mobil Exploration & Production Inc. as a joint venture partner. Details for the Karluk Ice Island were found in Bungo et al. (1990). The seabed where the island was constructed was silty

sand, with a friction angle of 36°. The island was located in 7.3 m of water. Construction of the ice island began on December 13, 1988 and was completed on January 20, 1989 (39 days). The average rate of spray ice build-up was 0.9 m/day once the island had grounded. Approximately 613 hours of spraying were required to achieve the required volume of ice.

The freeboard of the island was approximately 6.7 m, while the average core thickness was 14.3 m with a diameter of 270 m. The final ice volume of the island was approximately 697 000 m³. The maximum horizontal design load for the Karluk Ice Island was 367 MN, with a load factor of 1.5 for lateral stability. The average measured spray ice density after construction was completed was 614 kg/m³. Five in-place inclinometers at three locations and six manual inclinometer stations were used to monitor horizontal movement of the island. The in-place inclinometers measured maximum movements of 17.5 mm, 52.5 mm and 57.5 mm around the perimeter of the island. These movements occurred radially, moving away from the island centre and were attributed to settlement of the island under self-weight. It was concluded that movement was minimal and did not impose constraints on or limitations to the drilling. This was the maximum drilling area movement reported of the four ice islands.

Nipterk Ice Island

Nipterk spray ice island was constructed in the Canadian Beaufort Sea in 1988. The well operator was Esso Resources Canada Limited, in partnership with Chevron Canada, Petro Canada, Home Oil, AT&S and Gulf Canada. Details for the Nipterk Ice Island were obtained from Poplin and Weaver (1991); Weaver et al. (1991); Poplin (1989); and Weaver (1988). The Nipterk Ice Island was located near the Mackenzie River delta, approximately 6 km from Pelly Island. This location was more exposed that either the Mars or Angasak Ice Islands, the seabed soils were weaker and as a result of its proximity to the Mackenzie River delta, the water was less saline (and warmer). The island was located in approximately 6.5 m of water. The water column, in mid-November, 1988, was freshwater to a depth of 4 m below the water surface, and 15 ppt saline water below that. The seabed was a stiff overconsolidated silt, with a thin over-layer of very soft silty clay. The average minimum soil strength was 12 kPa and the soil was cohesive. The effective adhesion between the soil and the ice was estimated to be between 0.85 and 0.95 of the basic soil strength. Construction began on November 28, 1988, and was completed on January 20, 1989 (53 days). Layers were applied in thicknesses ranging from 1.0 m to 3.0 m. The island grounded unevenly, due to the roughness of the first year ice sheet.

The average freeboard over the working surface of the island was 4.15 m, with a freeboard of 3.7 m elsewhere. The final spray ice volume was approximately 825 000 m³. The design island diameter was 320 m, while the working surface diameter was 150 m. The average density in the ice island freeboard was 580 kg/m³. The surrounding consolidated level ice thickness was approximately 1.3 m on January 20. The design ice thickness, for May 1, was 2.0 m. The design ice load was calculated to be 600 MN, with a design sliding resistance of 970 MN. Three in-place inclinometers and five manual inclinometers were used to monitor horizontal movement of the ice island. All data was collected in real time. There was no significant horizontal movement during the early stages of the monitoring period. From Julian Day 86 to Julian Day 110, movement was detected; approximately 25 mm within the working area and a maximum

amount of 100 mm in the outer perimeter. By the end of the season in April, the total movement recorded was 200 mm along the seabed. The design limit was 150 mm/event. The major ice loading events were considered to be thermal events.

SLIDING STABILITY ANALYSIS

Basic concepts

It is important to identify and define the key parameters for the sliding resistance of the spray ice. The simplest concept for the sliding of the ice pad is to assume that the ice pad fails globally and is pushed off site by the advancing ice sheet. There are three different potential modes for this to occur:

1. Failure along the ice-seabed interface.
2. Failure through the seabed.
3. Failure in the ice.

Local failure and failure through the spray ice are not addressed here. In this paper, only failure along the ice-seabed interface or through the seabed is considered. The sliding resistance corresponds to the scenario that produces the lowest force. In this paper, failure is defined as gross movement of the ice island. Here, an ice island is considered to be essentially a deformable body. The movement may further be considered to occur in two stages, where stress deformation occurs with the commencement of the driving force, followed by the initiation of sliding movement along the seabed (see Figure 2). It may be possible to differentiate between the two types of movement, where the former occurs primarily in the surface of the spray ice, by examining detailed movement records. Where such records were not available, and it was unclear if sliding occurred along the seabed, movement was assumed to be purely stress deformation (that is, no failure along or through the seabed, nor through the ice).
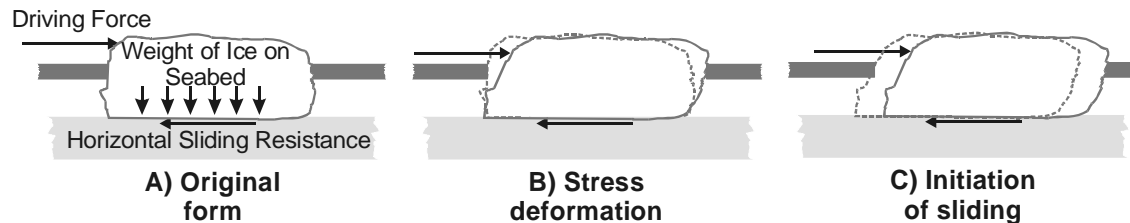

Fig. 2. Schematic illustration of the mechanism of global sliding along the seabed. Deformation and movement are greatly exaggerated for clarity

The horizontal sliding resistance, F_H, can be related to the normal force, N, (i.e the weight of the ice) on the sea bottom as follows:

$$F_H = Ac + N \tan \beta \ , \tag{1}$$

where A is the horizontal surface area of the structure, c is a constant and β is a friction angle. Weaver and Poplin (1997) used a similar formula, and indicated that c may be considered as an adhesion factor. Equation 1 is analogous to the expression of shear resistance along a plane within soils. In that case, c and β become the cohesion and angle of internal friction of the soil, respectively. It should be emphasized that in the present work, it is assumed that slip could take place at the interface between the ice and the soil or through the seabed. Therefore the friction parameters, c and β, are necessarily equal to the above mentioned soil parameters. The cohesion and angle of internal friction of the soil give upper bounds for the values of c and β.

212

The mechanics of sliding and friction resistance at the interface is not as well understood as the failure of soils. It is possible, however, to consider two extreme cases that are analogous to soil failure. In the one case, the shear resistance is linearly proportional to the normal force, and Equation 1 would be reduced to

$$F_H = N \tan \beta = f N \ , \tag{2}$$

where f is a friction coefficient. This case is similar to failure in sand. The stability is directly related to the weight of the ice island. In the other case, shear resistance would have a constant value, independent of the normal force, as

$$F_H = Ac \ . \tag{3}$$

This case corresponds to failure of clay. Note that in this case, the stability is not directly related to the weight of the island, but is dictated by the area of the ice island. In this paper, the stability of the ice islands will be examined in terms of these two extreme cases. Movement was recorded for two of the islands – Karluk and Nipterk. Karluk was built on a sandy seabed so Equation 2 is used to quantify the stability. Nipterk was built on a clay seabed so Equation 3 is used for this case. To do the analysis, information on the horizontal driving force, the normal force (weight of the ice island for Equation 2) and the area of the ice island (for Equation 3) is required in order to solve for β or c.

The normal force on the seabed is a function of the ice thickness and aerial extent, ice density and water depth. Stevens et al. (1984) derived the following equation to calculate the normal force for an ice pad constructed using spray ice:

$$N_s = [\, (1 - e_s) \, (\rho_i - \rho_w) \, d \, g + \rho_s \, Z_s \, g \,] \, A \ , \tag{4}$$

where N_s is the normal force due to spray ice, e_s is the sprayed ice void ratio, ρ_w is the water density, ρ_i is the density of ice either in rubble blocks or in spray ice granules (kg/m^3), d is the water depth (m), ρ_s is the bulk average density of spray ice above water (kg/m^3), Z_s is the sprayed ice thickness (m) and A is the surface area (m^2). The values that were used for the parameters in the equations (i.e. porosity, density, etc.) were taken from the original source whenever possible. If a value was not known, a reasonable value was assumed.

To estimate the possible horizontal driving force on the ice island, recent analysis of full-scale ice loads was used. Timco and Johnston (2004) analyzed the global loads on all of the caisson structures that were used in the Beaufort Sea. They found that the load was a function of the ice thickness, ice macrostructure and the failure mode of the ice. They produced a predictive equation for the average global load as

$$F_H = T_{fm} \, w \, h \ , \tag{5}$$

where the F_H is the driving force (in MN) on the structure, w is the width of the structure, h is the ice thickness and T_{fm} is a failure-mode parameter. In the present case, where the ice pads were usually surrounded by landfast ice, long-term creep loads would predominate so a value of 0.83 MN/m^2 was used for the failure mode parameter. Note that this value for the driving force represents a realistic value of the load that would be lower than the design value for the island.

Table 2 provides a summary of the ice properties and analysis results for each of the spray ice structures. Most values were gleaned from the published reports and papers, listed in the reference section of this report, although some values were assumed for each site. The calculated values of the normal force and driving force for each ice structure are shown in Table 2. The calculated average ice driving force on the ice islands

ranged from 360 to 522 MN, while the normal loads varied between 980 and 1600 MN. Any reported values concerning either the cohesion or the angle of internal friction of the seabed are also noted.

Table 2. Summary of ice island parameters (Values in bold were assumed)

Ice island name		Mars	An-gasak	Karluk	Nipterk
e_s (spray ice void ratio)		**0.6**	**0.64**	**0.6**	0.64
rho_w (water density)	kg/m³	**1020**	**1020**	**1020**	**1020**
rho_i (density of spray ice granules)	kg/m³	**900**	850	**900**	**900**
rho_s (bulk average density of spray ice above water)	kg/m³	641	700	614	580
d (water depth)	m	7.6	5.5	7.3	6.5
Z_s (sprayed ice freeboard)	m	7.6	6.1	6.7	3.73
D (average island diameter)	m	215	180	235	320
A (surface area – circular shape assumed)	m²	36200	25400	43200	80400
N_s (vertical normal force)	MN	1600	980	1600	1490
w (width of structure at waterline)	m	290	214	271	380
h (design ice thickness)	m	**1.9**	2.0	**1.9**	1.9
F_H (ice driving force/global load)	MN	460	360	430	522
Island movement?		unsure	unsure	yes	yes
Total amount of movement (any direction)	mm	-	-	58	250
Deformation of ice island	mm	-	-	58	50
Sliding movement	mm	-	-	0	200
Design seabed internal friction angle	°	n/a	30	36	n/a
Design seabed cohesive strength	kPa	48	18	-	12

Movement of Karluk

Bungo et al. (1990) reported that there was movement of the Karluk Ice Island. As shown in Figure 3, however, the movement appeared to occur radially away from the centre of the island. As a result, it is likely that this radial deformation was due to settlement of the island, rather than deformation from the surrounding ice sheet (i.e. island sliding). Thus, the Karluk Ice Island was stable with respect to the horizontal driving force. Since the island was stable, a friction coefficient cannot be determined from Equation 2. However, it is interesting to note that the ratio of the horizontal-to-vertical loads (i.e. the driving force / island weight) ratio is estimated to be 0.27. Since the island didn't slide, the friction coefficient had to be higher than this value.

Movement of Nipterk

At Nipterk, a maximum amount of movement of 25 mm was detected within the working surface perimeter, along the seabed. At the outer edge, the maximum movement recorded by the end of the season was 250 mm. For this island, the report by Poplin and

Weaver (1991) provides plots that detail the data obtained from the onsite slope indicators and inclinometers. An example from one outer edge station is shown in Figure 4. This plot illustrates that the movement of the ice island is a combination of sliding and shear deformation. Of the 250 mm of movement recorded at the outer edge of the ice pad, approximately 50 mm corresponds to a simple shear deformation of the pad, and the remaining 200 mm appears to result from sliding along the seabed. The deformation is considered in terms of both of the movement mechanisms shown in Figure 3c. A simple analysis of the shear deformation suggests that the effective shear modulus for the ice pad for long-term loading (months) is on the order of 2 MPa. With regard to overall sliding of the ice island, Nipterk was built on a clay seabed so Equation 3 can be used to estimate on overall cohesive strength. Using the as-built area of 80 400 m^2 and a horizontal driving force of 522 MN (from Equation 5), a large-scale cohesive strength of 7 kPa is determined. Since the average minimum strength of the seabed was 12 kPa, this suggests that failure took place along the ice-seabed interface.
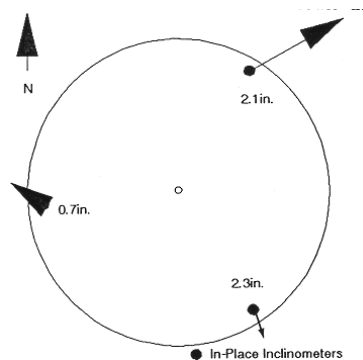

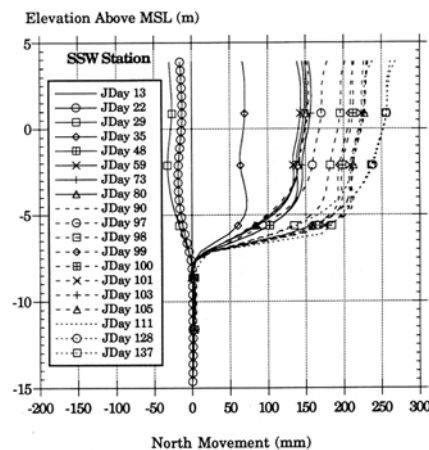Fig. 3. Recorded ice island movements for Karluk (from Bungo et al., 1990)

Fig. 4. Movement of Nipterk Ice Island, showing movement variations with depth.
Movement at the seabed is approximately 200 mm (from Poplin and Weaver, 1991)

SUMMARY

A review has been presented of four ice islands that were built in the Beaufort Sea. An examination of the stability of the islands indicates that these structures can be quite stable with respect to sliding movements if they are designed properly. An analysis was presented to attempt to quantify the stability. The movement that was detected at Karluk and Nipterk was not catastrophic in nature. Rather, it was generally a creeping process that resulted in cumulative displacement over the season of use. In the instances where larger movements occurred over a short period of time (a few days), this movement was still considered to be within acceptable tolerances. Although the concepts used here are

quite simple and straightforward, they provide some insight into the stability of the islands on a large scale. The work described here is part of a report (Barker and Timco, 2004) that examines the stability of these four ice islands, as well as three relief well ice pads, three ice barriers and a field study of grounded spray ice.

ACKNOWLEDGMENTS

REFERENCES

Barker, A. and Timco, G. (2004) Sliding Resistance of Grounded Spray Ice Structures. PERD/CHC Report CHC-TR-017. Ottawa, Canada.

Bungo, W., Masterson, D.M., Kenny, J. and Gamble, R. (1990) Karluk Ice Island. *Proceedings of the 9th International Offshore Mechanics and Arctic Engineering Symposium (OMAE'90)*, Houston, U.S.A. Vol. IV, pp. 9-17.

Funegard, E.G., Nagel, R.H. and Olson, G.G. (1987) Design and Construction of the Mars Ice Island. *Proceedings of the 6th International Offshore Mechanics and Arctic Engineering Symposium (OMAE'87)*, Houston, U.S.A. Vol IV, pp 25-32.

Goff, R.D. and Masterson, D. M. (1986). Construction of a Sprayed Ice Island for Exploration, *Proceedings of the 5th International Offshore Mechanics and Arctic Engineering Symposium (OMAE'86)*, Tokyo, Japan. Vol IV, pp 105-112.

Golder Associates (1986) Esso Resources Canada Limited Design Review Angasaak L-03 Spray Ice Island, Cape Dalhousie, N.W.T. *Golder Associates Confidential Report 862-2056*. Calgary, Canada.

Golder Associates (1984) Report to Esso Resources Canada Limited On Geotechnical Analysis of Kadluk Spray Ice Island. *Golder Associates Confidential Report 842-2039*. Calgary, Canada.

Kemp, T.S. (1984) Grounded Ice Pads as Drilling Bases in the Beaufort Sea. *Proceedings of the 7th International Symposium on Ice (IAHR'84)*, Hamburg, Germany. Vol. III, p.175-186.

Mellor, M., 1983. Mechanical Behavior of Sea Ice. US Army CRREL Monograph 83-1, Hanover, N.H., USA.

Poplin, J.P. (1991) Nipterk P-32 Spray Ice Island Ablation Protection Experiment. *Esso Resources Canada Confidential Report ERCL.RS.89.24*. Calgary, Canada.

Poplin, J.P. and Weaver, J.S. (1991) Nipterk P-32 Spray Ice Island Analysis of Island Performance. *Esso Resources Canada Ltd. Confidential Report ERCL.RS.91.27*. Calgary, Canada.

Stevens, G.S., Kemp, T.S., and Foster, R.J. (1984) An Engineering Assessment of the Kadluk O-07 Relief Well Ice Pad. *Esso Resources Canada Confidential Report ERCL.RS.84.23*. Calgary, Canada.

Timco, G.W. and Johnston, M. (2004) Ice Loads on the Caisson Structures in the Canadian Beaufort Sea. *Cold Regions Science and Technology (in press)*.

Weaver, J.S. (1988) Nipterk P-32 Spray Ice Island Design Report. *Esso Resources Canada Ltd. Confidential Report ERCL.RS.88.17*. Calgary, Canada.

Weaver, J.S. (1987) Angasak L-03 Spray Ice Island Stability Verification Report. *Esso Resources Canada Ltd. Confidential Report ERCL.RS.87.04*. Calgary, Canada.

Weaver, J.S. and Foster, R.J. (1986) Design of Angasak L-03 Spray Ice Island. *Esso Resources Canada Ltd. Confidential Report ERCL.RS.86.15*. Calgary, Canada.

Weaver, J.S. and Gregor, L.C. (1988) The Design, Construction and Verification of the Angasak Spray Ice Exploration Island. *Proceedings of the 7th International Offshore Mechanics and Arctic Engineering Symposium (OMAE'88)*, Houston, U.S.A. pp. 177-183.

Weaver, J.S. and Poplin, J.P. (1997) A case history of the Nipterk P-32 spray ice island. *Canadian Geotechnical Journal*. Vol.34, p.1-16, NRC Research Press, Ottawa.

Weaver, J.S., Poplin, J.P. and Croasdale, K.R. (1991) Spray Ice Islands for Exploration in the Canadian Beaufort Sea. *Proceedings of the 10th International Offshore Mechanics and Arctic Engineering Symposium (OMAE'91)*, Stavangor, Norway. Vol. IV, pp. 17-22.